2023

Spatial processing of conspecific signals in weakly electric fish: from sensory image to neural population coding

Oak Everette Milam
West Virginia University, oemilam@mix.wvu.edu

Spatial processing of conspecific signals in weakly electric fish:

from sensory image to neural population coding

Oak Milam

A dissertation submitted
to the Eberly College of Arts and Sciences
at West Virginia University

in partial fulfillment of the requirements for the degree of

Doctor of Philosophy in
Biology

Gary Marsat, Ph.D., Chair
Sadie Bergeron, Ph.D.
Kevin Daly, Ph.D.
Sarah Farris, Ph.D.
Jorge Mejias, Ph.D.

Department of Biology

Morgantown, West Virginia
2023

Keywords: signal localization, topographic maps, network modeling, neural coding, pyramidal neurons

Abstract:

Spatial processing of conspecific signals in weakly electric fish:
from sensory image to neural population coding

Oak Milam

In this dissertation, I examine how an animal's nervous system encodes spatially realistic conspecific signals in their environment and how the encoding mechanisms support behavioral sensitivity. I begin by modeling changes in the electrosensory signals exchanged by weakly electric fish in a social context. During this behavior, I estimate how the spatial structure of conspecific stimuli influences sensory responses at the electroreceptive periphery. I then quantify how space is represented in the hindbrain, specifically in the primary sensory area called the electrosensory lateral line lobe. I show that behavioral sensitivity is influenced by the heterogeneous properties of the pyramidal cell population. I further demonstrate that this heterogeneity serves to start segregating spatial and temporal information early in the sensory pathway. Lastly, I characterize the accuracy of spatial coding in this network and predict the role of network elements, such as correlated noise and feedback, in shaping the spatial information. My research provides a comprehensive understanding of spatial coding in the first stages of sensory processing in this system and allows us to better understand how network dynamics shape coding accuracy.

Acknowledgements

I've been incredibly fortunate to have met so many wise, kind, funny, and encouraging, positive influences throughout the years of my academic studies. For the sake of brevity, I would like to especially thank a few people who have shown their continual support over the duration of my research.

I'd like to begin by crediting some of the especially inspiring teachers I've had. From time to time, I still think about: some of Ed Booten's words of wisdom; Dr. Zach Fowler's contagious positivity and outlook; Dr. Joe Morton's genuine curiosity and easy-goingness; Dr. Andrew Dacks's humor and constructive criticism; Dr. Stephanie Young and Dr. Sue Raylman for always being there to help and providing me with opportunities. Thank you for (often indirectly) molding my perspective and motivation on teaching and research.

Next, I want to acknowledge my family. My mom for always being reliable and organized and my dad for always being supportive. My brother, Jay, for just being there and being yourself, really. You have no idea how much that means.

To the BLEST family, thanks for all the antics, you guys mean the world to me, here's to a century more.

To all the lads in the Plumtown server, thank you for all the good times and just being down to do anything all the time.

To the Zheng Family and Friends Vacation Squad, thank you for helping me relax a little bit and for inviting me to tag along as you all explore the world through bi-annual trips.

To my girlfriend, Jeongwi, for all the support and positivity.

To all the friends I met in grad school, we were all going through it together. Thanks, Dr. Lexie Schmidt and Dr. Becca Coltogirone, Sam Skibicki, Scott Arbet, Dr. Kristyn Lizbinski, Dr. Tyler Sizemore, and more.

To the Marsat Lab – To Dr. Kate Allen for all the sass, to Danielle for all the pranks, to Dr. Keshav Ramachandra for all of the everything really, to Robin, Ian, Sophia, and Jenna for all the extra help on this journey, and to the newest Marsat Lab cohort - Dakota and Elora (tell the fish that I'll miss them).

To my committee members, Drs. Sadie Bergeron, Kevin Daly, Sarah Farris, and Jorge Mejias, thank you for all the help, comments, and advice you have given me.

And to Dr. Gary Marsat, thank you the most. You've taught me nearly everything that I know about science and what it means to be a scientist. From you, I've become a better writer, learned how to code (neural, matlab, and HPC), gained an interest in PCs, embraced further my interest in the Korean language, heightened my analytical and quantitative skills, and realized what it really means to be a teacher, researcher, advisor, and mentor. Thank you.

To all who read this thesis, never stop learning. Go forth and prosper!

Table of Contents

Spatial processing of conspecific signals in weakly electric fish:

from sensory image to neural population coding

Chapter 1: Introduction – Part 1

Prologue

I introduce my dissertation with an insightful discussion of sensory systems and the challenges they must overcome to efficiently collect information from their surroundings. In particular, the challenge that I focus on is the sensory problem of localizing signals in three-dimensional space. I frame this problem around a reference animal, the weakly electric fish and its remarkable electrosensory system. These animals possess an aptitude for distinguishing very weak signals, relying only on the electric fields they generate to do so. What's even more interesting, is that they can do this even when environmental conditions confound the signal, making it difficult to process information accurately. However, these animals are not the only ones with finely tuned nervous systems, tailored for solving difficult sensory tasks. Several organisms have evolved general mechanisms to efficiently process this type of information.

Taking a comparative approach, I describe mechanisms that animals' nervous systems use to address the challenge of localizing signals in their environment. I present solutions that are either generalized or unique to the electrosensory system and highlight other similar findings that have been observed across different species and sensory modalities (e.g., auditory, visual, olfactory, and somatosensory). Along the way, I emphasize the importance of taking a neuroethological perspective for providing insights to elusive sensory questions.

Note: This first part of the introductory chapter has been published as:

"Milam, O. E., Ramachandra, K. L., & Marsat, G. (2019). Behavioral and neural aspects of the spatial processing of conspecifics signals in the electrosensory system. Behavioral Neuroscience, 133(3), 282."

Abstract

Localizing the source of a signal is often as important as deciphering the signal's message. Localization mechanisms must cope with the challenges of representing the spatial information of weak, noisy signals. Comparing these strategies across modalities and model systems allows a broader understanding of the general principles shaping spatial processing. In this review we focus on the electrosensory system of knifefish and provide an overview of our current understanding of spatial processing in this system, in particular, localization of conspecific signals. We argue that many mechanisms observed in other sensory systems, such as the visual or auditory systems, have comparable implementations in the electrosensory system. Our review therefore describes a field of research with unique opportunities to provide new insights into the principles underlying spatial processing.

Introduction

The role of sensory systems is to capture information about the environment. Although much of the behaviorally relevant information is contained in the quality and quantity of a signal, its spatial structure is also relevant (Bradbury & Vehrencamp, 2011; McGregor, 1993). Communication and conspecific signals carry much of their meaning in their spectral and temporal modulation: amplitude and frequency modulations in bird songs (Konishi, 1985; Lohr, Wright, & Dooling, 2003 Reid et al., 2005), colors of body ornaments (Doucet, Mennill, & Hill, 2007; Guilford & Dawkins, 1993; Keyser & Hill, 2000), or chirping patterns in weakly electric fish (Dunlap, DiBenedictis, & Banever, 2010; Engler, Fogarty, Banks, & Zupanc, 2000). Even for olfactory signals, the message is represented by the quality (i.e., odor identity) and quantity of the odor (Aragón, 2009; Daly et al., 2016; de Bruyne & Baker, 2008). In most cases, the receiver also tries to determine the location of the signal's source. Seeking out a signaling mate (Arikawa, Wakakuwa, Qiu, Kurasawa, & Stavenga, 2005; Byrne & Keogh, 2007; Mathis, 1990), localizing threats and the alarm calls they trigger in conspecifics (Cäsar, Zuberbühler, Young, & Byrne, 2013) or avoiding a competitor broadcasting its territorial claim (Bee, 2000; Behr, Knörnschild, & Von Helversen, 2009) are a few examples where the spatial aspect of the signal is key in guiding the behavior successfully. When localizing the source of a signal, sensory systems are faced with important challenges as a signal's directionality and strength can be weakened as it propagates through the environment (Bradbury & Vehrencamp, 2011).

Decades of research on the neural and behavioral mechanisms underlying signal localization in various modalities and model systems have led to rich insight into how these challenges are met. As always, comparing solutions across modalities and species can reveal

core principles of a mechanism and key adaptation permitting new functions. The study of sensory processing in weakly electric fish has provided important contributions to this comparative approach to understanding neural processing. An extensive literature on the temporal processing of electrosensory signals is matched by a relatively smaller but growing literature focused on the spatial aspects of communication signals. We provide in this review an overview of our current knowledge on the spatial processing of electrocommunication signals, but most importantly we point out key challenges faced by this system and commonalities with other sensory systems. We argue that the difficulty in localizing weak signals, signals in noise, or simply localizing accurately requires sensitive and efficient mechanisms that share many resemblances across modalities.

The electrosensory system

The ability to sense electric fields is thought to have evolved early in the vertebrate lineage (Bodznick & Northcutt, 1981) and is developmentally derived from lateral line placodes (Modrell, Bemis, Northcutt, Davis, & Baker, 2011). Electroreception was lost in teleost fish, but regained at least twice (in Osteoglossomorpha and Ostariophysi) thereby explaining the presence of electroreceptors in a variety of species, including catfish, elephantnose fish and knifefish (see Baker, Modrell, & Gillis, 2013 for a recent review on the topic). In teleosts, electroreceptors are thought to have evolved as a modification of neuromast (Baker et al., 2013). Beyond their detailed evolutionary trajectory, electroreceptor origin is clearly linked to the lateral line and mechanosensory system, similar to the origin of vertebrate auditory receptors (Duncan & Fritzsch, 2012). As a reflection of their similar evolutionary origin, both

electroreceptors and auditory receptors travel along the VIIIth cranial nerve (Carr, Maler, & Sas, 1982). Ampullary receptors are the most common type of electroreceptors across species, but in two orders of teleost (Gymnotiformes and Mormyriformes) a second type of electroreceptor evolved - tuberous receptors (Szabo, 1974). Where ampullary receptors are sensitive to low-frequency electric signals, such as the ones produced by contracting muscles, tuberous receptors are sensitive to high frequencies (Bennett, Sandri, & Akert, 1989; Maler, 2009a; Maler, 2009b; Hopkins, 1976) and their evolution accompanies the evolution of electric organs (EO) that generate high-frequency weak electric fields (Fig 1). Derived from a modified muscle or a modified nerve terminal, EO produce pulsatile or continuously oscillating electric fields (Kramer, 1996). Weakly electric fish (Gymnotiformes and Mormyriformes) thereby possess an active electrosense where the electric organ discharges (EOD; Lissmann, 1958) are perceived by electroreceptors on the skin. Anything in their environment that is more or less resistive than water will cause a distortion of this electric field that will cast an “electric shadow” (Rasnow, 1996) on the sensory surface (we refer to the electrosensory sensorium as the “sensory surface” throughout the review). They rely heavily on this active sense to navigate, localize prey, but also to communicate and interact with conspecifics (Bullock, Hopkins, Popper, & Fay, 1986; Lissmann, 1963). Although Gymnotiformes and Mormyriformes have many similarities in the way they use and process electric signals, the fact that they evolved this active electric sense independently also leads to significant differences, in particular at the neural level. To facilitate the discussion in this review, we will focus on knifefish (Gymnotiformes), and more specifically the wave type species (e.g., glass knifefish or ghost knifefish) that produce

continuous EODs rather than pulsed EODs (Bass 1986; Bennett, 1971); we will simply refer to them as weakly electric fish.

Knifefish are typically nocturnal species and thus rely heavily on this active electrosense to perceive their environment. The sensory image caused by objects close to them is quite accurate thanks to a relatively high density of receptors over the entire surface of the skin (Carr et al., 1982); allowing them to be efficient hunters of invertebrate prey (Nelson & MacIver, 1999). Similarly, they can locate and identify a conspecific based on the EOD it produces or mediate social interactions via electrocommunication signals such as chirps (Engler & Zupanc, 2001). The sensitivity of their ability to locate each other based on this sense is easily observable both in the field or in the lab (see below). For example, they will chase each other at high speed in a noisy environment with multiple other signal sources or locate each other at such distances that they must base this detection on extremely weak signals.

Localization of conspecifics

The localization of conspecific signals is a different sensory problem to the localization of small objects such as prey items. An object close to the body will cause a local disturbance in the EOD which will be picked up by a limited number of receptors on the corresponding portion of the skin (Rasnow, 1996). The localization strategy in this case is likely to be closer to visual localization or localization in the somatosensory system where exclusive activation of a subset of receptors encodes location in a labeled line code (Cichy & Teng, 2017; Hartmann & Bower, 2001; Krekelberg, Kubischik, Hoffmann, & Bremmer, 2003; Okada & Toh, 2006). Localizing a conspecific based on the EOD it produces cannot rely on this strategy since the sender's EOD

will impact the majority of electroreceptors over the entire skin surface (Kelly, Babineau, Longtin, & Lewis, 2008). Therefore, localization of conspecifics probably relies on comparison of the input at the various receptors and location would be computed by the nervous system based on the differences. This task shares similarities with localization in the auditory system, which relies on comparisons of binaural input (Brand, Behrend, Marquardt, McAlpine, & Grothe, 2002; Carr & Konishi, 1990; Jeffress, 1948). Localization in the electrosensory system might therefore be described as a hybrid mechanism that relies on a labeled line strategy for passive objects (e.g., small prey) that cause a local electrical disturbance, but needs to compute the spatial information about active electro-generating sources (e.g., conspecifics). As such, the electrosensory system is faced with many of the same challenges faced by the auditory or the visual system when localizing signal sources in complex environments. Whether it is a question of localization accuracy (e.g., auditory system), localizing in a noisy environment (cocktail party problem in the auditory system; Cherry, 1953; Liberman, Harris, Hoffman, & Griffith, 1957) or foreground-background separation (visual system; Ölveczky, Baccus, & Meister, 2003), there is a rich literature documenting the various neural and behavioral mechanisms in place to face these challenges.

The electrosensory system has a long history of contribution to our understanding of sensory processing (Bastian & Heiligenberg, 1980). Issues of temporal coding have been particularly well explored in this system (Gabbiani, Metzner, Wessel, & Koch, 1996; Krahe, Bastian, & Chacron, 2008). Understanding localization in the electrosensory system has focused heavily on the spatial aspect of prey capture or the localization of small objects (Babineau, Lewis, & Longtin, 2007; Caputi & Budelli, 2006; Nelson & MacIver, 1999; Rasnow, 1996). Less is

known about the spatial processing of conspecific signals, but there are several new studies and a growing interest in the topic (Kelly et al., 2008). Our goal in this review is to provide an overview of what is known about localization of conspecific signals in weakly electric fish, pointing out along the way how this model system can contribute to our general understanding of sensory processing. We will first discuss the behavioral aspects of conspecific localization to provide a good understanding of the tasks that must be carried out by the nervous system. We will then describe the neural mechanisms underlying spatial processing and point out the issues that remain poorly understood. Finally, we compare the electrosensory system with other modalities to highlight the common challenges they face and discuss the similarities and differences in how they accomplish these tasks.

Behavior and signal properties

This electrosense is advantageous for navigating at night or in murky waters. Their ability to navigate and locate prey based on this sense is well documented (Nelson & MacIver, 1999; Postlethwaite, Psemeneki, Selimkhanov, Silber, & MacIver, 2009; Stamper, Roth, Cowan, & Fortune, 2012; Von Der Emde, Schwarz, Gomez, Budelli, & Grant, 1998). Similarly, they also rely heavily on this electrosense when interacting with conspecifics to identify, communicate and locate each other. Identity can be determined from the EOD pattern (Fig 2a): depending on the species; EOD frequency; shape or pulse pattern can be used to identify conspecifics from individuals of another species (Zupanc, Sîrbulescu, Nichols, & Ilies, 2006) or even differentiate amongst conspecifics (Zakon, Oestreich, Tallarovic, & Triefenbach, 2002). In wave type species,

the EOD frequency (and possibly shape; Kolodziejski, Sanford, & Smith, 2007; Petzold, Marsat, & Smith, 2016) is perceived indirectly.

Indeed, when two or more individuals come into close proximity, the electric fields of each fish summate, and the resulting field contains amplitude and phase modulations, collectively known as a "beat" (Fig 2b; Heiligenberg, 1991). The beat frequency is equal to the frequency difference between the EOD of the sender and receiver (note that both fish send and both fish receive but we use this terminology throughout this article to describe the perspective we use (Stamper, Madhav, Cowan, & Fortune, 2012). Furthermore, phase modulations can indicate whether the other fish has an EOD frequency higher or lower than its own (see Carlson & Kawasaki, 2007; Metzner, 1999; Stamper et al., 2012 for more information). Determining beat frequency is important since each fish has a baseline EOD frequency and thus individual discrimination can be based on this signal. In some species, EOD frequency is sexually dimorphic leading beat frequencies to be lower during same-sex interactions and higher for male-female pairs (Engler & Zupanc, 2001). Since beat frequency can indicate species, sex, maturity and even individual identity, many species react differently when exposed to beat signals of various frequencies. For example, the rate of production of certain communication signals in black ghost or brown ghost knifefish depends on the beat frequency (Hupé, Lewis, & Benda, 2008). The most common type of communication signal produced by these fish -chirps- are brief increases in EOD frequency (see Kolodziejski et al., 2007 for more info).

Sensitivity of conspecific detection and localization

In wave type fish, the beat signal results from the presence of a conspecific (see Fig 2), and, therefore, carries information about a conspecific's location. The beat signal will strengthen as the conspecific gets closer and the strength of the signal across the sensory surface (i.e., the body's surface) correlates with its relative position. Both lab and field studies clearly show that they monitor this information to detect the presence and position of a conspecific. In an insightful field study, Henninger et al (Henninger, Krahe, Kirschbaum, Grewe, & Benda, 2018) used grids of electrodes placed in river streams and creeks to triangulate and follow individuals in their natural environment during long periods of time. Besides revealing the behavioral and communication dynamic happening during various types of interactions -including courtship or aggression- this study showed the range of detection of conspecifics via this electrosense. Although their data suggests that fish routinely communicate with each other over distances of up to 30 cm, it also shows that two fish can detect and assess a conspecific at distances of 1 meter or more. For example, they showed that a resident fish-initiated attacks on an intruder located as far as 1.7 m away. To emphasize how challenging this task is, they estimated the strength of the sender's signal and showed that a fish 30 cm away creates a signal of 10 µV/cm and that a fish 1.7 m away causes a signal smaller than 1 µV/cm. Note also that this data suggests that these weak signals were not only detected, but also localized since it guided the resident to launch an attack directed at the intruder.

Laboratory studies confirm the sensitivity of this system in detecting and locating a conspecific. Fish adjusted their EOD output (i.e., the response called "envelope tracking") when presented with beats of 10-15% contrast (Metzen, Huang, & Chacron, 2018) which would

correspond to a conspecific 20-30 cm away (Fotowat, Harrison, & Krahe, 2013). In another study, fish exposed to a conspecific signal presented from various distances regularly produced chirps only in response to the stimuli located fairly closely (10 cm; Zupanc et al., 2006). However, conditioned responses to weak signals demonstrated that fish could detect signals weaker than 1 μV/cm corresponding to a distance of up to 1.6 m (Knudsen, 1974; Knudsen, 1975). Therefore, despite coming to their conclusion through very different methods, the field and laboratory studies provide very similar estimates and identify a certain range within which fish actively interact with each other (e.g., chirp or envelope tracking) and a wider range delineating the limits of their detection and localization ability.

Conspecific localization and EOD temporal modulation

Information about conspecific location is present in two aspects of the signal: its temporal modulations and its spatial structure (see next section). Temporal modulations are indeed imparted by the relative movement of two fish. As a sender moves closer and further from the receiver, the beat will proportionally increase and decrease in strength (Fig 2c). The strength of the beat is also called its “contrast” and contrast modulations are called the “envelope signal”. The characteristics of these envelope signals have been determined experimentally by recording the signals received by a fish exposed to one or several other moving conspecifics (Fotowat et al., 2013; Yu et al., 2012). Since movement is relatively slow, envelope signals are typically low frequency (<10 Hz). The data also confirmed that the beat elicited by a conspecific nearby can be strong (often above 50% contrast at <10 cm), but decreases quickly with distance (a few % at 30 cm; Fotowat et al., 2013) since these electric fields decrease in strength as a

function of the cube of the distance (Caputi, Aguilera, Pereira, & Rodríguez-Cattáneo, 2013). Furthermore, these recordings illustrate another important principle that influences the properties of electric signals. The strength of the signal is not simply related to the distance but also to the relative orientation of the receiver and sender "dipoles" (Rasnow, Assad, & Bower, 1993). To simplify, the EO can be thought of as a stimulus dipole and electroreceptors are sensing dipoles detecting the potential difference across the skin. Electric fields are characterized by isopotential lines and a sensing dipole positioned parallel to an isopotential line would not pick up the signal even if it is close to the stimulus dipole (Fig 1; Assad & Bower, 1997; Rasnow et al., 1993). Consequently, the strength of the envelope can decrease to zero as the fish moves away or as it rotates 90° making the envelope signal picked up by a given receptor ambiguously related to the location of the sender.

Envelope signals are common in various modalities. In the visual system they are linked to the ability to distinguish contrast based visual contours (Grosof, Shapley, & Hawken, 1993). They are also used by the auditory system for speech perception and sound localization (Lohuis & Fuzessery, 2000; Smith, Delgutte, & Oxenham, 2002). The electrosensory system has provided important insight into how these signals are processed by the nervous system (see next section), but we do not yet know how they are used to gauge the distance of the sender. Furthermore, azimuth and elevation of the sender relative to the receiver is not encoded in this temporal signal, it can only be estimated by comparing the strength of the signal across the sensory surface.

Electrosensory image

The sensory surface is well suited to capture the spatial aspect of the sensory environment. Most of the body surface of knifefish contains a high density of electroreceptors each capturing the electrical potential within its vicinity (Carr, Maler, & Sas, 1982). Distortion of the fish's own EOD caused by its environment can thus be mapped on this spatially organized sensory array. Distortions experienced by these fish can be categorized as either a passive electric image or an active electric image. The active electric image arises when an object or animal that is more or less conductive than the surrounding water locally influences the strength of the electric field generated by the fish. For example, a conductive prey item near the head (Fig 3) will locally increase the strength of the electric field and cast an "electrical shadow" (or a bright spot in this case) on the skin. A series of seminal studies using modeling, physiological and behavioral approaches have detailed the characterization of the electrosensory image of prey items during hunting behaviors (Nelson & MacIver, 1999; Nelson, MacIver, & Coombs, 2002). The authors measured the 3D relative position of the fish and its prey, modeled the electrosensory image that would result, estimated the activation strength of the various receptors and reconstructed a 3D activation map of the sensory surface. They determined that black ghost knifefish typically detect prey when they are 1-2 cm away that elicit a signal of 1-3 μV and can potentially detect a signal as weak as 0.2 μV. These studies point out once again the extreme sensitivity of this system and provide a clear understanding of how these signals are represented at the periphery. The neural mechanisms underlying prey localization and detection are also a good example of sophisticated neural processing strategies used to accomplish challenging tasks (see

next section; Chacron & Bastian, 2008; Clarke, Longtin, & Maler, 2014; Jung, Longtin, & Maler, 2016).

A conspecific in close proximity to the receiver will also cast such an active electrosensory image -albeit a bigger one- but few studies have characterized this sensory image. In a recent study combining behavioral recordings and modeling of the electric field and sensory image, Pedraja et al (2016) showed that this active image could guide behavior during aggressive encounters. However, they showed that the passive electrosensory image (see below), rather than the active one, was better correlated with the initiation of attack behavior at close range. This study also indicates that the image of the conspecific is fairly sharp at close range (a small portion of receptors are strongly activated and the others much more weakly), thereby giving a clear labeled-line representation of conspecific location. In contrast, the image elicited by a conspecific further away (>10 cm) is uniformly weak, thus detection most likely involves pooling all the responses together to average out the noise and localization must rely on comparing the weak responses to determine the even-weaker differences among them. This analysis highlights once again the challenging task that this system must perform. Although it is still not clear to what degree they rely on the passive image versus a combination of passive and active images in close range interactions, the active image cannot underlie the ability to detect and localize conspecifics far away (Knudsen, 1975).

They must thus rely on the passive electrosensory image to detect and localize distant conspecifics. The passive image consists of the spatial pattern of distortion of the receiver EOD caused by the sender EOD. It is important to point out that this terminology, although well defined for prey and for pulse species, is more ambiguous for wave-type species since this

passive image is the result of both sender and receiver's active signals (EODs and the resulting beat). Furthermore, the passive and active components will both be perceived through modulations of the receiver's own EOD and thus, are not truly different images but different components of the electrosensory image. We nevertheless use this terminology for consistency with previous studies (e.g., Pedraja, Perrone, Silva, & Budelli, 2016).

The strength of the beat signal at different points on the receiver's skin will vary with position and orientation of the sender. A sender located in front, for example, would cause stronger beats on the rostral than caudal end of the receiver. The detailed activation pattern of the sensory surface also depends on receptor orientation (e.g., dorsal receptors are nearly orthogonal to the nearby receptors on the side of the body). For this reason, the activation pattern of areas like the head will be more complex than for relatively flat area like the side of the mid-body. Several researchers have modeled the electrosensory image caused by a conspecific either fixed (Kelly, Babineau, Longtin, & Lewis, 2008) or approaching (Castelló, Aguilera, Trujillo-Cenóz, & Caputi, 2016; Gómez-Sena, Pedraja, Sanguinetti-Scheck, & Budelli, 2014) the focal fish. Despite being extremely valuable data, the studies typically have simplifications that make evaluating the strength of the input for all electroreceptors more difficult. For example, the models looking at conspecific signals were either limited to 2D or considered receptors only along a line on the side of the fish or did not take into account the various orientation of receptors. This complexity will be most obvious for regions like the head where receptors very close to one another will have very different orientation and thus very different activation levels. Considering how receptor activation will depend on the relative orientation, in 3D, of the receptor relative to the stimulus, further studies are required to

obtain a detailed characterization of the sensory image of conspecifics. An incomplete understanding of the spatial structure of these sensory signals limits our ability to understand how the sensory system extracts this spatial information. Nevertheless, a rich literature on sensory processing in this system documents many of the neural processes relevant to this task.

Sensory system and neural processing

Representation of space in sensory systems, for example through topographic mapping, is a key feature in most modalities. In the electrosensory system, the sensory images activate electroreceptors distributed everywhere across the skin. Ampullary receptors (mediating low-frequency passive electrosensation; see Introduction) are less numerous (~700 total in brown ghost knifefish) compared to tuberous receptors (~13,000-17,000 total; Carr et al., 1982). The density of ampullary and tuberous receptors varies across the body surface. Regions of the mouth, face, and head are higher in receptor density, resulting in the formation of an electrosensory fovea. Similar to other sensory systems, this foveal arrangement of receptors permits a higher resolution of sensory input and its location near the mouth is well suited to guide the final stages of prey capture.

There are two kinds of tuberous receptors involved in active electrosensation: T-units and P-units. Time coding units (T-units) are few in number and form a separate channel early in the sensory pathway through spherical cells of the electrosensory lateral line lobe (ELL) and onto a dedicated layer of the Torus semicircularis (Ts; Maler, Sas, & Rogers, 1981). Most tuberous receptors are amplitude coding (or probability coding units: P-units), providing direct input to ELL pyramidal cells. P-units are solely responsible for encoding the amplitude of the fish's own

EOD and the amplitude modulations (AMs) arising from electrolocation and electrocommunication (Nelson, Xu, & Payne, 1997). All tuberous receptors split three ways providing trifurcated input unilaterally to the centromedial segment (CMS), centrolateral segment (CLS), and the lateral segment (LS), whereas ampullary receptors project exclusively to the medial segment (MS) of the ELL (Heiligenberg & Dye, 1982). Pyramidal cells across the different maps and different layers of the ELL (deep, intermediate or superficial) vary in their response properties (e.g., low-pass to high pass) or receptive field size and polarity (ON-center or OFF-center cells; Krahe, Bastian, & Chacron, 2008; Saunders & Bastian, 1984). The three tuberous-driven maps thus have properties adapted for processing different signals. For example, CMS is crucially involved in the jamming avoidance response (JAR), certain stages of prey capture might rely more heavily on CLS, while LS is best at encoding communication signals (Maler, 2009b ; Marsat, Proville, & Maler, 2009; Metzner & Juranek, 1997). ELL neurons project to the Ts in the midbrain and to areas providing feedback to the ELL (see below). Ts has a laminar organization and a complex network of inputs, outputs and connections between layers. Electrosensory input to the Ts is somatotopically conserved and restricted specifically to the dorsal Ts (Carr et al, 1981). The dorsal Ts is divided into twelve laminae, of which layers 3, 5, 6, 7, 8b, and 8d receive electrosensory input. Cells that respond to communication stimuli likely lie within the deeper layers of the Ts. At higher levels the electrosensory pathway splits as Ts projects to the optic tectum (TeO) involved in spatial processing, to the nucleus electrosensorius (nE) processing communication signals, and the preglomerular nucleus (PG) that mediates connectivity with the forebrain (Fig 4; Giassi, Ellis, & Maler, 2012; Zupanc & Horschke, 1997). As expected, extensive feedback from forebrain areas but also from mid and

hindbrain areas interconnect these regions; most are not discussed further here (Bell & Maler, 2005; Giassi et al., 2012).

The processing of conspecific signals has been most extensively studied at the receptor and ELL levels and so we focus on the early sensory processing in the next sections of this review. Conspecific stimuli cause both phase and amplitude modulations in the input signal (Stamper, Fortune, & Chacron, 2013; Stamper et al., 2012; Yu et al., 2012). While phase information relayed by the T-unit receptors is essential to generate the JAR behavioral response, the bulk of the processing at this early stage focuses on the AM. Most notably, the beat AM present during conspecific interactions must be detected, localized and its frequency determined. As is typical with early stages of sensory processing, receptors encode the AM fairly linearly and ELL pyramidal cells -although possessing important non-linearities- still represent the shape of a broad range of AM signals in modulations of their firing rate. Various response properties and coding mechanisms have been described at this level such as interspike interval (ISI) correlations to reduce noise (Ratnam & Nelson, 2000), bursting to improve feature detection (Gabbiani, Metzner, Wessel, & Koch, 1996) or decorrelation to enhance information bandwidth and coding accuracy (Marsat & Maler, 2010). We also have a detailed understanding of how communication signals, chirps more specifically, are encoded in the early sensory pathway. Chirp coding crucially depends on the frequency of the beat that is present in the background of these interactions (Marsat, Longtin, & Maler, 2012; Walz, Grewe, & Benda, 2014). For example, the receptors can synchronize or de-synchronize in response to a chirp depending on whether the beat is low or high frequency (Benda, Longtin, & Maler, 2006) and ELL neurons might respond with bursts only for some chirp-beat combinations (Allen & Marsat, 2018; Benda

et al., 2006). For both chirp and beat coding, Ts neurons respond more sparsely and selectively (Vonderschen & Chacron, 2011) although some neurons still encode the signal AM in detail. Although the coding properties alluded to above could influence the conspecific localization mechanism, we will focus below on two mechanisms that play a large role in this process, namely envelope coding and beat cancellation.

We described in the behavior section how the movements of interacting fish would cause an envelope modulation - a signal that could serve to gage distance between individuals. Several recent publications have clarified the neural mechanisms underlying envelope coding (Huang, Metzen, & Chacron, 2018; Metzen & Chacron, 2014; Savard, Krahe, & Chacron, 2011; Thomas, Metzen, & Chacron, 2018). For firing rate to reflect the envelope strength, a non-linear transformation must happen. To illustrate this point, consider an envelope signal that decreases as if the conspecific was moving away. During this decrease in envelope (beat contrast), the mean EOD strength that reaches the receptors does not change, it still varies around the same amplitude of the fish's own EOD. Therefore, if mean firing rate is to change, even though mean EOD strength does not change, the nervous system must implement a non-linear transformation. Several mechanisms might contribute to the envelope coding mechanism. At weaker intensities, ovoid cells can perform this task (Middleton, Longtin, Benda, & Maler, 2006) and direct feedback can enhance the sensitivity of the envelope responses (Huang et al., 2018). At higher intensities, the receptors provide the main mechanism implementing this non-linear transformation. Due to the threshold and saturation of receptors, the incoming signal is half-rectified and then low-pass filtered at the synapse with the

pyramidal cells (Savard et al., 2011). These mechanisms extracting the envelope strength could therefore contribute to evaluating conspecific distance.

The ELL receives both direct feedback from the nucleus praeminentialis (nP; see Figs 4, 5) and indirect feedback from cerebellar granular cells (EGp; Figs 4, 5).The encoding of beats in the ELL is also influenced by indirect feedback inputs (Joseph Bastian, 1986a, 1986b). The role of the latter in cancelling the response to beats has been extensively documented (Bol, Marsat, Harvey-Girard, Longtin, & Maler, 2011; Chacron, Doiron, Maler, Longtin, & Bastian, 2003). A subset of pyramidal cells, the superficial and to some degree the intermediate cells, receive massive parallel fibers inputs onto their apical dendrites. Plasticity at these synapses adjusts the relative contribution of each fiber so that the overall input is in antiphase to the feedforward input from the receptors thereby reducing the strength of the response in these cells (Bol et al., 2011; Harvey-Girard, Lewis, & Maler, 2010). This mechanism operates for relatively low frequency beats but does not cancel the responses to beat frequencies higher than 15-20 Hz (Chacron, Maler, & Bastian, 2005). This feedback only affects a subset of cells; it does not influence the response of deep pyramidal cells and cancellation in the CMS and LS segments is less pronounced. Nevertheless, since it affects the coding of the beat, and because beat strength can mediate the localization of conspecifics, this feedback can potentially influence the localization mechanism (see below).

Topographic representation and spatial information

Each receptor on the skin captures the strength of the electric signal at a given point on the skin and thus the pattern of activation of the array of electroreceptors covering the body will

reflect the spatial structure of the electrosensory image elicited by the presence of a conspecific. This spatial pattern of activation of receptors is conserved through the topographic projection into the ELL. Thereby each of the four segments of the ELL (from medial to lateral) is organized as a topographic map of the sensory surface (Lannoo, Maler, & Tinner, 1989). The three maps sensitive to EOD (CMS, CLS and LS) differ in size and in the shape of their topographic representation (see Krahe & Maler, 2014). CMS is the largest map containing ~2800 pyramidal cells (in brown ghost knifefish) and the head representation is disproportionately big compared to the trunk. At the other extreme, LS is the smallest segment (~900 pyramidal cells on each side) and the head representation occupies a smaller portion of the maps compared to CMS. Pyramidal cells are organized in columnar functional units where three ON cells and three OFF cells located at various depths (deep, superficial or intermediate) have receptive fields with similar centers. Each of the six pyramidal cells within a column has different response properties and connectivity thus representing complementary channels of information. Taking digital images as an illustration, each column would represent a pixel and the spatial resolution of the sensory image on one side of the body would thus be of 150, 235 or 470 total pixels (i.e., columns) for LS, CLS and CMS segments respectively (Maler, 2009b).

As suggested by the anatomy, the receptive fields of ELL cells vary from segment to segment with smaller receptive fields in CMS (6–14 mm^2 corresponding to the area covered by 25–50 P-units), than CLS (26–60 mm^2/100–240 P-units), and much larger receptive fields in LS (160–360 mm^2/640–1400 P-units; Bastian, Chacron, & Maler, 2002; Shumway, 1989a; Shumway, 1989b). The segments also vary in amount of overlap between the receptive fields of neighboring cells (larger in LS than CMS). Pyramidal cells have a classical center receptive field

and a surround receptive field with an ON-center/OFF-surround (or vice versa) pattern similar to the well-known phenomenon in the visual system. The size of the surround relative to the center also varies across maps with LS maps having proportionally smaller surrounds and CMS having larger surrounds.

These differences in feedforward convergence and receptive field sizes could lead to differences in spatial representation and sensitivity. The small receptive fields are often associated with high spatial resolution, but lower sensitivity and might thus be geared towards detecting nearby small objects such as prey. Larger receptive fields are typically thought to mediate lower spatial resolution but higher sensitivity, since the input from many receptors are pooled and the noise can be averaged out. They would be best at responding to weak, distant signals that cast spatially extended (diffuse) images such as a distant conspecific. The use of smaller receptive fields and higher density of receptors for higher spatial accuracy might be the simplest scenario, but it is not the only possible processing strategy. For example, it was shown that accurate localization can be achieved with a broad receptive field if the neurons responded with high signal-to-noise ratio (Snippe & Koenderink, 1992). No matter what strategy is used, differences in spatial mapping across the ELL should support the efficient processing of spatial information from a variety of signals.

The topographic representation is preserved in the Ts where many of the layers contain a map of the body surface (Carr, Maler, Heiligenberg, & Sas, 1981). Similarly, the tectum is topographically organized but the other targets of Ts (nE and PG) are not (Fig 4). In non-electrosensory fish species, the tectum is largely driven by visual inputs and directs visually guided behaviors. It is thus no surprise that this structure receives electrosensory inputs in

species that rely heavily on this sense to guide motor behavior. While the tectum projects to locomotive motor areas, the nE projects to electromotor areas to control EOD and communication signal generation. Note that nE and tectum are interconnected through feedback loops, therefore; a communication signal from a conspecific processed in nE can influence the spatial processing of the conspecific location in tectum or the spatially directed behavior it generates.

The role of spatial differences in receptor activation has been highlighted in studies of the jamming avoidance response (Carlson & Kawasaki, 2007). However, spatial representation and coding of an active conspecific signal has not been detailed explicitly at any level of the nervous system. In contrast, spatial coding of passive objects has been the focus of several behavioral and neurophysiological studies (e.g., Caputi & Budelli, 2006; Nelson & MacIver, 1999; Sicardi et al., 2000). The electrosensory image of a daphnia at the time of detection can be as weak as 0.2 µV and covers a small (2-3 cm diameter) diffuse area of the body surface (Chen, House, Krahe, & Nelson, 2005). This very weak signal barely causes any increase in the firing rate of electroreceptors or ELL pyramidal cells and researchers have investigated the mechanism that permits such a sensitive detection. For example, it was suggested that a 0.2 µV prey signal would elicit an increase in firing rate of 0.2 spikes corresponding to about $1/10^{th}$ the SD of baseline firing rate (i.e., noise).

The most obvious way to solve this problem is to pool and average the information over many receptors. Theoretical calculations based on the strength and size of these signals and the convergence of electroreceptors onto pyramidal cells of various maps determined that, given certain assumptions, the LS could achieve reliable detection of 0.2 µV prey signals but those

assumptions remain to be tested (Maler, 2009b). Coding accuracy could also be optimized and a noise-reducing mechanism to do so has been identified. The spiking pattern of electroreceptors at baseline is not random and displays negative serial correlation in interspike intervals (i.e., short interval followed by long and vice-versa) due to an adaptation process (Ratnam & Nelson, 2000). This pattern reduces the low-frequency content of baseline noise, thus enhancing the ability to detect the low-frequency signals typical of prey stimuli (Chacron, Lindner, Maler, Longtin, & Bastian, 2005; Chacron, Longtin, & Maler, 2001).

It was further suggested that prey signals would cause a slight disruption in this patterned receptor spike train and that pyramidal cells could extract this change in pattern (Jung et al., 2016; Nesse, Marsat, Longtin, & Maler, 2012). Although these mechanisms were revealed by focusing on prey capture mechanisms, they are also relevant to the detection of distant conspecific signals, and we expect that these concepts will be explored when investigating the mechanisms permitting sensitive conspecific detection and localization.

Network dynamic and spatial processing

Localization of a passive object like prey differs from localizing the active signal of a conspecific for several reasons. The sensing volume for prey or small passive objects is limited to a few cm around the body and even large objects, such as a tank wall, do not significantly affect the strength of the EOD signal when it is more than 10 cm away (Chen et al., 2005; Fotowat et al., 2013). Passive objects that are detected cause a disturbance of the EOD over a limited area of the skin (a spot for a prey, one side of the body for a wall, etc.). In contrast, a conspecific at distances of more than 10 cm causes a very diffuse image where the signal

strength at most points on the receiver's body differs only by small amounts (Pedraja et al., 2016). Furthermore, active conspecific signals will cause a complex activation pattern of the sensory surface because of the relative orientation of the sender fish EO and cutaneous receptor orientation. Consequently, two receptors situated equally far from the sender could perceive signals of very different strengths if they are oriented differently (e.g., along the ventral-dorsal axis for receptors on the back and medial-lateral for receptors on the side). In other words, the activation of the receptor array is not simply related to the x, y, z position of the conspecific but also to its orientation.

Nevertheless, no matter what the relationship is between the spatio-temporal pattern of activation of the array of receptors and conspecific location, it carries the spatial information necessary for localization. As described above, the feedforward circuit preserves a spatially accurate representation of the sensory image due to its localized receptive field. The ELL network contains a variety of elements that can influence spatial representation, each driven by more or less localized receptive fields (Fig 5). Most notably, two types of feedback inputs are known to influence pyramidal cell responses. While the feedback pathway through bipolar cells of the nP is poorly understood, the inputs from stellate cells are well characterized. It is driven by a receptive field slightly larger than the pyramidal cell it projects to. This feedback has been proposed to function as a "searchlight" (Berman & Maler, 1999) and recent papers by (Clarke et al., 2014; Clarke & Maler, 2017), demonstrated how this feedback enhances the response to moving prey-like stimuli. This mechanism could also play a role in shaping the response to conspecifics in close proximity, but it is unlikely that it will affect responses to more distant individuals since its modus operandi relies on the activation of relatively small receptive fields.

The feedback through nP's stellate cells has also been shown to enhance the response to envelope signals elicited by moving conspecifics (Metzen et al., 2018). The authors of this study showed that the sensitivity of a specific electromotor reaction to the envelope signals of medium to low strength (10-15% contrast) required this input. A 10-15% contrast corresponds to a fish 20-25 cm away (Fotowat et al., 2013) and it is unclear how this feedback affects the processing of signals from more distant individuals. Nevertheless, it would be interesting to determine whether this feedback pathway shapes the spatial representation of conspecific signals, particularly for a conspecific at short to medium distances.

The indirect feedback through the EGp is described in the section above as mediating a cancellation of the response to beats, and thus could also affect the spatial representation of conspecific signals. The precise extent of the receptive field driving this feedback has been shown to be very large and thus is well suited to provide an input that reflects the activation pattern over a large area of the sensory surface. As described in the next section, this type of spatially diffuse input has been shown in other systems to shape spatial processing through background suppression and contrast enhancement, so we suggest it could influence spatial representation in this system too.

Discussion

We have outlined some of the challenges faced by weakly electric fish when trying to detect and locate a conspecific and presented some of the mechanisms involved in spatial processing in this system. We have argued in the introduction that the electrosensory system can compare in some ways with the visual system but in others with the auditory system. We hope that

some of the insight presented along the way has reinforced this statement. For example, we pointed out that topographic mapping from the periphery all the way to the optic tectum that can guide locomotion is a feature shared with the visual system. On the other hand, the auditory system must "compute space" by comparing the signal at the two ears. For conspecific signals that are not in the immediate vicinity, this same process must happen and considering the shared developmental and evolutionary origins we speculate that solutions to this common problem could share some features. To stress further the potential for insight we can obtain from comparing these sensory systems, we point out below a few important mechanisms that the auditory or visual system utilizes to perform challenging tasks and explain how they can relate to the electrosensory system.

Sound localization has been thoroughly studied in a variety of systems but research on the barn owl, with its exquisite accuracy in sound localization, has a particularly rich history of insightful studies (Grothe, 2018). Research by Konishi, Knudsen, Carr and others have unraveled how the interaural time differences (ITD) of sound arrival at each ear, and interaural level differences (i.e., amplitude; ILD) enhanced, combined and how they support localization accuracy of just a few degrees (Carr & Konishi, 1990; Knudsen, 1981; Konishi, 1973). This corresponds to ITDs of a few μs and champions the sensitivity of most vertebrates' auditory systems. Electrolocation of conspecific fish cannot rely on timing differences since the speed of light would not give rise to significant differences. However, the electrosensory signal will cause differences in amplitude similar to the ILD used by the owl auditory system. In this system, localization on the vertical plane (elevation) relies heavily on ILD and sensitivity to these cues first arises in the posterior nucleus of the ventral lateral lemniscus where neurons receive

excitation from one ear and inhibition from the other (Takahashi & Keller, 1992). In mammals, ILD sensitivity contributes to the localization on the horizontal plane (at least for high frequency sounds) and a binaural comparison occurs in the lateral superior olive. There, excitatory inhibitory inputs combine with contralateral inhibitory inputs driven indirectly by globular bushy cells driven by a large number of auditory receptors (Grothe & Pecka, 2014). Contralateral inhibition enhancing binaural contrast is common in auditory systems and can interact with the temporal processing of the signals (Koch & Grothe, 2000) to enhance sound localization specifically for behaviorally relevant signal patterns (Marsat & Pollack, 2005). The neural circuitry to perform a similar operation is present in the ELL of knifefish (Fig 6). The indirect feedback is driven by spatially diffuse inputs and can attenuate the response to conspecific signals particularly relevant in some interactions (i.e., low frequency beats). For a pyramidal cell that is only weakly excited by the conspecific signal because it is not ideally located relative to the conspecific location, the feedback might draw its inputs from a region that is maximally stimulated by the conspecific and thus the beat would be effectively cancelled in these pyramidal cells. For cells strongly excited by the feedforward stimulation from the conspecific, the feedback might not completely cancel the beat response. Although this mechanism is simply a hypothesis and remains to be tested, the elements to implement it seem to be present.

Beyond localizing a single signal, the auditory system might be faced with the “cocktail party problem” where it must attend to one signal among many (Cherry, 1953). The mechanisms allowing the resolution of this issue have also been thoroughly investigated (e.g., Middlebrooks et al., 2017) and still lead to new discoveries regularly (e.g., Popham, Boebinger, Ellis,

Kawahara, & McDermott, 2018). Listening to a communication signal with only one ear in a noisy environment makes extracting the message more difficult than if binaural hearing is used. It is suggested that sound location allows to segregate elements from one stream and top-down feedback inputs allow the enhanced coding of this signal stream (for a review on the topics see Haykin & Chen, 2005). Although most of the mechanisms suggested to contribute to solving the cocktail party problem focused on cortical network, mechanisms present as early as the dorsal cochlear nucleus have been suggested (Pressnitzer, Sayles, Micheyl, & Winter, 2008). It is common to see electric fish locate and chase one another in cluttered environments even when other conspecifics are present (e.g., Henninger fig 2; Henninger et al., 2018). Thus, we argue that they are likely faced with a similar "cocktail party problem". This suggestion naturally leads to the question of how this issue is solved in the electrosensory system. Considering the proposed role of the direct feedback input from nP as a "searchlight" mechanism (i.e., a sort of low-level spatial attention mechanism) we suggest that it could contribute to segregating competing signals by enhancing the response (as in Metzen et al., 2018) to the most salient one.

Mechanisms of scene analysis, such as the ones involved in solving the cocktail party problem, are also central issues in visual processing. In particular, foreground-background separation is required when trying to attend to an object – when fixating a moving object for example. Background suppression is largely influenced by the activity of wide field, polyaxonal amacrine cells. These polyaxonal amacrine cells mediate retinal ganglion cell (RGC) selectivity of an object over the background (Ölveczky et al., 2003). This background suppression mechanism relies on the amacrine cells receiving input from a wide receptive field surround and

suppressing RGC activity (Baccus, Olveczky, Manu, & Meister, 2008). As in the auditory mechanism described above, or the electrosensory mechanisms hypothesized, this visual mechanism enhancing spatial processing relies on inhibition with a different receptive field as its target, emphasizing that this contrast enhancement procedure is a common strategy in scene analysis (see Fig 6).

The remarkable sensitivity of sensory systems has been the focus of a variety of studies in the auditory system (Fettiplace & Hackney, 2006; Hill & Boyan, 1977; Knudsen & Konishi, 1979), visual system (Jacobs et al., 2009), olfactory system (Daly, Carrell, & Mwilaria, 2007) and others. Mechanisms underlying the ability to detect extremely weak prey stimuli have been identified in weakly electric fish and are likely relevant to the detection of similarly weak conspecific signals. One of the mechanisms identified by Jung et al (2016), relies on a finely balanced inhibition and excitation from feedforward inputs. Balanced inhibition and excitation is a staple feature of many neural networks (e.g., cortex; Haider, 2006) and is involved in shaping sensory tuning in various systems (e.g., Anderson, Carandini, & Ferster, 2000). We also described how the presence of ISI correlation in receptors spike train enhances coding accuracy by decreasing variability, a process observed in a variety of neurons (e.g., Farkhooi, Strube-Bloss, & Nawrot, 2009). Several other mechanisms enhance the sensitivity of this system but have not been discussed here (e.g., bursting serving the same function in this system as in others; Krahe & Gabbiani, 2004) for lack of space or because they are less obviously relevant to processing the spatial aspect of conspecific signals.

Finally, it should be noted that behavioral strategies can contribute to the localization process. A good example of this phenomenon is calling song localization in crickets. Females will

approach a song source in zig-zag patterns but the angle of each turn is much greater than the angular resolution of localization in the frontal field (Schöneich & Hedwig, 2010). This suggests that the cricket lateralizes the sound, turns coarsely in that direction and after a few steps re-evaluates whether the sound is still coming from that side or not. This zig-zag behavioral strategy can thus be explained by the reliance on accurate lateralization rather than all around accurate localization. In elephantnose (mormyrid) electric fish, behavioral strategies might also hint at the sensory mechanism in place. An individual moving towards a conspecific will tend to follow electric field lines rather than moving straight towards it (Schluger & Hopkins, 1987). This pattern arises presumably from the fish aiming to balance the strength of the electric field on each side of the body. Various active sampling strategies are also used in different organisms to enhance a sensory signal (Schroeder, Wilson, Radman, Scharfman, & Lakatos, 2010). A well described example is the microsaccades used in the visual system to prevent firing rate adaptation, thereby preventing the fading of visual images representations (Schroeder et al., 2010). Similarly, knifefish use the motions of their body to enhance the localization of nearby objects (Stamper, et al., 2012). Furthermore, Heiligenberg found that tail bending enhances the electric image/shadow that the object of interest casts on the fish's body (Heiligenberg, 1975; see also Sim & Kim, 2011). A variety of object localization and detection mechanisms involving movement have been suggested (Hofmann, Sanguinetti-Scheck, Gómez-Sena, & Engelmann, 2017; Pedraja et al., 2018; Pourziaei, Lewis, Huang, & Lewis, 2019; Sim & Kim, 2011), and should be discussed in a separate dedicated review .

Behavioral tests in knifefish have not yet identified behavioral strategies that are used during conspecific localization specifically (rather than simply object localization) and could be

the topic of future experiments. In particular, it would be useful to test explicitly whether the fish can accurately localize other distant individuals at any azimuth or if they simply rely on a lateralization of the signals.

In conclusion, we would like to reiterate that weakly electric fish accomplish difficult tasks when detecting and localizing conspecifics. Many of these challenges resemble those faced by most modalities but the particularities of the electrosense allows us to probe the generality versus specificity of mechanisms observed across these sensory systems. Researchers studying weakly electric fish are continuing to build on a rich history of contribution to our understanding of behavior and its neural basis. Spatial processing in this system is one of the lines of research that has many unanswered questions and the potential for insightful discoveries.

References

Allen, K. M., & Marsat, G. (2018). Task-specific sensory coding strategies are matched to detection and discrimination performance. *The Journal of Experimental Biology*, *221*(6), jeb170563.

Anderson, J. S., Carandini, M., & Ferster, D. (2000). Orientation Tuning of Input Conductance, Excitation, and Inhibition in Cat Primary Visual Cortex. *Journal of Neurophysiology*, *84*(2), 909–926.

Aragón, P. (2009). Conspecific male chemical cues influence courtship behaviour in the male newt Lissotriton boscai. *Behaviour*, *146*(8), 1137–1151.

Arikawa, K., Wakakuwa, M., Qiu, X. D., Kurasawa, M., & Stavenga, D. G. (2005). Sexual dimorphism of short-wavelength photoreceptors in the small white butterfly, Pieris rapae crucivora. *Journal of Neuroscience*, *25*(25), 5935–5942.

Assad, C., & Bower, J. M. (1997). Electric field maps and boundary element simulations of electrolocation in weakly electric fish. *Engineering and Applied Science*.

Babineau, D., Lewis, J. E., & Longtin, A. (2007). Spatial Acuity and Prey Detection in Weakly Electric Fish. *PLoS Computational Biology*, *3*(3), e38.

Baccus, S. A., Olveczky, B. P., Manu, M., & Meister, M. (2008). A retinal circuit that computes object motion. *The Journal of Neuroscience : The Official Journal of the Society for Neuroscience*, *28*(27), 6807–6817.

Baker, C. V. H., Modrell, M. S., & Gillis, J. A. (2013). The evolution and development of vertebrate lateral line electroreceptors. *Journal of Experimental Biology*, *216*(13), 2515–

Bastian, J. (1986a). Gain control in the electrosensory system: a role for the descending

projections to the electrosensory lateral line lobe. *Journal of Comparative Physiology A*, *158*(4), 505–515.

Bastian, J. (1986b). Gain control in the electrosensory system mediated by descending inputs to the electrosensory lateral line lobe. *The Journal of Neuroscience*, *6*(2), 553–562.

Bastian, J., Chacron, M. J., & Maler, L. (2002). Receptive field organization determines pyramidal cell stimulus-encoding capability and spatial stimulus selectivity. *Journal of Neuroscience*, *22*(11), 4577–4590

Bastian, J., & Heiligenberg, W. (1980). Neural correlates of the jamming avoidance response ofEigenmannia. *Journal of Comparative Physiology A*, *136*(2), 135–152.

Bee, M. A. (2000). Male green frogs lower the pitch of acoustic signals in defense of territories: a possible dishonest signal of size? *Behavioral Ecology*, *11*(2), 169–177.

Behr, O., Knörnschild, M., & Von Helversen, O. (2009). Territorial counter-singing in male sac-winged bats saccopteryx bilineata: Low-frequency songs trigger a stronger response. *Behavioral Ecology and Sociobiology*, *63*(3), 433–442.

Bell, C. C., & Maler, L. (2005). Central neuroanatomy of electrosensory systems in fish. In T. H. Bullock, C. D. Hopkins, A. N. Popper, & R. R. Fay (Eds.), *Electroreception* (Vol. 21, pp. 68–111). New York: Springer.

Benda, J., Longtin, A., & Maler, L. (2006). A synchronization-desynchronization code for natural communication signals. *Neuron*, *52*(2), 347–358.

Bennett, M. V. L. (1971). Electroreception. *Fish Physiology*, *5*, 493–574.

Bennett, M. V. L., Sandri, C., & Akert, K. (1989). Fine structure of the tuberous electroreceptor of the high-frequency electric fish, Sternarchus albifrons (gymnotiformes). *Journal of*

Neurocytology, *18*(2), 265–283.

Berman, N. J., & Maler, L. (1999). Neural architecture of the electrosensory lateral line lobe: adaptations for coincidence detection, a sensory searchlight and frequency-dependent adaptive filtering. *Journal of Experimental Biology*, *202*(10).

Bodznick, D., & Northcutt, R. G. (1981). Electroreception in lampreys: evidence that the earliest vertebrates were electroreceptive. *Science*, *212*(4493), 465–467.

Bol, K., Marsat, G., Harvey-Girard, E., Longtin, A., & Maler, L. (2011). Frequency-Tuned Cerebellar Channels and Burst-Induced LTD Lead to the Cancellation of Redundant Sensory Inputs. *Journal of Neuroscience*, *31*(30), 11028–11038.

Bradbury, J. W., & Vehrencamp, S. L. (2011). *Principles of animal communication* (2nd ed.). Sunderland, Mass., Mass.: Sinauer Associates.

Brand, A., Behrend, O., Marquardt, T., McAlpine, D., & Grothe, B. (2002). Precise inhibition is essential for microsecond interaural time difference coding. *Nature*, *417*(6888), 543–547.

Bullock, T. H., Hopkins, C. D., Popper, A. N., & Fay, R. R. (1986). *Electroreception*. *Eletroreception*.

Byrne, P. G., & Keogh, J. S. (2007). Terrestrial toadlets use chemosignals to recognize conspecifics, locate mates and strategically adjust calling behaviour. *Animal Behaviour*, *74*(5), 1155–1162.

Caputi, A. A., Aguilera, P. A., Carolina Pereira, A., & Rodríguez-Cattáneo, A. (2013). On the haptic nature of the active electric sense of fish. *Brain Research*, *1536*, 27–43.

Caputi, A. A., & Budelli, R. (2006). Peripheral electrosensory imaging by weakly electric fish. *Journal of Comparative Physiology A*, *192*(6), 587–600.

Carlson, B. A., & Kawasaki, M. (2007). Behavioral responses to jamming and "phantom" jamming stimuli in the weakly electric fish Eigenmannia. *Journal of Comparative Physiology A: Neuroethology, Sensory, Neural, and Behavioral Physiology*, *193*(9), 927–941.

Carr, C. E., Maler, L., Heiligenberg, W., & Sas, E. (1981). Laminar organization of the afferent and efferent systems of the torus semicircularis of Gymnotiform fish: Morphological substrates for parallel processing in the electrosensory system. *Journal of Comparative Neurology*, *203*(4), 649–670.

Carr, C. E., Maler, L., & Sas, E. (1982). Peripheral organization and central projections of the electrosensory nerves in gymnotiform fish. *Journal of Comparative Neurology*, *211*(2), 139–153.

Carr, C., & Konishi, M. (1990). A circuit for detection of interaural time differences in the brain stem of the barn owl. *The Journal of Neuroscience*, *10*(10), 3227–3246.

Cäsar, C., Zuberbühler, K., Young, R. J., & Byrne, R. W. (2013). Titi monkey call sequences vary with predator location and type. *Biology Letters*, *9*(5).

Castelló, M. E., Aguilera, P. A., Trujillo-Cenóz, O., & Caputi, A. A. (2016). Electroreception in Gymnotus carapo: pre-receptor processing and the distribution of electroreceptor types. *The Journal of Experimental Biology*, *21*(Pt 21), 3279–3287.

Chacron, M. J., & Bastian, J. (2008). Population coding by electrosensory neurons. *Journal of Neurophysiology*, *99*(4), 1825–1835.

Chacron, M. J., Doiron, B., Maler, L., Longtin, A., & Bastian, J. (2003). Non-classical receptive field mediates switch in a sensory neuron's frequency tuning. *Nature*, *423*(6935), 77–81.

Chacron, M. J., Lindner, B., Maler, L., Longtin, A., & Bastian, J. (2005). Experimental and

theoretical demonstration of noise shaping by interspike interval correlations. *Fluctuations and Noise in Biological, Biophysical, and Biomedical Systems III*, *5841*, 150–163.

Chacron, M. J., Longtin, A., & Maler, L. (2001). Negative Interspike Interval Correlations Increase the Neuronal Capacity for Encoding Time-Dependent Stimuli. *The Journal of Neuroscience*, *21*(14), 5328–5343.

Chacron, M. J., Maler, L., & Bastian, J. (2005). Feedback and feedforward control of frequency tuning to naturalistic stimuli. *Journal of Neuroscience*, *25*(23), 5521–5532.

Chen, L., House, J. L., Krahe, R., & Nelson, M. E. (2005). Modeling signal and background components of electrosensory scenes. *Journal of Comparative Physiology. A*, *191*(4), 331–345.

Cherry, E. C. (1953). Some Experiments on the Recognition of Speech, with One and with Two Ears. *The Journal of the Acoustical Society of America*, *25*(5), 975–979.

Cichy, R. M., & Teng, S. (2017). Resolving the neural dynamics of visual and auditory scene processing in the human brain: A methodological approach. *Philosophical Transactions of the Royal Society B: Biological Sciences*, *372*(1714).

Clarke, S. E., Longtin, A., & Maler, L. (2014). A Neural Code for Looming and Receding Motion Is Distributed over a Population of Electrosensory ON and OFF Contrast Cells. *Journal of Neuroscience*, *34*(16), 5583–5594.

Clarke, S. E., & Maler, L. (2017). Feedback Synthesizes Neural Codes for Motion. *Current Biology*, *27*(9), 1356–1361.

Daly, K. C., Bradley, S., Chapman, P. D., Staudacher, E. M., Tiede, R., & Schachtner, J. (2016). Space Takes Time: Concentration Dependent Output Codes from Primary Olfactory

Networks Rapidly Provide Additional Information at Defined Discrimination Thresholds. *Frontiers in Cellular Neuroscience*, *9*, 515.

Daly, K. C., Carrell, L. A., & Mwilaria, E. (2007). Detection versus perception: physiological and behavioral analysis of olfactory sensitivity in the moth (Manduca sexta). *Behavioral Neuroscience*, *121*(4), 794–807.

de Bruyne, M., & Baker, T. C. (2008). Odor detection in insects: Volatile codes. *Journal of Chemical Ecology*, *34*(7), 882–897.

Doucet, S. M., Mennill, D. J., & Hill, G. E. (2007). The Evolution of Signal Design in Manakin Plumage Ornaments. *The American Naturalist*, *169*(S1), S62–S80.

Duncan, J. S., & Fritzsch, B. (2012). Evolution of sound and balance perception: Innovations that aggregate single hair cells into the ear and transform a gravistatic sensor into the organ of corti. *Anatomical Record*, *295*(11), 1760–1774.

Dunlap, K. D., DiBenedictis, B. T., & Banever, S. R. (2010). Chirping response of weakly electric knife fish (Apteronotus leptorhynchus) to low-frequency electric signals and to heterospecific electric fish. *The Journal of Experimental Biology*.

Engler, G., Fogarty, C. M., Banks, J. R., & Zupanc, G. K. (2000). Spontaneous modulations of the electric organ discharge in the weakly electric fish, Apteronotus leptorhynchus: a biophysical and behavioral analysis. *Journal of Comparative Physiology. A*, *186*(7–8), 645–660.

Engler, G., & Zupanc, G. (2001). Differential production of chirping behavior evoked by electrical stimulation of the weakly electric fish, Apteronotus leptorhynchus. *Journal of Comparative Physiology A*, *187*(9), 747–756.

Farkhooi, F., Strube-Bloss, M. F., & Nawrot, M. P. (2009). Serial correlation in neural spike trains: Experimental evidence, stochastic modeling, and single neuron variability. *Physical Review E - Statistical, Nonlinear, and Soft Matter Physics*, *79*(2), 1–10.

Fettiplace, R., & Hackney, C. M. (2006). The sensory and motor roles of auditory hair cells. *Nature Reviews Neuroscience*, *7*(1), 19–29.

Fotowat, H., Harrison, R. R., & Krahe, R. (2013). Statistics of the Electrosensory Input in the Freely Swimming Weakly Electric Fish Apteronotus leptorhynchus. *Journal of Neuroscience*, *33*(34), 13758–13772.

Gabbiani, F., Metzner, W., Wessel, R., & Koch, C. (1996). From stimulus encoding to feature extraction in weakly electric fish. *Letters to Nature*, *384*, 564–567.

Giassi, A. C. C., Ellis, W., & Maler, L. (2012). Organization of the gymnotiform fish pallium in relation to learning and memory: III. Intrinsic connections. *Journal of Comparative Neurology*, *520*(15), 3369–3394.

Gómez-Sena, L., Pedraja, F., Sanguinetti-Scheck, J. I., & Budelli, R. (2014, April 1). Computational modeling of electric imaging in weakly electric fish: Insights for physiology, behavior and evolution. *Journal of Physiology Paris*. Elsevier.

Grosof, D. H., Shapley, R. M., & Hawken, M. J. (1993). Macaque V1 neurons can signal "illusory" contours. *Nature*, *365*(6446), 550–552.

Grothe, B. (2018). How the Barn Owl Computes Auditory Space. *Trends in Neurosciences*, *41*(3), 115–117.

Grothe, B., & Pecka, M. (2014). The natural history of sound localization in mammals--a story of neuronal inhibition. *Frontiers in Neural Circuits*, *8*, 116.

Guilford, T., & Dawkins, M. S. (1993). Receiver Psychology and the Design of Animal Signals. *Trends in Neurosciences*, *16*(11), 430–436.

Haider, B. (2006). Neocortical Network Activity In Vivo Is Generated through a Dynamic Balance of Excitation and Inhibition. *Journal of Neuroscience*, *26*(17), 4535–4545.

Hartmann, M. J., & Bower, J. M. (2001). Tactile responses in the granule cell layer of cerebellar folium crus IIa of freely behaving rats. *The Journal of Neuroscience*, *21*(10), 3549–3563.

Harvey-Girard, E., Lewis, J., & Maler, L. (2010). Burst-induced anti-hebbian depression acts through short-term synaptic dynamics to cancel redundant sensory signals. *Journal of Neuroscience*, *30*(17), 6152–6169.

Haykin, S., & Chen, Z. (2005). *The Cocktail Party Problem*. *Neural computation* (Vol. 17).

Heiligenberg, W. (1975). Theoretical and experimental approaches to spatial aspects of electrolocation. *Journal of Comparative Physiology A*, *103*(3), 247–272.

Heiligenberg, W. (1991). Sensory control of behavior in electric fish. *Current Opinion in Neurobiology*, *1*(4), 633–637.

Heiligenberg, W., & Dye, J. (1982). Labeling of electroreceptive afferents in a Gymnotoid fish by intracellular injection of HRP - the mystery of multiple maps. *Journal of Comparative Physiology. A*, *148*(3), 287–296.

Henninger, J., Krahe, R., Kirschbaum, F., Grewe, J., & Benda, J. (2018). Statistics of natural communication signals observed in the wild identify important yet neglected stimulus regimes in weakly electric fish. *The Journal of Neuroscience*.

Hill, K. G., & Boyan, G. S. (1977). Sensitivity to frequency and direction of sound in the auditory system of crickets (Gryllidae). *Journal of Comparative Physiology*, *121*(1), 79–97.

Hofmann, V., Sanguinetti-Scheck, J. I., Gómez-Sena, L., & Engelmann, J. (2017). Sensory Flow as a Basis for a Novel Distance Cue in Freely Behaving Electric Fish. *The Journal of Neuroscience*, *37*(2), 302–312.

Hopkins, C. D. (1976). Stimulus filtering and electroreception: Tuberous electroreceptors in three species of Gymnotoid fish. *Journal of Comparative Physiology A*, *111*(2), 171–207.

Huang, C. G., Metzen, M. G., & Chacron, M. J. (2018). Feedback optimizes neural coding and perception of natural stimuli. *ELife*, *7*(514), 398–7493.

Hupé, G. J., Lewis, J. E., & Benda, J. (2008). The effect of difference frequency on electrocommunication: Chirp production and encoding in a species of weakly electric fish, Apteronotus leptorhynchus. *Journal of Physiology Paris*, *102*(4–6), 164–172.

Jacobs, A. L., Fridman, G., Douglas, R. M., Alam, N. M., Latham, P. E., Prusky, G. T., & Nirenberg, S. (2009). Ruling out and ruling in neural codes. *Proceedings of the National Academy of Sciences of the United States of America*, *106*(14), 5936–5941.

Jeffress, L. A. (1948). A place theory of sound localization. *Journal of Comparative and Physiological Psychology*. US: American Psychological Association.

Jung, S. N., Longtin, A., & Maler, L. (2016). Weak signal amplification and detection by higher-order sensory neurons. *Journal of Neurophysiology*, *115*(4), 2158–2175.

Kelly, M., Babineau, D., Longtin, A., & Lewis, J. E. (2008). Electric field interactions in pairs of electric fish: Modeling and mimicking naturalistic inputs. *Biological Cybernetics*.

Keyser, A. J., & Hill, G. E. (2000). Structurally based plumage coloration is an honest signal of quality in male blue grosbeaks. *Behavioral Ecology*, *11*(2), 202–209.

Knudsen, E. (1974). Behavioral thresholds to electric signals in high frequency electric fish.

Journal of Comparative Physiology, *91*(4), 333–353.

Knudsen, E. I. (1975). Spatial aspects of the electric fields generated by weakly electric fish. *Journal of Comparative Physiology A*, *99*(2), 103–118.

Knudsen, E. I. (1981). The Hearing of the Barn Owl. *Scientific American*, *245*(6), 112–125.

Knudsen, E. I., & Konishi, M. (1979). Mechanisms of sound localization in the barn owl (Tyto alba). *Journal of Comparative Physiology A*, *133*(1), 13–21.

Koch, U., & Grothe, B. (2000). Interdependence of spatial and temporal coding in the auditory midbrain. *Journal of Neurophysiology*, *83*(4), 2300–2314.

Kolodziejski, J. a, Sanford, S. E., & Smith, G. T. (2007). Stimulus frequency differentially affects chirping in two species of weakly electric fish: implications for the evolution of signal structure and function. *The Journal of Experimental Biology*, *210*(Pt 14), 2501–2509.

Konishi, M. (1973). How the Owl Tracks Its Prey: Experiments with trained barn owls reveal how their acute sense of hearing enables them to catch prey in the dark. *American Scientist*, *61*(4), 414–424.

Konishi, M. (1985). Birdsong: From Behavior to Neuron. *Annual Review of Neuroscience*, *8*(1), 125–170.

Krahe, R., Bastian, J., & Chacron, M. J. (2008). Temporal processing across multiple topographic maps in the electrosensory system. *Journal of Neurophysiology*, *100*(2), 852–867.

Krahe, R., & Gabbiani, F. (2004). Burst firing in sensory systems. *Nature Reviews Neuroscience*, *5*(1), 13–23.

Krahe, R., & Maler, L. (2014). Neural maps in the electrosensory system of weakly electric fish. *Current Opinion in Neurobiology*, *24*, 13–21.

Kramer, B. (1996). *Electroreception and communication in fishes*. *Progress in Zoology* (Vol. 42). Gustav Fischer.

Krekelberg, B., Kubischik, M., Hoffmann, K., & Bremmer, F. (2003). Neural correlates of visual localization and perisaccadic mislocalization, *37*, 537–545.

Lannoo, M. J., Maler, L., & Tinner, B. (1989). Ganglion cell arrangement and axonal trajectories in the anterior lateral line nerve of the weakly electric fish Apteronotus leptorhynchus (Gymnotiformes). *Journal of Comparative Neurology*, *280*(3), 331–342.

Liberman, A. M., Harris, K. S., Hoffman, H. S., & Griffith, B. C. (1957). The Discrimination of Speech Sounds within and across Phoneme Boundaries. *Journal of Experimental Psychology*, *54*(5), 358–368.

Lissmann, H. W. (1958). on the Function and Evolution of Electric Organs in Fish. *Journal of Experimental Biology*, *35*(1), 156-.

Lissmann, H. W. (1963). Electric Location by Fishes. *Scientific American*, *208*(3), 50–59.

Lohr, B., Wright, T. F., & Dooling, R. J. (2003). Detection and discrimination of natural calls in masking noise by birds: estimating the active space of a signal. *ANIMAL BEHAVIOUR*, *65*, 763–777.

Lohuis, T. D., & Fuzessery, Z. M. (2000). Neuronal sensitivity to interaural time differences in the sound envelope in the auditory cortex of the pallid bat. *Hearing Research*, *143*(1–2), 43–57.

Maler, L. (2009). Receptive field organization across multiple electrosensory maps. I. Columnar organization and estimation of receptive field size. *Journal of Comparative Neurology*, *516*(5), 376–393.

Maler, L. (2009). Receptive field organization across multiple electrosensory maps. II. Computational analysis of the effects of receptive field size on prey localization. *Journal of Comparative Neurology*, *516*(5), 394–422.

Maler, L., Sas, E. K. B., & Rogers, J. (1981). The cytology of the posterior lateral line lobe of high-frequency weakly electric fish (gymnotidae): Dendritic differentiation and synaptic specificity in a simple cortex. *The Journal of Comparative Neurology*, *195*(1), 87–139.

Marsat, G., Longtin, A., & Maler, L. (2012). Cellular and circuit properties supporting different sensory coding strategies in electric fish and other systems. *Current Opinion in Neurobiology*, *22*(4), 686–692.

Marsat, G., & Maler, L. (2010). Neural heterogeneity and efficient population codes for communication signals. *Journal of Neurophysiology*, *104*(5), 2543–2555.

Marsat, G., & Pollack, G. S. (2005). Effect of the temporal pattern of contralateral inhibition on sound localization cues. *Journal of Neuroscience*, *25*(26), 6137–6144.

Marsat, G., Proville, R. D., & Maler, L. (2009). Transient signals trigger synchronous bursts in an identified population of neurons. *Journal of Neurophysiology*, *102*(2), 714–723.

Mathis, A. (1990). Territorial salamanders assess sexual and competitive information using chemical signals. *Animal Behaviour*, *40*(5), 953–962.

McGregor, P. K. (1993). Signalling in territorial systems: a context for individual identification, ranging and eavesdropping. *Philosophical Transactions - Royal Society of London, B*, *340*(1292), 237–244.

Metzen, M. G., & Chacron, M. J. (2014). Weakly electric fish display behavioral responses to envelopes naturally occurring during movement: implications for neural processing. *J. Exp.*

Biol., *217*(Pt 8), 1381–1391.

Metzen, M. G., Huang, C. G., & Chacron, M. J. (2018). Descending pathways generate perception of and neural responses to weak sensory input. *PLOS Biology*, *16*(6), e2005239.

Metzner, W. (1999). Neural circuitry for communication and jamming avoidance in gymnotiform electric fish. *The Journal of Experimental Biology*, *202*(Pt 10), 1365–1375.

Metzner, W., & Juranek, J. (1997). A sensory brain map for each behavior? *Proceedings of the National Academy of Sciences*, *94*(26).

Middleton, J. W., Longtin, A., Benda, J., & Maler, L. (2006). The cellular basis for parallel neural transmission of a high-frequency stimulus and its low-frequency envelope. *Proceedings of the National Academy of Sciences of the United States of America*, *103*(39), 14596–14601.

Modrell, M. S., Bemis, W. E., Northcutt, R. G., Davis, M. C., & Baker, C. V. H. (2011). Electrosensory ampullary organs are derived from lateral line placodes in bony fishes. *Nature Communications*, *2*(1), 3142–3146.

Nelson, M. E., & MacIver, M. A. (1999). Prey capture in the weakly electric fish Apteronotus albifrons: Sensory acquisition strategies and electrosensory consequences. *The Journal of Experimental Biology*, *202*(10), 1195–1203.

Nelson, M. E., MacIver, M. A., & Coombs, S. (2002). Modeling Electrosensory and Mechanosensory Images during the Predatory Behavior of Weakly Electric Fish. *Brain, Behavior and Evolution*, *59*(4), 199–210.

Nelson, M. E., Xu, Z., & Payne, J. R. (1997). Characterization and modeling of P-type electrosensory afferent responses to amplitude modulations in a wave-type electric fish. *Journal of Comparative Physiology A*, *181*(5), 532–544.

Nesse, W. H., Marsat, G., Longtin, A., & Maler, L. (2012). Detection of weak sensory signals by molecular dynamic transformations of interspike interval sequence. In *Cosyne* (p. III-73). Salt Lake City.

Okada, J., & Toh, Y. (2006). Active tactile sensing for localization of objects by the cockroach antenna. *Journal of Comparative Physiology A: Neuroethology, Sensory, Neural, and Behavioral Physiology*, *192*(7), 715–726.

Ölveczky, B. P., Baccus, S. A., & Meister, M. (2003). Segregation of object and background motion in the retina. *Nature*, *423*(6938), 401–408.

Pedraja, F., Hofmann, V., Lucas, K. M., Young, C., Engelmann, J., & Lewis, J. E. (2018). Motion parallax in electric sensing. *Proceedings of the National Academy of Sciences*, *115*(3), 573–577.

Pedraja, F., Perrone, R., Silva, A., & Budelli, R. (2016). Passive and active electroreception during agonistic encounters in the weakly electric fish Gymnotus omarorum. *Bioinspiration and Biomimetics*, *11*(6), 065002.

Petzold, J. M. J. M., Marsat, G., & Smith, G. T. T. (2016). Co-adaptation of electric organ discharges and chirps in South American ghost knifefishes (Apteronotidae), *110*(3).

Popham, S., Boebinger, D., Ellis, D. P. W., Kawahara, H., & McDermott, J. H. (2018). Inharmonic speech reveals the role of harmonicity in the cocktail party problem. *Nature Communications*, *9*(1).

Postlethwaite, C. M., Psemeneki, T. M., Selimkhanov, J., Silber, M., & MacIver, M. A. (2009). Optimal movement in the prey strikes of weakly electric fish: A case study of the interplay of body plan and movement capability. *Journal of the Royal Society Interface*, *6*(34), 417–

433.

Pourziaei, B., Lewis, G. M., Huang, H., & Lewis, J. E. (2019). Spatiotemporal model for depth perception in electric sensing. *Journal of Theoretical Biology*, *461*, 157–169.

Pressnitzer, D., Sayles, M., Micheyl, C., & Winter, I. M. (2008). Perceptual Organization of Sound Begins in the Auditory Periphery. *Current Biology*, *18*(15), 1124–1128.

Rasnow, B. (1996). The effects of simple objects on the electric field of Apteronotus. *Journal of Comparative Physiology A*, *178*(3), 397–411.

Rasnow, B., Assad, C., & Bower, J. M. (1993). Phase and amplitude maps of the electric organ discharge of the weakly electric fish, Apteronotus leptorhynchus. *Journal of Comparative Physiology A*, *172*(4), 481–491.

Ratnam, R., & Nelson, M. E. (2000). Nonrenewal statistics of electrosensory afferent spike trains: implications for the detection of weak sensory signals. *The Journal of Neuroscience : The Official Journal of the Society for Neuroscience*, *20*(17), 6672–6683.

Reid, J. M., Arcese, P., Cassidy, A. L. E. V., Hiebert, S. M., Smith, J. N. M., Stoddard, P. K., … Keller, L. F. (2005). Fitness Correlates of Song Repertoire Size in Free-Living Song Sparrows (Melospiza melodia). *The American Naturalist*, *165*(3), 299–310.

Saunders, J., & Bastian, J. (1984). The physiology and morphology of 2 types of electrosensory neurons in the weakly electric fish Apteronotus leptorhynchus. *Journal of Comparative Physiology*, *154*(2), 199–209.

Savard, M., Krahe, R., & Chacron, M. J. (2011). Neural heterogeneities influence envelope and temporal coding at the sensory periphery. *Neuroscience*, *172*, 270–284.

Schluger, J. H., & Hopkins, C. D. (1987). Electric fish approach stationary signal sources by

following electric current lines. *The Journal of Experimental Biology*, *130(12*), 359–367.

Schöneich, S., & Hedwig, B. (2010). Hyperacute directional hearing and phonotactic steering in the cricket (Gryllus bimaculatus deGeer). *PLoS ONE*, *5*(12).

Schroeder, C. E., Wilson, D. A., Radman, T., Scharfman, H., & Lakatos, P. (2010). Dynamics of Active Sensing and perceptual selection. *Current Opinion in Neurobiology*, *20*(2), 172–176.

Shumway, C. A. (1989). Multiple electrosensory maps in the medulla of weakly electric gymnotiform fish. I. Physiological differences. *The Journal of Neuroscience : The Official Journal of the Society for Neuroscience*, *9*(12), 4388–4399.

Sicardi, E. A., Caputi, A. A., & Budelli, R. (2000). Physical basis of distance discrimination in weakly electric fish. *Physica A: Statistical Mechanics and Its Applications*, *283*(1), 86–93.

Sim, M., & Kim, D. (2011). Electrolocation based on tail-bending movements in weakly electric fish. *Journal of Experimental Biology*, *214*(14), 2443–2450.

Smith, Z. M., Delgutte, B., & Oxenham, A. J. (2002). Chimaeric sounds reveal dichotomies in auditory perception. *Nature*, *416*(6876), 87–90.

Snippe, H. P., & Koenderink, J. J. (1992). Discrimination thresholds for channel-coded systems. *Biological Cybernetics*, *66*(6), 543–551.

Stamper, S. A., Fortune, E. S., & Chacron, M. J. (2013). Perception and coding of envelopes in weakly electric fishes. *Journal of Experimental Biology*, *216*(13).

Stamper, S. A., Madhav, M. S., Cowan, N. J., & Fortune, E. S. (2012). Beyond the Jamming Avoidance Response: weakly electric fish respond to the envelope of social electrosensory signals. *Journal of Experimental Biology*, *215*(23), 4196–4207.

Stamper, S. A., Roth, E., Cowan, N. J., & Fortune, E. S. (2012). Active sensing via movement

shapes spatiotemporal patterns of sensory feedback. *Journal of Experimental Biology*, *215*(9), 1567–1574.

Szabo, T. (1974). Anatomy of the Specialized Lateral Line Organs of Electroreception BT - Electroreceptors and Other Specialized Receptors in Lower Vertrebrates. In T. H. Bullock, A. Fessard, P. H. Hartline, A. J. Kalmijn, P. Laurent, R. W. Murray, … A. Fessard (Eds.) (pp. 13–58). Berlin, Heidelberg: Springer Berlin Heidelberg.

Takahashi, T., & Keller, C. (1992). Commissural connections mediate inhibition for the computation of interaural level difference in the barn owl. *Journal of Comparative Physiology A*, *170*(2), 161–169.

Thomas, R. A., Metzen, M. G., & Chacron, M. J. (2018). Weakly electric fish distinguish between envelope stimuli arising from different behavioral contexts. *The Journal of Experimental Biology*, *221*(15), jeb178244.

Von Der Emde, G., Schwarz, S., Gomez, L., Budelli, R., & Grant, K. (1998). Electric fish measure distance in the dark. *Nature*, *395*(6705), 890–894.

Vonderschen, K., & Chacron, M. J. (2011). Sparse and dense coding of natural stimuli by distinct midbrain neuron subpopulations in weakly electric fish. *Journal of Neurophysiology*, *106*(6), 3102–3118.

Walz, H., Grewe, J., & Benda, J. (2014). Static frequency tuning properties account for changes in neural synchrony evoked by transient communication signals. *Journal of Neurophysiology*, *112*(May), 752–765.

Yu, N., Hupé, G., Garfinkle, C., Lewis, J. E., Longtin, A., & Fortune, E. (2012). Coding Conspecific Identity and Motion in the Electric Sense. *PLoS Computational Biology*, *8*(7), e1002564.

Zakon, H., Oestreich, J., Tallarovic, S., & Triefenbach, F. (2002). EOD modulations of brown ghost electric fish: JARs, chirps, rises, and dips. *Journal of Physiology, Paris*, *96*(5–6), 451–458.

Zupanc, G. K. H., & Horschke, I. (1997). Neurons of the posterior subdivision of the nucleus preopticus periventricularis project to the preglomemlar nucleus in the weakly electric fish, Apteronotus leptorhynchus. *Brain Research*, *774*(1–2), 106–115.

Zupanc, G. K. H., Sîrbulescu, R. F., Nichols, A., & Ilies, I. (2006). Electric interactions through chirping behavior in the weakly electric fish, Apteronotus leptorhynchus. *Journal of Comparative Physiology A*, *192*(2), 159–173.

Figures and Legends

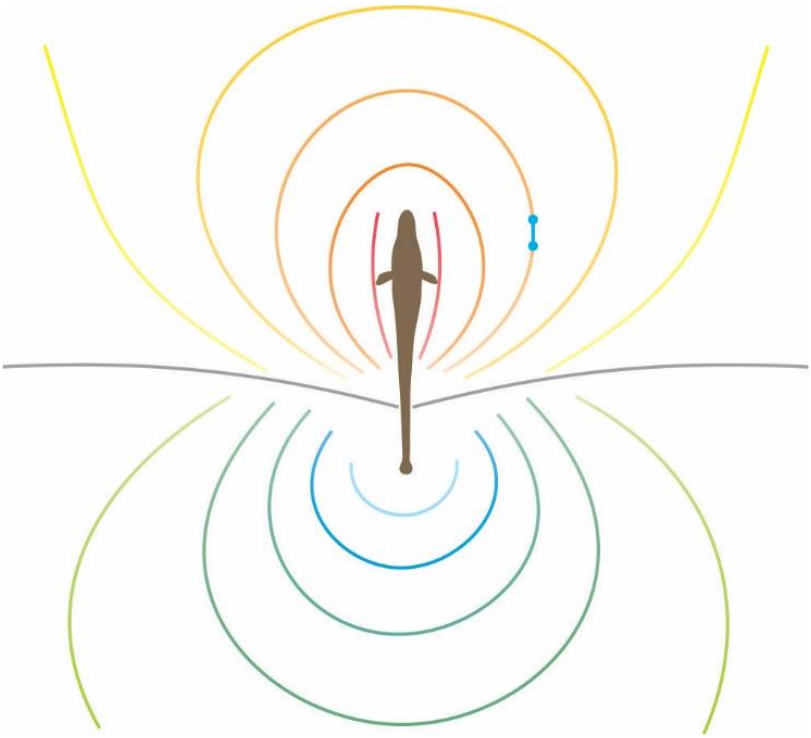

Figure 1. Spatial structure of an Apteronotus leptorhynchus' weakly electric field. Illustration of an *Apteronotus leptorhynchus*, brown ghost knifefish, (center) surrounded by its electric field. Multicolored isopotential lines project outward from the fish. A small receiving dipole (blue) is shown measuring along an isopotential line (orange). The electric field potential is highest close to the fish and decreases as a function of distance. The gray line depicts the zero-potential plane of the fish's electric field.

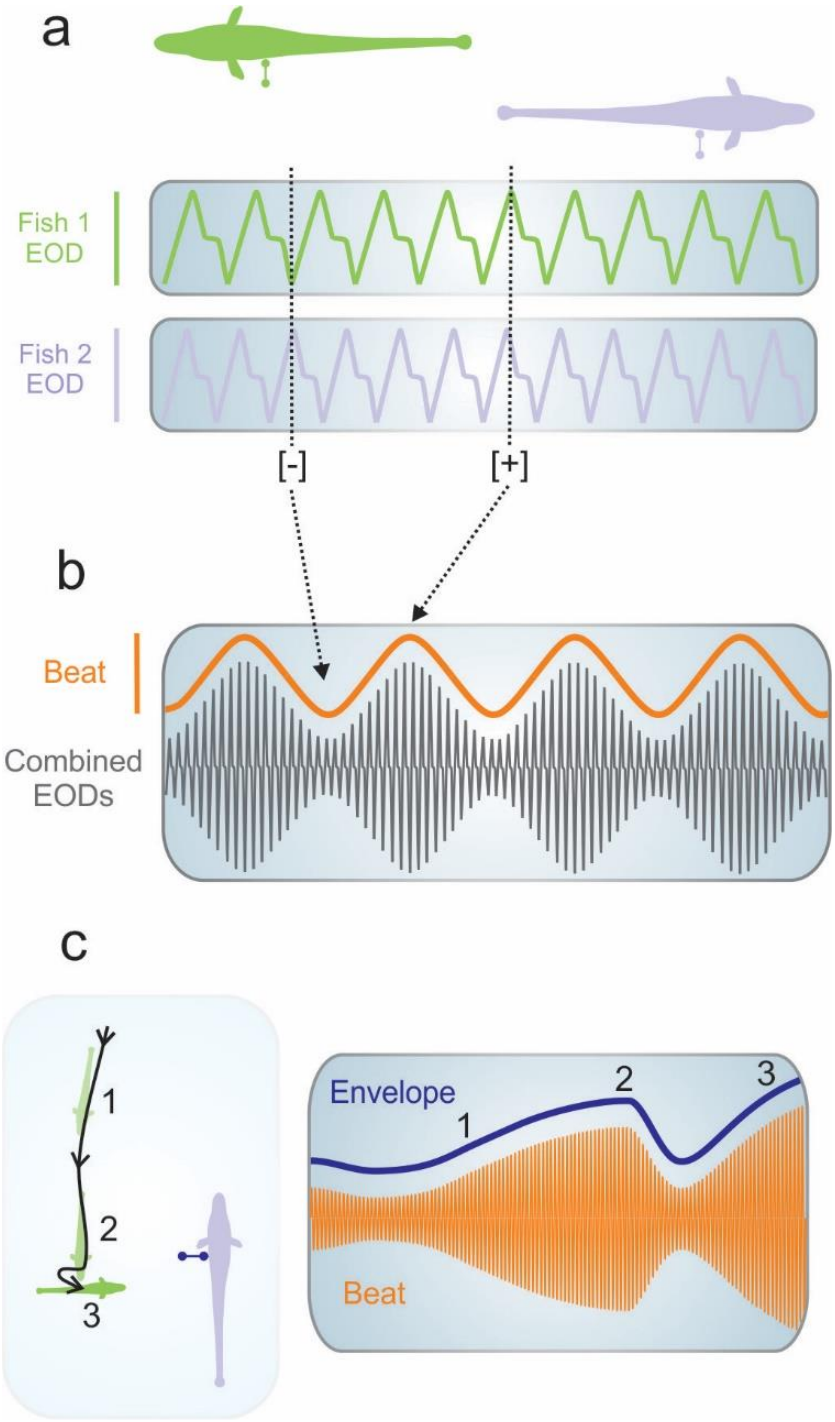

Figure 2. Conspecific signals and the influence of spatial interaction.

(a). Two separate, individual fish are depicted with receiving dipoles (green and purple) measuring their respective EODs. EODs are shown as continuous quasi-sinusoidal waveforms that differ slightly in frequency. Differences in frequency cause changes in phase, as depicted by the dotted black lines. Interactions of EOD waveform peaks and troughs create suppressions and additions in amplitude and are represented by [-] and [+], respectively.

(b). A depiction of the combined EODs of two static fish. Constructive and destructive interferences created by EOD phase differences result in the formation of a “beat” (orange).

Arrows point to examples of decreases and increases of beat strength caused by EOD interactions.

(c). Amplitude modulations of the beat (beat of the beat) result in the formation of an "envelope". Receiving dipole recordings (blue) from a stationary, receiver fish (purple) shows how the envelope strength changes as a function of distance as well as orientation. (1) A distant, sender fish will produce a weaker envelope that increases in strength as the sender fish approaches. (2) Envelope strength greatly increases when the two fish are in close proximity but quickly decreases as the zero potential plane of the sender fish crosses over the receiving dipole. (3) The strength of the envelope is affected not only by distance but also by orientation, with an optimal orientation resulting in greater envelope strength.

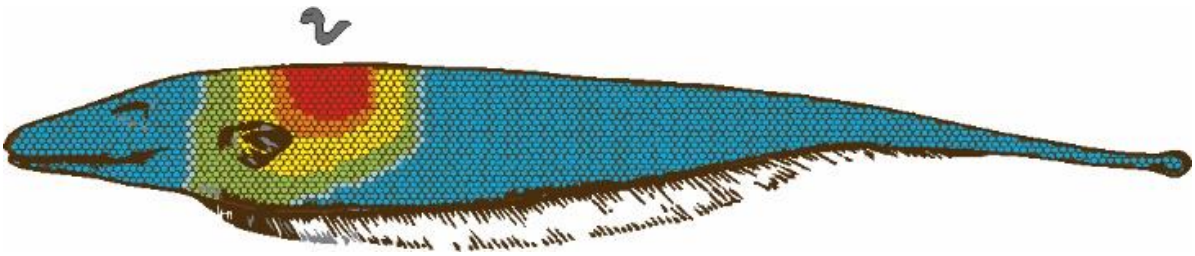

Figure 3. Local activation of the receptor array enables spatial localization of prey.

A representation of the tuberous electroreceptor array on an *Apteronotus leptorhynchus*. Local electrokinetic signals from a small prey item create a gradient of activation along the sensory surface of the body. Warmer and cooler colors depict a higher and lower amount of receptor activation, respectively. This pattern of receptor activity provides sensory information for spatially localizing prey.

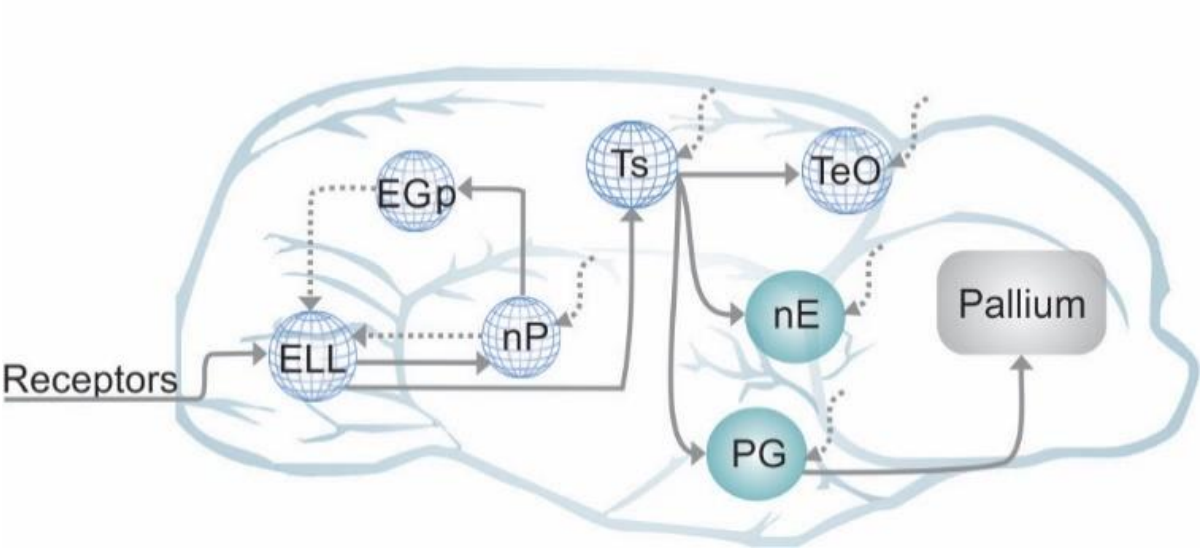

Figure 4. Electrosensory pathway and topographically mapped brain regions.

A depiction of an *Apteronotus leptorhynchus* brain with labeled brain regions and their respective connections. Electroreceptor afferents provide sensory input to the electrosensory lateral line lobe (ELL). The ELL is topographically mapped (globe symbol) and influenced by indirect feedback from the caudal lobe of the cerebellum (EGp) and by direct feedback from the nucleus praeminentialis (nP). Sensory information from the hindbrain ELL projects to the midbrain torus (Ts). Connections from the Ts project further to the optic tectum (TeO), the nucleus electrosensorius (nE), and the preglomerular nucleus (PG). A topographic organization is conserved to brain regions as far as TeO but is lost in the forebrain dorsal telencephalon (pallium). Dashed arrows represent brain areas additionally influenced by the pallium, though connections and interactions with the pallium have been less studied.

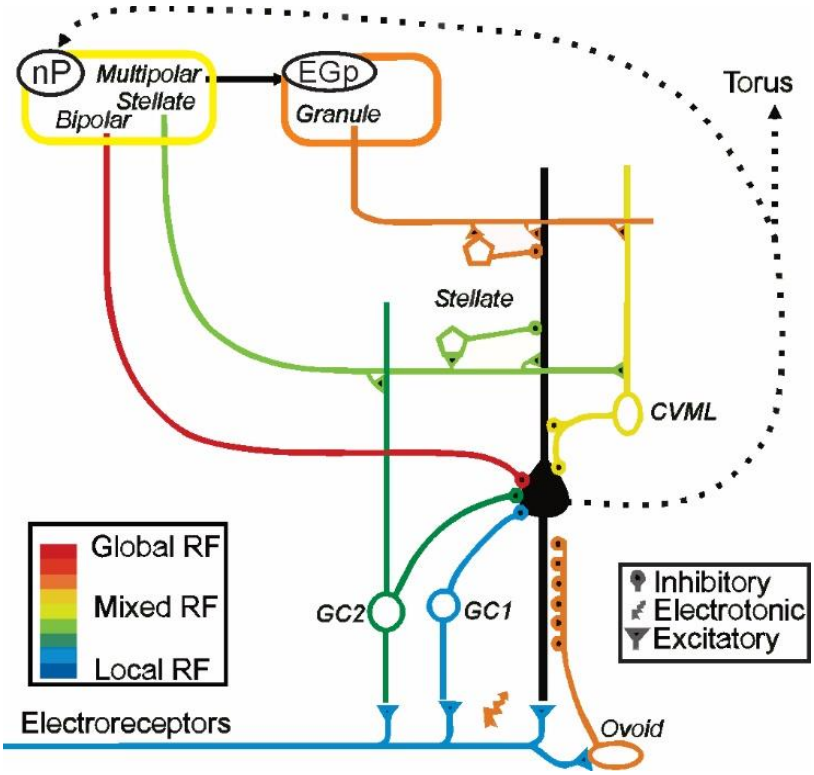

Figure 5. Circuitry of the ELL and immediate projections. A simplified schematic of the electrosensory lateral line lobe (ELL) focusing on a particularly relevant set of connections with pyramidal cells is depicted. The progressive, cool to warm color scheme shows the size of receptive fields for a given cell type. More local receptive fields are depicted by cooler colors (blue and green), global receptive fields are shown in warmer colors (red and orange), and mixed receptive fields are shown with an intermediate color scheme (yellow), as described within the lower left box of the figure. Each electroreceptor provides sensory input to the ELL. Within the ELL, initial input is received by granule cells (GC1 and GC2), ovoid cells, and pyramidal cells (black hub). Pyramidal cells are the sole output neurons of the ELL, sending sensory information to the midbrain Torus semicircularis. A major source of input to ELL pyramidal cells comes from feedback pathways through the nucleus praeminentialis (nP) and the caudal lobe of the cerebellum (EGp). Stellate cells of the nP regulate the local direct feedback pathway (green) and form the basis of the "sensory searchlight" hypothesis. Bipolar cells of the nP provide global direct feedback, however the role of bipolar cells and global direct feedback has not been extensively studied. An indirect feedback pathway from the nP travels through the EGp and influences pyramidal

cell activity. This schematic is not a comprehensive diagram of ELL connections, as other less obviously relevant pathways are not shown for the purpose of clarity.

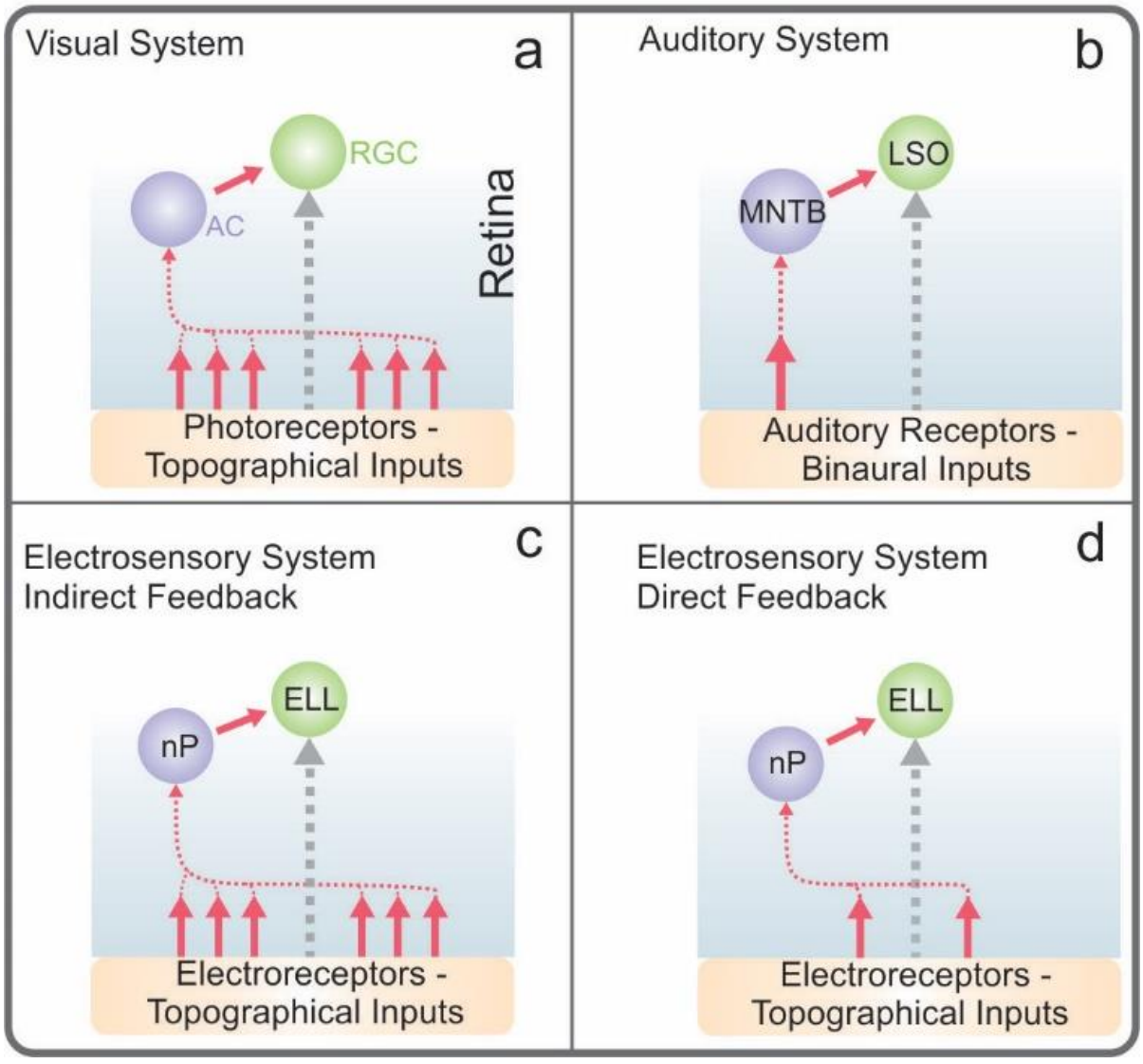

Figure 6. Shared network elements and potential feedback / lateral inputs contributing to localization and spatial processing.

In the visual system **(a)**, photoreceptors convey topographically organized visual input to retinal ganglion cells (RGCs) through additional layers of retinal circuitry. Most notably, amacrine cells (AC) influence RGC output and contribute to mechanisms such as background-suppression. A simplified depiction of sound localization in the mammalian auditory system is shown in panel **(b)**. Binaural input from the ipsilateral side is sent to the lateral superior olive (LSO), while sensory input from the contralateral side is sent to the LSO by way of the medial nucleus of the

trapezoid body (MNTB). Direct excitatory input to the LSO and indirect inhibitory input illustrate an early mechanism of spatial processing in the auditory system**.** Panels **(c)** and **(d)** show how electroreceptors provide topographical input to the ELL through a feedforward pathway, while the nucleus praeminentialis (nP) provides two forms of feedback input onto the ELL, an indirect feedback **(c)** and a direct feedback **(d)**. Compared to the visual and auditory systems described above, different modes of feedback in the electrosensory system house shared network elements and are potentially involved in localization and spatial processing. In all panels, we color the pathway leading to feedback inputs or lateral inputs in red and the direct feedforward pathway in gray. Note that these diagrams are intended as simplified flow-charts.

Chapter 1: Introduction – Part 2

Prologue

I continue the introduction of my dissertation with a primer that focuses specifically on neural coding of weak signals across biological sensory systems. In the first part of Chapter 1, we provided support that weakly electric fish excel at encoding signals emitted by other weakly electric fish, even when conditions are unfavorable. However, it is unclear whether the mechanisms used by the electrosensory system are generalizable to other modalities. In this second part of Chapter 1, I expand on how different sensory systems operate to encode weak signals. In particular, I provide an encyclopedic-style discussion on the behavioral and neural mechanisms of weak signal coding. Importantly, this sensory challenge is one that nearly all organisms must face and requires that nervous systems adjust, in several ways, their typical coding strategies. Whether it be navigating the environment, finding food, or even escaping a potentially lethal situation, the survival of an organism can heavily depend on the sensitivity of the nervous system to encode weak signals reliably.

Taking a comparative perspective, I provide a general overview of the early sensory pathways across modalities including the visual, auditory, olfactory, somatosensory, and electrosensory systems. In particular, I discuss three aspects of the nervous system (receptive field structure, adaptation, and feedback), that share similarities between modalities and contribute to modulating the sensitivity for weak signal coding. Using a neuroethological approach, I base this discussion on observable behaviors and delineate how the nervous system supports each behavior.

Abstract

A central goal in neuroscience is to understand how sensory systems can efficiently and sensitively encode natural, ethologically-relevant stimuli while suppressing noise and redundant sensory input. Experimental and theoretical research, in all modalities, seeks to establish core principles by which these processes take place and provide a broader understanding of how these principles generalize across sensory modalities. Although extensive progress has been made over the last few decades, much less is known about the cellular and network strategies used by the nervous system to encode weak sensory signals particularly. In this focused primer, I delineate a selection of key physiological mechanisms and neural response properties that allow the nervous system to flexibly adapt its selectivity and enhance its sensitivity to increase the sensory limits.

I begin by providing a brief overview on neural dynamics and the functional organization principles of sensory systems that are relevant to the coding of weak signals. Afterwards, I describe several neural strategies for encoding weak signals across sensory modalities, focusing on three key mechanisms: feedback, receptive field interactions, and adaptation via short-term synaptic plasticity. In addition, I provide examples of behavioral strategies that may optimize weak signal coding. Lastly, I present an integrated perspective, describing how a combination of the mechanisms discussed may function together to accomplish this challenging task.

Introduction

For most neurons, the spiking response is the fundamental unit of information transmission in the nervous system and there are entire fields of research dedicated to quantifying how neurons can encode, transform, and convey information through patterns of action potentials (Rieke et al., 1999; Bullock et al., 2005). Information can be encoded in the mean firing rate (i.e., how many action potentials occur within a certain window of time), in precise temporal patterns of action potentials within a spike train, and from the timing of one neuron's spiking activity relative to others in a population (Rieke et al., 1999).

Research on neural coding principles led to the development and proposal of constraining theories based on computationally and biophysically efficient properties of biological systems. This concept was most notably formulated by Horace Barlow in his proposed "Efficient Coding Hypothesis", stating that evolutionary pressures have driven nervous systems to encode sensory stimuli with as few action potentials as possible to limit computational load and increase metabolic efficiency (Barlow, 1961). Experimental support for this notion has been documented throughout different stages of the nervous system, but is most evident at higher levels of processing where the spiking activity of neurons is generally more sparse (Koch and Laurent, 1999; Lewicki, 2002; Denève and Machens, 2016). A key challenge in this respect is to reduce redundancy to improve efficiency while at the same time preserving and maximizing sensitivity. This discussion will focus on how this is achieved and the way the nervous system is organized enables these mechanisms to be implemented.

The organization of sensory systems has a hierarchical structure where a stimulus is first received by receptors at the periphery and its information must be conveyed throughout

different functional regions and layers of the central nervous system (Liang et al., 2012; Lyons-Warren et al., 2012). One structural organizing principle that determines how the stimulus is encoded is the use of a "labeled line" code where the identity of the neurons responding to a given stimulus feature specifies the information being represented. The clearest example of this principle is a topographic representation of space that is mapped in the early pathways and often preserved throughout higher level brain regions. In a topographic map, the peripheral spatial region where a neuron responds preferentially to a given stimulus is defined as the neuron's receptive field. Therefore, the activation of a neuron's receptive field at the periphery provides information about a signal's spatial structure (Peterson et al., 2001; Seriès et al., 2004). A neuron's response strength will depend on the signal's content (e.g., its temporal properties) and its location (Zhang and Sejnowski, 1999). Thus, by having multiple neurons with receptive fields that differ in their structure and spatial extent encoding different aspects of the stimulus, each neuron can encode a portion of the stimulus better and reduce redundancy across the population.

Organization principles are not the only aspects of the nervous system that influence the efficiency of neural coding and the dynamics of the spiking response has a key influence on the coding scheme. In particular, a neuron's spiking history at pre-synaptic and post-synaptic sites can largely influence a neuron's spiking state, and its capacity to encode information in a context-dependent manner (Dayan and Abbott, 2001). There is now strong experimental and theoretical support for the role of active dendrites and synaptic sites in shaping the representation of sensory inputs. Combining the fact that synapses are plastic with the vast number of synaptic sites and highly intricate connectivity patterns of neurons within a network

lead to a flexibility that allows the system to fine tune to the properties of the signals it must encode. One specific example has been reported in weakly electric fish, where mechanisms of fast short-term depression (FSTD) operate to decrease the variability of the rate of synaptic output, thereby reducing noise (Khanbabaie et al., 2010). Under the context of weak signal coding, it is thus not surprising that synaptic plasticity can enhance the coding of weak signals at the cellular and circuit levels.

This adaptation of a neuron's response to the statistics of the natural sensory input (e.g., Woolley et al., 2006); is not entirely a bottom-up or local process. A bottom-up process refers to the fact that more peripheral inputs are relayed to the first-way station more centrally, then to the next, and so on. Growing evidence suggests the crucial role of top-down processes governed via feedback inputs that modify the feedforward on different temporal and spatial scales (Metzen et al., 2018; Pak et al., 2019). This feedback is often a precise and complex process achieved through the recruitment of several networks or cell-types (Maler, 2007; Boyd et al., 2012; Markopoulos et al., 2012; Layton et al., 2014; Clarke et al., 2015; Hofmann and Chacron, 2019). Feedback has been shown to significantly change the firing activity patterns of neurons in a population, alter the precision of temporal synchrony, and largely influence phasic responses and feature preferences (Bol et al., 2011; Marsat et al., 2012; Mejias et al., 2013; Tuthill et al., 2014; Liang et al., 2017). Thus, feedback plays an important role in optimizing neural coding of ethologically relevant sensory input, including weak signals by enhancing the responses to some features while filtering-out others.

Receptive field structure

Across biological sensory systems, receptive fields of neurons cover the spatial extent of sensory sensitivity across the periphery and vary in their size, shape, and selectivity to stimuli (Woolsey and Van der Loos., 1970; Maler, 2009; Nishino et al., 2018; Turner et al., 2018). Receptive fields are often largely overlapping, leading to redundant and synergistic coding that is especially prevalent in the early stages of sensory processing. Redundancy is theoretically less efficient due to multiple neurons coding for the same information. That said, some amount of redundancy does offer many advantages as redundancy can help to overcome noisiness in signal transmission and signal coding. In this case, redundancy might act as a failsafe mechanism, a means to reduce error through redundant coding of the stimulus' range (Schneidman et al., 2003; Latham and Nirenberg, 2005).

In the visual system, space is encoded via a labeled line coding strategy and this topographic organization preserves the stimulus' spatial structure. One well studied cell type in the early visual pathway is the retinal ganglion cells (RGC), which have a classical receptive field center-surround topography. In a center-surround organization, the center and surround are arranged in a pair of concentric circles, with different center and surround activation patterns. ON-centers will depolarize when stimulated with an increase in stimulus intensity on the receptive field center. They will be hyperpolarized when the surround is stimulated and respond to decreases in stimulus intensity. This leads to a varied, more complex response when both center and surround are stimulated to different extents. OFF-centers respond in the opposite fashion. RGCs serve as the sole output neuron of the retina, and I will explain below that the center-surround organization of the receptive field has a heavy influence on the information transmitted through different aspects of the neural response. Furthermore, there is a rich

literature documenting their connectivity and physiological response properties with respect to various bipolar and amacrine interneurons (Masland, 2001; Masland, 2012). The intricate connectivity patterns to interneurons within the retina can shape their physiological responses to a wide range of stimulus patterns as described in the next paragraph (Rodieck and Stone, 1965; Famiglietti and Kolb, 1976).

In the early stages of visual processing, thresholding can be influenced by neural mechanisms such as local contrast enhancement and redundancy reduction through receptive field surrounds (Durant et al., 2007). Generally, for receptive field centers, the threshold can be influenced by connections between bipolar cells and RGCs, whereas alterations to the threshold for receptive field surrounds occur largely through bipolar cell and amacrine cell interactions (Takeshita and Gollisch, 2014). For neurons with a center-surround receptive field organization (e.g., RGCs), the extent of the magnitude of surround suppression depends heavily on the spatial structure of the visual stimulus. Natural visual scenes contain visual stimuli that vary in size and intensity. Often, these visual signals can be received by multiple receptive fields leading to many neurons encoding similar visual stimuli. This redundant, overlapped coding of visual signals can be described as spatially correlated coding. RGCs are one neuron type that has been shown to encode weak visual signals by reducing spatial correlations. These spatial correlations can be reduced by introducing sparsifying nonlinearities through mechanisms such as gain control, thresholding, refractoriness, and overlapping receptive field antagonisms, that help to improve the efficiency of the neural code (Gollisch and Meister, 2008; Pitkow and Meister, 2012). Below, I describe a few common mechanistic functions as well as their contributions to weak signal coding.

One way the retinal network helps to enable a reduction in spatial correlations and increase its sensitivity is through receptive field antagonisms formed by contextual interactions between RGCs, bipolar cells, horizontal cells, and amacrine cells. Bipolar cells create excitatory synapses onto RGCs, acting as nonlinear synaptic subunits within the RGC's receptive field center. A RGC's receptive field surround is created in part by amacrine and/or horizontal cells, and can impact the responses of bipolar cells. The strength of the receptive field surround changes the degree of rectification of the nonlinear bipolar cell subunits. This results in a neural circuit for flexible spatial integration and adjustable sensitivity to a range of spatial contrasts across different visual stimuli. Receptive field antagonisms create distinct modes of operation, where a weaker/hyperpolarizing surround is associated with nonlinear integration, and a depolarizing surround is associated with linear integration (Turner et al., 2018). Thus, the surround can dictate the neuron's sensitivity to different stimulus' spatial structure by modifying the amount of integration of visual information at the receptive field center.

Many forms of synaptic and intrinsic mechanisms have been identified as a potential source of spatial contrast gain control in retinal networks. In RGCs, levels of intrinsic ionic conductance are changed by fluctuations in stimulus luminance and contrast, causing transformations to the threshold. At the synaptic level, bipolar cells provide input to RGCs, allowing RGCs to adapt to changes in local contrast.

Neural populations within the retinal network divide the inputs they receive to different types of cells while shifting their dynamic range for stimulus coding. This heterogeneity in cell types and response properties is another advantageous way the visual system is able to reduce spatial correlations for increased coding efficiency. Differences in refractoriness or response

latency within a neural population has been shown to be a candidate mechanism implemented by the visual system to detect changes in stimulus contrast across a visual scene (Gollisch and Meister, 2008). Where a mixed population of RGCs with fast/slow and ON/OFF cells encode information about visual stimulus identity by responding at different latencies, and with higher responses to regions of a visual scene with higher contrast levels.

Somatotopically-organized maps are a key feature of the whisker-barrel system, with receptive fields conserved in the ascending pathway that correspond to specific regions of the face containing vibrissae. (Woolsey and Van der Loos, 1970). In layer 4 of the primary somatosensory cortex, clusters of neurons form barrels with topology that is matched to the whiskers along the snout. This organization enables the deflection of a single whisker to be represented as a spatially localized, multicolumn region of neural activity, allowing stimulus location to be coded quickly with few spikes per neuron (Peterson and Diamond, 2000; Peterson et al., 2001). The somatosensory system of rats displays a remarkable capacity for very fine texture discrimination, capable of detecting 30 µm grooves spaced at 90 µm intervals (Carvell and Simons, 1990). Rats rival humans in their ability to detect very small differences in textures through an active sensing strategy termed, “whisking”. Arabzadeh and colleagues have found that when whisking, rats sweep their vibrissae against an object of interest, generating kinetic signatures in the whisker-barrel cortex that vary with texture profile and whisker velocity (Arabzadeh et al., 2005). This insightful study also suggests that even a single whisker can transmit a large amount of somatosensory information to central processing areas, providing support for similar behavioral findings.

In experiments using naturalistic wall tracking, rats must use active whisking strategies to navigate through winding paths in a virtual reality environment. Sofroniew and colleagues found that neurons in layer 4 responded with graded activation and were sufficient to guide locomotion in a wall tracking, navigation task. This research suggests that the barrel cortex interprets increases in spike rate as a distance measure for calculating the next locomotor response, where distance from whisker to wall could be coded as inversely proportional to the spiking activity in layers 2/3, and 4 of the primary somatosensory cortex. However, neurons in layer 5 produced a more complex response, exhibiting close to a monotonic tuning curve, suggesting that a population of these gaussian tuned neurons could allow for higher coding accuracy (Sofroniew et al., 2015). Findings from a recent modeling study have found that activity in layer 4 neurons directly suppressed the activity of neurons in layer 5 via deep, fast-spiking inhibition. The results from this insightful modeling study suggests that the population level response of layer 4 helps to sharpen the spatial representation of neurons in layer 5, improving the feature selectivity of somatosensory cortical output (Pluta et al., 2015).

The receptive field surround of neurons in the somatosensory barrel cortex has been shown to influence neural activity at cellular and population levels. Complex somatosensory stimuli, as opposed to single whisker stimulation, induced noticeably sharper receptive fields, as an effect of adaptation. This enables the surround to facilitate, instead of suppressing, the responses to the whisker of interest. More optimal stimulation of the receptive field increased the firing rate of neurons within layers 4, 5, and 6, while having little effect on the firing rate of neurons in layers 2 and 3. These results suggest that the role of the surround helps to increase the range of stimulus discrimination during active sensing (Ramirez et al., 2014). Another insightful study by

Pluta and colleagues shows that the surround input can greatly change the amplitude of the neural response and modulate the preference of spatial coding at the single neuron level. This study also describes how the integration of surround input at the population level can provide a smoothened representation of the scanned space (Pluta et al., 2017).

In the olfactory system, encoding an odor's spatial distribution involves comparing intensity inputs and timing differences between bilateral olfactory organs. Cockroaches can encode the spatial position of a pheromone to locate a signaling mate by capitalizing on antennatopic organization of olfactory sensory neurons and subsequent compartmentalization of projection neurons into different compartments of the mushroom body (Nishino et al., 2018). Changes in the spatial geometry of an olfactory stimulus are further encoded in the excitatory and inhibitory receptive fields of macroglomerular projection neurons. In comparison to the visual system, largely overlapping receptive fields of small receptive field projection neurons can permit high spatial resolution at minimal spatial scales and enhance edge detection of odor plumes (De Bruyne and Baker, 2008). For projection neurons with small receptive fields, there are observable response latencies depending on receptive field location relative to antenna placement (Nishino et al., 2018). This dynamic sensory information is constantly updated as the animal navigates and actively samples its spatial environment.

In the electrosensory system, multiple topographic maps in the electrosensory lateral line lobe (ELL) are comprised of a heterogeneous network of ON and OFF-type pyramidal cells (Heiligenberg and Dye, 1982; Shumway, 1989; Maler, 2009). The body of weakly electric fish is covered with electroreceptors, whose afferents provide trifurcated, unilateral input to the maps of the ELL: the lateral segment (LS), centro-lateral segment (CLS), and centro-medial

segment (CMS; for review see Krahe and Maler, 2014; Milam et al., 2019). Pyramidal cells within each map vary in their response properties and receptive field parameters (Chacron et al., 2001; Krahe et al., 2008). Receptive fields in the LS map are the largest, the CMS map contains the smallest receptive fields, and receptive fields in the CLS map are intermediate. Different neural maps are specialized for certain behavioral tasks (Maler, 2007; Allen and Marsat, 2018). The CMS map having the smallest receptive fields might be better for small prey detection or resolving finer details at close range, given the higher spatial resolution that small receptive fields support (Nelson and MacIver, 1999). In contrast, the LS map with much larger receptive fields might be a more sensitive map that is better for long range communication with other weakly electric fish (Litwin-Kumar et al., 2012; Allen and Marsat, 2019). This is a reasonable assumption, as a viable solution would be to trade high spatial resolution for greatly increased sensitivity at a much lower spatial resolution.

In vivo recordings have shown that pyramidal cells across maps of the ELL displayed similar levels of correlation even though they differ in receptive field overlap. Using a modeling approach, Hoffman and colleagues showed that overlapping receptive field centers alone cannot determine correlations, but by varying the size and gain of the receptive field surround, they were able to match the experimentally observed correlated activity (Hoffman and Chacron, 2017). Thus, differences in the antagonistic center-surround receptive field organization across the multiple topographic maps of the ELL change the correlations among pyramidal cells, thereby affecting their redundancy and coding efficiency.

Enhanced sensitivity through neural adaptation and synaptic plasticity

Synaptic plasticity occurs in many synapses of key neurons across the central nervous system and plays a critical role in shaping how sensory input is encoded. The dynamics of synaptic plasticity occur across a spectrum of temporal and spatial scales, capable of affecting both cellular and circuit states (Abbott and Regehr, 2004). Occurring on a time scale of milliseconds, short-term synaptic plasticity is a neurophysiological phenomenon that is dependent on the history of pre- and post-synaptic neural activity. From a network perspective, synaptic plasticity can allow for increased information coding by inducing flexible activity patterns within a finite pattern of connection. (Abraham and Bear, 1996; Abbott and Nelson, 2000).

One well-studied form of short-term synaptic plasticity is stimulus-response adaptation, where neurons adapt to either the stimulus intensity or the timing of stimulus occurrence. For example, some neurons display adaptation that can be mediated by synaptic plasticity and reduce the strength of the response to a repeated stimulus. (Schwartz and Simoncelli, 2001; Fu et al., 2014; Wissig and Kohn, 2013). Adaptation can also alter tuning by suppressing some responses more than others. Adaptation has been shown to reduce redundancy, improve discriminability, and mediate the feature-specificity of neurons in order to benefit distinct modes of adaptation (Ganmor et al., 2010; Ozuysal and Baccus, 2012; Piazza et al., 2018).

A notable sensory modality to highlight the role of neural adaptation is the visual system, known for its remarkable sensitivity and capable of detecting as little as a single photon of light (Rieke and Baylor, 1998). After photon absorption under extreme light conditions, a light-dependent gain modulation produces a dynamic change in the detection threshold occurring over a temporal span of several seconds, thus modulating the visual system's sensitivity (Tinsley

et al., 2016). More generally, adaptation in the visual system has been shown to play a large role in allowing sensitivity to a wide range of contrast levels. In the retina, reducing the inhibitory activity of tonically active amacrine cells has been shown to be necessary to increase the sensitivity of the retina to weak visual stimuli (i.e., low-contrast; Kastner et al., 2019). Another functional example occurs further along in the early visual pathway, where magnocellular neurons of the lateral geniculate nucleus (LGN) display strong adaptation to visual contrast, whereas parvocellular neurons show little to no adaptation. This strong adaptation to visual contrast helps neurons in the magnocellular pathway to have higher light/dark contrast detection and to enhance their sensitivity to visual stimuli with low spatial frequency. The ability of magnocellular neurons of the LGN to detect changes in contrast levels is important for visual search related tasks, edge detection, and changes in luminance (Solomon et al., 2004).

Neural adaptation to specific stimuli is also a common mechanism in olfaction (Stopfer and Laurent, 1999). In the context of sensory processing, odor adaptation is a mechanism that allows the olfactory system to adjust its sensitivity at different stimulus intensities to prevent saturation and maintain high sensitivity to olfactory stimuli. In the locust, projection neurons show a quick, intensity-adaptation response when exposed to a repeated stimulus yet respond with better synergy and precision with other projection neurons in the antennal lobe circuits (Assisi et al., 2007). A recent study on the AWC olfactory neuron in *C. elegans* describes how a history based adaptive-threshold mechanism helps to continuously filter noise and improve sensory detection of odor concentration (Levy and Bargmann, 2019). This insightful work also predicts animal navigation decisions based on the adaptive odor concentration threshold.

Similar findings in the whisker-barrel somatosensory system have suggested that adaptation in the whisker system is an optimal neural strategy to encode signal strengths that are greater than the baseline stimulus signal (Adibi et al., 2010; Adibi et al., 2012).

Remarkably, the auditory system can encode a wide range of sound levels while maintaining high accuracy (Batchelor and Wilson, 2019; Zirkelbach et al., 2019; Ihlefeld et al., 2019). In certain areas of the auditory system, changes in firing rate are positively correlated with increasing sound level, but such changes are restricted to a subset of the entire range of auditory signals that are possible to encode. Dean and colleagues found that midbrain auditory neurons in the guinea pig adapt to the mean and variance of sound-level distributions to fine-tune accurate encoding of sound level based on the local environment, thus forming a dynamic range of adaptive hearing that is context dependent (Dean et al., 2005). A well-established study on the investigation of distance coding mechanisms in the bat *Myotis*, observed an interesting phenomenon called the “paradoxical latency shift” (see Figure 2). Neurons which displayed this phenomenon responded to low amplitude sounds at a shorter latency than high amplitude sounds, thus serving as a potential mechanism for encoding weak signals that occur over short timescales (Sullivan, 1982).

In the electrosensory system, one potential neural mechanism used to facilitate the detection of weak signals in the early sensory pathway, is to increase the sensitivity of a postsynaptic neuron by utilizing the correlated structure of input via short-term synaptic plasticity (Lüdtke and Nelson, 2006). This mechanism was proposed in an insightful modeling study by Lüdtke and Nelson, where they tested the theoretical capability of weak signal coding at the electrosensory afferent level. The authors proposed a two-part mechanism that relies on

negatively correlated interspike intervals (ISIs) and a fast short-term synaptic plasticity component. Under these conditions, they demonstrated that weak signal detection performance was increased due to synaptic plasticity serving as a way for the sensory system to address the computational challenge of representing conditional firing probabilities. From their findings, they speculated that neurons with high firing rates might be matched by small synaptic time constants.

Mechanisms of fast short-term depression (FSTD) can decrease the variability of the rate of synaptic output to reduce noise (Khanbabaie et al., 2010). The decreased variability of ON-type pyramidal cell excitatory postsynaptic potentials (EPSPs) also results in a decreased gain caused by a lowered EPSP amplitude. In *Apteronotus*, this form of FSTD operates through a one-to-one linear relationship, where shorter (longer) ISIs result in smaller (larger) EPSP amplitude. The kinetics of FSTD act on a timescale of approximately 1.5ms, uniquely quicker than other standard forms of STD. Similarly, electroreceptor P-units display low levels of gain when encoding low-frequency signals due to negative ISI correlations (Ratnam and Nelson, 2000; Chacron et al., 2001; Goense and Nelson 2003; Chacron et al., 2005). Together, negative ISI correlations in combination with the noise and gain reducing effects of fast short-term synaptic plasticity present an interesting and open area of research for understanding how weak signals are encoded in early processing pathways. Therefore, it is essential to have a detailed characterization of different mechanisms that increase coding performance at the detection threshold level, where firing rate changes are insignificant (Nesse et al., 2021).

Adaptation in the electrosensory system can allow for precise encoding of natural communication signals (Benda et al., 2006). Benda and colleagues showed that different forms

of adaptation can shift the onset of the frequency-intensity curve having been shown to affect gain linearly in biophysical experiments. They later demonstrated how changing the variability of spike thresholding and adaptation state, results in a shift of the frequency-intensity curve and dynamic gain modulation (Benda et al., 2010). Thus, whether the electrosensory system relies on a combination of previously defined neural mechanisms involving synaptic plasticity or novel ones for encoding weak signals remains an open area of research.

Flexible selectivity by network feedback

A common theme across sensory systems is the modification of feedforward input by top-down feedback. In many systems, the number of feedback pathways far outweighs the number of feedforward pathways, suggesting that feedback makes essential contributions to sensory processing (Markov et al., 2014; Zagha, 2020). Across modalities many neurons display higher sensitivity (i.e., lower detection thresholds) to amplitude modulations in higher sensory processing areas of the brain. One possibility for this observed heightened sensitivity is that feedback plays a key role in driving and adaptively lowering detection thresholds to encode signals of interest.

Feedback has been shown to be a critical component of visual perception. Recent studies have started to investigate the role of feedback for encoding illusory contours. The encoding and perception of illusory contours have revealed the importance of thalamocortical feedback to layer V1 of the visual cortex in mice and from V4 to V1 for lateral contours in primates (Liang et al., 2017, Pak et al., 2019). Thus, the encoding of illusory contours aided by feedback can be

thought of as a task of weak visual signal coding, where the nervous system must infer a complete signal using only a limited subset of visual cues.

An incredible finding that is gaining more experimental support is that a finely tuned balance of excitatory and inhibitory activity can optimize neural coding performance, and is a candidate mechanism for encoding weak signals (Dodla et al., 2006; Large et al., 2016; Beiderbeck et al., 2018; Lankarany et al., 2019). In the auditory system, a precise timing of inhibition to increase the spatial sensitivity to weak sounds relies on finely-tuned timing changes through interaural time difference (ITD) and input latencies generated by interaural level difference (ILD) on the order of microseconds (Schnupp and Carr, 2009; Beiderbeck et al., 2018). Neurons in the lateral superior olive (LSO) participate in comparing the timing and amplitude strength of incoming sound levels. If precisely timed, glycinergic inhibition of LSO neurons can facilitate spiking to increase the limits of sound source detection (Brand et al., 2002). Specifically, in neural networks with high spontaneous firing rates, selective and precise inhibition through lateral inhibition or feedback can sharpen the differences among parallel inputs and increase the signal-to-noise ratio. Investigating the effects of feedback and a balance of excitation and inhibition on weak signal coding by heterogeneous networks of neurons is one area of research that remains largely unexplored.

The organization of the olfactory system could be thought of as inherently noise limiting (Sachse and Galizia, 2003). The nature of odors is typically lingering and occurring in irregular intervals. The circuitry of the antennal lobe may have intrinsically low spike thresholds, but could have improved selectivity through finely tuned inhibition and feedback modulation (Laurent, 2002). An example of this in the early olfactory pathway can be seen in mitral and

tufted cells of the olfactory bulb. Activation of pyramidal cells of the olfactory cortex in vivo, strongly suppressed odor-evoked excitation and enhanced odor-evoked inhibition in mitral and tufted cells. In this study, feedback had little effect on the spontaneous firing rates, but the overall effect of cortical feedback on olfactory bulb mitral and tufted cells was an increase in odor-evoked inhibition. This cortical feedback can act to suppress background activity through broad inhibition and help shape the responses of olfactory bulb output neurons through temporally precise action potentials (Boyd et al., 2012; Markopoulos et al., 2012).

Behavioral and neural experiments on spatial interaction between conspecifics in the electrosensory system allude to a high level of sensitivity for detecting weak signals (Henninger et al., 2018; Jung et al., 2016). On the sensory side, this elevated sensitivity could be enhanced by cerebellar feedback and the cancellation of reafferent signals. The ELL receives indirect, global feedback inputs that have been shown to cancel the response to beats produced by global amplitude modulations from the electric fields generated by interacting electric fish. Superficial pyramidal cells in the ELL receive parallel fiber input onto their apical dendrites (Bastian et al., 2004). The contribution of each fiber is adjusted by plastic synapses so that the total input is antiphase to the feedforward input from electroreceptors, cancelling the strength of the neural response (Bol et al., 2011; Mejias et al., 2013). Recent findings from field studies in the electrosensory system allude to their remarkable capacity for detecting very weak electric signals (<1μV) from over 1.7 meters away (e.g., Henninger et al., 2018); despite the large self-generated modulations that are cancelled by feedback. This challenging task involves not only the ability to detect a weak signal, but also to discriminate between the even smaller

differences between low contrast/low amplitude signals and background signals (Jung et al., 2016; Longtin et al., 2019).

Feedback has also been shown to mediate spatial attention by balancing polarity to establish a focal distance during object motion-tracking in the electrosensory system (Clarke and Maler, 2017). This top-down mechanism occurs through a nested inner and outer loop. The outer feedback loop synthesizes a neural code for motion reversal in ELL pyramidal cells and the inner feedback loop regulates the outer feedback loop by reducing pyramidal cell bursting and lowering responses to interfering sensory input. Thus, ELL feedback includes a strong positive feedback loop, tightly constrained by delayed negative feedback, resulting in a nonlinear influence on the response to approaching or receding objects.

Additionally, Metzen and colleagues have shown that the threshold for detecting weak electrosensory signals in an envelope is approximately 9% stimulus contrast (corresponding to a conspecific 20-30 cm away, Fotowat et al., 2013; see also Chapter 1: Introuction - Part 1 for more information on envelope signals); and the perception of weak signals embedded in an envelope relies on a closed-loop feedback mechanism (Metzen et al., 2018).

Many examples of feedback mechanisms in the early levels of the auditory system relate to self-generation of sound or to learning and memory of auditory signals (Köppl et al., 2000; Theunissen and Shaevitz, 2006; Tschida and Mooney, 2012). A smaller, but growing body of literature on the role of the inferior colliculus and the descending auditory pathways from the auditory cortex details other ways that feedback can influence the neural response (Huffman and Henson, 1990; Lee and Sherman, 2010). One excellent example of a feedback reliant mechanism to help encode weak auditory signals is prepulse inhibition, a highly robust

phenomenon that serves as a pre-attentive form of sensory gating. Prepulse inhibition of the startle response is an inhibitory mechanism driven by a weak, subthreshold stimulus that serves to reduce the magnitude of a much stronger, following stimulus (Li et al., 2009). Many examples of sensory gating occur at the level of the midbrain, but have been shown to be present as early as the first synaptic level of the brainstem in vertebrates (Tabor et al., 2018).

Discussion

In this primer, I compared the early sensory pathway and nervous system architecture across sensory modalities, describing how different neural mechanisms and network strategies could allow for enhanced neural coding of weak signals. Though these strategies operate via different biophysical, cellular, or network mechanisms across sensory systems, the general neural coding principles share commonality and are likely applicable to the task at hand.

I described how the receptive field structure and the spatiotemporal properties of receptive fields in the early sensory pathway enables a dynamic range of stimulus encoding. The largely overlapping organization of antagonistic center and surround receptive fields helps to reduce spatial correlations for increased neural coding efficiency. I also highlighted how mechanisms such as short-term synaptic plasticity, lateral inhibition, gain control, and dynamic spike thresholds modulate the neural response in an adaptive manner to improve network flexibility for weak signal coding. Lastly, I explained that the role of neural feedback is versatile and enhances the system's sensitivity by suppressing background activity through inhibition, cancelling responses in certain conditions, influencing temporal synchrony, and adapting to repetitive stimuli. These mechanisms are prevalent across sensory modalities, generally

operating in parallel and to different degrees depending on the sensory task. Though the scope of this primer focuses on common features of neural systems, this summary is not exhaustive, as many other mechanisms could be contributing to the neural coding of weak signals.

Many neural strategies for optimizing the encoding of weak signals may depend on applying refined behavioral strategies to enhance a signal of interest. Such hallmark active sensing behaviors include edge detection and tracking of weak odor plumes in moth olfaction, as well as foveal sampling in the visual and electrosensory systems, to name a few examples (see Enikolopov et al., 2018; Pedraja et al., 2019). While studying prey capture, a recent study found that certain bat species take advantage of their angle of approach with respect to the background surface to increase the signal to noise ratio of a prey echo. Such acoustically camouflaged prey items would normally have their weak prey echoes masked by background echoes from other objects in the natural environment (Geipel et al., 2019). These behavioral observations hint at a finely tuned nervous system that uses precise behavioral strategies to help optimize signal detection and localization, through largely unknown neural mechanisms.

Parts of this primer focus on the notion of optimizing signal coding efficiency at the cost of lowering spatial correlations and reducing redundant coding. It would be especially interesting to investigate how efficiency and redundancy trade off as the signal-to-noise ratio changes for different sensory stimuli in key neurons of the early sensory pathways. Additionally, dissecting the mechanisms of cellular and network function in a variety of stimulus conditions will be crucial for uncovering higher order processing and neural population dynamics. Pursuing these avenues of research will help us better understand how the nervous system transforms physical

signals from the environment into a neural code usable by the organism, provided a common theme of neural architecture and shared cellular and network strategies.

References

Abbott, L. F., & Nelson, S. B. (2000). Synaptic plasticity: taming the beast. *Nature neuroscience*, *3*(11s), 1178.

Abbott, L. F., & Regehr, W. G. (2004). Synaptic computation. *Nature*, *431*(7010), 796.

Abraham, W. C., & Bear, M. F. (1996). Metaplasticity: the plasticity of synaptic plasticity. *Trends in neurosciences*, *19*(4), 126-130.

Adibi, M., & Arabzadeh, E. (2010). A comparison of neuronal and behavioral detection and discrimination performances in rat whisker system. *Journal of neurophysiology*, *105*(1), 356-365.

Adibi, M., Diamond, M. E., & Arabzadeh, E. (2012). Behavioral study of whisker-mediated vibration sensation in rats. *Proceedings of the National Academy of Sciences*, *109*(3), 971-976.

Allen, K. M., & Marsat, G. (2018). Task-specific sensory coding strategies are matched to detection and discrimination performance. *Journal of Experimental Biology*, *221*(6), jeb170563.

Allen, K. M., & Marsat, G. (2019). Neural Processing of Communication Signals: The Extent of Sender–Receiver Matching Varies across Species of Apteronotus. *eNeuro*, *6*(2).

Arabzadeh, E., Zorzin, E., & Diamond, M. E. (2005). Neuronal encoding of texture in the whisker sensory pathway. *PLoS biology*, *3*(1), e17.

Assisi, C., Stopfer, M., Laurent, G., & Bazhenov, M. (2007). Adaptive regulation of sparseness by feedforward inhibition. *Nature neuroscience*, *10*(9), 1176.

Baker, C. A., Ma, L., Casareale, C. R., & Carlson, B. A. (2016). Behavioral and single-neuron sensitivity to millisecond variations in temporally patterned communication signals. *Journal of Neuroscience*, *36*(34), 8985-9000.

Barlow, H. B. (1961). Possible principles underlying the transformation of sensory messages. *Sensory communication*, *1*, 217-234.

Bastian, J., Chacron, M. J., & Maler, L. (2004). Plastic and nonplastic pyramidal cells perform unique roles in a network capable of adaptive redundancy reduction. *Neuron, 41*(5), 767-779.

Batchelor, A. V., & Wilson, R. I. (2019). Sound localization behavior in Drosophila melanogaster depends on inter-antenna vibration amplitude comparisons. *Journal of Experimental Biology*, *222*(3), jeb191213.

Beiderbeck, B., Myoga, M. H., Müller, N. I., Callan, A. R., Friauf, E., Grothe, B., & Pecka, M. (2018). Precisely timed inhibition facilitates action potential firing for spatial coding in the auditory brainstem. *Nature communications*, *9*(1), 1771.

Benda, J., Longtin, A., & Maler, L. (2006). A synchronization-desynchronization code for natural communication signals. *Neuron*, *52*(2), 347-358.

Brand, A., Behrend, O., Marquardt, T., McAlpine, D., & Grothe, B. (2002). Precise inhibition is essential for microsecond interaural time difference coding. *Nature*, *417*(6888), 543.

Bol, K., Marsat, G., Harvey-Girard, E., Longtin, A., & Maler, L. (2011). Frequency-tuned cerebellar channels and burst-induced LTD lead to the cancellation of redundant sensory inputs. *Journal of Neuroscience*, *31*(30), 11028-11038.

Boyd, A. M., Sturgill, J. F., Poo, C., & Isaacson, J. S. (2012). Cortical feedback control of olfactory bulb circuits. *Neuron, 76*(6), 1161-1174.

Bullock, T. H., Bennett, M. V., Johnston, D., Josephson, R., Marder, E., & Fields, R. D. (2005). The neuron doctrine, redux. *Science*, *310*(5749), 791-793.

Carvell, G. E., & Simons, D. J. (1990). Biometric analyses of vibrissal tactile discrimination in the rat. *Journal of Neuroscience*, *10*(8), 2638-2648.

Clark, D. A., Benichou, R., Meister, M., & da Silveira, R. A. (2013). Dynamical adaptation in photoreceptors. *PLoS computational biology*, *9*(11), e1003289.

Clarke, S. E., Longtin, A., & Maler, L. (2015). The neural dynamics of sensory focus. *Nature communications*, *6*, 8764.

Clarke, S. E., & Maler, L. (2017). Feedback synthesizes neural codes for motion. *Current Biology, 27*(9), 1356-1361.

Chacron, M. J., Longtin, A., & Maler, L. (2001). Negative interspike interval correlations increase the neuronal capacity for encoding time-dependent stimuli. *Journal of Neuroscience*, *21*(14), 5328-5343.

Chacron, M. J., Maler, L., & Bastian, J. (2005). Electroreceptor neuron dynamics shape information transmission. *Nature neuroscience*, *8*(5), 673.

Dayan, P., & Abbott, L. F. (2001). *Theoretical neuroscience* (Vol. 806). Cambridge, MA: MIT Press.

De Bruyne, M., & Baker, T. C. (2008). Odor detection in insects: volatile codes. *Journal of chemical ecology*, *34*(7), 882-897.

Dean, I., Harper, N. S., & McAlpine, D. (2005). Neural population coding of sound level adapts to stimulus statistics. *Nature neuroscience*, *8*(12), 1684.

Denève, S., & Machens, C. K. (2016). Efficient codes and balanced networks. *Nature neuroscience*, *19*(3), 375.

Dodla, R., Svirskis, G., & Rinzel, J. (2006). Well-timed, brief inhibition can promote spiking: postinhibitory facilitation. *Journal of neurophysiology*, *95*(4), 2664-2677.

Durant, S., Clifford, C. W., Crowder, N. A., Price, N. S., & Ibbotson, M. R. (2007). Characterizing contrast adaptation in a population of cat primary visual cortical neurons using Fisher information. *JOSA A*, *24*(6), 1529-1537.

Enikolopov, A. G., Abbott, L. F., & Sawtell, N. B. (2018). Internally generated predictions enhance neural and behavioral detection of sensory stimuli in an electric fish. *Neuron*, *99*(1), 135-146.

Famiglietti, E. V., & Kolb, H. (1976). Structural basis for ON-and OFF-center responses in retinal ganglion cells. *Science*, *194*(4261), 193-195.

Fotowat, H., Harrison, R. R., & Krahe, R. (2013). Statistics of the electrosensory input in the freely swimming weakly electric fish Apteronotus leptorhynchus. *Journal of Neuroscience, 33*(34), 13758-13772.

Fu, Y., Tucciarone, J. M., Espinosa, J. S., Sheng, N., Darcy, D. P., Nicoll, R. A., ... & Stryker, M. P. (2014). A cortical circuit for gain control by behavioral state. *Cell*, *156*(6), 1139-1152.

Gabbiani, F., Metzner, W., Wessel, R., & Koch, C. (1996). From stimulus encoding to feature extraction in weakly electric fish. *Nature*, *384*(6609), 564.

Ganmor, E., Katz, Y., & Lampl, I. (2010). Intensity-dependent adaptation of cortical and thalamic neurons is controlled by brainstem circuits of the sensory pathway. *Neuron*, *66*(2), 273-286.

Geipel, I., Steckel, J., Tschapka, M., Vanderelst, D., Schnitzler, H. U., Kalko, E. K., ... & Simon, R. (2019). Bats actively use leaves as specular reflectors to detect acoustically camouflaged prey. *Current Biology*, *29*(16), 2731-2736.

Goense, J. B. M., & Ratnam, R. (2003). Continuous detection of weak sensory signals in afferent spike trains: the role of anti-correlated interspike intervals in detection performance. *Journal of Comparative Physiology A*, *189*(10), 741-759.

Gollisch, T., & Meister, M. (2008). Rapid neural coding in the retina with relative spike latencies. *science*, *319*(5866), 1108-1111.

Gussin, D., Benda, J., & Maler, L. (2007). Limits of linear rate coding of dynamic stimuli by electroreceptor afferents. *Journal of neurophysiology*, *97*(4), 2917-2929.

Heiligenberg, W., & Dye, J. (1982). Labelling of electroreceptive afferents in a gymnotoid fish by intracellular injection of HRP: the mystery of multiple maps. *Journal of comparative physiology*, *148*(3), 287-296.

Henninger, J., Krahe, R., Kirschbaum, F., Grewe, J., & Benda, J. (2018). Statistics of natural communication signals observed in the wild identify important yet neglected stimulus regimes in weakly electric fish. *Journal of Neuroscience*, *38*(24), 5456-5465.

Hofmann, V., & Chacron, M. J. (2017). Differential receptive field organizations give rise to nearly identical neural correlations across three parallel sensory maps in weakly electric fish. *PLoS computational biology, 13*(9), e1005716.

Hofmann, V., & Chacron, M. (2019). Novel functions of feedback in electrosensory processing. *Frontiers in integrative neuroscience*, *13*, 52.

Huang, C., Resnik, A., Celikel, T., & Englitz, B. (2016). Adaptive spike threshold enables robust and temporally precise neuronal encoding. *PLoS computational biology, 12*(6), e1004984.

Huang, C. G., Metzen, M. G., & Chacron, M. J. (2018). Feedback optimizes neural coding and perception of natural stimuli. *ELife*, *7*, e38935.

Huffman, R. F., & Henson Jr, O. W. (1990). The descending auditory pathway and acousticomotor systems: connections with the inferior colliculus. *Brain research reviews*, *15*(3), 295-323.

Ihlefeld, A., Alamatsaz, N., & Shapley, R. M. (2019). Population rate-coding predicts correctly that human sound localization depends on sound intensity. *eLife*, *8*.

Jung, S. N., Longtin, A., & Maler, L. (2016). Weak signal amplification and detection by higher-order sensory neurons. *Journal of neurophysiology*, *115*(4), 2158-2175.

Kastner, D. B., Ozuysal, Y., Panagiotakos, G., & Baccus, S. A. (2019). Adaptation of inhibition mediates retinal sensitization. *Current Biology*, *29*(16), 2640-2651.

Khanbabaie, R., Nesse, W. H., Longtin, A., & Maler, L. (2010). Kinetics of fast short-term depression are matched to spike train statistics to reduce noise. *Journal of neurophysiology*, *103*(6), 3337-3348.

Krahe, R., Bastian, J., & Chacron, M. J. (2008). Temporal processing across multiple topographic maps in the electrosensory system. *Journal of Neurophysiology*, *100*(2), 852-867.

Krahe, R., & Maler, L. (2014). Neural maps in the electrosensory system of weakly electric fish. *Current opinion in neurobiology*, *24*, 13-21.

Koch, C., & Laurent, G. (1999). Complexity and the nervous system. *Science*, *284*(5411), 96-98.

Köppl, C., Manley, G. A., & Konishi, M. (2000). Auditory processing in birds. *Current opinion in neurobiology*, *10*(4), 474-481.

Lankarany, M., Al-Basha, D., Ratté, S., & Prescott, S. A. (2019). Differentially synchronized spiking enables multiplexed neural coding. *Proceedings of the National Academy of Sciences*, *116*(20), 10097-10102.

Large, A. M., Vogler, N. W., Mielo, S., & Oswald, A. M. M. (2016). Balanced feedforward inhibition and dominant recurrent inhibition in olfactory cortex. *Proceedings of the National Academy of Sciences*, *113*(8), 2276-2281.

Latham, P. E., & Nirenberg, S. (2005). Synergy, redundancy, and independence in population codes, revisited. *Journal of Neuroscience, 25*(21), 5195-5206.

Laurent, G. (2002). Olfactory network dynamics and the coding of multidimensional signals. *Nature reviews neuroscience*, *3*(11), 884.

Lee, C. C., & Sherman, S. M. (2010). Drivers and modulators in the central auditory pathways. *Frontiers in neuroscience*, *4*, 14.

Lewicki, M. S. (2002). Efficient coding of natural sounds. *Nature neuroscience*, *5*(4), 356.

Levy, S., & Bargmann, C. I. (2019). An adaptive-threshold mechanism for odor sensation and animal navigation. *Neuron*.

Li, L., Du, Y., Li, N., Wu, X., & Wu, Y. (2009). Top–down modulation of prepulse inhibition of the startle reflex in humans and rats. *Neuroscience & Biobehavioral Reviews*, *33*(8), 1157-1167.

Liang, H., Gong, X., Chen, M., Yan, Y., Li, W., & Gilbert, C. D. (2017). Interactions between feedback and lateral connections in the primary visual cortex. *Proceedings of the National Academy of Sciences*, *114*(32), 8637-8642.

Liang, X., Zhao, L., & Liu, Z. (2012). Enhancing weak signal transmission through a feedforward network. *IEEE transactions on neural networks and learning systems*, *23*(9), 1506-1512.

Litwin-Kumar, A., Chacron, M. J., & Doiron, B. (2012). The spatial structure of stimuli shapes the timescale of correlations in population spiking activity. *PLoS Computational Biology*, *8*(9), e1002667.

Longtin, A., Yu, N., Hupe, G. J., & Lewis, J. E. (2019). Electrosensory contrast signals for interacting weakly electric fish. *Frontiers in integrative neuroscience*, *13*, 36.

Lüdtke, N., & Nelson, M. E. (2006). Short-term synaptic plasticity can enhance weak signal detectability in nonrenewal spike trains. *Neural computation*, *18*(12), 2879-2916.

Luo, J., Macias, S., Ness, T. V., Einevoll, G. T., Zhang, K., & Moss, C. F. (2018). Neural timing of stimulus events with microsecond precision. *PLoS biology*, *16*(10), e2006422.

Lyons-Warren, A. M., Hollmann, M., & Carlson, B. A. (2012). Sensory receptor diversity establishes a peripheral population code for stimulus duration at low intensities. *Journal of Experimental Biology*, *215*(15), 2586-2600.

Maler, L. (2007). Neural strategies for optimal processing of sensory signals. *Progress in brain research*, *165*, 135-154.

Maler, L. (2009). Receptive field organization across multiple electrosensory maps. I. Columnar organization and estimation of receptive field size. *Journal of Comparative Neurology*, *516*(5), 376-393.

Markopoulos, F., Rokni, D., Gire, D. H., & Murthy, V. N. (2012). Functional properties of cortical feedback projections to the olfactory bulb. Neuron, 76(6), 1175-1188.

Markov, N. T., Vezoli, J., Chameau, P., Falchier, A., Quilodran, R., Huissoud, C., ... & Barone, P. (2014). Anatomy of hierarchy: feedforward and feedback pathways in macaque visual cortex. *Journal of Comparative Neurology*, *522*(1), 225-259.

Marsat, G., & Maler, L. (2010). Neural heterogeneity and efficient population codes for communication signals. *Journal of neurophysiology*, *104*(5), 2543-2555.

Marsat, G., & Maler, L. (2011). Preparing for the unpredictable: adaptive feedback enhances the response to unexpected communication signals. *Journal of neurophysiology*, *107*(4), 1241-1246.

Marsat, G., Longtin, A., & Maler, L. (2012). Cellular and circuit properties supporting different sensory coding strategies in electric fish and other systems. *Current opinion in neurobiology*, *22*(4), 686-692.

Masland, R. H. (2001). The fundamental plan of the retina. *Nature neuroscience*, *4*(9), 877.

Masland, R. H. (2012). The neuronal organization of the retina. *Neuron*, *76*(2), 266-280.

Mejias, J. F., Marsat, G., Bol, K., Maler, L., & Longtin, A. (2013). Learning contrast-invariant cancellation of redundant signals in neural systems. *PLoS Comput Biol, 9*(9), e1003180.

Metzen, M. G., Huang, C. G., & Chacron, M. J. (2018). Descending pathways generate perception of and neural responses to weak sensory input. *PLoS biology*, *16*(6), e2005239.

Milam, O. E., Ramachandra, K. L., & Marsat, G. (2019). Behavioral and neural aspects of the spatial processing of conspecifics signals in the electrosensory system. *Behavioral neuroscience*, *133*(3), 282.

Nelson, M. E., & Maciver, M. A. (1999). Prey capture in the weakly electric fish Apteronotus albifrons: sensory acquisition strategies and electrosensory consequences. *Journal of Experimental Biology*, *202*(10), 1195-1203.

Nesse, W. H., Maler, L., & Longtin, A. (2021). Enhanced signal detection by adaptive decorrelation of interspike intervals. *Neural Computation*, *33*(2), 341-375.

Nishino, H., Iwasaki, M., Paoli, M., Kamimura, I., Yoritsune, A., & Mizunami, M. (2018). Spatial receptive fields for odor localization. *Current biology*, *28*(4), 600-608.

Ozuysal, Y., & Baccus, S. A. (2012). Linking the computational structure of variance adaptation to biophysical mechanisms. *Neuron*, *73*(5), 1002-1015.

Pak, A., Ryu, E., Li, C., & Chubykin, A. A. (2019). Top-Down Feedback Controls the Cortical Representation of Illusory Contours in Mouse Primary Visual Cortex. *Journal of Neuroscience*.

Pedraja, F., Hofmann, V., Goulet, J., & Engelmann, J. (2019). Task related sensorimotor adjustments increase the sensory range in electrolocation. *Journal of Neuroscience*.

Petersen, R. S., & Diamond, M. E. (2000). Spatial–temporal distribution of whisker-evoked activity in rat somatosensory cortex and the coding of stimulus location. *Journal of Neuroscience, 20*(16), 6135-6143.

Petersen, R. S., Panzeri, S., & Diamond, M. E. (2001). Population coding of stimulus location in rat somatosensory cortex. *Neuron, 32*(3), 503-514.

Piazza, E. A., Theunissen, F. E., Wessel, D., & Whitney, D. (2018). Rapid Adaptation to the Timbre of Natural Sounds. *Scientific reports*, *8*(1), 13826.

Pitkow, X., & Meister, M. (2012). Decorrelation and efficient coding by retinal ganglion cells. *Nature neuroscience*, *15*(4), 628.

Pluta, S., Naka, A., Veit, J., Telian, G., Yao, L., Hakim, R., ... & Adesnik, H. (2015). A direct translaminar inhibitory circuit tunes cortical output. *Nature neuroscience, 18*(11), 1631-1640.

Pluta, S. R., Lyall, E. H., Telian, G. I., Ryapolova-Webb, E., & Adesnik, H. (2017). Surround integration organizes a spatial map during active sensation. *Neuron, 94*(6), 1220-1233.

Ramirez, A., Pnevmatikakis, E. A., Merel, J., Paninski, L., Miller, K. D., & Bruno, R. M. (2014). Spatiotemporal receptive fields of barrel cortex revealed by reverse correlation of synaptic input. *Nature neuroscience, 17*(6), 866-875.

Ratnam, R., & Nelson, M. E. (2000). Nonrenewal statistics of electrosensory afferent spike trains: implications for the detection of weak sensory signals. *Journal of Neuroscience*, *20*(17), 6672-6683.

Rieke, F., & Baylor, D. A. (1998). Single-photon detection by rod cells of the retina. *Reviews of Modern Physics*, *70*(3), 1027.

Rieke, F., Warland, D., Van Steveninck, R. D. R., & Bialek, W. S. (1999). *Spikes: exploring the neural code* (Vol. 7, No. 1). Cambridge: MIT press.

Rodieck, R. W., & Stone, J. (1965). Analysis of receptive fields of cat retinal ganglion cells. *Journal of neurophysiology*, *28*(5), 833-849.

Sachse, S., & Galizia, C. G. (2003). The coding of odour-intensity in the honeybee antennal lobe: local computation optimizes odour representation. *European journal of neuroscience*, *18*(8), 2119-2132.

Schneidman, E., Bialek, W., & Berry, M. J. (2003). Synergy, redundancy, and independence in population codes. *Journal of Neuroscience, 23*(37), 11539-11553.

Schnupp, J. W., & Carr, C. E. (2009). On hearing with more than one ear: lessons from evolution. *Nature neuroscience*, *12*(6), 692.

Schulze, L., Henninger, J., Kadobianskyi, M., Chaigne, T., Faustino, A. I., Hakiy, N., ... & Judkewitz, B. (2018). Transparent Danionella translucida as a genetically tractable vertebrate brain model. *Nature methods*, *15*(11), 977.

Schwartz, O., & Simoncelli, E. P. (2001). Natural signal statistics and sensory gain control. *Nature neuroscience*, *4*(8), 819.

Seriès, P., Latham, P. E., & Pouget, A. (2004). Tuning curve sharpening for orientation selectivity: coding efficiency and the impact of correlations. *Nature neuroscience*, *7*(10), 1129.

Shumway, C. A. (1989). Multiple electrosensory maps in the medulla of weakly electric gymnotiform fish. I. Physiological differences. *Journal of Neuroscience*, *9*(12), 4388-4399.

Sofroniew, N. J., Vlasov, Y. A., Hires, S. A., Freeman, J., & Svoboda, K. (2015). Neural coding in barrel cortex during whisker-guided locomotion. *Elife, 4*, e12559.

Solomon, S. G., Peirce, J. W., Dhruv, N. T., & Lennie, P. (2004). Profound contrast adaptation early in the visual pathway. *Neuron*, *42*(1), 155-162.

Stopfer, M., & Laurent, G. (1999). Short-term memory in olfactory network dynamics. *Nature*, *402*(6762), 664.

Sullivan 3rd, W. E. (1982). Possible neural mechanisms of target distance coding in auditory system of the echolocating bat *Myotis lucifugus*. *Journal of neurophysiology*, *48*(4), 1033-1047.

Tabor, K. M., Smith, T. S., Brown, M., Bergeron, S. A., Briggman, K. L., & Burgess, H. A. (2018). Presynaptic inhibition selectively gates auditory transmission to the brainstem startle circuit. *Current Biology*, *28*(16), 2527-2535.

Takeshita, D., & Gollisch, T. (2014). Nonlinear spatial integration in the receptive field surround of retinal ganglion cells. *Journal of Neuroscience*, *34*(22), 7548-7561.

Theunissen, F. E., & Shaevitz, S. S. (2006). Auditory processing of vocal sounds in birds. *Current opinion in neurobiology*, *16*(4), 400-407.

Tinsley, J. N., Molodtsov, M. I., Prevedel, R., Wartmann, D., Espigulé-Pons, J., Lauwers, M., & Vaziri, A. (2016). Direct detection of a single photon by humans. *Nature communications*, *7*, 12172.

Tschida, K., & Mooney, R. (2012). The role of auditory feedback in vocal learning and maintenance. *Current Opinion in Neurobiology*, *22*(2), 320-327.

Turner, M. H., Schwartz, G. W., & Rieke, F. (2018). Receptive field center-surround interactions mediate context-dependent spatial contrast encoding in the retina. *Elife, 7*, e38841.

Wissig, S. C., & Kohn, A. (2013). The influence of surround suppression on adaptation. *J. Neurosci*, *33*(2), 532-543.

Woolley, S. M., Gill, P. R., & Theunissen, F. E. (2006). Stimulus-dependent auditory tuning results in synchronous population coding of vocalizations in the songbird midbrain. *Journal of Neuroscience*, *26*(9), 2499-2512.

Woolsey, T. A., & Van der Loos, H. (1970). The structural organization of layer IV in the somatosensory region (SI) of mouse cerebral cortex: the description of a cortical field composed of discrete cytoarchitectonic units. *Brain research*, *17*(2), 205-242.

Zagha, E. (2020). Shaping the Cortical Landscape: Functions and Mechanisms of Top-Down Cortical Feedback Pathways. *Frontiers in Systems Neuroscience*, *14*, 33.

Zhang, K., & Sejnowski, T. J. (1999). Neuronal tuning: To sharpen or broaden?. *Neural computation*, *11*(1), 75-84.

Zirkelbach, J., Stemmler, M., & Herz, A. V. (2019). Anticipatory neural activity improves the decoding accuracy for dynamic head-direction signals. *Journal of Neuroscience*, *39*(15), 2847-2859.

Chapter 2

Prologue

There has been extensive research on how wave-type weakly electric fish use their electric sense when foraging for food. Small prey items such as aquatic worms, will strongly stimulate only a very small portion of the total electroreceptor array (i.e., local stimulus). Signals generated by conspecifics (e.g., other weakly electric fish), stimulate the entire array of electroreceptors with different beat strengths at various points along the fish's body (i.e., global stimulus). The exact pattern of stimulation changes based on one fish's location, distance, and/or orientation relative to the other fish in three-dimensional space. Understanding the spatio-temporal structure of the signal as it reaches the receptors is essential to clarify how this signal is processed throughout the nervous system. Therefore, we must have a complete characterization of where the receptors are located and what the strength of the signal is at those locations to fully understand the sensory dynamic that occurs during realistic behavioral scenarios.

In this chapter, I estimate the strength of the electric signal reaching the electroreceptive periphery during social interaction. To do so, I map out the electroreceptor array, implement an electric field model to simulate weakly electric fish interaction in a variety of spatial contexts, and use the signal strength as a stimulus input for an electroreceptor population comprised of 8,195 leaky integrate-and-fire, computational models. My results provide a quantitative description of the signal as it reaches each receptor, thereby enabling us to estimate the limits of sensory detection and investigate more precisely the transformation imposed by the nervous system.

Note: This chapter was submitted for publication as:

"Ramachandra, K. L., Milam, O. E., Pedraja, F., Cornett, J., & Marsat, G. (2023). Detection and localization of conspecifics in ghost knifefish are influenced by the relationship between the spatial organization of receptors and signals. Current Biology. Submitted"

My contribution to this manuscript consisted of the histological characterization of the receptors' locations and distribution, in addition to the enhancement of the EI model with spatially distributed receptors. I also contributed to the writing of the manuscript.

Abstract

The detection and localization of signals relies on arrays of receptors and their spatial organization plays a key role in setting the accuracy of the system. Electrosensory signals in weakly electric ghost knifefish are captured by an array of receptors covering their body. While we know that spatial resolution for small objects, such as prey, is enhanced near the head due to a high receptor density, it is not clear how receptor organization influences the processing of global and diffuse signals from conspecifics. We investigated the detection and localization accuracy for conspecific signals and determined how they are influenced by the organization of receptors. To do so we modeled the signal, its spatial pattern as it reaches the sensory array, and the responses of the heterogeneous population of receptors. Our analysis provides a conservative estimate of the accuracy of detection and localization (specifically azimuth discrimination) of a conspecific signal. We show that beyond 20 cm the conspecific signal is less than a few percent the strength of the baseline self-generated signal. As a result, detection and localization accuracy decreases quickly for more distant sources. Detection accuracy at distances above 40 cm decreases rapidly and detection at the edge of behaviorally observed ranges might require attending to the signal for several seconds. Angular resolution starts to decrease at even shorter distances (30 cm) and distant signals might require behavioral or neural coding mechanisms that have not been considered here. Most importantly, we show that the higher density of receptors rostrally enhances detection accuracy for signal sources in front of the fish, but contributes little to the localization accuracy of these conspecific signals. We discuss parallels with other sensory systems and suggest that our results highlight a general principle. High receptor convergence in systems with spatially diffuse signals contributes to

detection capacities, whereas in systems with spatially delineated signals, receptor density is associated with better spatial resolution.

Introduction

Whether it is the early detection of a predator, the accurate localization of a mate, or finding food sources based on weak cues, the sensitive detection and localization of sensory signals can be an advantage. Signal detection and localization typically rely on an array of sensory receptors; their sensitivity, number, and spatial organization play a key role in setting the accuracy of the system. For example, visual resolution is enhanced by the high receptor density in the retina's fovea, sound localization is largely enabled by the binaural configuration of the auditory system, and moths can detect the presence of just a few pheromone molecules due to the number and convergence of olfactory receptors (Ashida and Carr, 2011; Provis et al., 2013; Rospars et al., 2014). While the spatial structure and size of the receptor array clearly shape the sensitivity of the system, it is not always clear how the configuration of the receptors is related to detection accuracy versus localization.

The electrosensory system in fish is an exquisite example of sensitivity. In ghost knifefish in particular, survival depends on navigating, detecting prey, and communicating through this active sense. They generate a constant weak electric field with their electric organ (EO) and any distortions of this field by preys or objects in their environment are picked up by an array of receptors covering the skin of the fish (Nelson et al., 1997; Pedraja et al., 2014). Distortions from an object or prey will impact only a spatially defined subset of receptors on the corresponding portion of skin onto which the electric image (EI) of the object is projected. By activating the corresponding portions of the topographic maps higher in the sensory system,

spatial information is encoded in a sort of labeled-line code reminiscent of the way the visual or somatosensory system is organized. Furthermore, similar to these modalities (i.e., fovea of the retina), regions of higher receptor density towards the head and snout of the fish provides a higher spatial resolution particularly useful in the last stage of prey capture as the target approaches the fish's mouth (MacIver et al., 2001; Nelson and Maciver, 1999). They also detect and communicate with one another through this electric sense (Allen & Marsat, 2018; Knudsen, 1975; Petzold et al., 2016). The ongoing electric organ discharge (EOD) is a spatially diffuse signal that can reach globally all the receptors of the other fish's body. Localization of such signals would thus have to rely on differences in the signal strength at different input locations, similar to the way the auditory system compares binaural inputs to localize sound sources (see Milam et al., 2019, for review). While it is clear that the high rostral density of receptors can enhance the spatial accuracy for objects, it is not clear how it influences the processing of diffuse and global signals from another fish's EOD. More specifically, we are interested in determining how the spatial organization and density of receptors interact with the spatial structure of EOD signals to influence the detection and localization of conspecific signals.

The EOD generated by the long EO located in the caudal 2/3 of the fish can be approximated as a dipole whose polarity switches during each EOD cycle (Rasnow et al., 1993). The resulting signal is a quasi-sinusoidal output with frequencies between 500 Hz and 1000 Hz (in *A. leptorhynchus*, the focal species in this paper; Zupanc and Maler, 1993). Although weak, this signal will travel several tens of cm and will permit the long-range detection of the conspecific (Pedraja et al., 2016). Behavior studies demonstrated that frequent interactions occur at distances of 30 cm or less, but there is evidence from field studies that these fish might

be able to detect and navigate toward one another at distances in the 1-meter range (this upper limit has not been quantified systematically; Henninger et al., 2018; Stamper et al., 2012; Stamper et al., 2013; Zupanc et al., 2006). These distant signals will reach the receptors with low intensity as the strength of electric signals decreases exponentially with distance. The signal from a distant fish will combine with the signal of the fish's own EOD resulting in a combined electric field with sinusoidal amplitude modulations designated as the beat. If the distant fish's signal reaches the focal fish with an amplitude $1/10^{th}$ the strength of the self-generated EOD, this beat modulation will have an amplitude of $1/10^{th}$ the undisturbed EOD. These weak beat contrasts are the signals that must be encoded to detect a conspecific and differences in contrast at receptors across the fish's body constitute the localization cues. The mathematical framework to estimate the strength and structure of the electric field during social interactions has been detailed in previous studies (Caputi and Budelli, 2006; Castello et al., 2000; Gómez-Sena et al., 2014; Kelly et al., 2008). It can be used to quantify the strength of the signal as it reaches each receptor to obtain a complete characterization of the sensory input structure due to an approaching conspecific.

Ghost knifefish possess several types of electroreceptors, we focus here on p-unit tuberous receptors that constitute the vast majority of electroreceptors, are tuned specifically to encode conspecific signals, and are responsible for encoding the amplitude of these beat contrasts (Bennett et al., 1989). Previous estimates of p-units receptor density range from 9-15 per mm^2 on the head region to 0.6-3.4 over the trunk area (Carr et al., 1982). A thorough quantification of receptor density as a function of dorso-ventral/rostro-caudal location in *A. leptorhynchus* is not yet available. Receptor sensitivity and response properties have been extensively studied

and several neural models of p-units are available (Benda et al., 2005; Chacron et al., 2005; Goense and Ratnam, 2003; Gussin et al., 2007; Nelson et al., 1997; Ratnam and Nelson, 2000). This large population of several thousand receptors will converge to the primary sensory area in the hindbrain, the electrosensory lateral line lobe, and the information is then transmitted down the sensory pathway (Lannoo et al., 1989; Maler et al., 1991). To estimate the information carried by the population of receptors about realistic signals, two key elements must be considered. First, we must take into account the response properties of the receptors, their sensitivity/noisiness, and their heterogeneity across the population. Second, we must consider the structure of the stimuli and how signals from different locations will cause input strengths that vary across the receptor positions.

In this paper, we aim to clarify how spatially realistic signals from conspecifics are encoded by the population of electroreceptors. Our approach includes using a model of the fish's electric field to quantify the EI strength at each receptor location. This input drives a model of the p-unit population consisting of heterogeneous leaky-integrate-and-fire units calibrated based on the extensively documented properties of this population. We then use a decoding analysis to estimate the information that can be extracted from the receptor population and provide a conservative estimate of the expected detection and localization accuracy. We specifically hypothesize that the high density of receptors rostrally will enhance detection and localization accuracy, particularly in the frontal quadrant. We tested this hypothesis by altering the structure and density of the receptor population and confirming that detection accuracy depends on receptor density. Surprisingly, we show that localization is relatively less influenced by receptor density and that the high rostral density does not enhance localization accuracy for

frontal azimuth. Our results highlight the intricate relationship between the spatial structure of signals and the spatial organization of sensory receptors.

Methods

Quantification of electroreceptor distribution

Weakly electric brown ghost knifefish, *Apteronotus leptorhynchus*, were obtained from a tropical fish supplier (Segrest Farms, FL, USA). Fish care and use were approved by West Virginia University IACUC.

Fish were euthanized then fixed in a 50mL aliquot containing a 40mL solution of 4% paraformaldehyde, and preserved for up to 7 days. After tissues were completely fixed, 5mg of eosin Y was added to the aliquot containing the preserved fish. Stained fish were analyzed under a fluorescent microscope with a light wavelength of 530nm. A stereotaxic system was used to move the fish and place a $1mm^2$ sampling grid at different locations along the fish's body, tuberous receptors inside the grid were visually identified and counted. We collected 581 samples from 18 fish measuring on average 14 cm in length.

A coarse 3D mesh model of the fish was created using Maya 2019 (Autodesk, Inc) based on average measurements of our fish and images of the rostral, dorsal, and lateral profiles. The quadrangle mesh model has 218 planar faces. For each face, the corresponding measured receptor densities were averaged. Average receptor densities for each face were mapped along a rostro-caudal and dorsal-ventral plane. A 3-dimensional 5^{th}-degree polynomial was fitted to obtain a smooth, interpolated, estimate of receptor density as a function of body location.

Using a more detailed mesh model (the same used for EI calculation; see below), we randomly generated receptor locations for each face according to our density function.

EI model

The electric image model used in this study was based on the established methods developed by Caputi and Budelli (Caputi and Budelli, 1995; Caputi and Budelli, 2006; Caputi et al., 1998), and implemented using software developed by Rother (Rother et al., 2003). More details on the model can be found in these publications and it is described here briefly. The EI model requires the creation of a reconstruction of the geometry and electrical properties of the fish bodies and their placement in the surrounding water. This information is used to calculate the transcutaneous voltage at specific nodes along the skin of the fish. The model makes the following assumptions:

1. All the media are ohmic Therefore, $J(x) = \sigma(x)E(x), \sigma(x) > 0$ (1)

Where J(x) is the current density at point x and E(x) is the electric field at the same point.

2. There are no capacitive effects so at no point in space is there an accumulation of charge. $\frac{\delta p(x)}{\delta(t)} = 0$ (2)
3. The model is an electrostatic approximation (Bacher, 1983)
4. The fish and other objects that make up the environment are immersed in an infinite water medium. Each object in the environment is covered by a thin resistive layer (the skin in the case of the fish), which can be homogeneous or heterogeneous.

The model is based on the charge density equation which, under the above assumptions, implies that the charge generated by the sources f(x) is equal to the charge diffusion:

$$\frac{\delta p(x)}{\delta(t)} = f(x) - \nabla.J(x) \quad (3)$$

Combining equations 1 and 2 we get

$$\nabla.J(x) = f(x) \Rightarrow \sigma\nabla.E(x) = f(x) \quad (4)$$

The electric field E(x) can be expressed as $E(x) = -\nabla\varphi$ therefore:

$$\sigma\nabla^2\varphi(x) = -f(x) \quad (5)$$

Equation (5) is a partial differential equation known as the Poisson equation and can be solved for every point in space, in our case the fish boundaries by using the boundary element method (BEM) as proposed by Assad (Assad and Bower, 1997). The method determines the boundary conditions by solving a linear system of M•N equations for M poles and N nodes, with the unknown variables being the transepithelial current density and voltage at each node (Pedraja et al., 2014). The shape of the 3D fish mesh model consists of 49 ellipses composed of 17 nodes each (i.e., 835 nodes) defining 1,666 triangular faces between the nodes (Rother et al., 2003). The size of the fish was kept constant at 14 cm in length in this paper and the water conductivity is 300 µS and the skin and internal conductivity of the fish were 100 and 10,000 µS respectively. The 2 poles for each fish were positioned 9.3 and 10.5 cm from the rostral tip of our 14 cm fish. We use the middle of this dipole (i.e., the center of our “electric organ”) to define the position from which the signal originates.

Calculations of signal strength at receptor locations

We calculate the transdermal voltage when only the focal fish is present (*Vf*) or when both focal and sender fish are present (*Vfs*), in which case the peak voltage is determined at the top

of the beat cycle (EODs in phase). The strength of the EI caused by the sender fish at each node *i* on the surface of the focal fish was defined as a contrast *c*:

$$c = \frac{Vfs_i - Vf_i}{Vf} \quad (6)$$

The contrast value for receptor location within each triangular face was interpolated from the values at the nodes that define the face using a barycentric coordinates system. Considering a triangle with values *N* at the nodes (vertices) and coordinates *X, Y, Z*. A receptor inside the triangle will have a contrast value *R* according to the weighted value of the nodes. The weights *W* can be found by solving:

$$X_R = W1 \cdot X_{N1} + W2 \cdot X_{N2} + W3 \cdot X_{N3} \quad (7)$$

$$Y_R = W1 \cdot Y_{N1} + W2 \cdot Y_{N2} + W3 \cdot Y_{N3} \quad (8)$$

$$Z_R = W1 \cdot Z_{N1} + W2 \cdot Z_{N2} + W3 \cdot Z_{N3} \quad (9)$$

And contrast at the receptor location is calculated as:

$$R = W1 \cdot N1 + W2 \cdot N2 + W3 \cdot N3 \quad (10)$$

Although the EI model was thoroughly calibrated based on experimental recording on actual fish (Pedraja et al., 2014; Pedraja et al., 2016), we performed transcutaneous recordings on 3 pairs of fish and verified that the transdermal voltage contrast values that we are calculating correspond to the range of values that can be measured experimentally.

Receptor Modeling

We used a leaky integrate and fire (LIF) framework to model the receptors. The model includes noise σ and adaptation current with conductance g_α and reversal potential E_α, and is driven by an input *I*. The membrane voltage is calculated as:

$$\tau_m \frac{dV}{dt} = E_m - V + R_m(I + \sigma - g_\alpha(V - E_\alpha)) \quad (11)$$

The initial parameters of the model were based on existing models (Benda et al., 2005; Carlson and Kawasaki, 2006; Chacron et al., 2001; Nelson et al., 1997). Particularly, the noise was the product of a strength variable A_σ and a random process (specifically, two Ornstein–Uhlenbeck processes; refer to Chacron et al., 2001, for details). Adaptation current α was adjusted to match the time course of adaptation described experimentally (Benda et al., 2005). Conductance g_α is augmented by Δ_α after each spike and decays with time constant τ_α. When the membrane voltage reaches the threshold V_T it is reset to V_R and kept constant during a refractory period t_R. The input I to these p-unit model neurons replicates the input they would receive from receptor cells during social interactions. A sinusoidal EOD carrier signal with amplitude A_{EOD} was created with a frequency of 1000 Hz (the upper range of the naturally occurring EOD frequencies in this species was used for convenience), and modulated with a sinusoidal amplitude modulation (the "beat") of 30 Hz (other AM envelopes are used to validate our model, see Supplementary Material). This AM envelope signal was adjusted to a specific contrast as specified in the Results. A contrast of 0% indicates that the baseline EOD is unmodulated. Whereas a beat contrast of 100% causes the EOD amplitude to be 0 during the trough and twice the baseline EOD amplitude at the peak of the beat. To emulate the current direction and sensitivity as the signal passes through the receptor cells before it reaches the p-unit neurons, the modulated EOD is halfwave rectified after a baseline bias β was subtracted.

Parameters were adjusted to create a prototypical neuron with response properties matched to published data (Bastian, 1981; Benda et al., 2005; Chacron et al., 2005; Grewe et al., 2017; Gussin et al., 2007b; Nelson et al., 1997; Ratnam and Nelson, 2000). We used a wide

range of response parameters to validate our model: firing rate, coefficient of variation, response sensitivity to random amplitude modulations, response sensitivity and time course to steps and responses to beat stimuli (see Supplementary Figure S1). This prototypical neuron with response properties matched to the average experimental values served as our original seed; this set of parameter values are given in Supplementary Information Table S1.

We then used this original seed to create a heterogeneous population that replicates the range of response properties observed experimentally through an iterative process of diversifying the population and constraining the response properties. A heterogeneous array of parameters sets was created (8,000 sets) from the original seed values by slightly varying randomly several parameters: t_R, R_m, τ_m, V_T, A_σ, τ_α, Δ_α, and β. From this array, 12 seeds were selected by choosing sets of parameters that, again, best replicate the average response properties. These sets were further diversified randomly, and from these new arrays, 26 seeds were chosen by selecting neurons that replicate the average coding properties, but that span the range of spontaneous firing rates measured experimentally (Chacron et al., 2001; Gussin et al., 2007; Ratnam and Nelson, 2000). From these 26 seeds, the parameter sets were further diversified, and we retained 9,200 sets of parameters by rejecting sets for which the response properties do not fit in the range of response properties determined experimentally. Therefore, our pool of neurons replicates the average and range of response properties measured experimentally. From this pool, 5 equivalent but different populations of 8,195 receptors were created by randomly assigning one of the 9,200 neurons to each receptor location. All data shown in the results reflect averages across these 5 populations.

Decoding analysis

Population responses to different stimuli were compared with our decoding analysis to determine how accurately signals could be detected or discriminated considering the differences in response patterns for these stimuli. The framework used for our decoder has been described and validated thoroughly in previous publications (Marsat et al., 2023; Allen and Marsat, 2018; Allen and Marsat, 2019; Allen et al., 2021; Marsat and Maler, 2010). It was shown that this analysis measure is directly correlated with the information content of the responses about the stimuli. We describe the method briefly here. Importantly, the only difference with the established measure described in Marsat et al. (2023), is that we do not use the detailed time-course of each neural response (i.e., the full spike trains), but use the peak-to-though firing rate to quantify the response of the neuron. To calculate the peak-to-trough firing rate, the binarized spike trains are smooth with a sliding square window of 16.67 ms (half a beat cycle) to obtain an instantaneous firing rate. For each beat cycle, the difference between the maximum of the instantaneous firing rate and the minimum gives us our measure of peak-to-trough firing rate. These peak-to-trough measures can be averaged over several cycles of the beat, or we can use the values for single beat cycles as specified in the different Results section. When no beat stimulus is provided, the analysis is unchanged and the peak-to-trough is calculated over each consecutive 33.34 ms segments of response (i.e., a 30 Hz period).

Pairs of responses are compared by the analysis: responses to stimuli from two different azimuths are compared in the angular resolution analysis while in the detection analysis the response to the sender fish's signal is compared to the response when no second fish is present (i.e., baseline firing due to the focal fish's own signal). For each individual neuron *i* (out of *n*

total neurons*)*, the similarity between the probability distributions *P(x)* of responses (the peak-to-trough firing rate *x*) to the two stimuli (*R* and *B*) is calculated based on the area difference $\Omega_{(P_R,P_B)}$ between the two distributions:

$$\Omega_{(P_{Ri},P_{Bi})} = \sum_x |P_{Ri}(x) - P_{Bi}(x)| \quad (12)$$

AD values are normalized to 1 across the *n* neurons to obtain a weight W:

$$W_i = H_0(\Omega_{(P_{Ri},P_{Bi})} - \frac{1}{n}\sum_n \Omega_{(P_{Rn},P_{Bn})} + 1) \quad (13)$$

where H_0 is the Heaviside step function. The peak-to-trough firing rates for each neuron are multiplied with these weights before being used in our Euclidean distance calculations (see below). As a consequence of this weighting, the neurons that respond very differently to the two stimuli will contribute more to Euclidean distance between the population responses and the neurons that respond similarly to the two stimuli will contribute little to the Euclidean distance. Since the sum of the weight for a population is 1, the overall firing rate of the population is unchanged by the weighting procedure.

The Euclidean distance *D* between pairs of weighted responses (R_a and R_b) is calculated between responses to the same stimulus or between responses to the two different stimuli being compared:

$$D = \sqrt{\sum_{nt}(R_a - R_b)^2} \quad (14)$$

These Euclidean distances are used to determine how well an ideal observer could discriminate between responses to the two stimuli. The distribution of distances between responses to the same stimulus D_{xx} and the distribution of distances between responses to the two different stimuli, D_{xy}, are used for an ROC analysis. In this analysis, a threshold distance *T* is varied. For each threshold, the probability of non-discrimination (P_D) is calculated as the sum of $P(D_{xy}>T)$

and the probability of false discrimination *(P_F)* is calculated as the sum *$P(D_{xx}>T)$*. The error rate *E* is taken as the minimum error across threshold given:

$$E = \frac{1}{2}P_F + \frac{1}{2}(1 - P_D) \quad (15)$$

This error rate is used in the various parts of the result as specified therein, and we consider that reliable detection or discrimination happens when the error rate is below 0.05.

Results

Since ghost knifefish can detect and localize each other based on the electric signals they continuously emit; both fish are thus senders and receivers at the same time. To simplify the description of our results we describe the fish for which we describe the electric image (EI) and sensory responses as the focal fish. The "other" fish that needs to be detected and localized by the focal fish is designated as the sender fish. A number of studies have characterized the EI that one fish causes on another fish's body (Kelly et al., 2008; Pedraja et al., 2016). The results presented in these papers are not always easily related to electrophysiological studies because many experiments on the responses of sensory neurons in this system calibrate the signals as a relative contrast in the measured voltage. For example, many studies present the response properties to conspecific signal of 5-10% contrast (Fotowat et al., 2013; Metzen et al., 2018). Since our goal is to use the estimate of signal strength as an input to neuron models that match their known response properties, we quantify the EI strength as a relative contrast in the transdermal potential difference. If the signal from the sender is as strong as the focal fish's own baseline signal at a given point on their body, the signal strength will be 100% and the EOD

will vary from close to 0 mV (at the trough of the beat) to twice the baseline EOD strength (at the peak of the beat cycle).

Expressing the signal as a contrast highlights the challenges that the fish encounters when interacting with a conspecific due to the rapid decay of signal strength with distance. Figure 1 displays the signal strength during a common scenario a sender fish approaching and then moving away from the focal fish. When the fish are separated by only a few centimeters (position 2), the EI has a strong gradient that goes from a strong signal (25% contrast) on portions of the body closest to the sender to a very weak signal close to 0% contrast. For convenience, we will refer to the region of the electric image with the strongest signal as the hot spot. While this hotspot is well defined when the sender is close-by, the EI is much more diffuse when the sender is further away and there is a weaker gradient between the hotspot and the areas with a weaker signal. For example, in Fig 1B, the difference between the hot spot near the head (position 1) or tail (position 3) is less than 1% stronger than the portions with the weakest signal. The positions 1 and 3 depicted here correspond to a distance (30 cm) at we know fish can detect each other and display active interactions (Henninger et al., 2018; Zupanc and Maler, 1993; Zupanc et al., 2006). The known extreme sensitivity of this system is thus highlighted here since detecting the sender 30 cm away involves detection of a 1% modulation, and localizing this signal requires deciphering a gradient in this signal of less than 1% across the body surface.

The EI stimulates an array of receptors covering the fish's skin and the spatial structure of this sensory array will dictate how the spatial structure of the signal is captured. Receptor density for different portions of the fish's body has been characterized in a closely related

species (Carr et al., 1982), but we needed a more detailed quantification of variations in receptor density across the fish's body (Fig 2A). Our data confirm the general organization of receptor density: a region of high density on the snout and head, of medium density on the dorso-rostral portion of the trunk that decreases both ventrally and caudally (Fig 2B). Based on this spatially precise empirical data, we incorporated a population of p-unit receptor locations on the 3D mesh model used for EI calculations that varies smoothly in density as a function of rostro-caudal and dorso-ventral position (Fig 2C). In the rest of this study, we will use an "average" fish that measures 14 cm long and includes ~8,195 receptor locations.

We calculated the stimulus intensity for each receptor location for the various iterations of the EI calculation; the result for the 3 positions illustrated in Fig 1 is shown in Fig 3A (note that for this figure, the blue-red color scale covers the contrast range for each position). We wanted to quantify how the strength of the EI changes with the position of the sender relative to the focal fish. To do so, we ran the model for 864 relative positions where the two fish are at 12 distances that vary from nearly touching to 75 cm apart and for 72 different azimuths around the focal fish while always having the sender fish's heading towards the focal fish. To estimate the maximal strength of the signal for each location, we used the strength of the signal at the center of the hot spot on the focal fish. We plot this value as a color scale at the position of the middle of the electric organ of the sender fish (Fig 3B). We can see that the strength of the signal decreases sharply with distance as expected. The portions of the figure with contrast above 20% (yellow-white shades) represent positions where the fish are nearly touching (with the sender fish head-on). The decrease in signal strength with distance follows the expected

power law such that contrast drops to 10% by 10-15 cm and is only a few percent when the sender is 20-30 cm away (Fig 3C).

The EI model helps us quantify the cues that the sensory system can use to detect and localize the source of these signals. To better understand the accuracy with which detection and localization could occur, the strength of these signal must be compared with the noise that the sensory system experiences. We therefore use the deterministic model of EI signal strength described above as an input to a population of model neurons that includes realistic noise. We based our receptor model on established parameters of leaky-integrate-and-fire that includes adaptation, noise, and a refractory period, to replicate the response properties of p-units (Benda et al., 2005; Chacron et al., 2005; Grewe et al., 2017; Gussin et al., 2007; Nelson et al., 1997). Based on this prototype p-unit model, with properties matched to the average characteristics of p-units, we diversified the model parameters to create a heterogeneous population matching the range of properties observed experimentally (see Methods for details). For the model to provide a biologically reasonable estimate of how accurately this population encodes spatial cues, it is vital to calibrate the sensitivity, heterogeneity and noisiness of the responses to reflect the measured properties of the neurons. Our calibration involved matching the model responses to published values for a range of stimulus types and analysis methods (see Methods and Supplementary Figure S1). The population is then stimulated with conspecific signals (beat stimuli) at intensity levels that is dictated by the EI image for various relative fish positions. Figure 4 shows the response pattern of the population for two of the positions used in Figure 1 and 3. Response strength is quantified as the difference between the peak and though of the instantaneous firing rate during each stimulus

cycle (here normalized relative to spontaneous activity). We can see differences in response strength due to the spatial contrast in the EI but also differences across receptors due to heterogeneity that makes some neurons more sensitive.

Firing rate modulation across one stimulus cycle replicates the experimentally measured sensitivity (Fotowat et al., 2013; Henninger et al., 2018; Pedraja et al., 2014; Pedraja et al., 2016; Zupanc et al., 2006) The strength of the electric image quickly decreases with distances and reaches levels below 1% contrast at ranges where the fish still detect and interact with each other (e.g., 30 cm). Our model replicates the fact that for these weak signals, the response modulation is barely above variations in firing rate that naturally occur in the absence of a second fish (Fig 5). Figure 5C shows that, although the responses for nearby fish (14 cm and 22.5 cm in this figure) are visibly different from spontaneous response, signals from more distant fish (40 cm, 75 cm in this figure) cause much more subtle differences in response strength. This is true when looking at the distribution of responses for cycles of the beat, for responses averaged across time (gray or color portion of the distribution plots), or overall responses averaged across time and neurons (white lines).

The sensitivity with which a conspecific signal would be detected will depend on the coding and decoding mechanisms implemented by the nervous system. It is beyond the scope of this article to explore all possible coding and decoding algorithms that could contribute to the sensitivity of the system, but as a first step towards understanding the sensitivity of this system, we aim to provide a lower-bound on accuracy. To do so, we only consider peak-to-trough firing rate to quantify response strength as it is the most salient aspect of the response that varies with stimulus strength. The responses of individual receptors will be combined at higher levels

of the nervous system and this can help average out noise in the responses. However, the way these responses are combined would require various assumptions, matched to the architecture of high brain areas, that would lead to a complex modeling effort and speculations on decoding procedure. For this reason, and to remain within a “lower-bound” perspective, we map each population response in Euclidean space where each dimension represents the response strength of a neuron (i.e., response strength is not averaged across neurons). Reliable detection would occur if the strength of the population response is markedly different from the response when no signal is present; in other words, when the stimulus response is far from baseline responses in this Euclidean space representation. Our analysis therefore uses a weighted Euclidean distance followed by an ROC analysis to quantify the reliability with which stimulus responses can be differentiated from baseline. This analysis could be done on “instantaneous responses”, considering the response of the population (peak-to-trough for each receptor) for a single cycle of the stimulus which would give us a response accuracy (i.e., probability of error) for each fish positions. Behavioral responses typically occur after attending the signal for a certain period of time, and more accurate detection occurs after several seconds of the stimulus than after the first cycle. We therefore integrate the response of each neuron across time (average the peak-to-trough across several beat cycles) to estimate how detection accuracy would change as information is accumulated with time. We consider that accurate detection occurs when less than 5% detection error would occur and plot the amount of time that accurate detection would require (see Fig 6). Our analysis shows that accurate detection could occur within a single cycle of the stimulus for fish that are within 20 cm of the focal fish (Fig 6A, 6C). Detection accuracy decreases with distance and thus it takes more time to reliably

detect the stimulus. As a result, a fish 60-70 cm away would require integrating the signal for several seconds to be able to reliably tell that another fish is present.

Detection accuracy is undoubtedly influenced by the fact that thousands of receptors contribute to transmitting this information. The distribution of these receptors is not uniform across the fish's body. In particular, the rostral end of the fish (head region) has a density of receptors 5-10 times higher than the caudal end (tail region). We hypothesize that this foveal organization supports an enhanced sensitivity in the frontal quadrant relative to the fish. Alternatively, the increased density in receptors plays an important role in localizing small objects like prey with higher resolution, but does not enhance perception of conspecific in specific regions of space. This is a plausible alternative because conspecific signals cause a more diffuse EI that stimulates a majority of the receptors over the receiver's body. To test our hypothesis, we reduced the density of receptors to make it uniform over the entire body and equal to the low density found at the caudal end of the fish (Supplementary Figure S2). Our resulting population has 2,770 receptors compared to 8,195 for the full population. The difference in detection sensitivity is displayed in Figure 6B and reveals the enhancement in sensitivity afforded by the increased density in the rostral portion of the body. The difference is negligeable when the sender is very close because accuracy is high and a decrease in the number of receptors encoding the stimulus is not sufficient to affect performance. For very distant signals (e.g., 75 cm), the lower rostral density causes a decrease in sensitivity that is fairly uniform across azimuth (see also Supplementary Figure S3). This can be explained by the fact that distant signals cause diffuse EI patterns that vary by less than 1% across the body (e.g., see Figure 1). As a result, the head region is stimulated at a level nearly identical to the tail

region even if the sender fish is located behind the focal fish. There is, however, a clear difference as a function of azimuth for medium distances (35-50 cm; Figure 6B and Supplementary Figure S3). The higher density of receptors on the head provides a clear advantage in detection accuracy in the frontal quadrants (i.e., requires less time until accurate detection occurs). We further verified the idea that having a larger population of receptors allows the population to encode the presence of the stimulus more reliably by decreasing further the density of our uniform population of receptors by 2-, 4- and 8-fold (resulting in population sizes of 1,385, 693 and 347 receptors respectively). Our analysis confirms that a higher density of receptors allows more accurate detection for distances where the signal is faint (Figure 6C).

We next inquire about the spatial information about the angular position of the sender fish relative to the focal fish: its azimuth (in front=0°; behind= 180°). To do so, we compare the responses to stimuli at various positions and quantify how reliably these responses could be discriminated based on the same weighted Euclidean distance analysis used above. Error probability will thus depend on two factors, angular separation between the two stimuli and duration of stimulus evaluated whereas in our previous detection analysis the latter was the only factor considered. To be able to display our results conveniently, we chose to keep the duration of the stimulus integration to 1s. This value is a compromise between expecting accurate angular discrimination instantaneously (~1 cycle) and expecting the sender fish to remain in a relatively fixed position for seconds in order for angular position to be accurately estimated. Using this 1s integration time, we determined the angle that needed to separate two stimuli to lead to reliable discrimination (<5% error) and call this value angular resolution

(Figure 7). Our results show that angular resolution is accurate to a few degrees (<5°) when the sender is within 10-20 cm and decreases sharply between 20 and 40 cm such that beyond 40 cm, azimuth could not be reliably determined (angular resolution>180°). If we repeat the analysis using different integration times (Fig 7B); as expected, the sharp decrease in angular resolutions moves from being for positions 20 cm away when a single cycle of the beat is considered to being 40-50 cm away when 3.3s of the stimulus is being averaged. Our analysis suggests that for the most distant positions tested (75 cm) angular position could not be resolved even when the stimulus is being integrated for several seconds. Together with the results of Figure 6, these finding thus suggest that for the more distant signals only detection would occur, and the position of the sender would not be accurately determined without relying on additional behavioral or neural mechanisms (see Discussion).

Angular resolution does not appear to be equally good for a given distance as a function of the azimuth of the sender (e.g., front vs. side vs. back). This can be seen in Figure 7A where the color patterns around the focal fish are not perfectly circular. In particular, worse angular resolution occurs at a shorter distance in the back quadrant compared to the front. We suspected that the way we equalized distance across angle could cause a bias. The center of the focal fish is taken as the average receptor position and the center of the sender as the middle between the two emitting poles that constitute the EOD source. Center-to-center distance and azimuth were used to set our relative positions. In this arrangement, a fish at 130° (in the back quadrant, see fish illustrated in Fig 7A) rotating 5° would not only change azimuth but also come closer to the focal fish if we consider the two closest points on each fish's bodies. Note that this is not an issue in our detection analysis since our accuracy measure does not depend

on the comparisons between two stimuli locations but only on the absolute location of a single stimulus. We therefore repeated our angular resolution analysis by comparing angular resolutions where the distance between the rostral tip of the sender and the closest point on the body of the receiver is kept constant (the dots in Fig 8A show the positions of the rostral tip of the sender used in our analysis). We found that angular resolution is better in the frontal quadrants than at the back (Fig 8A, 8C). Surprisingly, it is not best directly in front of the focal fish (0°) but rather on the side (90°). Since we expected the high density of receptors on the head of the fish to help enhance localization accuracy, we hypothesize that angular resolution is particularly good as the edge of the hotspot caused by the sender sweeps across the region of high receptor density (which could correspond to sender positions around ~90°). To test the contribution of higher receptor density towards the heads, we repeated the analysis with the "uniform" receptor population used in the previous section that has an equally low receptor density across the whole body. This uniform population of receptors did not perform much worse than our full population, and in particular there is no striking difference directly in front (0°) or the side (90°) of the fish where resolution is best. Azimuth determination was not possible (angular resolution>180°) when the fish were two body lengths apart (28 cm) but at one body length, the higher density of receptors provided a small advantage. Specifically, there are only a few spots at ~45° and ~125° where the higher receptor density on the rostral portion of the body helps to enhance angular resolution (Fig 8B, 8C). We confirm that decreasing the population density further decreases angular resolution and this is particularly obvious for more distant stimuli (one body length), where localization is still possible but angular resolution is not great (Fig 8D).

Our results demonstrate that the angular resolution is relatively poor at the back and is slightly better on the side than the front. This effect cannot be attributed to the higher density of receptor towards the head. Therefore, we questioned whether this effect could be due to the geometry of the fish's body and how it interacts with the geometry of the electric field. We hypothesize that a small change in angle on the side will cause a relatively bigger change in the electric image than a similar angle difference at the back. A sender fish at 90° azimuth would have its EI hotspot centered on the flat surface of the side of the focal fish whereas for frontal (0°) or caudal (180°) azimuth, the EI hotspots are centered on the pointy rostral and caudal ends of the fish. We quantified how much difference in EI a sender at various azimuth would cause on the focal fish and integrated this difference across the body surface. We found that it correlates strongly with the differences in angular resolution that we have estimated for various azimuth and distances (Figure 8E). Our analysis supports the conclusion that differences in angular resolution as a function of azimuth is in part due to the geometry of the fish and their electric fields.

Discussion

By using a model of weakly electric fish EI and carefully normalizing how we calculate the distance between the relevant points on the two fish, we presented a clear quantification of the strength of the EI as a function of distance. Our results suggest that strong signals of more than a few percent beat contrast, only occur at distances below 15-20 cm. This finding is in agreement with empirical data and consistent with the fact that when two fish actively interact (e.g., chasing each other and courtship), they are typically in close proximity (Fotowat et al.,

2013; Zupanc and Maler, 1993).The relationship we show is quantitatively informative only in a simplified case: a given fish size (and EOD strength) with a fixed heading angle (sender head-on towards focal fish). The strength of the electric image as a function of distance will depend on environmental factors (water conductivity), the individuals interacting (their size and EOD strength), and on moment-by-moment changes in the relative heading angle of each fish. All these factors could be taken into account in a more extensive analysis of EI during social interactions, but it is beyond the scope of our paper. It is also important to point out that additional improvements on the model could provide additional details on the structure and dynamics of the EI such as replicating the bending of the fish's body or having the EO modeled with more spatio-temporal details rather than being a simple fixed dipole. We note that since the strength of the EI at a given receptor location depends on distance and relative heading angles, the strength of the beat AM (i.e., its envelope) cannot serve as a reliable indicator of distance or movement towards/away. Rather, reliable spatial information must take into account the differences in EI strength over the body of the receiver. This is obvious for localizing the azimuth of the target but can also help resolve the distance since a fish close-by will cause EIs with sharper contrasts across the body while distant fish will elicit more uniform EIs.

We used, for the first time in this system, a model of the full population of receptors, replicating their heterogeneous response properties and their spatially realistic input patterns. This allowed us to provide a conservative estimate of the detection range that this sensory input could support. We found that, depending on how the information is extracted, detection would still be possible at 75 cm. This range is comparable to behavioral interactions that report instances where a fish detected and moved towards another or simply interacted electrically

with one another at ranges above 60 cm (Henninger et al., 2018; Stamper et al., 2012; Yu et al., 2012). Our sensitivity estimates might, in fact, come short of the sensitivity observed behaviorally, but this might be because we intentionally provide a conservative estimate. Our estimate relies on a decoding analysis that does not try to replicate sophisticated decoding procedures that could be implemented by the nervous system. Our analysis uses a "Euclidean distance" perspective to quantify similarity in responses where the response of each neuron is kept as separate dimensions. The nervous system will, in various steps of its pathway, combine neural responses and thereby average out noise. An optimized procedure (e.g., using a principal component approach) could be implemented but it would need to be tailored to each stimulus/task being considered. Any realistic attempt to leverage the convergence of receptor input that is performed by higher sensory area would be a major undertaking that could not be simply added to this study. We also use a simple measure of response strength (peak-to-trough firing rate) and although it is likely one of the key elements of the response, other aspects could be considered. Particularly, synchrony among receptors has been shown to encode frequency modulations that occur during communication (Benda et al., 2006; Metzen et al., 2020). It is possible that changes in synchrony occur as the stimulus strength changes and encode information that could enhance the detection and localization accuracy. Further experiments are required to better understand the importance of population synchrony in this context. Other neural mechanisms could be present and enhance the sensitivity of the system. We know for example that the presence of negative correlations in inter-spike intervals suppresses noise at low frequencies and could enhance the coding of low-frequency stimuli (lower than the frequency we use in this paper; Chacron et al., 2001). For this reason, we propose that our

sensitivity estimates are conservative estimates that can serve as a starting point in estimating the limits in detection and localization abilities.

Our analysis indicates that reliable detection or localization would require integration of the signals over a certain period of time by higher brain areas. This is a realistic perspective as behavioral performance in various systems will be more accurate for ongoing than for brief stimuli (Dizon and Litovsky, 2004; Gai et al., 2013). For example, estimates of the direction of motion in a “random dot display” integrates over time in the visual system of primates to reach a reliable decision after seconds of attending the stimulus (Ditterich et al., 2003; Kim and Shadlen, 1999). For weakly electric fish, it is not unrealistic to assume that the stimulus can be integrates over several hundred ms to support accurate detection and localization, but it is not clear that this integration could occur over tens of seconds particularly when relative movement could require location estimate to be updated frequently. As a first step, our analysis considered spatially fixed signals, but it will thus be imperative in future studies, to take into account both the spatial and temporal dynamic of the conspecific signals. According to this perspective, localization accuracy, and thus behavioral decisions, depends on the spatial dynamic during the interaction. Moreover, this spatial dynamic can be leveraged as a means to collect spatial information. Various behavioral strategies can contribute to localizing a stimulus. For example, when localization is difficult, movements towards the target that result in the signal strength increasing can help confirm the position of the second fish (Fagan et al., 2013; Kaushik et al., 2020). Lateralization, rather that precise azimuth localization, can be used while a fish moves towards a target: if a stimulus is perceived as coming from the left or right, corrective turns realign the target. The individual would therefore move towards the target in a

zig-zag pattern; this mechanism has been proposed to contribute to behavior in various systems (Beetz and el Jundi, 2023; Gerhardt et al., 2023; Pollack et al., 1984).

Detection could rely on the convergence of the whole population of receptors thereby efficiently averaging out noise. Furthermore, the high receptor density rostrally improves detection for frontal azimuth because the EI hotspot will be centered on this high receptor density area and thus lead to a high convergence of strong responses. Localization, however, must rely on comparison of the EI strength across the body. When comparing the responses to stimuli from different azimuths, our analysis focuses on the neural responses that differ between the stimuli by weighing heavily the contribution of these neurons. This procedure to optimize the extraction of spatial information is essential because the EI might differ only slightly between two stimuli and thus the responses of most neurons will be identical across the stimuli locations. For localization, it is thus the convergence of the responses of a subset of neurons, that differ in activation between the locations being compared, that can support the accurate discrimination of azimuth. Surprisingly, we found that the high density of receptors on the rostral portion of the fish does not lead to a better discrimination of the frontal azimuth. This result could reflect the fact that the receptors on the head will have a stronger difference in response at the edge of the hot spot elicited by the sender moving across these receptor locations. We suggest that this would occur as the leading, or trailing, edge of the hotspot sweeping across high density areas. This could explain the modest increases in spatial resolution due to the increased rostral receptors density that we observed around 60° and 120°. This is in contrast with the contribution of the high density of receptors during prey capture (i.e., small objects) where localization accuracy is enhanced for the head and snout

regions. The structure and convergence of receptors thus play different roles in the detection and localization of objects and conspecifics: while high density and convergence contribute markedly to spatial coding of objects, it mostly contributes to detection accuracy for conspecific signals.

In other systems, regions of high receptor density are typically associated with high spatial resolution. It is the case of the foveal region of the retina and of high receptor density regions of the somatosensory system like the fingers or lips in humans (Catania and Catania, 2015; Dacey, 1994; Nakamura et al., 1998). In other systems faced with spatially diffuse signals, like the auditory or olfactory systems, the extraction of spatial information typically relies on the comparisons between a limited number of input (e.g., 2 ears) and high convergence of receptors is more tightly involved with the accurate detection, rather that localization, of the signals (Carr and MacLeod, 2010; Chapman, 1982; Okada and Toh, 2006; Schnupp and Carr, 2009). Our result on the electrosensory system suggests that this is a general principle guiding the relationship between signal structure and the organization of the sensory arrays. We argue that for signals that are spatially diffuse, receptor density and convergence will benefit detection abilities and spatial information is extracted by comparing inputs at different locations without relying on a higher number of inputs to enhance localization. For signals that are spatially localized, a topographic mapping system is advantageous and localization accuracy directly depends on the spatial resolution of the input array. The electrosensory system provides a powerful way to compare these systems and reveal organizing principles because it processes both localized and diffuse signals for which receptor organization and convergence play different roles.

References

Allen, K. M. and Marsat, G. (2018). Task-specific sensory coding strategies are matched to detection and discrimination performance. *J Exp Biol* **221**, jeb170563.

Allen, K. M. and Marsat, G. (2019). Neural Processing of Communication Signals: The Extent of Sender–Receiver Matching Varies across Species of Apteronotus. *eNeuro* **6**,.

Allen, K. M., Salles, A., Park, S., Elhilali, M. and Moss, C. F. (2021). Effect of background clutter on neural discrimination in the bat auditory midbrain. *J Neurophysiol* **126**, 1772–1782.

Ashida, G. and Carr, C. E. (2011). Sound localization: Jeffress and beyond. *Curr Opin Neurobiol* **21**, 745–751.

Assad, C. and Bower, J. M. (1997). Electric field maps and boundary element simulations of electrolocation in weakly electric fish. *Engineering and Applied Science* **PhD**,.

Bacher, M. (1983). A new method for the simulation of electric fields, generated by electric fish, and their distorsions by objects. *Biol Cybern* **47**, 51–58.

Beetz, M. J. and el Jundi, B. (2023). The influence of stimulus history on directional coding in the monarch butterfly brain. *J Comp Physiol A Neuroethol Sens Neural Behav Physiol*.

Benda, J., Longtin, A. and Maler, L. (2005). Spike-Frequency Adaptation Separates Transient Communication Signals from Background Oscillations. *Journal of Neuroscience* **25**, 2312–2321.

Benda, J., Longtin, A. and Maler, L. (2006). A synchronization-desynchronization code for natural communication signals. *Neuron* **52**, 347–358.

Bennett, M. V. L., Sandri, C. and Akert, K. (1989). Fine structure of the tuberous electroreceptor of the high-frequency electric fish,Sternarchus albifrons (gymnotiformes). *J Neurocytol* **18**, 265–283.

Caputi, A. and Budelli, R. (1995). The electric image in weakly electric fish: I. A data-based model of waveform generation in Gymnotus carapo. *J Comput Neurosci* **2**, 131–147.

Caputi, A. A. and Budelli, R. (2006). Peripheral electrosensory imaging by weakly electric fish. *Journal of Comparative Physiology A* **192**, 587–600.

Caputi, A. A., Budelli, R., Grant, K. and Bell, C. C. (1998). The electric image in weakly electric fish: physical images of resistive objects in Gnathonemus petersii. *J Exp Biol* **201**, 2115–28.

Carlson, B. A. and Kawasaki, M. (2006). Ambiguous Encoding of Stimuli by Primary Sensory Afferents Causes a Lack of Independence in the Perception of Multiple Stimulus Attributes. *Journal of Neuroscience* **26**, 9173–9183.

Carr, C. E. and MacLeod, K. M. (2010). Microseconds Matter. *PLoS Biol* **8**, e1000405.

Carr, C. E., Maler, L. and Sas, E. (1982). Peripheral organization and central projections of the electrosensory nerves in gymnotiform fish. *J Comp Neurol* **211**, 139–153.

Castello, M. E., Aguilera, P. A., Trujillo-Cenoz, O. and Caputi, A. A. (2000). Electroreception in Gymnotus carapo: pre-receptor processing and the distribution of electroreceptor types. *Journal of Experimental Biology* **203**,.

Catania, K. C. and Catania, E. H. (2015). Comparative studies of somatosensory systems and active sensing. *Sensorimotor Integration in the Whisker System* 7–28.

Chacron, M. J., Longtin, A. and Maler, L. (2001). Negative interspike interval correlations increase the neuronal capacity for encoding time-dependent stimuli. *J Neurosci* **21**, 5328–43.

Chacron, M. J., Maler, L. and Bastian, J. (2005). Electroreceptor neuron dynamics shape information transmission. *Nat Neurosci* **8**, 673–678.

Chapman, R. F. (1982). Chemoreception: the significance of receptor numbers. *Adv Insect Physiol* **16**, 247–356.

Dacey, D. M. (1994). Physiology, Morphology and Spatial Densities of Identified Ganglion Cell Types in Primate Retina. *Ciba Found Symp* **184**, 12–34.

Ditterich, J., Mazurek, M. E. and Shadlen, M. N. (2003). Microstimulation of visual cortex affects the speed of perceptual decisions. *Nature Neuroscience 2003 6:8* **6**, 891–898.

Dizon, R. M. and Litovsky, R. Y. (2004). Localization dominance in the median-sagittal plane: Effect of stimulus duration. *J Acoust Soc Am* **115**, 3142–3155.

Fagan, W. F., Lewis, M. A., Auger-Méthé, M., Avgar, T., Benhamou, S., Breed, G., Ladage, L., Schlägel, U. E., Tang, W. W., Papastamatiou, Y. P., et al. (2013). Spatial memory and animal movement. *Ecol Lett* **16**, 1316–1329.

Fotowat, H., Harrison, R. R. and Krahe, R. (2013). Statistics of the Electrosensory Input in the Freely Swimming Weakly Electric Fish Apteronotus leptorhynchus. *Journal of Neuroscience* **33**, 13758–13772.

Gai, Y., Ruhland, J. L., Yin, T. C. T. and Tollin, D. J. (2013). Behavioral and modeling studies of sound localization in cats: Effects of stimulus level and duration. *J Neurophysiol* **110**, 607–620.

Gerhardt, H. C., Bee, M. A. and Christensen-Dalsgaard, J. (2023). Neuroethology of sound localization in anurans. *J Comp Physiol A Neuroethol Sens Neural Behav Physiol* **209**, 115–129.

Goense, J. B. M. and Ratnam, R. (2003). Continuous detection of weak sensory signals in afferent spike trains: The role of anti-correlated interspike intervals in detection performance. *J Comp Physiol A Neuroethol Sens Neural Behav Physiol* **189**, 741–759.

Gómez-Sena, L., Pedraja, F., Sanguinetti-Scheck, J. I. and Budelli, R. (2014). Computational modeling of electric imaging in weakly electric fish: Insights for physiology, behavior and evolution. *Journal of Physiology-Paris* **108**, 112–128.

Grewe, J., Kruscha, A., Lindner, B. and Benda, J. (2017). Synchronous spikes are necessary but not sufficient for a synchrony code in populations of spiking neurons. *Proc Natl Acad Sci U S A* **114**, E1977–E1985.

Gussin, D., Benda, J. and Maler, L. (2007). Limits of Linear Rate Coding of Dynamic Stimuli by Electroreceptor Afferents. *J Neurophysiol* **97**, 2917–2929.

Henninger, J., Krahe, R., Kirschbaum, F., Grewe, J. and Benda, J. (2018). Statistics of natural communication signals observed in the wild identify important yet neglected stimulus regimes in weakly electric fish. *J Neurosci* 0350–18.

Kaushik, P. K., Renz, M. and Olsson, S. B. (2020). Characterizing long-range search behavior in Diptera using complex 3D virtual environments. *Proc Natl Acad Sci U S A* **117**, 12201–12207.

Kelly, M., Babineau, D., Longtin, A. and Lewis, J. E. (2008). Electric field interactions in pairs of electric fish: Modeling and mimicking naturalistic inputs. *Biol Cybern* **98**, 479–490.

Kim, J. N. and Shadlen, M. N. (1999). Neural correlates of a decision in the dorsolateral prefrontal cortex of the macaque. *Nature Neuroscience 1999 2:2* **2**, 176–185.

Knudsen, E. I. (1975). Spatial aspects of the electric fields generated by weakly electric fish. *Journal of Comparative Physiology ? A* **99**, 103–118.

Lannoo, M. J., Maler, L. and Tinner, B. (1989). Ganglion cell arrangement and axonal trajectories in the anterior lateral line nerve of the weakly electric fish Apteronotus leptorhynchus (Gymnotiformes). *Journal of Comparative Neurology* **280**, 331–342.

MacIver, M. A., Sharabash, N. M. and Nelson, M. E. (2001). Prey-capture behavior in gymnotid electric fish: motion analysis and effects of water conductivity. *Journal of Experimental Biology* **204**,.

Maler, L., Sas, E., Johnston, S. and Ellis, W. (1991). An atlas of the brain of the electric fish Apteronotus leptorhynchus. *J Chem Neuroanat* **4**, 1–38.

Marsat, G. and Maler, L. (2010). Neural Heterogeneity and Efficient Population Codes for Communication Signals Marsat G, Maler L. Neural heterogeneity and efficient population codes for communication signals. *J Neurophysiol* **104**, 2543–2555.

Marsat, G., Daly, K. C. and Drew, J. A. (2023). Characterizing neural coding performance for populations of sensory neurons: comparing a weighted spike distance metrics to other analytical methods. *bioRxiv* 778514.

Metzen, M. G., Huang, C. G. and Chacron, M. J. (2018). Descending pathways generate perception of and neural responses to weak sensory input. *PLoS Biol* **16**, e2005239.

Metzen, M. G., Hofmann, V. and Chacron, M. J. (2020). Neural Synchrony Gives Rise to Amplitude- and Duration-Invariant Encoding Consistent With Perception of Natural Communication Stimuli. *Front Neurosci* **14**, 79.

Milam, O. E., Ramachandra, K. L. and Marsat, G. (2019). Behavioral and Neural Aspects of the Spatial Processing of Conspecifics Signals in the Electrosensory System. *Behavioral Neuroscience* **133**, 282–296.

Nakamura, A., Yamada, T., Goto, A., Kato, T., Ito, K., Abe, Y., Kachi, T. and Kakigi, R. (1998). Somatosensory Homunculus as Drawn by MEG. *Neuroimage* **7**, 377–386.

Nelson, M. E. and Maciver, M. A. (1999). Prey capture in the weakly electric fish Apteronotus albifrons: sensory acquisition strategies and electrosensory consequences. *J Exp Biol* **202**, 1195–203.

Nelson, M. E., Xu, Z. and Payne, J. R. (1997). Characterization and modeling of P-type electrosensory afferent responses to amplitude modulations in a wave-type electric fish. *Journal of Comparative Physiology A* **181**, 532–544.

Okada, J. and Toh, Y. (2006). Active tactile sensing for localization of objects by the cockroach antenna. *J Comp Physiol A Neuroethol Sens Neural Behav Physiol* **192**, 715–726.

Pedraja, F., Aguilera, P., Caputi, A. A., Budelli, R. and Nobel, S. (2014). Electric Imaging through Evolution, a Modeling Study of Commonalities and Differences. *PLoS Comput Biol* **10**, e1003722.

Pedraja, F., Perrone, R., Silva, A. and Budelli, R. (2016). Passive and active electroreception during agonistic encounters in the weakly electric fish Gymnotus omarorum. *Bioinspir Biomim* **11**, 065002.

Petzold, J. M., Marsat, G. and Smith, G. T. (2016). Co-adaptation of electric organ discharges and chirps in South American ghost knifefishes (Apteronotidae). *J Physiol Paris* **110**, 200–215.

Pollack, G. S., Huber, F. and Weber, T. (1984). Frequency and temporal pattern-dependent phonotaxis of crickets (Teleogryllus oceanicus) during tethered flight and compensated walking. *Journal of Comparative Physiology A* **154**, 13–26.

Provis, J. M., Dubis, A. M., Maddess, T. and Carroll, J. (2013). Adaptation of the central retina for high acuity vision: Cones, the fovea and the avascular zone. *Prog Retin Eye Res* **35**, 63–81.

Rasnow, B., Assad, C. and Bower, J. M. (1993). Phase and amplitude maps of the electric organ discharge of the weakly electric fish, Apteronotus leptorhynchus. *Journal of Comparative Physiology A* **172**, 481–491.

Ratnam, R. and Nelson, M. E. (2000). Nonrenewal statistics of electrosensory afferent spike trains: implications for the detection of weak sensory signals. *J Neurosci* **20**, 6672–83.

Rospars, J. P., Grémiaux, A., Jarriault, D., Chaffiol, A., Monsempes, C., Deisig, N., Anton, S., Lucas, P. and Martinez, D. (2014). Heterogeneity and Convergence of Olfactory First-Order Neurons Account for the High Speed and Sensitivity of Second-Order Neurons. *PLoS Comput Biol* **10**, e1003975.

Rother, D., Migliaro, A., Canetti, R., Gómez, L., Caputi, A. and Budelli, R. (2003). Electric images of two low resistance objects in weakly electric fish. *Biosystems* **71**, 169–177.

Schnupp, J. W. H. and Carr, C. E. (2009). On hearing with more than one ear: lessons from evolution. *Nat Neurosci* **12**, 692–697.

Stamper, S. A., Madhav, M. S., Cowan, N. J. and Fortune, E. S. (2012). Beyond the Jamming Avoidance Response: weakly electric fish respond to the envelope of social electrosensory signals. *Journal of Experimental Biology* **215**, 4196–4207.

Stamper, S. A., Fortune, E. S. and Chacron, M. J. (2013). Perception and coding of envelopes in weakly electric fishes. *Journal of Experimental Biology* **216**,.

Yu, N., Hupé, G., Garfinkle, C., Lewis, J. E., Longtin, A. and Fortune, E. (2012). Coding Conspecific Identity and Motion in the Electric Sense. *PLoS Comput Biol* **8**, e1002564.

Zupanc, G. K. H. and Maler, L. (1993). Evoked chirping in the weakly electric fish Apteronotus leptorhynchus : a quantitative biophysical analysis. *Can J Zool* **71**, 2301–2310.

Zupanc, G. K. H., Sîrbulescu, R. F., Nichols, A., Ilies, I. (2006). Electric interactions through chirping behavior in the weakly electric fish, Apteronotus leptorhynchus. *J Comp Physiol A Neuroethol Sens Neural Behav Physiol* **192**, 159–173.

Figures and Legends

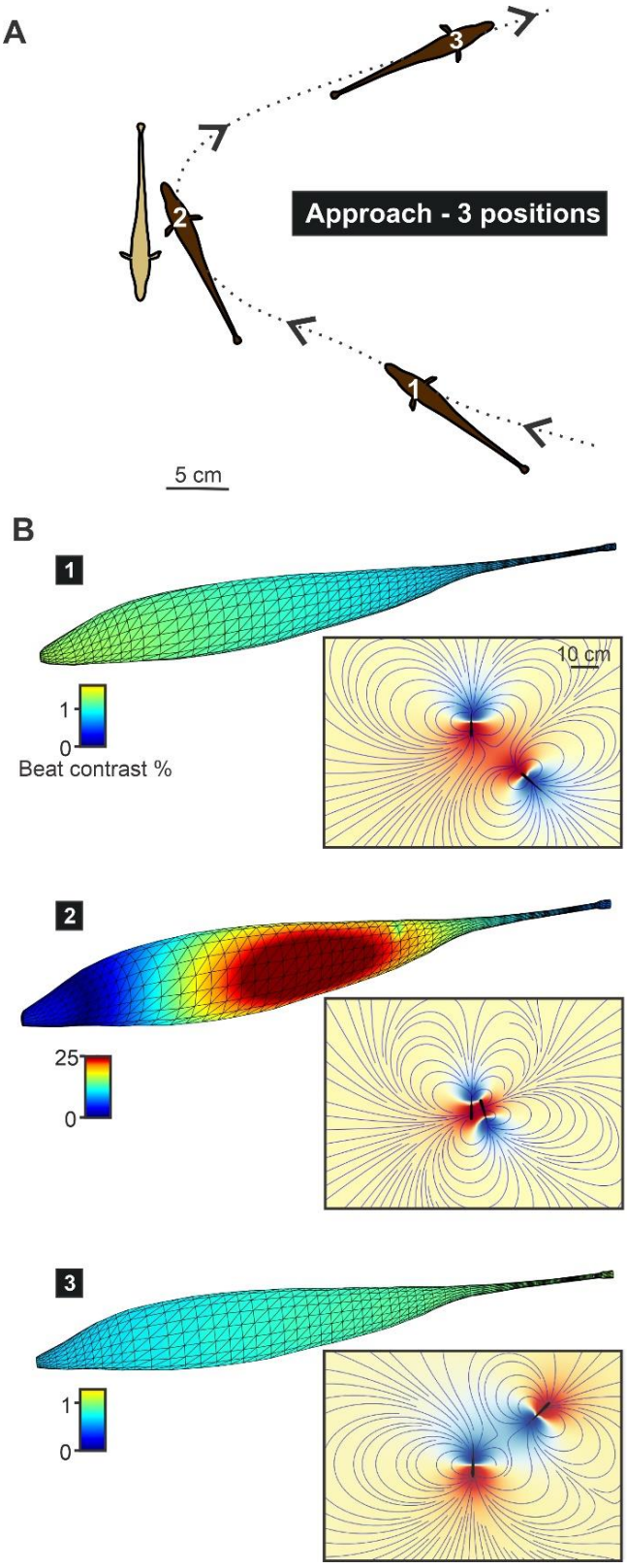

Figure 1: Model of the electric image during social interactions. The model takes into account the relative position of the two fish to estimate the strength of the EI caused by one fish (designated as "sender") onto the body of the other ("focal" fish). **A.** Three relative positions are illustrated here representing different phases of a fish approaching the focal fish. **B.** The EI is quantified based on the strength of the transdermal voltage at the peak of the beat AM caused by the interaction of the fish's EODs. The strength of this AM is then normalized to the baseline EOD strength (i.e., EOD amplitude when only the focal fish is present) to obtain an EI strength expressed as percent contrast. 0% contrast indicates that the signal from the sender fish has no impact on the receiver and 100% contrast indicates that the sender's signal is as strong as the focal fish's own EOD. We

can see that for the 2 more distant positions, the signal strength is weak (<1%) and there are only minute differences in signal strength across the receiver's body. When the sender is very close, however, a salient "hot spot" has a much stronger EI strength than other portions of the body (note the different color scales for each image). We show as an inset on the right, the electric field with current lines (gray lines) and the iso-potential lines are depicted for the near-field range as a color gradient (red or blue depending on polarity). The perspective in this inset is from the top as in A) while the EI illustrations in B) present a perspective of the side of the focal fish being approached by the sender.

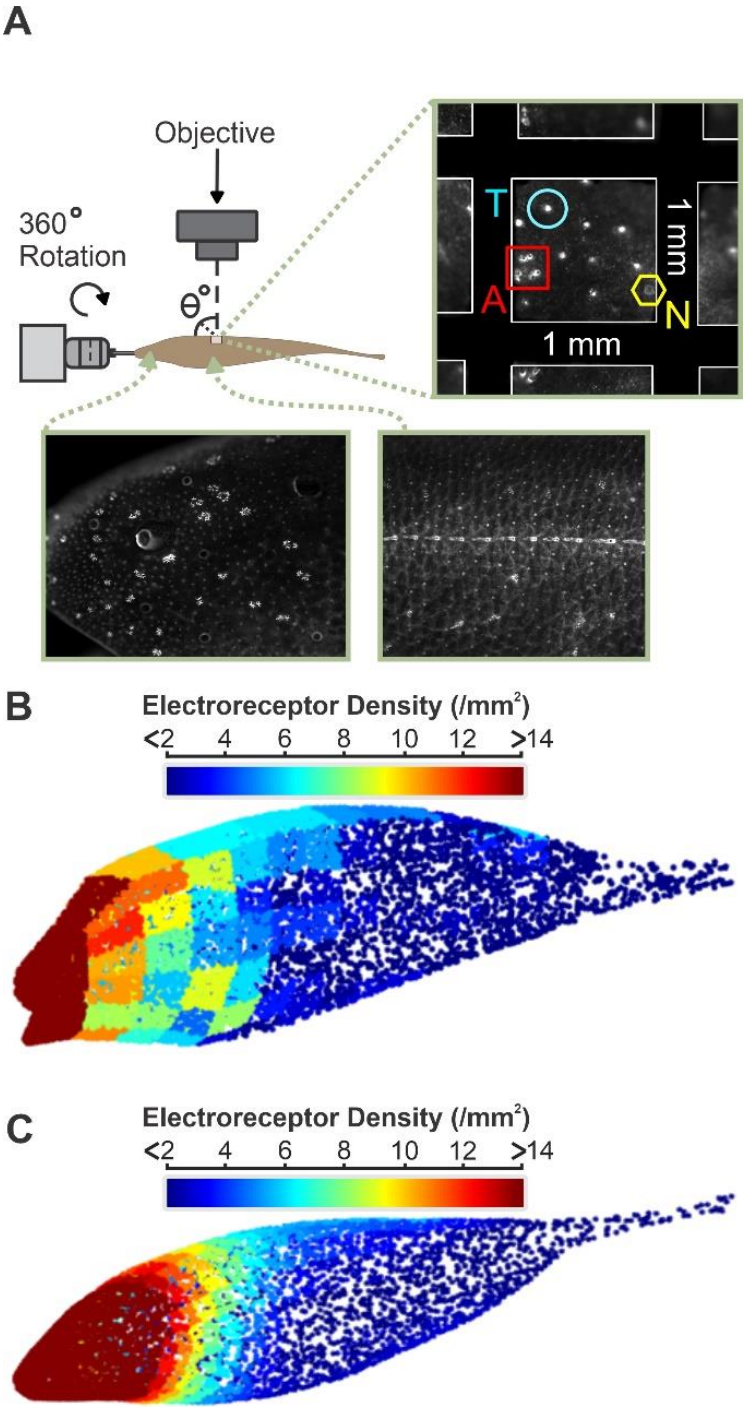

Figure 2: Spatial structure of the receptor array. A. Receptor density across the body of the fish was determined experimentally. Eosin Y stained specimen were examined and cutaneous receptors of different types were identified (e.g., Neuromast labelled N, ampullary labelled A, or tuberous receptors, labelled T in the inset on the top right). The number of tuberous receptors in $1mm^2$ areas was averaged across samples for each face of a coarse 3D mesh model of the fish (**B**). Receptor density as a function of body position was then smoothed by fitting a 5^{th} degree polynomial and mapped onto the fine mesh model used in the EI model (**C**). For each face of this 3D mesh, random receptor positions were selected according to the receptor density attributed to each face. The receptor positions that we generated are marked by the dots in B) and C) and their color reflect the density of receptors for the corresponding position.

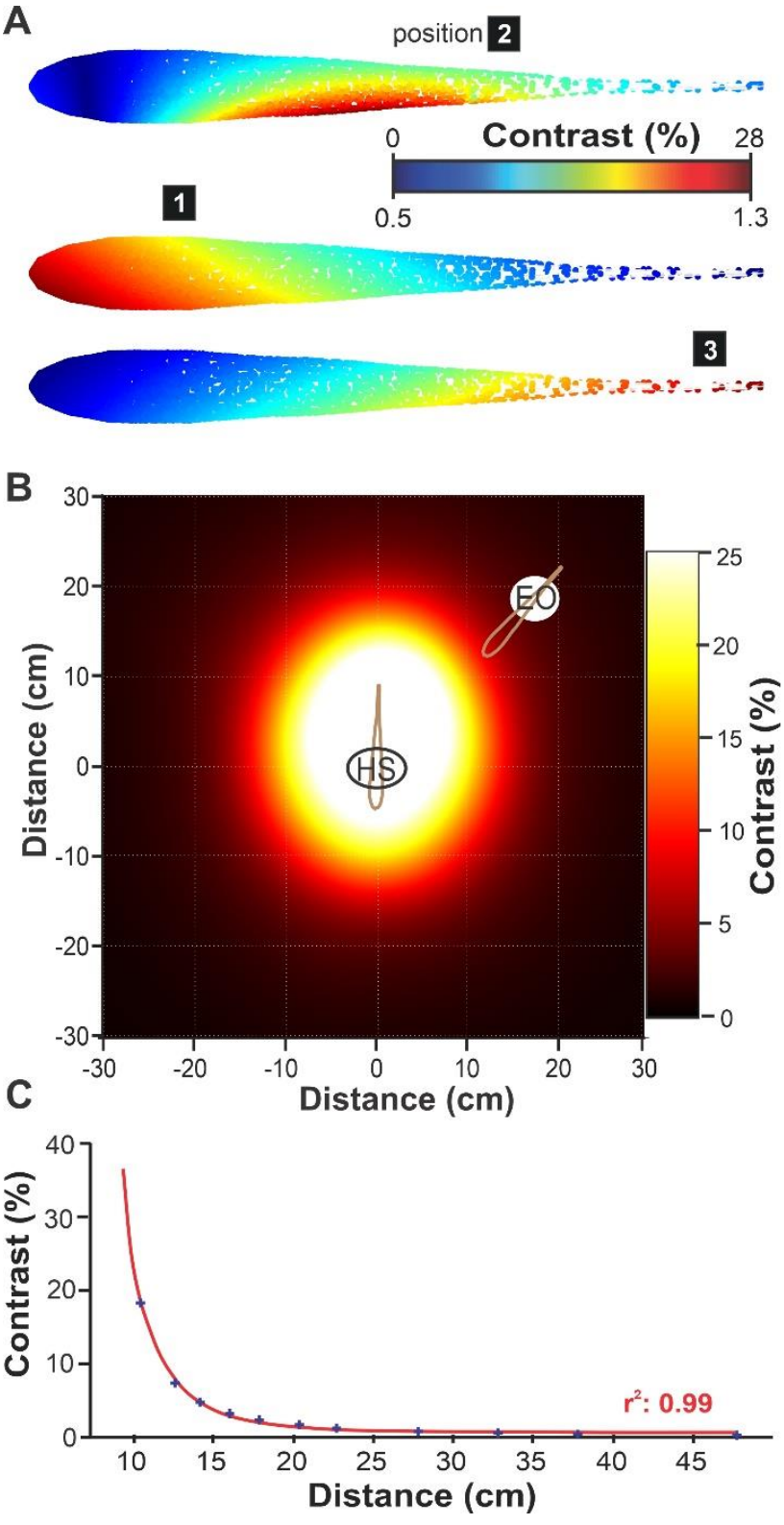

Figure 3: EI strength as a function of relative position of the two fish. A. The strength of the EI from the sender was calculated for each receptor position. It is displayed here for the 3 relative fish positions illustrated in Figure 1 (note the difference in color scale for position 2 vs 1 and 3). The focal fish are presented here from a top perspective. **B.** The strength of the electric image is characterized as a function of distance and azimuth. The EI for 864 relative positions (12 distances x 72 azimuths) was calculated and the strength of the signal in the "hot spot" (HS; taken as the average of the 5% most strongly activated receptors) is

depicted by the color scale. The position of the sender fish for position is based on the center of the EO and the data points have been repositioned to reflect the distance between the center of the HS on the focal fish and the EO of the sender rather than the center of the focal fish. The EI strength values (contrast %) have been interpolated between data points. **C.** Average contrast values in the HS across azimuth and for fish displayed as a function of the distance between the hot spot and EO centers. The relationship follows a cubic power law (red best fit curve: $c=1.6 \cdot 10^{4} \cdot x^{-3}$).

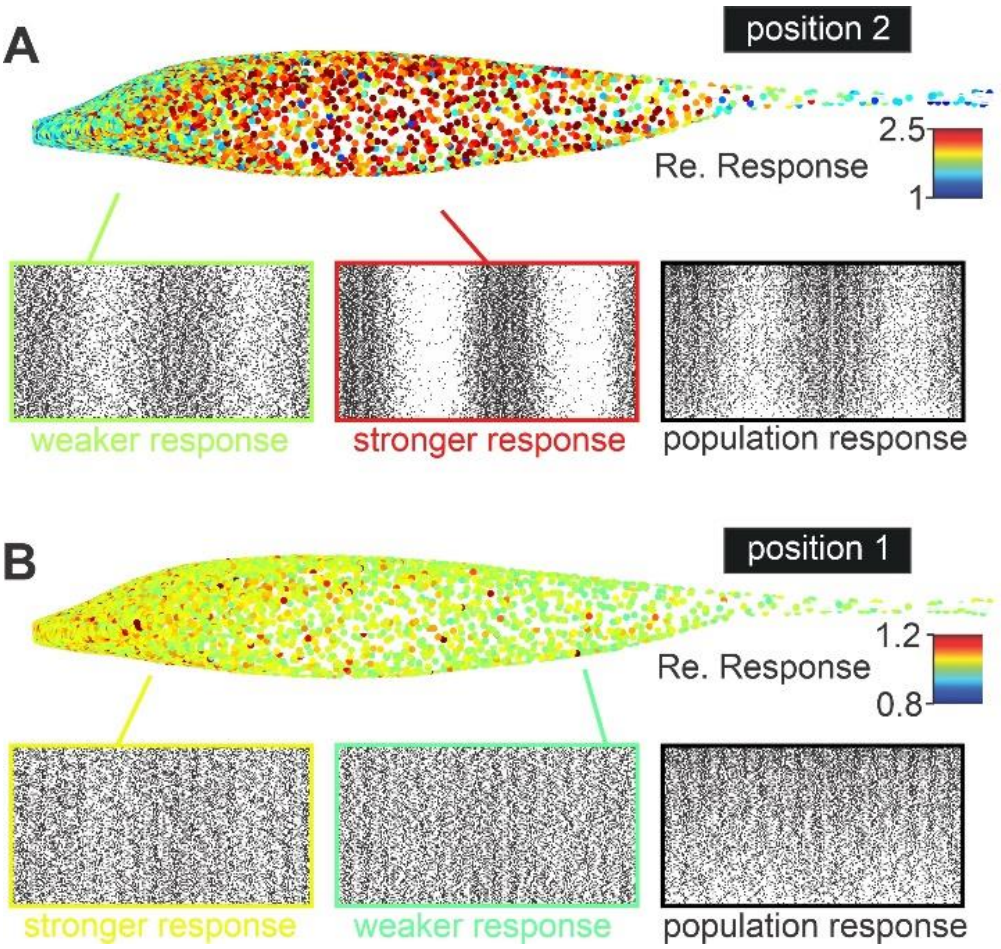

Figure 4: Heterogeneous population response in modeled receptors. A. LIF models with heterogeneous response properties were stimulated with realistic inputs that match the spatio-temporal structure of conspecific signals. In the color map (top), each receptor's response is quantified as the peak-to-trough firing rate modulation and normalized relative to spontaneous modulations in firing rate occurring when no second fish is present (i.e., a relative response of 1 reflects modulations in firing rate similar to spontaneous activity). The two raster plot insets on the left show the response patterns of two individual neurons from portions of the fish's body that are more or less strongly stimulated. The raster plot on the right shows the population response: we show a stack of 800 randomly selected receptor responses ordered from weakest peak-to-trough responses (bottom) to strongest responses (top). **B.** We display the same

elements as in panel A. but the position of the sender fish is more distant (position 1 of Figure 1) compared to nearby relative position used in A. (position 2 from Figure 1).

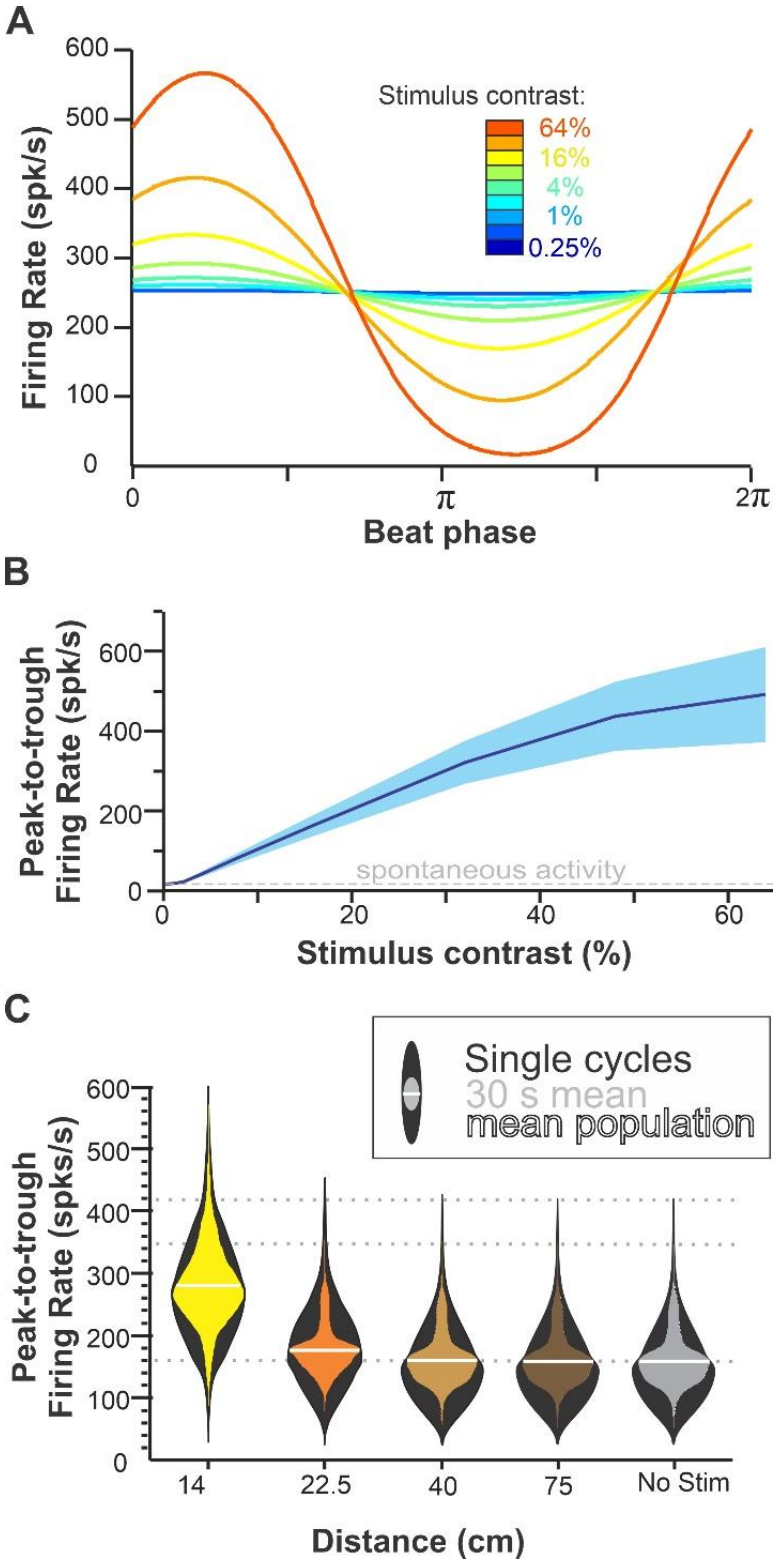

Figure 5: Sensitivity of the receptor model replicates responses to beat stimuli. A. Mean firing rate (averaged across all receptors) during a single cycle of a 30 Hz AM beat stimulus for different contrast intensity. The model produced modulations in firing of just a few spikes/s peak-to-trough for the weakest intensities and of a few hundred spikes/s for the stronger intensities. **B.** F-I curves display the strength of the response as a function of the stimulus intensity (mean across the population ± s.d.). Average peak-to-trough firing rate quantified in a similar way but during spontaneous activity (no sender fish) is display (gray dashed line) and we can see that for the weakest stimuli the average response is similar to spontaneous activity. Response sensitivity has been calibrated to match published data

(Bastian, 1981; Nelson et al., 1997; see also Methods and Supplementary Figure S1). **C.** The distribution of responses strength across the population of receptors is displayed for sender fish positioned at different distances (azimuth 90º). The outer distributions (black violin plots) show the variability of peak-to-trough firing rate on single cycles of the beat for single neurons. The inner distributions (colored violin plots) show the variability across neurons but for each neuron peak-to-trough firing rate is averaged across the whole stimulus (900 cycles, 30 s). The mean of this distribution (i.e., also averaged across neurons) is displayed as a white line. Dotted grid lines (in gray) are provided in the background to help notice minute differences in the distributions. The fact that only subtle differences between the distributions for stimuli at distances of 40 cm or more compared to responses in the absence of second fish highlights the difficulty in detecting these distant signals.

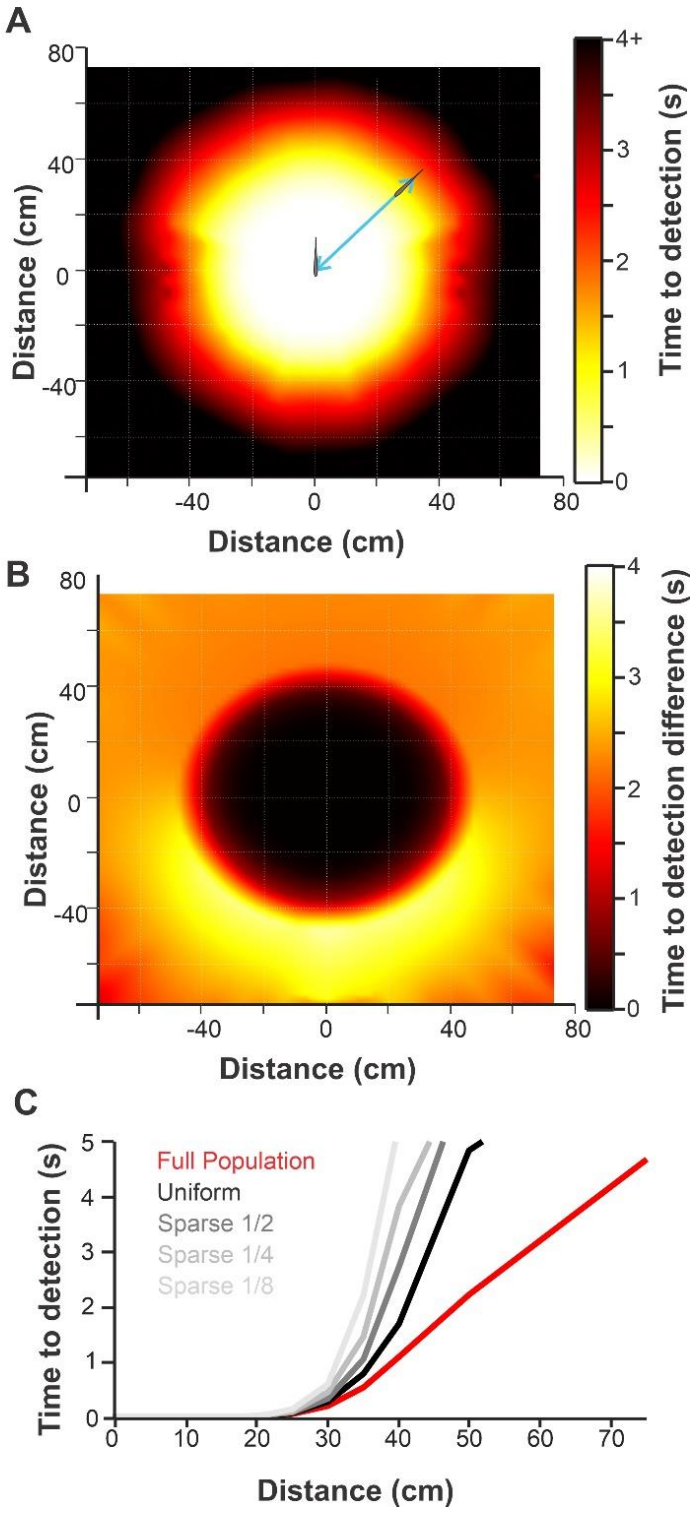

Figure 6: Estimates of detection sensitivity as a function of relative fish position and the influence of receptor density distribution. A. Detection sensitivity is quantified as the time it would take to reliably detect the presence of the sender's signal and is displayed as a function of the relative position of the sender. For each position (12 distances x 72 azimuth) the peak-to-trough responses of the population are compared to spontaneous responses. As peak-to-trough is averaged across cycles of the beat (increased time to detection), detection becomes more reliable because noise is averaged out. We display the stimulation time required for our decoder to reach reliable detection (<5% error; see Methods for more details). Each position is defined by the distance and azimuth between the center of the receptor positions in the focal fish and the center of the

EO in the sender fish. Values for each data point are then interpolated across space to obtain the smoothly varying color plots. **B.** Decrease in detection sensitivity (increased time to detection) caused by reducing the density of receptors in dense areas (i.e., making it uniformly low like the density in the caudal portion of the body). The decrease in density makes uniformly no difference nearby (black region). It uniformly increases time to detection when the sender is very distant (distant black area in panel A). It has a most pronounced effect at mid distance (40-50 cm) in the frontal azimuth (yellow area) where time to detection increases from 1-2 s to 2-6 s (see also Supplementary Figure S3) showing that the rostral high density of receptors can increase detection sensitivity in the frontal quadrant. C. The overall detection sensitivity (time to detection averaged across azimuth) decreased markedly at distances above 30 cm when receptor density is made uniformly low (black line compared to red line) and decreases further when receptor density is made even sparser (1/2, 1/4 or 1/8 the size of the uniform population; gray curves).

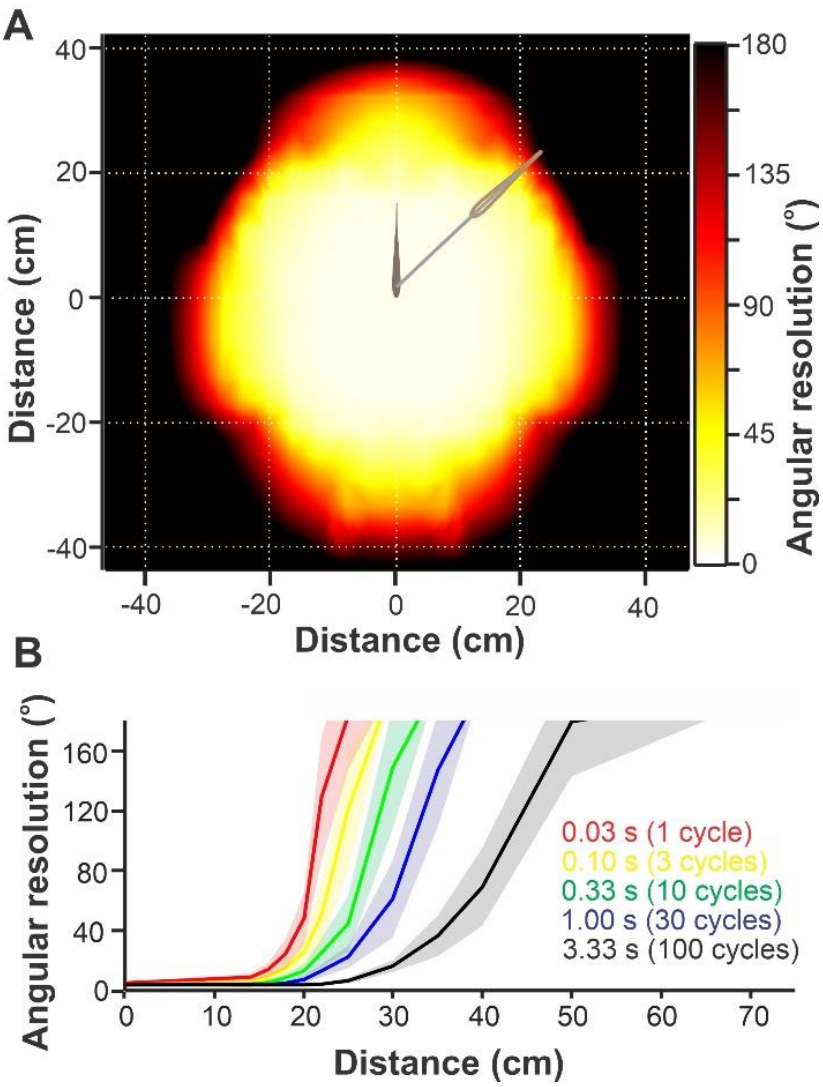

Figure 7: Estimates of angular resolution supported by the receptors' response accuracy. **A.** Angular resolution estimated as a function of distance and azimuth of the sender. The analysis is based on the average peak-to-trough firing rate (30 cycles average, i.e., 1 s) of each receptor for a given stimulus location. Population responses for a sender at a given test azimuth was compared, by our decoder, to responses for a sender at various angular displacement (clockwise or counter-clockwise; distance kept fixed). The smallest angle that allows 95% accurate discrimination between the responses was taken as the angular resolution. Failure to discriminate responses for stimuli locations 180º apart (black regions on the graph) indicates an inability to localize reliably the azimuth of the sender's location. Data points for 72 test azimuths and 12 distance (i.e., 864 positions) were generated, taking the center of receptors location for the focal fish and the center of the EO for the sender fish as position values. Data values are then interpolated to obtain the smoothly varying color plot. **B.** The angular resolution (mean ± s.d. across azimuth)

can be calculated based on peak-to-trough responses of the receptors to a single cycle of the stimulus or on the peak-to-trough averaged across several cycles. Averaging the response across cycles corresponds to a decoder that integrates the response across time to get a more accurate estimate of response strength. Consequently, angular resolution improves as the decoder integrates across more time, but in all cases we still see a sharp change in resolution from very accurate (e.g., at distances below 20 cm) to very poor (e.g., above 50 cm).

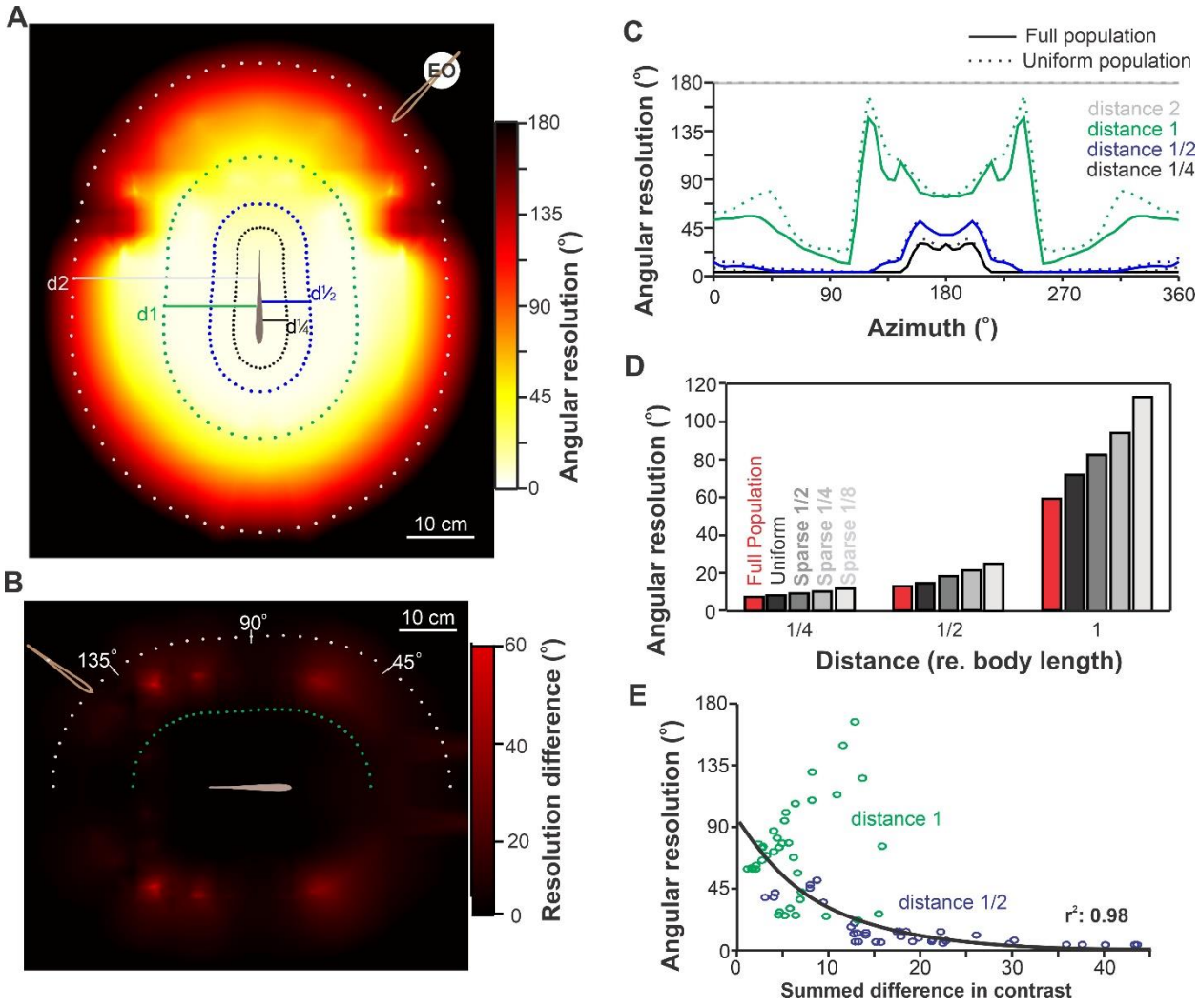

Figure 8: Receptor density and angular resolution as a function of azimuth. A. Angular resolution for a sender fish at various positions around the focal fish was calculated as in Figure 7, but the way distance is normalized across angles is different. We still compare, with our decoder, positions at different angles while keeping the distance equal. Here distance is set by the distance between the rostral tip of the sender and the closest point on the surface of the focal fish. The fish are thus separated by a fixed gap set to 1/4, 1/2, 1 or 2 body lengths (i.e., 3.5, 7, 14 and 28 cm respectively). In Figure 7, the gap between the fish was not consistent across azimuth since distance was set between the center of receptor locations in the focal fish

and center of the EO in the sender. For example, the rostral tip of the sender was closer to the skin of the receiver when it was at 180º than when it was at 0º. The positions of the rostral tip of the sender, for the 72 angles and 4 distances, are marked with dots on this figure. Datapoints for various positions are still mapped on the color graph at the position of the middle of the EOD of the sender and the color gradient interpolated between datapoints. **B.** Decreasing the density of receptors in dense areas (i.e., making receptor density uniformly as low as density in the caudal portion of the body) causes decreases in angular resolution. This resolution decrease is strongest in the red area of the graph. We note that this decrease is relatively limited and not concentrated in the frontal quadrant. **C.** Angular resolution as a function of azimuth, distance and receptor density. This is the same data used to generate panels A and B but shown here in 2D. The change in resolution as a function of azimuth is clearly visible even when receptor density is uniform across the body **D.** Angular resolution averaged across azimuths for different receptor density patterns. The full population is compared to a uniform lower density population or to populations made even sparser (1/2, 1/4 or 1/8 the uniform population). Decreasing the receptor density decreases angular resolution. **E.** Changes in EI for small angular displacements (averaged across 5°, 10° and 15° displacements) are compared across azimuth and related to the angular resolution of the system. For a given displacement, the difference in EI was characterized by integrating the difference in EI strength across the body surface. This EI difference was calculated for various azimuth and at the 2 distances (1 or 1/2 body length apart) that give medium angular resolutions. We show that the EI difference correlates with angular resolution with an exponential relationship (black best-fit curve, r^2=0.98).

Supplementary Information

Table S1: Model parameters used for the prototypic seed neuron (see Methods for details).

Description	Name	Value	Description	Name	Value
Membrane time constant (s)	τ_m	$15 \cdot 10^{-4}$	Noise strength (A)	A_σ	$15 \cdot 10^{-9}$
Lean reversal potential (V)	E_m	$-70 \cdot 10^{-3}$	Adaptation reversal potential (V)	E_α	$-80 \cdot 10^{-3}$
Membrane resistance (Ω)	R_m	$15 \cdot 10^{5}$	Adaptation increment (V)	Δ_α	$14.5 \cdot 10^{-8}$
Spiking threshold (V)	V_T	$-49 \cdot 10^{-3}$	Adaptation time constant (s)	τ_α	$50 \cdot 10^{-3}$
Reset potential (V)	V_R	$-70 \cdot 10^{-3}$	EOD amplitude (A)	A_{EOD}	$1.7 \cdot 10^{-7}$
Refractory period (s)	t_R	$9 \cdot 10^{-4}$	EOD baseline bias (A)	β	$3 \cdot 10^{-8}$

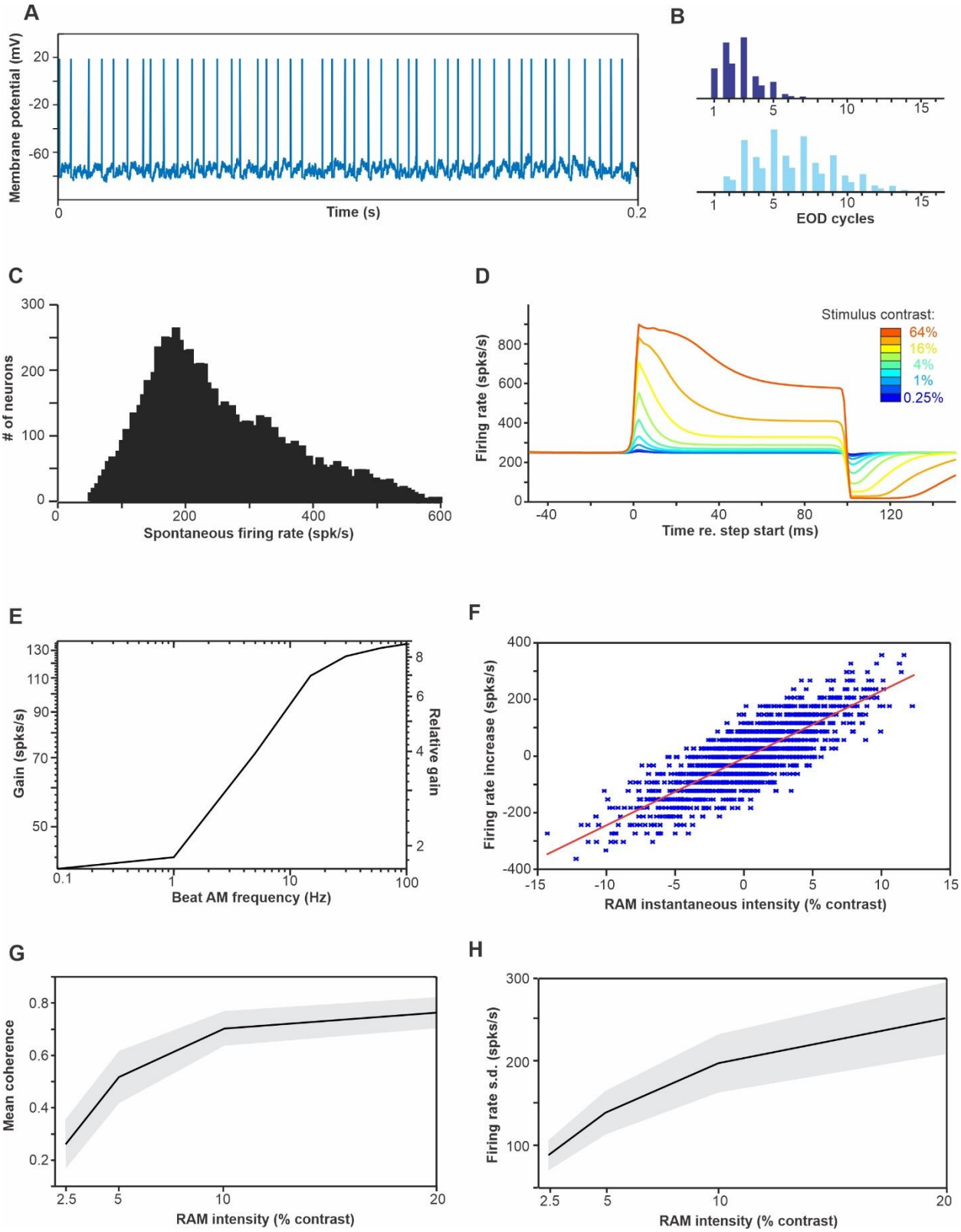
A
Membrane potential (mV)
20
-20
-60
0
Time (s)
0.2
B
1
5
10
15
1
5
10
15
EOD cycles
C
# of neurons
300
200
100
0
0
200
400
600
Spontaneous firing rate (spk/s)
D
Firing rate (spks/s)
800
600
400
200
0
Stimulus contrast:
64%
16%
4%
1%
0.25%
-40
0
40
80
120
Time re. step start (ms)
E
Gain (spks/s)
130
110
90
70
50
Relative gain
8
6
4
2
0.1
1
10
100
Beat AM frequency (Hz)
F
Firing rate increase (spks/s)
400
200
0
-200
-400
-15
-10
-5
0
5
10
15
RAM instantaneous intensity (% contrast)
G
Mean coherence
0.8
0.6
0.4
0.2
2.5
5
10
20
RAM intensity (% contrast)
H
Firing rate s.d. (spks/s)
300
200
100
2.5
5
10
20
RAM intensity (% contrast)

Figure S1: Average response properties of the heterogeneous population of modeled receptors.

A. Example of the membrane potential and spiking pattern of a model response (spontaneous activity). **B.** Inter-spike interval histogram of 2 different model neurons (spontaneous activity) showing phase locking to the EOD period and different firing tendencies. Note that the x axis is expressed in multiples of the EOD period but since we used an EOD frequency of 1,000 Hz for simplicity, this also corresponds to ms. **C.** Distribution of spontaneous firing rate across our entire population. This distribution was achieved by selecting 26 seed neurons with firing rates unevenly distributed along this range and diversifying model parameters based on these seeds (see Methods). This range and distribution replicates published data (Bastian, 1981; Grewe et al., 2017; Ratnam and Nelson, 2000). In particular, the mean spontaneous firing rate was 251 spk/s with a CV of 0.45. **D.** Responses to step increases in EOD intensity. The strength of the peak response, the steady-state response, and the adaptation time course was matched to published data (Benda et al., 2005). **E.** Response gain to beat stimuli of different AM frequencies. Although we did not explore systematically the response of our model at different beat frequencies in the results section, we calculated the gain for a range of AM frequencies. This analysis helps us to evaluate the sensitivity of the neurons (see the absolute scale on the left) and it also helps to assert that the adaptation dynamic replicates some of the tuning properties of the neurons (see the relative scale on the right; gain for an AM of 1 Hz is normalized to 1). This average gain curve is comparable to experimental data (Chacron et al., 2005; Nelson et al., 1997). **F.** Relative firing rate during random amplitude modulations. We replicated a published analysis of receptors sensitivity (Gussin et al., 2007a) that measure the

relative firing rate (relative to average) in successive 32 ms windows during the response to a low frequency (0 to 4 Hz) random amplitude modulation. We note that our scale is different than theirs: our ± 5% values correspond to the absolute contrast of the stimulus (i.e., s.d. of 10% contrast) whereas the scale in their Fig 3 has ± 50% being the min-to-max of their 10% contrast stimulus. When converted to the same scale, we find a gain slope of 23.7 spk/s/% (± 5.8 s.d.) comparable to the 17.7 spk/s/% (range 3.2 to 40.2) they found. **G.** Mean coherence at 10-30 Hz for random amplitude modulations (0-100 Hz) of different overall intensities (contrast). We qualitatively matched the coherence to values found in previous publications (Chacron et al., 2005; Grewe et al., 2017). **H.** Firing rate modulation in response to random amplitude modulations (0-300 Hz). We replicated the analysis in Grewe et al. (2017; see their figure S1A) that plots the standard deviation of the response (averaged over trials) as a function of stimulus contrast. Their population averages go from approximately 100 spk/s for 2.5% contrast to 200 spk/s at 20% contrast with a large variability among the population; we have a population average between 90 spk/s and 250 spk/s respectively.

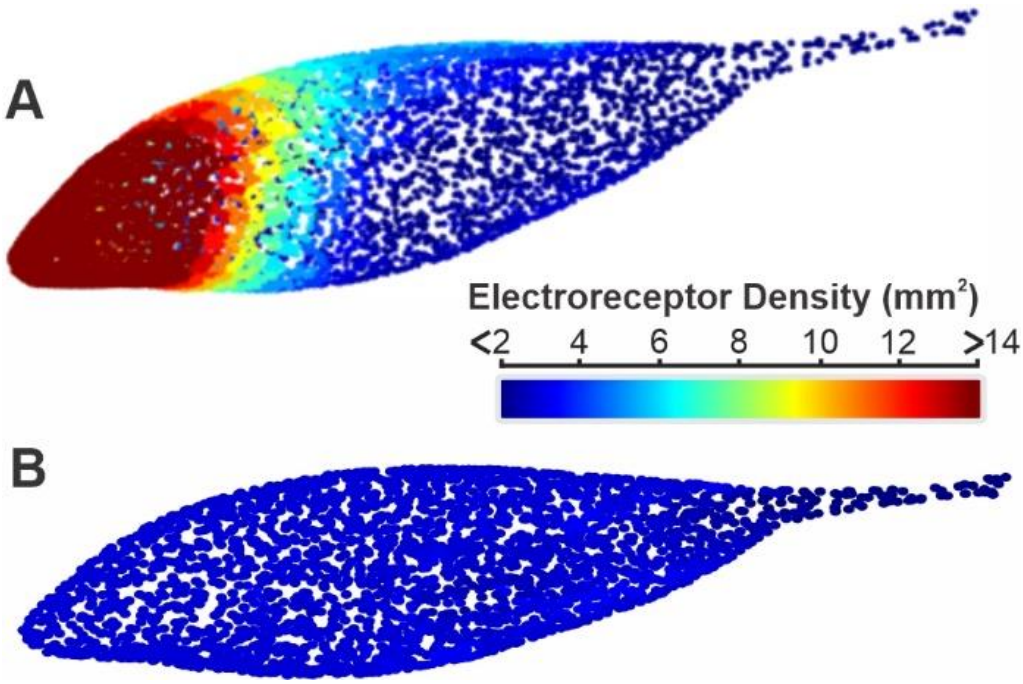

Figure S2: Receptor density compared between our full population (A) and our uniformly low-density population (B). Each dot shows the position of a receptor and the color reflects the density of receptor at this location. The uniform population was created by selecting, for each face of the mesh model, a subset of receptors from the full population to match the density of 2 receptors per mm^2.

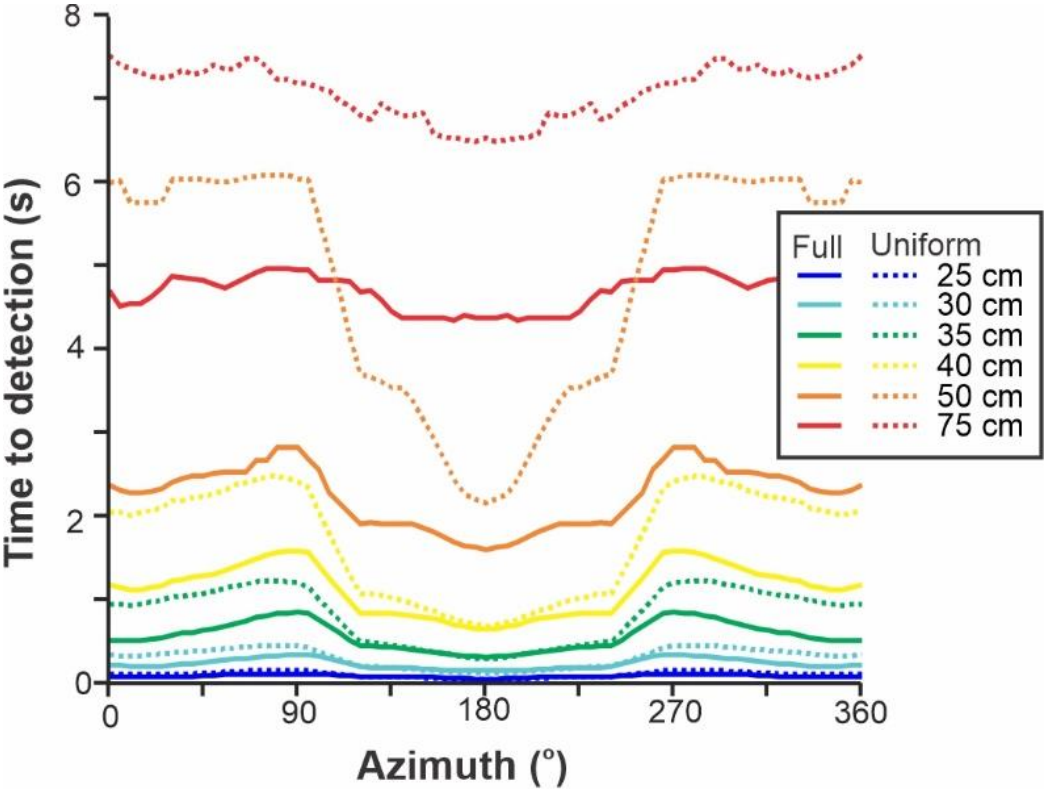

Figure S3: Detection performance as a function of source location and receptor structure. We compare a full population of receptors that includes a high density in rostral regions with a population that has a uniform density across the body matching the low density of the caudal region of the body (see Figure S2B). We present here the results for distances above 25 cm where we can see differences across azimuth and population structures. Our decoder considers that the response strength of receptors can be integrated across time and thus more noisy, weak responses require integration across longer periods to reach a reliable detection performance. We plot here the integration time required for our decoder to reach 95% detection accuracy and plot this here as a function of stimulus location.

Chapter 3

Prologue

The previous chapter demonstrates how social interaction between weakly electric fish affects the contrast and spatial pattern of the beat signal received by electroreceptors at the periphery and how accurately this signal is encoded. It is unknown how this spatial information is represented at the next level of sensory processing in the electrosensory lateral line lobe (ELL). In this chapter, I use a combination of neurophysiological and computational approaches to understand how the spatial information is represented by the population of pyramidal cells and clarify how the heterogeneity in the population influences coding. I demonstrate that spatial information begins to segregate at the level of the ELL by evaluating how well spatial information is encoded by populations of ELL pyramidal cells.

Note: This chapter has been submitted for publication as:

"Milam, O.E., and Marsat, G. (2023). Spatial coding of conspecifics in subpopulations of pyramidal cells of the gymnotiform electrosensory system. Frontiers in Neuroscience. Submitted"

I performed all of the experiments and data analysis. Gary Marsat helped in a supervisory role and in drafting the manuscript.

Abstract

Localizing the source of a signal requires sophisticated neural mechanisms and we are still uncovering the coding principles that support accurate spatial processing. Weakly electric fish can detect and localize distant conspecifics, but the way this spatial information is encoded is unclear. Here, we investigate the spatial representation of conspecific signals in the hindbrain to determine how the properties of the heterogenous population of pyramidal cells affect the spatial coding accuracy of conspecific signals. We hypothesize that specific subsets of cells provide more accurate spatial information about conspecific location. We stimulated the fish with an artificial signal that replicates both the spatial and temporal structure of conspecific signals. We recorded from cells with various receptive field positions covering the entire body surface and analyzed the spike train with spike-train distance metrics to determine how accurately the location of the stimulus is encoded. We found that some pyramidal cells (such as ON-type, and those within the deep layer) encode the spatial information more accurately while other subgroups (OFF-type, and superficial layer) provide less accurate information. Our results help us understand how the heterogeneity of a population of cells allow the efficient processing of signals and suggest that a segregation of the spatial information stream starts earlier in the sensory pathway.

Keywords: population coding, discrimination, localization, topographic maps, weakly electric fish

Introduction

Nervous systems must accurately encode sensory information about environmental stimuli and a central goal of neuroscience is to reveal how this is accomplished efficiently (Barlow, 1961; Bialek and Rieke, 1992; Bullock et al., 2005; Dayan and Abbott, 2001; Shannon, 1953). Courting a signaling mate or surviving an agonistic encounter between a competitor are a couple of behavioral examples where encoding spatial information reliably is essential for piloting social interaction (Bradbury and Vehrencamp, 2011; Pedraja et al., 2016). Yet, how this spatial information is represented by populations of neurons to guide such behaviors remains poorly understood. Here, we investigate the spatial coding accuracy of heterogeneous pyramidal cell populations in the hindbrain collected via *in-vivo* electrophysiological recordings.

Apteronotus leptorhynchus, a gymnotiform wave-type weakly electric fish, produces a continuous, quasi-sinusoidal, electric organ discharge (EOD) via an electric organ located in the tail (Lissmann, 1951; Lissmann, 1958). The EOD drives the baseline discharge of tuberous electroreceptors (P-units) distributed across the entire body. P-units are the electroreceptor type most relevant for encoding electrosensory input, used for communicating with conspecifics and navigating the environment (Bullock, 1969; Bullock, 1982). The afferents from each P-unit provide trifurcated, unilateral input to different subtypes of pyramidal cells located in the maps of the electrosensory lateral line lobe (ELL): the lateral segment (LS), centro-lateral segment (CLS), and centro-medial segment (CMS; for review see Krahe and Maler, 2014; Milam et al., 2019). Multiple topographic maps in the ELL are comprised of a heterogeneous network of ON and OFF-type pyramidal cells (Heiligenberg and Dye, 1982; Maler, 2009a; Shumway et al., 1989). Pyramidal cells are organized in a columnar layout, containing superficial, intermediate,

and deep-type pyramidal cells. Within each map, pyramidal cells vary in their response properties and center-surround receptive field parameters (Chacron et al., 2001; Krahe et al., 2008). Receptive fields in the LS map are the largest, the CMS map contains the smallest receptive fields, and receptive fields in the CLS map are intermediate. It has been suggested that different neural maps are specialized for certain behavioral tasks (Allen and Marsat, 2018; Maler, 2007). However, besides a few focused studies, little is known about how pyramidal cells (at the individual neuron or population level) respond to spatially realistic, conspecific stimuli (Kelly et al., 2008; Litwin-Kumar et al., 2012).

Recent field and lab studies on interacting weakly electric fish indicate that these animals possess an aptitude for detecting and localizing conspecific signals in their environment, even in conditions where sensory cues are limited (Zupanc and Maler, 1993; Stamper et al., 2012; Henninger et al., 2018; Knudsen, 1975; Berman and Maler, 1999; Yu et al., 2012; Fotowat et al., 2013; Jung et al., 2016). The diffuse nature of these signals (affecting peripheral receptors covering the entire body, i.e., “global signal”) suggests that the central nervous system must discriminate between small differences in the spatial signal to encode conspecific location accurately. Though behavioral observations clearly demonstrate their sensory capacity, how the nervous system accomplishes this task remains unknown. Our goal in this study is to understand how the primary electrosensory area of the nervous system encodes the location of a conspecific based on their self-generated signal. We aim to uncover how multiple receptor inputs are integrated by pyramidal cells in the hindbrain so that relevant spatial information is encoded in a way that enables accurate localization of conspecifics. We argue that efficient extraction of spatial information should involve implementing different neural streams and

codes. We hypothesize that a heterogeneous population of pyramidal cells uses different neural coding strategies for efficiently processing conspecific stimuli that vary based on their spatial parameters.

In this study, we directly compare neural heterogeneity at the lowest level of the electric fish's central nervous system – the ELL – and accurate neural coding of conspecific location. We first show that the spatially realistic, conspecific stimulus elicits responses from ELL pyramidal cells represented in both rate and temporal aspects of the spike train. After single cell analysis, we quantify a population response from a heterogeneous pool of pyramidal cells and demonstrate that information about the spatial stimulus is encoded in the pattern of the population response. We calculate the discrimination performance of the population and find that spatial stimuli are accurately and efficiently encoded. This confirms that combining sensory input from multiple pyramidal cell receptive fields yields higher discrimination performance for coding conspecific position. We separate the population into categories and reveal a pyramidal cell type specialization for spatial coding of conspecific information based on the aspect of the response used for discrimination. Finally, we assess neural coding performance across a range of stimulus spatial scales, and using a weighted analysis, confirm that a segregation of conspecific spatiotemporal information begins in the primary sensory area of weakly electric fish.

Materials and Methods

Animals

Wild-caught *Apteronotus leptorhynchus* were obtained from commercial fish suppliers. Tanks water conductivity were maintained at 200-300 µS and at temperatures of 26-27°C. All procedures were approved by the West Virginia University IACUC.

Electrophysiology

Surgical techniques were as previously described (Allen and Marsat, 2019; Marsat and Maler, 2010; Marsat et al., 2009). Briefly, *A. leptorhynchus* was anesthetized with tricane methanesulfonate (Western Chemical, Inc.) and respirated during surgery. A local anesthetic (Lidocaine HCL 2%, Hospira, Inc.) was applied, and the skin overlying the craniotomy site was removed. A fixed post with a circular opening was glued to a portion of the exposed skull for stability. The fish was immobilized with an injection of tubocurarine chloride pentahydrate (0.2 mg ml^{-1}, TCI). The experimental tank contained water with conductivity at 250 (±10) µS and temperature at 26 (±1) °C. The portion of the skull above the ELL was removed. A cone was secured to the fixed post, allowing top-down access to the exposed ELL. Melted resin was used to form a watertight seal between the ventral opening of the cone and the skull around the exposed ELL. ACSF was applied to the brain. This cone allows for full body submersion into the experimental tank during recordings while preventing the brain from coming in contact with tank water. Respiration was switched from general anesthesia to anesthetic-free water for respiration. *In vivo*, single-unit recordings of the lateral segment (LS) and centrolateral segment (CLS) were performed using metal-filled extracellular electrodes (Frank and Becker, 1964). Recordings were amplified (A-M Systems, Model 1700) and data recorded (Axon Digidata 1500 and Axoscope software, Molecular Devices) at a 20kHz sampling rate. Pyramidal cells of the LS

and CLS were identified based on the blood vessel landmarks, depth of penetration (in the dorsal-ventral plane), and response properties of the (Maler et al., 1991; Saunders and Bastian, 1984).

Stimulation

All stimuli were sampled at 20 kHz and created in MATLAB (MathWorks, Inc.). Our stimulation procedure replicates the amplitude modulations (AM) experienced during social interactions. The baseline EOD was recorded between the head and tail of the fish. Each EOD cycle triggered a sine wave generator (Rigol DG1022A) to output one cycle of a sinusoidal signal with matching frequency to the fish's EOD. This signal was then multiplied using a custom-built signal multiplier by the AM stimulus to create the desired modulation of the electric field. Stimuli were played through a custom made stimulus isolator into the experimental tank using one of three configurations: a global stimulation, via two 30.5 cm carbon electrodes arranged parallel to the longitudinal axis of the fish; a local stimulation, via two silver chloridized electrodes 0.5 cm apart positioned at various positions near the skin surface; an artificial conspecific stimulation (i.e., fishpole), via two silver chloridized electrodes embedded in agarose with a conductivity of 35 µS (Hupé and Lewis, 2008; Kelly et al., 2008; Walz et al., 2013). Stimulation for global and local configurations were adjusted to provide ~20% contrast relative to the baseline EOD strength.

The fishpole signal was calibrated to match the amplitude of the electric field potential of real fish recorded from 24 different positions and distances around the fish (n=7, of mixed gender and size). One of the silver wires represented the rostral end of the fishpole (5.5 cm

long), and the other silver wire represented the caudal end (0.1 cm long). The two wires were separated by 4 cm, yielding a fishpole with 9.6 cm in length and a zero-plane potential located at ~70% of the rostral to caudal body length, in accordance with previous observations (Assad and Bower, 1997). The solidified, agarose body was carved to match the body shape of a real fish. The fishpole was positioned in the experimental tank at three different orientations/azimuths (0, 45, 90°), and 7 different locations around the fish 10 cm away. The 7 locations were the operculum, mid-body, and the zero-potential plane for both ipsilateral and contralateral sides of the fish (6 locations), and 1 location directly caudal to the fish (see Figure 1A). We use the term, orthogonal, to describe stimulus positions where the rostral end of the fishpole is oriented toward the receiving fish. Sinusoidal AM (SAM) stimuli were 40 s long, modulated at 30 Hz, and were played through the fishpole during the experiments.

Data Analysis

All analyses described here were performed using MATLAB. Spike trains collected from experimental recordings were first binarized into a sequence of zeros (no spike) and ones (spike). The binarized sequence was transformed into instantaneous firing rates by convolution with a gaussian filter. We used either the binarized spike train or the instantaneous firing rate (see below) that were separated into 1 second, 50% overlapping segments. Statistical analyses were performed using the MATLAB statistical analysis toolbox and custom-made scripts. Data was tested using a 2-way (or n-way) ANOVA. Following all ANOVAs, post hoc comparisons were made using a Tukey-Kramer test. Mean differences were considered statistically significant when $p < 0.05$.

Gain

The stimulus-response gain (*G*) to SAM stimulation was calculated by:

$$G(f) = \sum Q\,(f) \qquad (1)$$

where *Q* is the power spectral density of the convolved spike train, *f* are the frequencies within ± 0.5 Hz of the target SAM frequency (30 Hz). A larger stimulus-response gain value indicates a larger response from the neuron to a stimulus at the target frequency.

Vector Strength

The strength of phase locking to SAM stimulation was calculated by:

$$s = \frac{\sqrt{(\sum {x_i}^2)+(\sum {y_i}^2))}}{p} \qquad (2)$$

where *p* is the number of spikes, and *x* and *y* are the sine and cosine phases of the stimulus at which the *i* spike occurs (Goldberg and Brown, 1969; Marsat and Pollack, 2004). The vector strength, *s*, quantifies the precision and clustering of responses to a given phase of the stimulus cycle, with 0 being equal response at all phases of the beat, and 1 being a perfectly precise response at a single phase of the beat.

Discrimination Analysis

Our discrimination analysis is based on a weighted Euclidean distance analysis that relates directly to the information carried by a population of neurons to discriminate between stimuli (see Marsat et al., 2023, for more details). Here, we compare stimuli from different locations and used one of three measurements to quantify response strength: mean firing rate, vector

strength, or gain for each 1 s response segment. A weight is assigned to each neuron for each pair of stimuli being compared. The weight is based on the Kullback-Leibler divergence in the response distributions for each stimulus. The weight is normalized to 1 across neurons within a population response, the response strength is then multiplied by this weight. Population responses are then taken as data point in Euclidean space where each dimension is the weighted response of one neuron in the population. An ensemble of population response is thus considered, each of which is composed of a random 1 s segment of response from a subset of *n* neurons from the population (*n* will be varied, see below). The Euclidean distance between responses to the same stimulus and across different stimuli are then compared. Larger distances indicate less similarity between spike trains. Stimuli that can be easily discriminated will elicit responses that are very different (i.e., large Euclidean distance) relative to the variability across responses to the same stimulus. The weighting procedure allows to optimize the decoding efficiency by assigning a stronger contribution to the Euclidean distance to neurons that carry more information about the difference in the stimuli. The distributions of Euclidean distances for responses to the same stimulus $P(D_{xx})$ and across the two stimuli being compared $P(D_{xy})$ are then used in a receiver operating characteristic (ROC) analysis. Receiver operating characteristic (ROC) curves were generated by varying a threshold distance value T; for each threshold, the probability of non-discrimination (P_D) is calculated as the sum of $P(D_{xy}>T)$ and the probability of false discrimination (P_F) is calculated as the sum $P(D_{xx}>T)$. The error probability is taken as the minimum error, *E,* across thresholds:

$$E = \frac{1}{2}P_F + \frac{1}{2}(1 - P_D) \qquad (3)$$

Error probability of 0.5 indicates chance-level discrimination while an error rate of 0 indicates that the responses are different enough to support perfectly accurate discrimination.

Efficiency Rate

The size of the population of neurons used in the discrimination analysis can be varied. If it is based on the information contained in a single neuron, discrimination will be less accurate than if the information from many neurons is considered. By plotting the error probability as a function of the number of neurons included in the analysis, we can estimate how quickly the error rate decreases with increasing population size. This rate of decrease is representative of efficiency in population coding since it reflects how much information each neuron contributes. Based on this principle, we quantify a population coding efficiency by fitting an exponential function to the error probability as a function of population size:

$$F(x) = \alpha e^{-\lambda x} \quad (4)$$

Where λ is the efficiency rate value and *x* is the neural population size. A higher efficiency rate value, the more efficient the population is at discriminating between conspecific stimuli presented from different spatial positions or orientations.

2D Activation Heatmaps

Two-dimensional activation heatmaps are valuable as a qualitative tool for visualizing differences in neural responses when the stimulus is presented from different spatial locations and orientations around the fish. We used a 3D model of a fish on which a population of electroreceptor locations have been placed (i.e., each dot on the fish) that was used previously

(Ramachandra et al., 2023). The receptive field center of each neuron was delineated experimentally by moving a local dipole across the body surface and determining the edge of the classical receptive field where the neurons responded with their characteristic ON-center or OFF-center responses. All tuberous receptor locations within a neuron's receptive field boundary were assigned to that neuron, such that one receptor could belong to several neurons' receptive field centers. Values from the neural response measures (e.g., firing rate, gain, vector strength) for a given stimulus were appended to all receptors within the neurons' receptive field centers, and then averaged so that each receptor's location represented a single activation value for all its represented neurons.

Results

Conspecific stimuli played from an artificial, conspecific dipole mimic (i.e., "fishpole"), were presented to an immobilized *A. leptorhynchus* while recording extracellularly from ELL pyramidal cells *in vivo*. After mapping the cell's receptive field, the fishpole stimulus was positioned at one of three orientations (0,45,90°), and one of seven spatial positions (Fig 1A; see Methods) around the immobilized fish in random combination until all combinations of spatial stimuli were used. To replicate the signals experienced when a conspecific is present, we replicated the beat AM (i.e., sinusoidal amplitude modulations of the fish's own EOD) and used, in this paper, a beat frequency of 30 Hz because all pyramidal cells respond strongly at this frequency.

We examined how the location or orientation of the stimulus fish would influence the pyramidal cell responses. We noticed obvious qualitative differences in the neural response

that ranged across the spectrum of temporal to rate aspects of the spike train. The stimulus-elicited changes in response pattern were heterogeneous with some neurons showing pronounced changes in their mean firing rate whereas other cells responded with clear differences in vector strength with little to no change in rate (Fig 1B). We could not readily identify a single aspect of the response that most clearly correlated with changes in stimulus position. We therefore used three measures in our analysis that cover the range of rate vs temporal coding: mean firing rate, gain (which reflect changes in both timing and rate of the response), and vector strength (i.e., how tightly the response is concentrated at one phase of the stimulus).

Our aim is to compare how accurately the population of pyramidal cells encode that spatial location of the stimulus. To do so, we compare pair-wise population responses to different stimuli locations and quantify how different the pattern of responses are. The similarity in response pattern is based on a weighted Euclidean distance analysis that tightly correlates with the amount of information that the population carries about stimuli differences (i.e., location). This analysis results in an estimate of the error rate in stimuli discrimination that would occur by comparing population responses. This error rate is estimated as a function of the number of neurons included in the population response, a faster decrease in error rate with increasing population size (efficiency λ in Figure 2) indicates that the neurons carry more spatial information. We found that all unique pairs of spatial stimuli were able to be discriminated effectively, with the average of all unique stimulus pairs being discriminated reliably (<5% error) with populations of less than 20 neurons (Fig 2B). Thus, this data showed that the spatial aspect of the conspecific stimulus was reliably encoded within the pattern of the population response.

Some neurons clearly changed their response pattern for different stimuli positions whereas others showed more subtle changes. By comparing subpopulations of neurons with clear difference for a given stimulus pair, to a subpopulation with less obvious differences, we demonstrate in Figure 2C how our efficiency measure reflects how accurately stimulus position is encoded in the response pattern.

ELL pyramidal cells are heterogenous and many differences in their response properties have been documented. Yet, it is not known whether the different subpopulations differ in their encoding of the spatial aspect of conspecific signals. To answer this question, we compare the coding accuracy across categories: ON-type vs OFF-type cells, neurons of the LS vs CLS maps, and superficial/intermediate vs deep pyramidal cells. ON and OFF-type pyramidal cells were easily distinguished based on their preference of stimulus polarity (increases vs decreases in stimulus amplitude). Location of each recorded neuron relative to the different ELL maps was estimated based on the stereotaxic position of the recording electrodes and on the response properties of the neurons (see Supplementary Figure S1). In this study, we focus on the LS and CLS segments that are most relevant for processing conspecific signals. Important differences exist between deep pyramidal cells and cells that are more superficial. We pooled together putative superficial and intermediate cells because they occupy a similar place in the circuitry of the electrosensory system whereas deep pyramidal cells are functionally separate (Maler, 2009b). We categorized deep-type pyramidal cells based on their characteristically high spontaneous firing rate, lower coefficient of variation, and their better synchronization to the EOD compared to superficial and intermediate-type pyramidal cells (S 1D; S 1E; Bastian, 1986; Bastian et al., 2002; Krahe et al., 2008).

The classical receptive field of each neuron was delineated based on their response to a small local dipole that was moved across rostro-caudal and ventro-dorsal locations. The neurons we recorded had receptive fields in various positions from head to tail (Fig 3A, 3B). We note that, while most electrophysiological studies avoid sampling cells from the fish's head because the typical experimental configuration has the fish's head close to -or above- the water surface, we performed the experiment with the fish completely submerged in a more realistic position. We did not observe striking differences in response properties for cells of the head, despite the fact that they receive inputs from much more densely pack receptors than pyramidal cells from the trunk of the fish. Receptive field size varied from cell to cell (Fig 3B). As expected, CLS neurons had smaller receptive field sizes than LS neurons (Carr et al., 1982; see also Supplementary Figure S2). The receptive field sizes for deep-type and superficial/intermediate-type pyramidal cells were similar (Maler, 2007; Maler, 2009b; Maler, 2009a).

To visualize how ELL pyramidal cells varied in their response to stimuli from different locations, we constructed two-dimensional activation heatmaps based on one of the three response strength measurements (see Fig 1). These heatmaps (Fig 4) highlight a few key observations. First, as expected, stimuli from different locations lead to clear differences in the pattern of activation across the body. Also, the heatmaps highlight the heterogeneity and variability in the response pattern of pyramidal cells. Although an overall pattern of activation is visible, with receptive field facing the stimulus location being more strongly activated, pyramidal cells showed uneven patterns of activation with movement relative to their receptive field. Finally, these heatmaps illustrate that different subpopulations of pyramidal cells might

have a more obvious relationship between their response strength and the stimulus location. Specifically, we displayed responses of ON vs. Off and deep vs. superficial/intermediate where the ON and the deep cells show clearer differences across stimuli locations.

Further analysis revealed that the discrimination error for specific spatial stimulus pairs varied based on the response measure used in the analysis. Overall, we found that using the mean firing rate of the vector strength to quantify the response led to better spatial coding than using the gain (Fig 5A). It is worth mentioning that we also investigated how the phase of the response changed with the spatial stimulus. Some neurons showed noticeable shifts in response phase to a conspecific stimulus changing either orientation or location (Supplementary Figure S3). However, this measure proved less informative for population analysis, when their responses were combined with either cells that also exhibited phase changes or cells that showed no phase changes in their response.

The full population was separated into distinct categories of pyramidal cell types, and we asked if specific pyramidal cell types would discriminate spatial stimuli more efficiently depending on the aspect of the spike train response used for discrimination. We found that ON-type pyramidal cells can discriminate the spatial stimulus more efficiently than OFF-type pyramidal cells across all three measures (Fig 5B). Similar to the full population, both ON and OFF-type pyramidal cells obtained the highest efficiency rate using the vector strength, and the lowest when using stimulus-response gain. This exact finding was also observed when comparing deep-type pyramidal cells vs superficial/intermediate-type pyramidal cells (Fig 5D). However, when comparing efficiency between CLS and LS pyramidal cells, there was a flip in the measures that resulted in the highest efficiency rate. The population of CLS neurons was found

to be most efficient when using mean firing rate, whereas the LS population was most efficient using vector strength (Fig 5C). The same trend is observed when comparing neurons with large receptive fields (> 0.2 body proportion) against neurons with small receptive fields (< 0.2 body proportion; Fig 5E). This might reflect the fact that LS neurons tend to have larger receptive fields than CLS neurons. Our data thus indicates that CLS and LS neurons encode spatial information with a different proportion of rate vs. temporal coding, with CLS cells relying more on rate coding compared to LS cells that encode spatial information better in the timing of the response.

An alternative approach to characterizing how different neurons encode spatial information is to describe the properties of neurons that carry relatively more information about stimulus location. Our decoding analysis assigns a weight to each neuron based on how different their response is to the stimuli locations being compared. This weight is based on the Kullback-Leibler divergence between response distributions which relates to the information present in the spike trains (Allen and Marsat, 2018; Allen and Marsat, 2019; Marsat and Maler, 2010; Marsat et al., 2023; van Rossum, 2001). By using the average weight assigned to a neuron across stimuli comparisons, we categorized the cells as being associated with high weights (> 0.7; Fig 6A) or low weights (< 0.7). Consequently, the cells in each group have a higher vs. lower coding efficiency (Fig. 6B). This approach is complementary to our previous analysis because it allows us to determine the characteristics of cells that encode spatial information particularly well. We found that the high-weight group carried more information in their response timing (i.e., vector strength; Fig 6B), whereas the low-weight group encoded more spatial information in their mean firing rate. Interestingly, this trend parallels the differences we observed

comparing LS and CLS cells and cells with large vs. small receptive fields (see Fig 5). Our analysis of cell properties in each weight category also confirms the previous findings. Specifically, cells in the high weight category had a higher average spontaneous firing rate, lower average coefficient of variation, and larger average receptive field size than neurons in the low weight category (Fig 6C; Fig 6D; Fig 6E). We verified that putative deep pyramidal cells were more likely to be in the high-weight category (Fig 6F).

The results presented in previous figures averaged the analysis of pairs of stimuli locations. We now ask if the difficulty in discriminating between spatial stimuli could be influenced by the proximity of the stimulation sites. For example, two spatial stimuli that are close to one another may be a more difficult discrimination task than two spatial stimuli that are far apart. We hypothesized that the differences we observed in spatial coding efficiency across cell types were even more apparent when considering only the more difficult discrimination tasks. Surprisingly, we found only modest differences in coding efficiency when comparing stimuli that are next to each other (ipsilateral, Fig 7) or on opposite sides of the body (contralateral). Overall, coding efficiency was better for coarse discrimination (contralateral) than fine discrimination (ipsilateral). The cell sub-type performing best, and the response properties encoding the most information were the same as noted in the previous analysis and there were no qualitative differences when considering coarse vs. fine discrimination tasks. Our stimuli locations and intensity mimicked a medium-sized fish relatively close to the fish being tested. Recent finding suggests that the spatial information present in the population of receptors should be relatively accurate for stimuli at these distances (Ramachandra et al. 2023). It is thus probable that even when comparing our closest stimuli locations, we are not testing the lower

limits of the cell's sensitivity. Using weaker stimuli (Supplementary Figure S5), placing the stimulus source further away or comparing locations with less separation would result in lower coding performance and potentially increase the modest differences we observe between fine and coarse discrimination tasks.

Discussion

We investigated spatial coding of conspecific stimuli by electrosensory neuron populations in the hindbrain. To do so, we performed *in-vivo* electrophysiological recordings on immobilized *A. leptorhynchus*, as an artificial dipole mimic (i.e., "fishpole") was used to stimulate from various positions within the experimental tank. Specifically, we targeted the topographic maps of the hindbrain ELL, which contain heterogeneous populations of pyramidal cells that vary in their anatomy and physiological response properties. Using our full dataset of recorded neurons, we found that this full population could discriminate accurately (< 5% error) between all unique pairs of spatial stimuli presented (see Methods). In addition to heterogeneity in anatomy and physiology, ELL pyramidal cells also vary in their functional connectivity based on their layer in the map. For example, pyramidal cells in the deep layer have no receptive field surround and do not receive feedback from either the nucleus praeminentialis or via cerebellar granular cells from the posterior eminentia granularis. In fact, deep pyramidal cells are the source of feedback to superficial and intermediate-type pyramidal cells in the ELL (Maler et al., 1991; Berman and Maler, 1999; see also Milam et al., 2019, for review). We therefore investigated how the discrimination ability differs between subpopulations in the ELL. Briefly, we found that: (1) ON-type pyramidal cells displayed lower error than OFF-type; (2) deep

pyramidal cells outperformed superficial and intermediate-type; (3) pyramidal cells with larger receptive fields were better than those with small receptive fields; and (4) LS neurons discriminated more accurately than CLS neurons on average. By far, the clearest difference we observed in spatial coding was between the deep and superficial pyramidal cell populations. Previous studies have shown that superficial pyramidal cells excel in temporal coding of communication signals (e.g., chirps). Interestingly, in this study we found that superficial cells performed poorly in encoding spatial information from conspecific signals. When contrasted with deep cells, which excelled in the same spatial coding task, this result complements findings from Vonderschen and Chacron (2011). In their study, they describe a dichotomy of sparse and dense coding strategies by neural subpopulations, downstream from the ELL in the midbrain torus semicircularis. Sparse coders in the torus were specialized for encoding sensory information related to specific chirp features, whereas dense coders were more broadly responsive to electrosensory stimuli. Similar to the torus, the ELL has a laminar structure, as well as a complex network of connections. Electrosensory input from the ELL to the torus is topographically conserved and confined to the dorsal torus (Carr et al., 1981). Downstream, the electrosensory pathway separates as the torus outputs: to the optic tectum involved in spatial processing; to the nucleus electrosensorius involved in processing communication signals; and to the preglomerular nucleus that mediates connectivity with the forebrain (Giassi et al., 2012; Zupanc and Horschke, 1997a; Zupanc and Horschke, 1997b). Topography is conserved to brain regions as far as the optic tectum, but is lost in the nucleus electrosensorius, the preglomerular nucleus, and the forebrain dorsal telencephalon (pallium). It is for this reason that the optic tectum is considered to be an important area for multisensory integration, and putatively an

ultimate localization center. Taken together, our findings suggest that the separation of spatial vs identity (e.g., communication) coding begins as early as the ELL with an early split starting between deep vs superficial pyramidal cells, albeit a large overlap in function. Further studies are needed to investigate spatial coding in higher brain areas where topography remains conserved.

Our results show that certain neural subpopulations allow for more accurate discrimination when using mean firing rate, while others encode more accurately in their response synchrony. We found that this pattern is most obvious when comparing population responses between the LS and CLS maps. Pyramidal cells in the LS map displayed less discrimination error when using vector strength, whereas CLS cells performed better, on average, when using mean firing rate. This response preference is indicative of a switch in the neural coding strategies used by different topographic maps. Several factors might be contributing to the differences in coding preference that we observed here, such as: receptive field parameters, adaptation, and the influence of feedback. Nonetheless, this finding provides an opportunity for speculation as to what measures of the spiking response are most relevant for spatial coding in downstream sensory areas. For example, it is unclear what aspects of the pyramidal cells' response influence spatial coding in the midbrain torus. While we know that dense coders in torus will modulate their firing rate with peak and trough of a conspecific beat, the strength of the response can be affected by the average number of spikes or by having a spike that clusters more around a single phase, such that both spike rate and timing could be relevant. Preferences in the neural response tailored to specific stimulus features have been well documented, some good examples being combinatorial and multiplexed neural codes (Bodnar and Bass, 1999; Lankarany

et al., 2019). For example, studies on human sound localization have shown how neurons that receive shared input can use asynchronous firing rate to encode the intensity of low-contrast features, while also using precise timing of synchronous spikes to encode high-contrast features (Lankarany et al., 2019). Similarly, other behavioral experiments on human sound localization have found that softer sounds can be perceived closer to the midline than louder sounds, favoring a rate-coding strategy (Ihlefeld et al., 2019). Furthermore, research on spatial navigation has shown that the time of firing can represent an animal's location within a place field, whereas the firing rate can represent the animal's velocity through the field (Huxter et al., 2003). Information can also be transmitted through short interspike intervals within a burst (Krahe and Gabbiani, 2004; Oswald et al., 2007). Thus, it is well supported that in heterogeneous neural populations spatial information about a conspecific's location can be represented in different aspects of the spiking response. Indeed, further studies are necessary to dissect the role of information coding related to conspecific location.

Our results demonstrate that spatial coding efficiency is high across most subpopulations of pyramidal cells in the ELL. Accurate discrimination between pairs of stimulus positions is possible using a small number of cells relative to the full population. Specifically, the discrimination accuracy is high for conspecifics located at distances of 10 cm away. At this distance, we are not testing stimuli at the edge of sensitivity, as recent studies have estimated that difficult discrimination tasks start at distances of approximately 30 cm away (Ramachandra et al., 2023). Furthermore, our discrimination analysis takes 1 s averages of neural responses and assumes that a decoder can integrate these inputs over time. If integrating over less time, because the neural system does not operate on long time scales or because the fish does not

remain in a fixed location, the discrimination accuracy will decrease. Moreover, this decoding analysis might not encompass the relevant aspect of the neural response, or could underestimate coding accuracy. An alternative decoding method might implement a principal component approach to average out noise more effectively. On the other hand, our analysis could also be overestimating the coding efficiency. In our analysis, we weigh each neuron and thus leverage the most informative neurons over those that provide less information. It is possible that this may not be the exact computation that subpopulations of ELL pyramidal cells are performing, as our measure relates directly to the amount of information present in the system (Marsat et al., 2023). Additionally, the gathering of information can be enhanced via active sensing behaviors. Such specialized and often stereotype-patterned behaviors occur across systems and include edge detection and tracking of odor plumes in moth olfaction, and foveal sampling in the visual and electrosensory systems, to name a few (Enikolopov et al., 2018; Pedraja et al., 2019). Certain bat species have been shown to take advantage of their angle of approach with respect to the background surface to increase the signal to noise ratio of a prey echo during prey capture behavior. Such acoustically camouflaged prey items would normally have their weak prey echoes masked by background echoes from other objects in the natural environment (Geipel et al., 2019). High accuracy steering towards the location of a sound source at a fixed azimuth has been documented in crickets (Schöneich and Hedwig, 2010). This finding suggests that localization ability could be high when integration over time can happen. Cricket zig-zag walking and other corrective repositioning behaviors, could help to re-evaluate the localization error during movement. Thus, localization during behavior should consider the motion component and that the process from sensory to motor and back is highly

dynamic. Further studies on the role of active sampling and dynamic sensorimotor adjustments are needed to better understand how the spatial aspect of signals are encoded by the nervous system.

Our results provide new insights for population coding of spatially realistic conspecific signals and what aspects of the neural response are most important for localization. Overall, our data suggests that the start of segregation of spatial processing occurs in ELL pyramidal cells. It is likely that the experimental findings we present here for quantifying spatial coding performance in pyramidal cells are generalizable to other sensory systems. The neural circuitry in the ELL contains several network elements that are shared across modalities, such as classical receptive field center-surround organization, topographic maps of the body, and feedback influences that contribute to shaping the neural code. Taken together, this study serves as foundational work for understanding how a primary sensory area of the hindbrain represents the location of conspecifics. Future studies will be necessary to gain a better understanding of the complex interaction between extracting the location and the “message” in sensory signals.

References

Allen, K. M. and Marsat, G. (2018). Task-specific sensory coding strategies are matched to detection and discrimination performance. *J Exp Biol* **221**, jeb170563.

Allen, K. M. and Marsat, G. (2019). Neural Processing of Communication Signals: The Extent of Sender–Receiver Matching Varies across Species of Apteronotus. *eNeuro* **6**,.

Assad, C. and Bower, J. M. (1997). Electric field maps and boundary element simulations of electrolocation in weakly electric fish. *Engineering and Applied Science* **PhD**,.

Barlow, H. B. (1961). Possible principles underlying the transformation of sensory messages. In *Sensory communication* (ed. Rosenblith, W. A.), pp. 217–234. Cambridge, MA: MIT press.

Bastian, J. (1986). Gain control in the electrosensory system: a role for the descending projections to the electrosensory lateral line lobe. *Journal of Comparative Physiology A* **158**, 505–515.

Bastian, J., Chacron, M. J. and Maler, L. (2002). Receptive field organization determines pyramidal cell stimulus-encoding capability and spatial stimulus selectivity. *Journal of Neuroscience* **22**, 4577–4590.

Berman, N. J. and Maler, L. (1999). Neural architecture of the electrosensory lateral line lobe: adaptations for coincidence detection, a sensory searchlight and frequency-dependent adaptive filtering. *Journal of Experimental Biology* **202**,.

Bialek, W. and Rieke, F. (1992). Reliability and information transmission in spiking neurons. *Trends Neurosci* **15**, 428–434.

Bodnar, D. A. and Bass, A. H. (1999). Midbrain combinatorial code for temporal and spectral information in concurrent acoustic signals. *J Neurophysiol* **81**, 552–563.

Bradbury, J. W. and Vehrencamp, S. L. (2011). *Principles of animal communication*. 2nd ed. Sunderland, Mass., Mass.: Sinauer Associates.

Bullock, T. H. (1969). Species differences in effect of electroreceptor input on electric organ pacemakers and other aspects of behavior in electric fish. *Brain Behav Evol* **2**, 85–118.

Bullock, T. H. (1982). Electroreception. *Annual Reviews of Neuroscience* **5**, 70.

Bullock, T. H., Bennett, M. V. L., Johnston, D., Josephson, R., Marder, E. and Fields, R. D. (2005). The neuron doctrine, redux. *Science (1979)* **310**, 791–793.

Carr, C. E., Maler, L., Heiligenberg, W. and Sas, E. (1981). Laminar organization of the afferent and efferent systems of the torus semicircularis of Gymnotiform fish: Morphological substrates for parallel processing in the electrosensory system. *Journal of Comparative Neurology* **203**, 649–670.

Carr, C. E., Maler, L. and Sas, E. (1982). Peripheral organization and central projections of the electrosensory nerves in gymnotiform fish. *Journal of Comparative Neurology* **211**, 139–153.

Chacron, M. J., Longtin, A. and Maler, L. (2001). Negative interspike interval correlations increase the neuronal capacity for encoding time-dependent stimuli. *J Neurosci* **21**, 5328–43.

Dayan, P. and Abbott, L. F. (2001). *Theoretical neuroscience: computational and mathematical modeling of neural systems*. Cambridge, MA: Academic Press.

Enikolopov, A. G., Abbott, L. F. and Sawtell, N. B. (2018). Internally Generated Predictions Enhance Neural and Behavioral Detection of Sensory Stimuli in an Electric Fish. *Neuron* **99**, 135-146.e3.

Fotowat, H., Harrison, R. R. and Krahe, R. (2013). Statistics of the Electrosensory Input in the Freely Swimming Weakly Electric Fish Apteronotus leptorhynchus. *Journal of Neuroscience* **33**, 13758–13772.

Frank, K. and Becker, M. C. (1964). Microelectrodes for recording and stimulation. In *Physical techniques in biological research* (ed. Nastuk, W. L.), pp. 23–84. New York: Academic Press.

Geipel, I., Steckel, J., Tschapka, M., Kalko, E. K. V, Peremans, H. and Correspondence, R. S. (2019). Bats Actively Use Leaves as Specular Reflectors to Detect Acoustically Camouflaged Prey. *Current Biology* **29**,.

Giassi, A. C. C., Ellis, W. and Maler, L. (2012). Organization of the gymnotiform fish pallium in relation to learning and memory: III. Intrinsic connections. *Journal of Comparative Neurology* **520**, 3369–3394.

Goldberg, J. M. and Brown, P. B. (1969). Response of binaural neurons of dog superior olivary complex to dichotic tonal stimuli: some physiological mechanisms of sound localization. *J Neurophysiol* **32**, 613–636.

Heiligenberg, W. and Dye, J. (1982). Labelling of electroreceptive afferents in a gymnotoid fish by intracellular injection of HRP: The mystery of multiple maps. *Journal of Comparative Physiology □ A* **148**, 287–296.

Henninger, J., Krahe, R., Kirschbaum, F., Grewe, J. and Benda, J. (2018). Statistics of natural communication signals observed in the wild identify important yet neglected stimulus regimes in weakly electric fish. *J Neurosci* 0350–18.

Hupé, G. J. and Lewis, J. E. (2008). Electrocommunication signals in free swimming brown ghost knifefish, Apteronotus leptorhynchus. *J. Exp. Biol.* **211**, 1657–1667.

Huxter, J., Burgess, N. and O'Keefe, J. (2003). Independent rate and temporal coding in hippocampal pyramidal cells. *Nature* **425**, 828–832.

Ihlefeld, A., Alamatsaz, N. and Shapley, R. M. (2019). Population rate-coding predicts correctly that human sound localization depends on sound intensity. *Elife* **8**,.

Jung, S. N., Longtin, A. and Maler, L. (2016). Weak signal amplification and detection by higher-order sensory neurons. *J Neurophysiol* **115**, 2158–2175.

Kelly, M., Babineau, D., Longtin, A. and Lewis, J. E. (2008). Electric field interactions in pairs of electric fish: Modeling and mimicking naturalistic inputs. *Biol Cybern* **98**, 479–490.

Knudsen, E. I. (1975). Spatial aspects of the electric fields generated by weakly electric fish. *Journal of Comparative Physiology ? A* **99**, 103–118.

Krahe, R. and Gabbiani, F. (2004). Burst firing in sensory systems. *Nat Rev Neurosci* **5**, 13–23.

Krahe, R. and Maler, L. (2014). Neural maps in the electrosensory system of weakly electric fish. *Curr Opin Neurobiol* **24**, 13–21.

Krahe, R., Bastian, J. and Chacron, M. J. (2008). Temporal processing across multiple topographic maps in the electrosensory system. *J Neurophysiol* **100**, 852–67.

Lankarany, M., Al-Basha, D., Ratté, S. and Prescott, S. A. (2019). Differentially synchronized spiking enables multiplexed neural coding. *Proc Natl Acad Sci U S A* **116**, 10097–10102.

Lissmann, H. W. (1951). Continuous Electrical Signals from the Tail of a Fish, Gymnarchus niloticus Cuv. *Nature* **167**, 201–202.

Lissmann, H. W. (1958). On the Function and Evolution of Electric Organs in Fish. *Journal of Experimental Biology* **35**, 156-.

Litwin-Kumar, A., Chacron, M. J. and Doiron, B. (2012). The Spatial Structure of Stimuli Shapes the Timescale of Correlations in Population Spiking Activity. *PLoS Comput Biol* **8**, e1002667.

Maler, L. (2007). Neural strategies for optimal processing of sensory signals. In *Progress in Brain Research*, pp. 135–154.

Maler, L. (2009a). Receptive field organization across multiple electrosensory maps. I. Columnar organization and estimation of receptive field size. *Journal of Comparative Neurology* **516**, 376–393.

Maler, L. (2009b). Receptive field organization across multiple electrosensory maps. II. Computational analysis of the effects of receptive field size on prey localization. *J Comp Neurol* **516**, 394–422.

Maler, L., Sas, E., Johnston, S. and Ellis, W. (1991). An atlas of the brain of the electric fish Apteronotus leptorhynchus. *J Chem Neuroanat* **4**, 1–38.

Marsat, G. and Maler, L. (2010). Neural Heterogeneity and Efficient Population Codes for Communication Signals Marsat G, Maler L. Neural heterogeneity and efficient population codes for communication signals. *J Neurophysiol* **104**, 2543–2555.

Marsat, G. and Pollack, G. S. (2004). Differential temporal coding of rhythmically diverse acoustic signals by a single interneuron. *J Neurophysiol* **92**, 939–948.

Marsat, G., Proville, R. D. and Maler, L. (2009). Transient Signals Trigger Synchronous Bursts in an Identified Population of Neurons Marsat G, Proville RD, Maler L. Transient signals trigger syn- chronous bursts in an identified population of neurons. *J Neuro-physiol* **102**, 714–723.

Marsat, G., Daly, K. C. and Drew, J. A. (2023). Characterizing neural coding performance for populations of sensory neurons: comparing a weighted spike distance metrics to other analytical methods. *bioRxiv* 778514.

Milam, O. E., Ramachandra, K. L. and Marsat, G. (2019). Behavioral and neural aspects of the spatial processing of conspecifics signals in the electrosensory system. *Behavioral Neuroscience* **133**, 282–296.

Oswald, A. M. M., Doiron, B. and Maler, L. (2007). Interval coding. I. Burst interspike intervals as indicators of stimulus intensity. *J Neurophysiol* **97**, 2731–2743.

Pedraja, F., Perrone, R., Silva, A. and Budelli, R. (2016). Passive and active electroreception during agonistic encounters in the weakly electric fish Gymnotus omarorum. *Bioinspir Biomim* **11**, 065002.

Pedraja, F., Hofmann, V., Goulet, J. and Engelmann, J. (2019). Task related sensorimotor adjustments increase the sensory range in electrolocation. *The Journal of Neuroscience* 1024–19.

Saunders, J. and Bastian, J. (1984). The physiology and morphology of two types of electrosensory neurons in the weakly electric fish Apteronotus leptorhynchus. *Journal of Comparative Physiology A* **154**, 199–209.

Schöneich, S. and Hedwig, B. (2010). Hyperacute directional hearing and phonotactic steering in the cricket (Gryllus bimaculatus deGeer). *PLoS One* **5**,.

Shannon, C. E. (1953). The lattice theory of information. *IRE Professional Group on Information Theory* **1**, 105–107.

Shumway, C. A., Koch, C., Wessel, R. and Gabbiani, F. (1989). Multiple electrosensory maps in the medulla of weakly electric gymnotiform fish. II. Anatomical differences. *J Neurosci* **9**, 4400–15.

Stamper, S. A., Madhav, M. S., Cowan, N. J. and Fortune, E. S. (2012). Beyond the Jamming Avoidance Response: weakly electric fish respond to the envelope of social electrosensory signals. *Journal of Experimental Biology* **215**, 4196–4207.

van Rossum, M. C. (2001). A novel spike distance. *Neural Comput* **13**, 751–763.

Vonderschen, K. and Chacron, M. J. (2011). Sparse and dense coding of natural stimuli by distinct midbrain neuron subpopulations in weakly electric fish. *J Neurophysiol* **106**, 3102–3118.

Walz, H., Hupé, G. J., Benda, J. and Lewis, J. E. (2013). The neuroethology of electrocommunication: How signal background influences sensory encoding and behaviour in Apteronotus leptorhynchus. *Journal of Physiology-Paris* **107**, 13–25.

Yu, N., Hupé, G., Garfinkle, C., Lewis, J. E., Longtin, A. and Fortune, E. (2012). Coding Conspecific Identity and Motion in the Electric Sense. *PLoS Comput Biol* **8**, e1002564.

Zupanc, G. K. and Horschke, I. (1997a). Reciprocal connections between the preglomerular nucleus and the central posterior/prepacemaker nucleus in the diencephalon of weakly electric fish, Apteronotus leptorhynchus. *Neuroscience* **80**, 653–67.

Zupanc, G. K. and Horschke, I. (1997b). Neurons of the posterior subdivision of the nucleus preopticus periventricularis project to the preglomerular nucleus in the weakly electric fish, Apteronotus leptorhynchus. *Brain Res* **774**, 106–15.

Zupanc, G. K. H. and Maler, L. (1993). Evoked chirping in the weakly electric fish Apteronotus leptorhynchus – a quantitative biophysical analysis. *Can J Zool* **71**, 2301–2310.

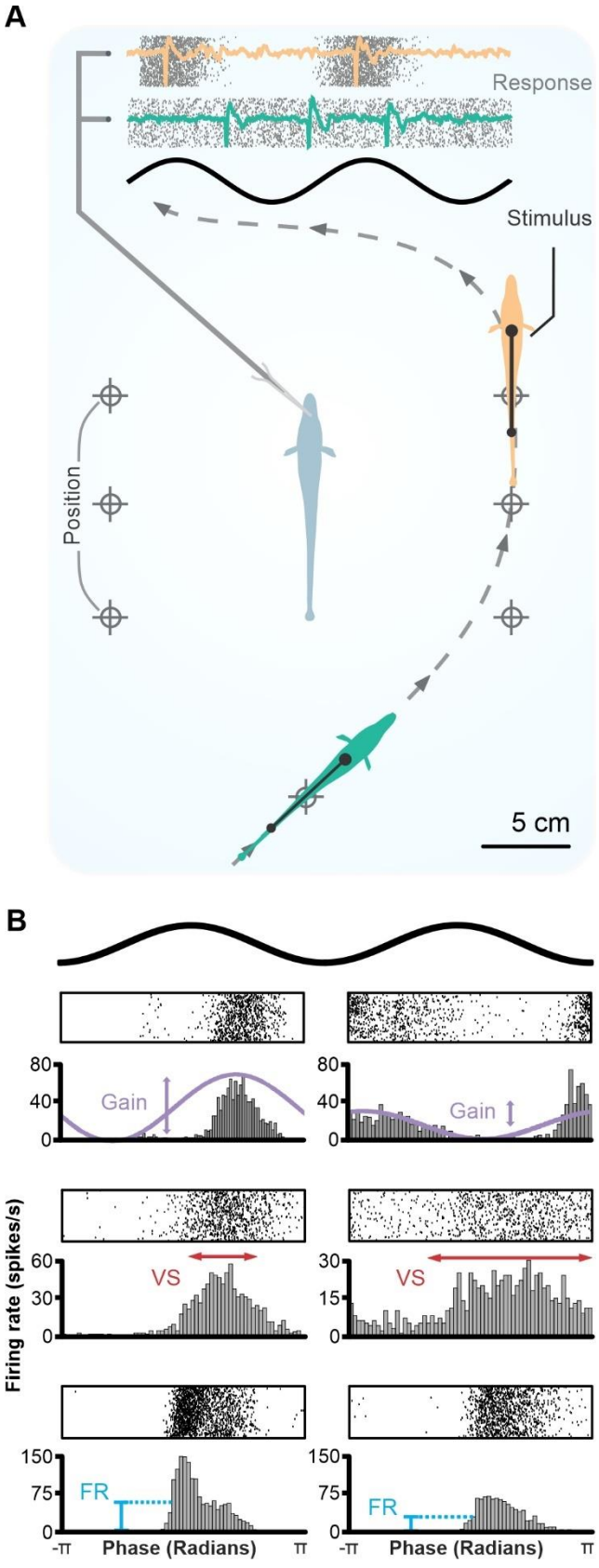

Figures and Legends

Figure 1. Spatially realistic conspecific signals and response strengths in the ELL.

(A) Schematic of the experimental design. An immobilized *A. leptorhynchus* (center, light blue) is stimulated using a conspecific dipole mimic (i.e., "fishpole") positioned at various spatial locations and azimuths around the experimental tank (at distances of 10 cm), while recording extracellularly from ELL pyramidal neurons *in vivo*. Neural responses to two cycles of the conspecific stimulus (top, black) are shown as raster plots layered with a trace of the raw neural recordings. The examples highlight differences in the pattern of the spike train responses for encoding spatial stimuli (orange and green).

(B) Measurement of response strength to stimulations with conspecific stimulus from different stimulation sites (yellow site for A.: left column; green site: right column). Raster plots of the response are shown above, and

the corresponding peristimulus time histogram (PSTH) are shown below. Changes in spatial location and orientation of the conspecific stimulus can elicit increases or decreases in the spike train response of ELL pyramidal cells. Responses to the spatial stimulus vary in stimulus-response gain (top, purple), vector strength (middle, red), and mean firing rate (bottom, blue).

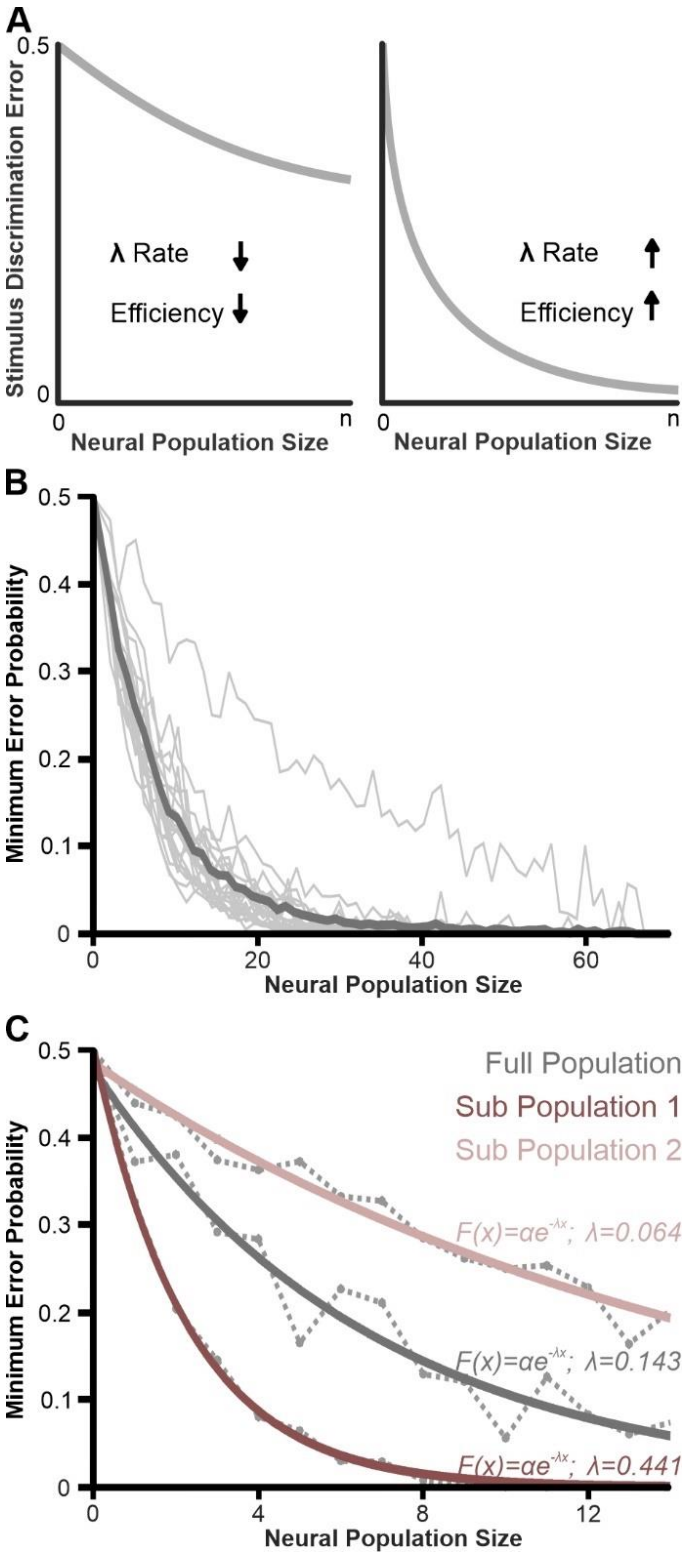

Figure 2. Coding efficiency quantified by the rate of decrease of the discrimination error as the information from more neurons are included in the analysis. **(A)** Schematic detailing how coding efficiency is related to the rate of discrimination error. For a pairwise stimulus discrimination task, the efficiency (λ) can be defined as the change in discrimination error as a function of neural population size. A slow decrease in error as the information from more neurons is pooled indicates a low coding efficiency (each neuron has little information or redundant information). A faster decrease (left plot compared to the right) indicates a higher efficiency. **(B)** Pairwise stimulus discrimination using vector strength on the full population of recorded pyramidal cells (n=70). All unique paired combinations of spatial stimuli are shown in the background (light gray), with the

mean across all stimulus pairs in the foreground (dark gray). A discrimination accuracy level of 95% is obtained with fewer than 20 neurons.

(C) Stimulus discrimination and efficiency across different neural populations. We selected two subsets of neuron (n=14 each): one where we could see obvious differences in responses between two stimuli locations and one where differences were not obvious. We used our analysis on these two subsets simply to illustrate the results expected from efficiently coding neurons (Sub-Population 1) and from a population with low coding efficiency.

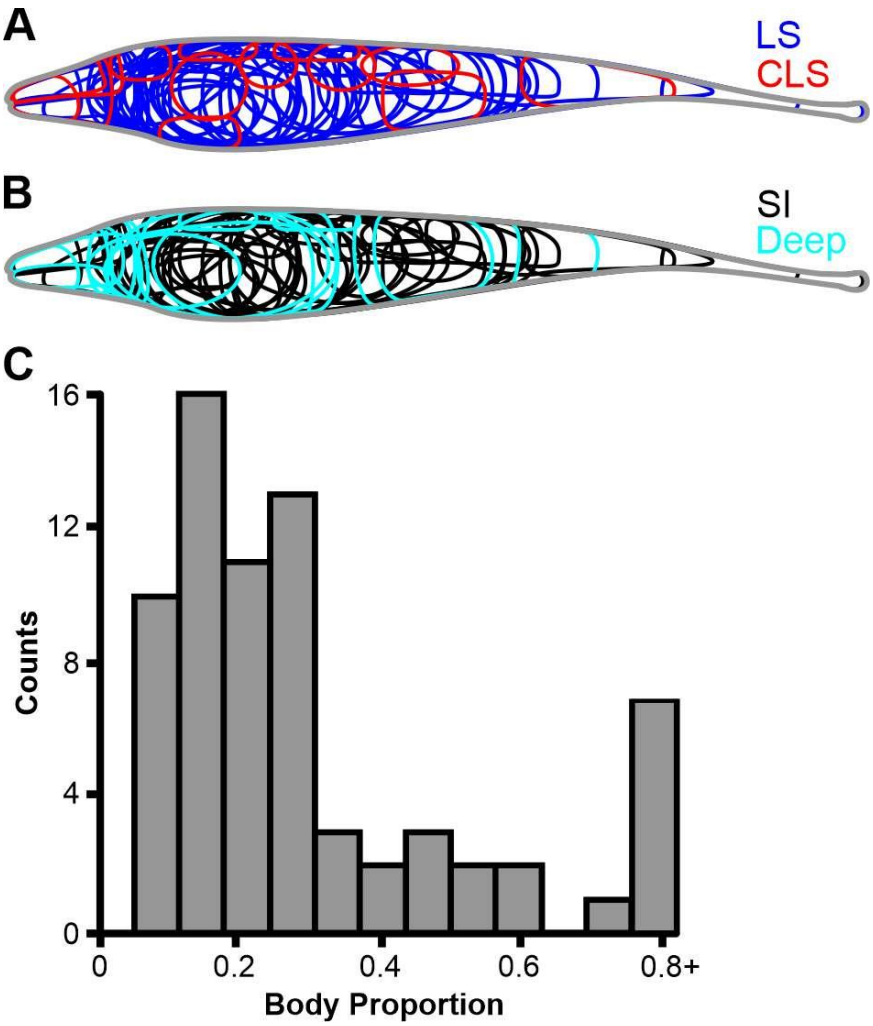

Figure 3. Receptive field of pyramidal cells sampled. **(A)** Boundaries of receptive field centers from recorded LS (n=55) and CLS (n=15) pyramidal cells on a two-dimensional outline of an *A. leptorhynchus*. **(B)** Boundaries of receptive field centers from recorded deep-type (n=18) and superficial/intermediate-type (n=52) pyramidal cells. **(C)** Histogram of all recorded pyramidal cell receptive field sizes (n=70). Size is represented as a fraction of the length in the rostro-caudal axis compared to the total body length.

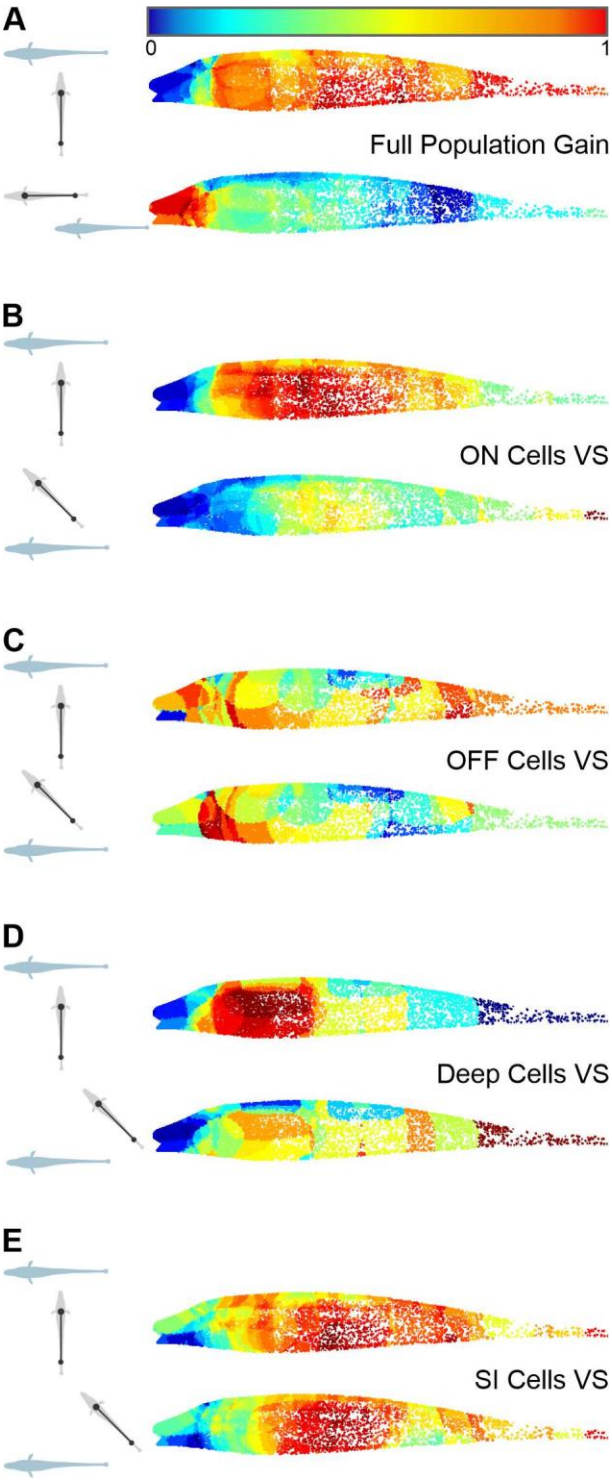

Figure 4. Responses to spatially realistic conspecific signals visualized as topographic heatmaps for different subsets of pyramidal cells.

The heatmaps allow a visualization of the population response to a conspecific stimulus played from various relative positions and orientations (shown on the left insets). Each colored point on the heatmap represents a putative receptor on the skin of the fish (see Methods and Ramachandra et al., 2023). A receptor can contribute to several neurons' receptive field and its color will reflect the average responses (e.g., gain) across these neurons. For each neuron to contribute equally to the heatmap, their responses are normalized to 1 where 1 is the strongest response of the neuron across all stimuli positions. In the 5 pairs of heatmaps presented here for different subpopulations of cells, we see differences across stimulus locations that vary from obvious (A, B, D) to more subtle (C, E)

(A) Heatmaps of the full population of recorded pyramidal cells (n=70) using gain as a response measure.

(B) Heatmaps of the ON-type pyramidal cells subpopulation (n=46) using vector strength as response measure.

(C) Heatmaps of the OFF-type pyramidal cells subpopulation (n=24) using vector strength as response measure.

(D) Heatmaps of the deep pyramidal cells subpopulation (n=18) using vector strength as response measure.

(E) Heatmaps of the superficial/intermediate pyramidal cells subpopulation (n=52) using vector strength as response measure.

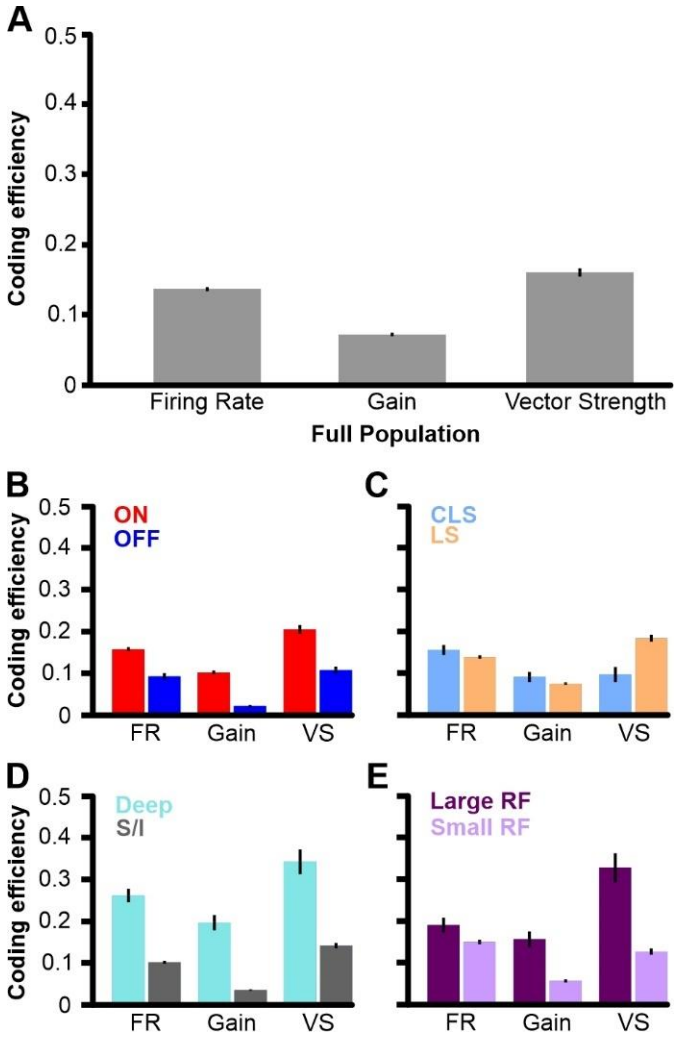

Figure 5. Spatial coding efficiency varies with pyramidal cell type and is dependent on the aspect of the neural response relevant for stimulus discrimination.

(A) Mean coding efficiency (± s.e. across stimuli pairs) of all pairwise stimulus combinations (orthogonal orientation; see Methods) using the full population (n=70). The highest efficiency is obtained when using vector strength to characterize neural responses; and the lowest efficiency is obtained when using response gain ($p < 0.0001$).

(B) Mean coding efficiency (± s.e. across stimuli pairs) for populations of ON (n=46) and OFF-type pyramidal cells (n=24). The highest efficiency results from vector strength, with the lowest efficiency from stimulus-response gain (ON - $p < 0.0001$, OFF - $p < 0.0001$). ON-type pyramidal cells have higher efficiency than OFF-type pyramidal cells across all measures ($p < 0.0001$).

(C) Mean coding efficiency (± s.e. across stimuli pairs) for populations of CLS (n=15) and LS pyramidal cells (n=55). There is a higher efficiency result from mean firing rate compared to gain for CLS ($p < 0.0001$), and for vector strength compared to gain for LS ($p < 0.0001$).

(D) Mean coding efficiency (± s.e. across stimuli pairs) for populations of deep (n=18) and superficial/intermediate-type pyramidal cells (n=52). The highest efficiency results from vector strength, with the lowest efficiency from stimulus-response gain (Deep - $p < 0.0001$, SI - $p < 0.0001$). Deep-type pyramidal cells have higher efficiency than superficial and intermediate-type pyramidal cells across all measures ($p < 0.0001$).

(E) Mean coding efficiency (± s.e. across stimuli pairs) for cells with large receptive fields (n=33) and small receptive fields (n=37). The highest efficiency results from using vector strength for large receptive field neurons ($p < 0.01$), and is highest using mean firing rate for small receptive field neurons ($p < 0.01$). Large receptive field pyramidal cells have higher efficiency than small receptive field pyramidal cells across all measures ($p < 0.0001$).

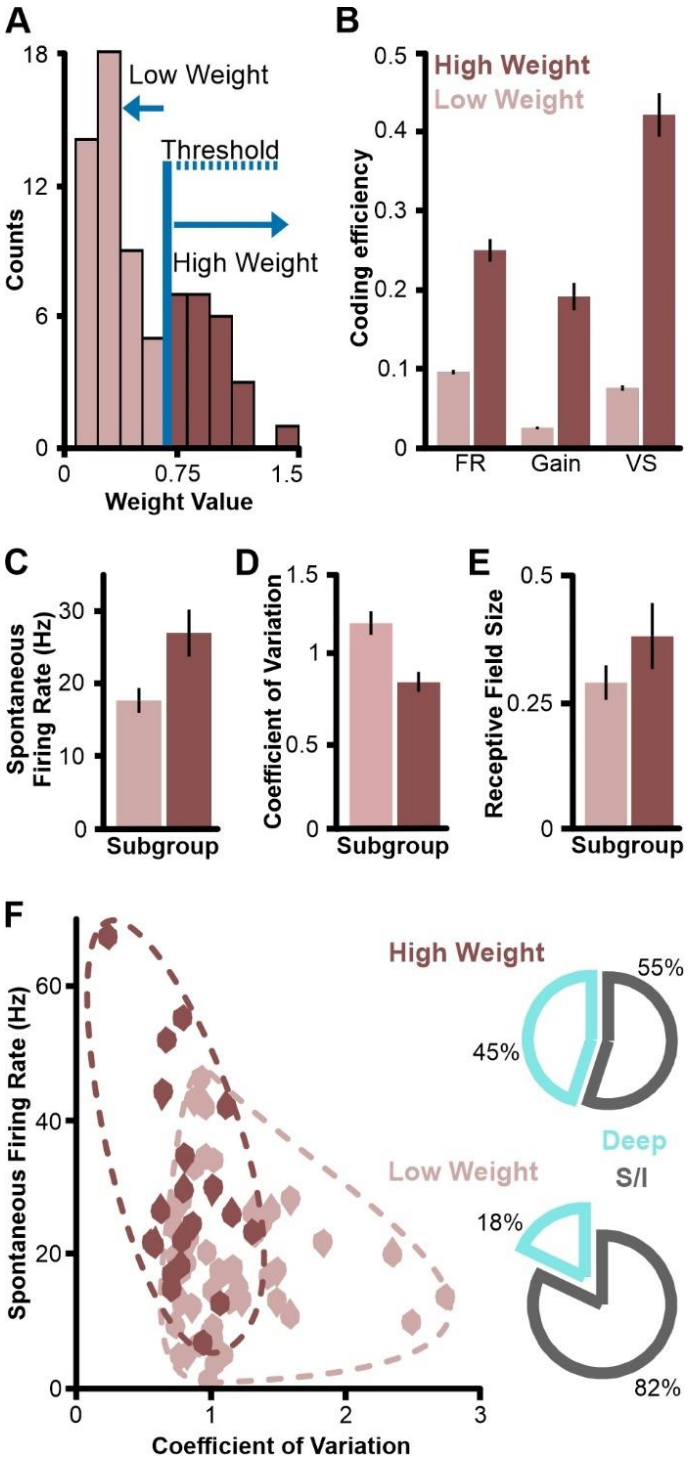

Figure 6. Properties of neurons with more informative responses.

(A) Distribution of average weight value assigned to each neuron in the analysis that reflects the separation in their response distribution to the stimuli being compared (here averaged across stimuli pairs). A threshold was established to divide this distribution with two peaks into two different populations of neurons (low weight in pink, n=50; high weight in red, n=20).

(B) Mean coding efficiency (± s.e. across stimuli pairs; orthogonal orientations only), of the two weight-groups show the expected overall difference, the high-weight performs much better ($p < 0.01$).

(C) The mean spontaneous firing rate (± s.e. across neurons) for the high-weight group is higher than that of the low-weight neurons ($p < 0.01$).

(D) The mean coefficient of variation (± s.e. across neurons) for the high-weight group is lower than that of the low-weight neurons ($p < 0.001$).

(E) The average receptive field size (± s.e. across neurons) for the high-weight group is higher than that of the low-weight neurons, though this difference is not statistically significant (p ~< 0.05).

(F) Scatter plot of spontaneous firing rate and coefficient of variation of every neuron in each weight category. We delineated the groups with a dashed line to highlight the separation/overlap between groups. Pie charts showing the proportion of deep pyramidal cell types within each weight category (right). Note that only 18 of 70 recorded neurons are deep pyramidal cells which represents 25.7%. deep pyramidal cells are thus under-represented in the low-weight group and over-represented in the high-weight group.

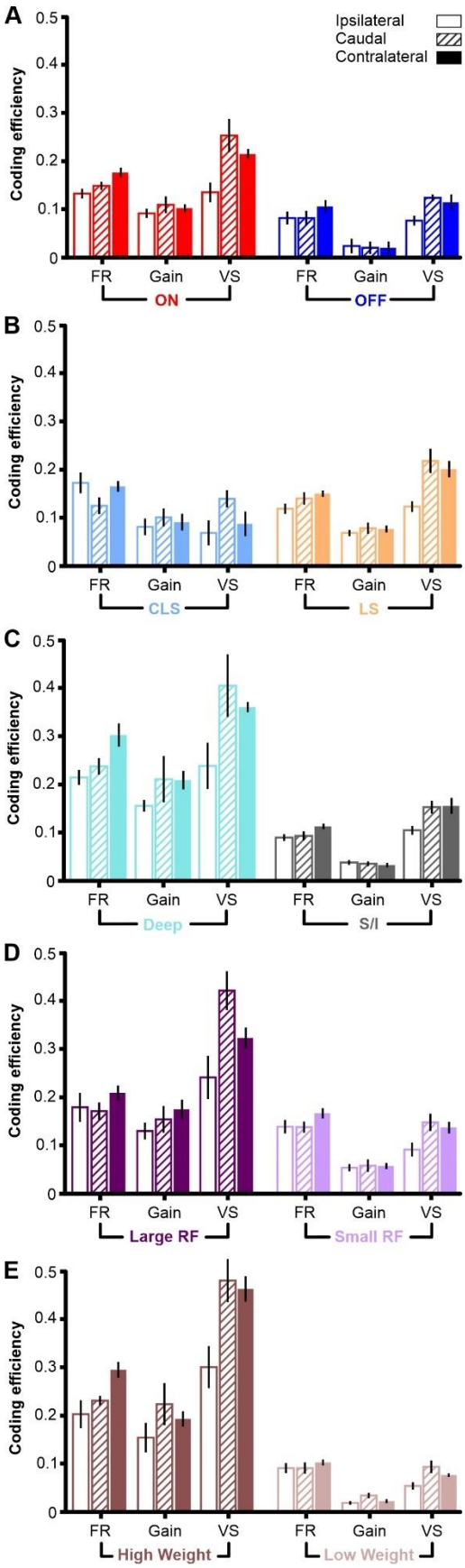

Figure 7. Fine and coarse spatial discrimination across cells-types and response measures.

Mean coding efficiency (± s.e. across stimuli pairs) for discrimination tasks where we compare: locations on the same side of the fish (ipsilateral); locations on opposite sides (contralateral); or locations on the sides compared to the caudal location. We compare different subpopulations and groups of pyramidal cells: **(A)** ON-type vs. OFF-type pyramidal cells; **(B)** CLS vs. LS, **(C)** deep-type vs. superficial/intermediate-type pyramidal cells; **(D)** large receptive field vs. small receptive field neurons, **(E)** high weight vs. low weight neurons.

Supplementary Information

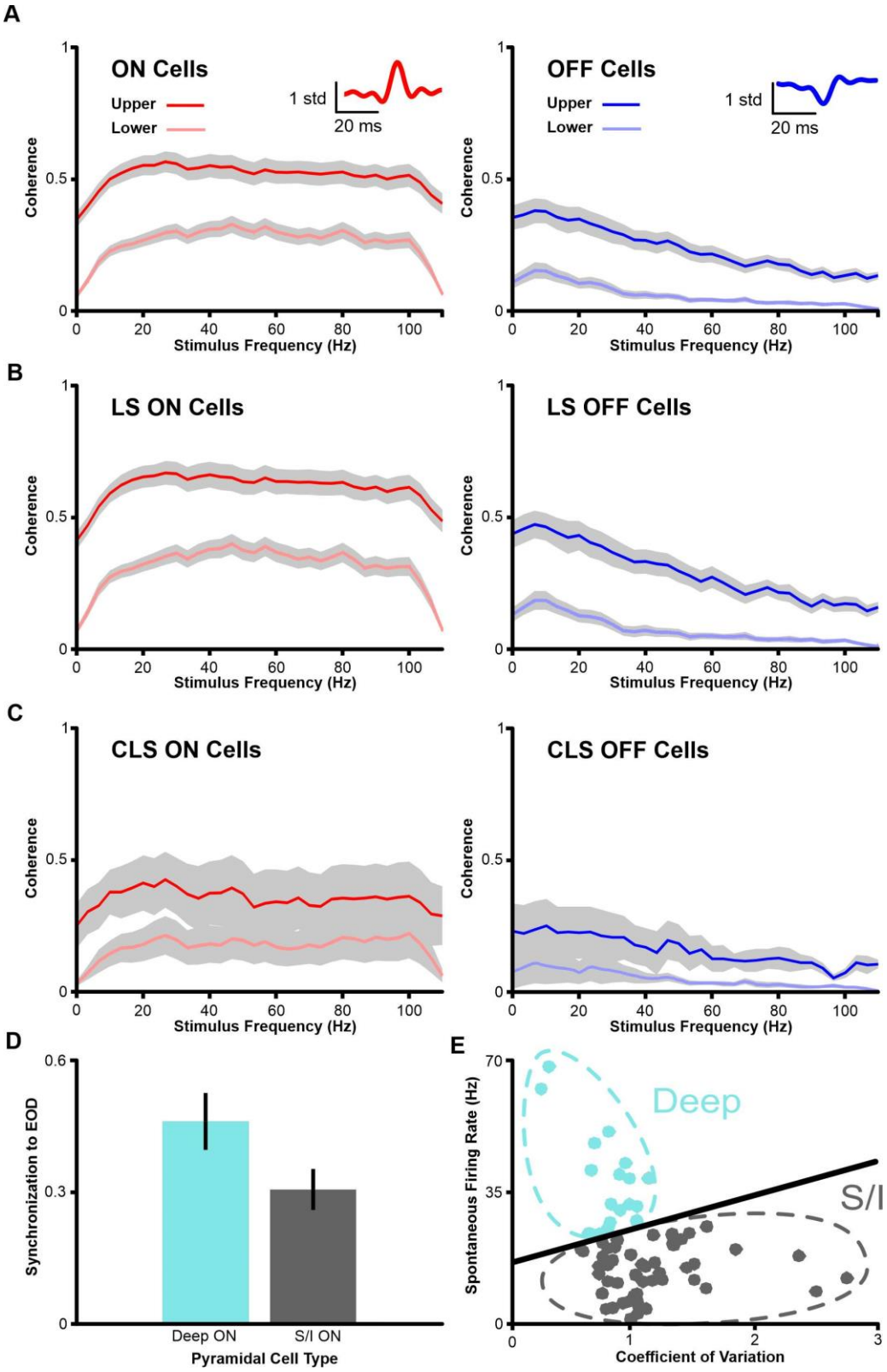

Supplemental Figure 1. Confirmation of pyramidal cell type.

(A) Upper and lower bound coherence of ON and OFF-type pyramidal cells. Insets show spike triggered average waveforms in response to RAM stimuli presented globally. Coherence analyses are standard and described in previous publications (Allen et al., 2019; Krahe et al., 2008). The upper-bound coherence reflects the coding accuracy including both linearly and non-linearly encoded information, whereas lower-bound coherence is based on the linear correlation between the stimulus and the response, gray shaded areas represent ±1 s.d. across neurons.

(B) Upper and lower bound coherence of LS ON and LS OFF-type pyramidal cells.

(C) Upper and lower bound coherence of CLS ON and CLS OFF-type pyramidal cells.

(D) Synchronization to the EOD between deep and superficial/intermediate-type pyramidal cells. The synchronization uses the vector strength measure (ranging from 0 to 1) in response to cycles of the EOD rather than cycles of a SAM stimulus. Deep-type pyramidal cells show higher EOD phase locking ($p < 0.05$). Vertical, black lines indicate ±1 s.e.

(E) Scatterplot of the baseline firing rate and coefficient of variation for each neuron recorded from the full population (n=70). Deep-type pyramidal cells are shown in blue, outlined manually for visualized grouping. Superficial and intermediate-type pyramidal cells are shown in black with manually outlined grouping to better visualize clustering of cells.

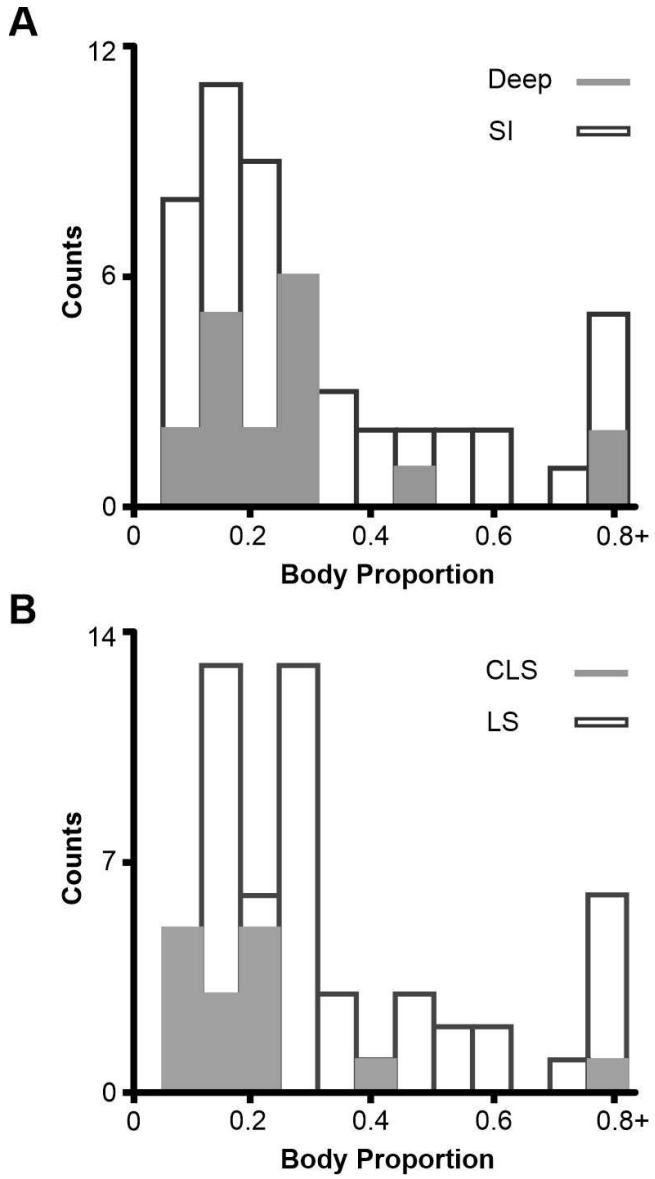

Supplemental Figure 2. Receptive field size by pyramidal cell type.

(A) Histogram of receptive field sizes measured as a fraction of total body proportion for deep and superficial/intermediate-type pyramidal cells.

(B) Histogram of receptive field sizes measured as a fraction of total body proportion for LS and CLS pyramidal cells.

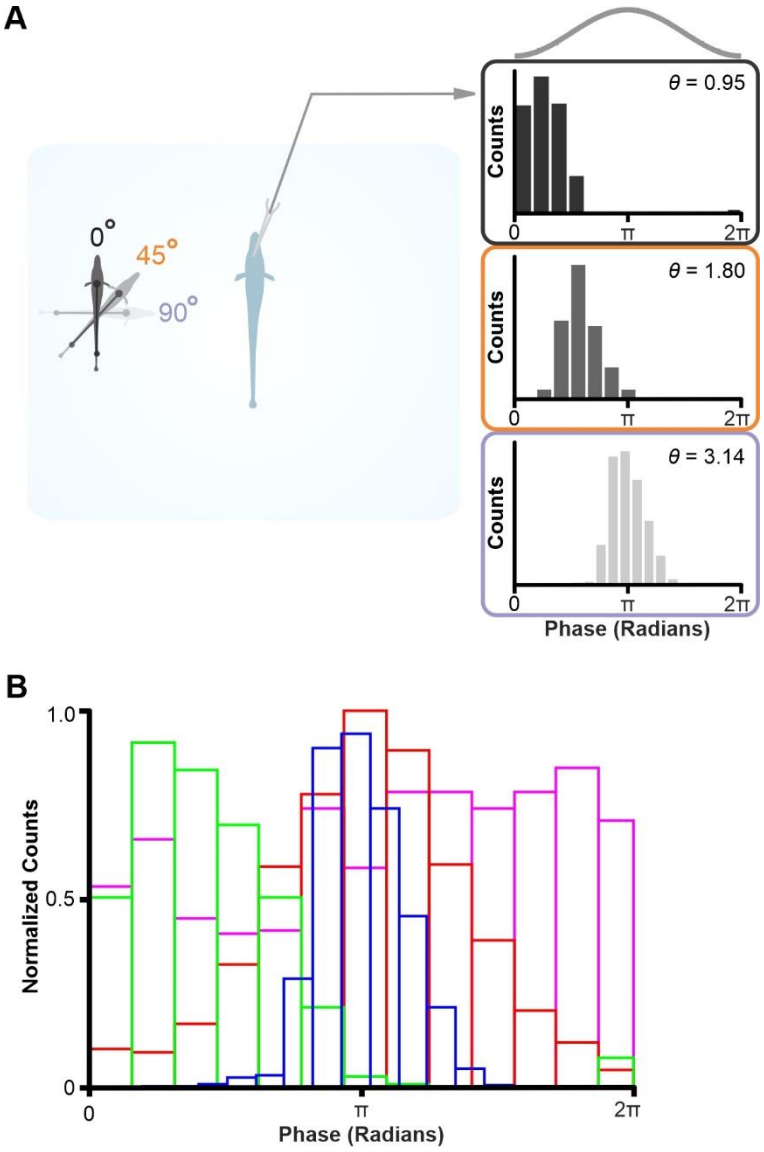

Supplemental Figure 3. Observed phase-shifted responses in ELL pyramidal cells.

(A) Effect of stimulus orientation a single ON-type ELL pyramidal cell. Certain neurons showed clear changes in phase to the spatially realistic conspecific stimulus. The average phase in the response is represented as θ.

(B) 4 ON-type ELL pyramidal cells and their phase response to a stimulus with orthogonal orientation and placed in a singular location ipsilaterally to the receptive field. Each pyramidal cell response is shown as an unfilled histogram in color scale (in similar fashion to A).

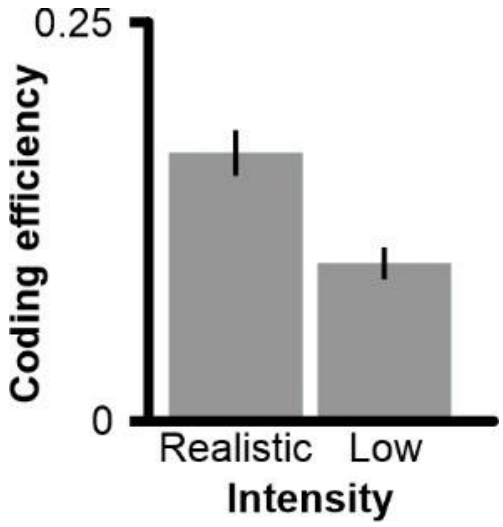

Supplemental Figure 5. Fishpole intensity and its effects on discrimination efficiency.

Discrimination efficiency of pyramidal cells (n=23) to the spatial stimulus using two different stimulus intensities. Discrimination occurs even at lower stimulus intensity ($p < 0.05$).

Chapter 4

Prologue

In the previous two chapters, I demonstrated how electrosensory signals reaching the periphery are modulated in contrast and spatial extent during social interaction, and that spatial information from conspecific signals are accurately encoded by pyramidal cells of the ELL in *A. leptorhynchus*. In the previous study, I characterized the spatial coding response of pyramidal cells through sampling and empirical recordings, which is essential for determining the response pattern and coding accuracy of the population. However, a complete population response requires extrapolating from a small representative sample to a full population of thousands of neurons. Furthermore, the electrophysiological approach offers few opportunities for manipulation that probe the role of different coding mechanisms.

In this chapter, I create a large-scale neural model of the ELL to perform a quantitatively accurate characterization of population coding of spatial information. Using this comprehensive analysis, I make predictions on how the network elements that contribute to the population response, such as noise correlations and feedback, influence the spiking activity of ELL pyramidal cells, and thus the spatial representation of conspecific signals.

Note: This chapter will serve as the base of an article that will be submitted as:
"Milam, O.E., and Marsat, G. (2024). Large-scale population modeling provides insights for localizing weakly electric fish."
I performed all of the experiments and data analysis. Gary Marsat helped in a supervisory role and in drafting the manuscript.

Abstract

How populations of sensory neurons encode the location of a conspecific remains a mostly unanswered question in neuroscience. We address this question by using a large-scale modeling approach of the electrosensory lateral line lobe (ELL) of gymnotid weakly electric fish, who display a remarkable sensitivity for localizing others in suboptimal conditions. Our specific goal is to determine how spatial coding in the ELL permits accurate conspecific localization. The ELL is comprised of a heterogeneous pyramidal cell population that is affected by several network elements, such as noise correlations and feedback. We hypothesize that spatial information is carried in the both firing rate and synchrony in the spiking response, and that this information is further shaped by noise correlations and feedback. To test our hypothesis, we created leaky integrate-and-fire model neurons of the 12 different pyramidal cell subtypes found in the topographic maps of the ELL and matched their responses to those reported *in-vivo*. We varied the parameters of each ELL neuron type and upscaled each model variant to create a full heterogeneous population of 4,620 neurons. We used previously published models of electric field simulation and electroreceptor populations, to provide as inputs to the ELL model. This allowed us to create population responses to spatially realistic conspecific stimuli. Using a weighted Euclidian decoder, we determined how accurately the population can discriminate between conspecific stimuli presented from different locations in three-dimensional space. We analyzed several aspects that affect the population response, and show that noise correlations impose a limit to spatial information at the population level. Overall, our results highlight that different sub-populations of ELL pyramidal cells contribute more spatial

information to the population code than others, and that noise correlations are detrimental for accurate localization of weakly electric fish.

Keywords: population coding, topographic mapping, feedback, electrosensory system, spatial processing

Introduction

Across sensory modalities, localizing communication signals from background noise is essential for guiding navigational behaviors. Several mechanisms for signal encoding have been studied extensively, both theoretically and experimentally (Allen and Marsat, 2018; Bodnar and Bass, 1997; Clarke et al., 2015; Franke et al., 2016; Gussin et al., 2007; Ihlefeld et al., 2019; Lankarany et al., 2019; Marsat et al., 2012; Seriès et al., 2004). Despite a growing body of literature, how populations of neurons represent the spatial aspect of communication signals remains poorly understood (Dayan and Abbott, 2001; Litwin-Kumar et al., 2012; Maler, 2007; Maler, 2018). This lack of knowledge in spatial processing is due in part to an incomplete understanding of several components that affect population coding, including: topographic representations of space; neural heterogeneity; signal and noise correlations; and network interactions such as feedback (Bastian et al., 2002; Bialek and Rieke, 1992; Chacron and Bastian, 2008; Hofmann and Chacron, 2017; Hofmann and Chacron, 2018; Krahe and Maler, 2014; Maler, 2009a; Maler, 2009b; Marsat and Maler, 2012; Mejias et al., 2013; Metzen et al., 2018; Milam et al., 2019; Simmonds and Chacron, 2015). *In-vivo* studies on spatial coding offer valuable insight, however these experimental frameworks often lack the resolution necessary for extrapolating a full population code. Here, we implement a large-scale modeling approach to investigate how heterogeneous pyramidal cell populations in topographic maps represent the spatial aspect of communication signals, thereby enabling accurate signal-source localization.

Apteronotus leptorhynchus, are a species of gymnotiform wave-type weakly electric fish and serve as an ideal model system for studying the neural basis of localization behavior. The neural

circuitry in the early electrosensory pathways is well characterized and amenable to experimental and modeling studies on spatial coding (Carr et al., 1981; Carr et al., 1982; Chacron et al., 2005a; Clarke and Maler, 2017; Maler et al., 1991). These fish possess a neurogenic electric organ located in their tail that discharges at high frequency to produce a carrier signal, called an electric organ discharge (EOD; Lissmann, 1958). High frequency discharges of the electric organ produce a continuous electric field surrounding the fish's body (Lissmann, 1951). Electroreceptors covering the entire body surface detect any perturbations impinging on the electric field (Bullock, 1969). These receptors transmit electrosensory information to the electrosensory lateral line lobe (ELL), where they synapse directly onto pyramidal cells (Carr et al., 1982; Maler et al., 1991). ELL pyramidal cells are the key neurons for electrosensory processing in the hindbrain, as they are the sole output to the midbrain torus semicircularis, creating a funnel for sensory information to higher processing areas (Carr et al., 1981). These neurons possess receptive fields with antagonistic center-surround organization, integrating hundreds to thousands of spatially localized electroreceptor inputs (Clarke et al., 2014; Maler, 2009b). The ELL population is known to be largely heterogeneous, varying in receptive field size, morphology, physiological response properties, and sensitivity to feedback (see Krahe and Maler, 2014; Maler, 2007; Milam et al., 2019 for review). Behavioral studies in the field and in the lab have shown that these fish can localize electrosensory signals generated by their conspecifics often in difficult conditions where the signal is weak, masked by several sources of noise, and/or in a cluttered environment (Henninger et al., 2018; Hupé and Lewis, 2008; Jung et al., 2016; Stamper et al., 2012a; Stamper et al., 2012b; Stamper et al., 2013). This implies that these fish are not only able to detect the conspecific signal in difficult conditions,

but that they can successfully discriminate the detected signal from other backgrounds signals over time to localize the signal's source. Recent studies on conspecific localization have characterized the electric image produced between interacting weakly electric fish, or have quantified conspecific beat and envelope coding without the signal's spatial component (i.e., under "global" configuration; Metzen et al., 2018; Pedraja et al., 2016; Stamper et al., 2013; Yu et al., 2012). Thus, there remains a current gap in knowledge of how the spatial aspect of a conspecific signal is encoded at the population level and topographically represented in the ELL.

Here, we used an electric field model to simulate spatial interaction between two weakly electric fish positioned in different locations (Ramachandra et al., 2023). The different stimulus locations create a series of electric images that represent changes in the beat contrast produced by the interacting electric fields. The resulting electric image is displayed onto a three-dimensional mesh model of a weakly electric fish that is covered with electroreceptors. Each electroreceptor is a leaky-integrate-and-fire model (with x, y, z coordinates) that responds to spatially localized changes in beat contrast (Ramachandra et al., 2023). The population of model electroreceptors provides current inputs to our ELL model. This ELL model is composed of leaky integrate-and-fire neurons with columnar-specific receptive field coverage, antagonistic center-surround organization, spike-frequency adaptation, and cancellation via a negative image feedback component. The model pyramidal cells are matched to the *in-vivo* responses of different pyramidal cell types in topographic maps of the ELL to a conspecific dipole mimic positioned in different locations (Milam and Marsat, 2023). Based on the output of the ELL model, we recreate an estimate of the location of the sender fish and assess the accuracy of the model. Overall, we argue that this population of model neurons can accurately

localize the position of a conspecific in three-dimensional space. Additionally, we investigate noise correlations and confirm that correlated noise provides a limitation on information content, but due to the small extent of spatial correlations, has only a small impact on the population code. Lastly, we show that a model feedback component shapes the spatial representation of conspecific signals. Taken together, our data corroborates the idea that generic principles of spatial processing are used across sensory modalities, since the way the early sensory system shapes spatial information shares design features with the visual and auditory systems.

Methods

Electroreceptor modeling

The electroreceptor model is based on a simple leaky integrate-and-fire framework that includes noise and spike-frequency adaptation. This electroreceptor model has been previously published in (Ramachandra et al., 2023), and the responses were matched to biologically accurate responses and in-line with other previously published electroreceptor models (see Benda et al., 2005; Chacron et al., 2005). Our full heterogeneous population of 8,195 different electroreceptor models were placed onto a 3D mesh model (as described in Ramachandra et al., 2023). The resulting combined input to the ELL model is the electroreceptor population response to the beat contrast created by conspecific electric field simulation in a variety of spatial configurations (for more information on the electric field model see Ramachandra et al., 2023; Pedraja et al., 2016).

LIF ELL model

The models of different ELL pyramidal cells are based on a leaky integrate-and-fire framework. The voltage evolves according to the following equation:

$$\tau_m \frac{dV}{dt} = -V + [I + \sigma\xi(t) - \mu(t)] + \Lambda\{-gV\}$$

When the membrane potential, *V*, crosses the spike threshold, V_{thresh}, a spike is recorded and *V* returns to the resting membrane potential. After the refractory period, τ_m, the voltage continues to integrate according to the leaky integrate-and-fire model equation above. The feedforward electroreceptor input is modeled as an input current, I, with noise, $\sigma\xi(t)$. The spike-frequency adaptation is modeled as, $\mu(t)$. The adaptation time constant is smaller in superficial-type pyramidal cells compared to intermediate-type pyramidal cells (Maler, 2009a; Maler, 2009b; Zhang and Chacron, 2016). Adaptation is also modeled to be slightly stronger in the LS than in CLS. The feedforward electroreceptor input is rectified as symbolized by the section of the equation in brackets, [. . .].

The receptive field surround is convolved with an alpha function, and low pass filtered with a first order Butterworth filter with a cutoff frequency of 50 Hz (Hofmann and Chacron, 2017). ON-type pyramidal cells have an excitatory polarity preference and respond to increases in stimulus amplitude, whereas OFF-type pyramidal cells have an inhibitory polarity preference that is mediated by synaptic connections with GABAergic inhibitory interneurons and respond to decreases in stimulus amplitude (Berman and Maler, 1998). This polarity preference is modeled by separating the input current, I, into two parts, I_{RFC} and I_{RFS}. The first part is the electroreceptors that contribute a current input via a receptive field center, I_{RFC}, and the other part composes the receptive field surround, I_{RFS}. For ON-type pyramidal cells, the receptive

field center is positive polarity and is subtracted from a positive polarity receptive field surround, as the input is in the same phase (Berman and Maler, 1999; Bratton and Bastian, 1990; Shumway and Maler, 1989). For OFF-type pyramidal cells, the receptive field center is negative polarity and is added to the receptive field surround that is positive polarity, as the input is in anti-phase due to interactions with GABAergic inhibitory interneurons affecting the receptive field center. The sizes of the receptive field centers were matched to those mapped during *in-vivo* electrophysiology experiments (Milam and Marsat, 2023). Receptive field centers were larger for the LS map than for the CLS map. Receptive field surrounds were made using an absolute distance around the perimeter of each receptive field center. The size of the surround varied for each pyramidal cell, with CLS pyramidal cells having a larger surround than LS, in accordance with previously published observations (Hofmann and Chacron, 2017; Maler, 2009a; Maler, 2009b; Shumway, 1989; Shumway et al., 1989).

Feedback input from the parallel fibers is modeled as a current input of strength, Λ. Due to a gap in the literature regarding the precise spatial extent of the feedback's receptive field coverage, the feedback input is modeled here as a negative image of the entire electroreceptor population response. The feedback is then convolved with an alpha function, and low pass filtered with a first order Butterworth filter with a cutoff frequency of 20 Hz (similarly to Chacron et al., 2005b; Simmonds and Chacron, 2015). The strength of the feedback is adjusted by a positive DC offset with a smaller offset for superficial-type pyramidal cells than for intermediate-type pyramidal cells. This replicates the inhibitory disynaptic input and results in a larger effect of cancellation in the superficial-type pyramidal cells (approximately 30% stronger), supported by experimental data (Bol et al., 2013; Marsat and Maler, 2012).

Network structure

The population of electroreceptor models positioned on a three-dimensional mesh model of an *Apteronotus leptorhynchus* is a key component to the ELL modeling process. This approach allows for each electroreceptor to have a coordinate in x, y, z, space. When paired with the electric field simulation model, the result is each electroreceptor receiving a precise spatial input of beat contrast. The network's architecture operates on a feedforward (bottom-up) configuration with a feedback (top-down) component (Berman and Maler, 1999; Clarke and Maler, 2017; Milam et al., 2019). The electroreceptors constitute the feedforward, providing direct input to the pyramidal cells in the ELL model network. Each pyramidal cell within a column (150 columns for LS; 235 for CLS) receives input from a cluster of electroreceptors within the receptive field center and surround. A column includes an ON-type and OFF-type of each different pyramidal cell layer (superficial, intermediate, and deep; Maler, 2009b). The feedback affects superficial-type and intermediate-type pyramidal cells, while deep-type pyramidal cells receive no feedback (Berman and Maler, 1999; Krahe and Maler, 2014; Maler, 2007; Maler, 2009a; Maler, 2009b; Milam et al., 2019). The feedback input is a negative image of the feedforward input with an added DC offset (Bol et al., 2013; Marsat and Maler, 2012; Mejias et al., 2013). The strength of the feedback is slightly stronger for superficial-type pyramidal cells than for intermediate-type pyramidal cells, and is set by the level of the DC offset with superficial-type pyramidal cells having a smaller DC offset (more cancellation).

Data analysis

All stimulation, modeling, and analyses described here were performed using MATLAB. Spike trains collected from leaky integrate-and-fire model simulation were first binarized into a sequence of zeros (no spike) and ones (spike). The binarized sequence was convolved with a gaussian filter and separated into 1 second, 50% overlapping segments. Discrimination errors are a type of statistical analysis as distributions are compared and a probability of error is calculated, therefore, additional statistical analyses were not necessary for the results presented here.

Gain

The stimulus-response gain (*G*) to SAM stimulation was calculated by:

$$G(f) = \sum Q\,(f)$$

where *Q* is the power spectral density of the convolved spike train, *f* are the frequencies within ± 0.5 Hz of the target SAM frequency (5 or 30 Hz). A larger stimulus-response gain value indicates a larger response from the neuron to a stimulus at the target frequency.

Vector strength

The strength of phase locking to SAM stimulation was calculated by:

$$s = \frac{\sqrt{(\sum {x_i}^2) + (\sum {y_i}^2)}}{n}$$

where *n* is the number of spikes, and *x* and *y* are the sine and cosine phases of the stimulus at which *i* occurs (Goldberg and Brown, 1969; Marsat and Pollack, 2004). The vector strength, *s*,

quantifies the precision of responses to a given phase of the stimulus cycle, with 0 being equal vectors or a flat response, and 1 being a perfectly precise response.

Discrimination analysis

The discrimination analysis relates directly to the information carried by a population of neurons to discriminate between stimuli (see Marsat et al., 2023, for more details). For our discrimination analysis, to compare our model's output to *in-vivo* recordings in the ELL that are from just one side of the brain, we perform this analysis using only the ipsilateral side of the brain (i.e., the fish's left side, Milam and Marsat, 2023). We compare stimuli from different locations and used one of three measurements to quantify response strength: mean firing rate, vector strength, or stimulus-response gain for each 1 s response segment with a 50% overlap between segments. A weight, based on the Kullback-Leibler divergence in the response distributions for each stimulus, is assigned to each neuron for each pair of stimuli being compared. The weight is then normalized to 1 across neurons within a population response, afterwards the response strength is multiplied by this weight. Population responses are represented as data points in Euclidean space, where each dimension is the weighted response of one neuron in the population. Several population responses are considered, each consisting of a random 1 s segment of response from a subset of *n* neurons from the population (*n* will vary, as described further). Euclidean distances between all possible stimulus pairs are then compared. Larger distances between stimulus pairs indicate less similarity between the responses. Stimuli that can be easily discriminated will elicit responses that are very different (i.e., a large Euclidean distance) relative to the variability across responses to the same

stimulus. The weighting procedure optimizes the decoding accuracy by assigning a stronger contribution to the Euclidean distance to neurons that carry more information about the difference between stimuli.

The probability distributions of the values in these matrices $P(D_{xy})$ *or* $P(D_{xx})$ were used for ideal observer analysis. Receiver operating characteristic (ROC) curves were generated by varying the threshold distance to separate responses to conspecific stimuli from different locations or orientations. ROC curves were generated by varying a threshold distance value *T*; for each threshold, the probability of non-discrimination (P_D) is calculated as the sum of $P(D_{xy}>T)$ and the probability of false discrimination (P_F) is calculated as the sum $P(D_{xx}>T)$. The error probability is taken as the minimum error, *E*, across thresholds:

$$E = \frac{1}{2}P_F + \frac{1}{2}(1 - P_D)$$

Three-dimensional population response heatmaps

Heatmaps were represented as an array of fixed points (tuberous electroreceptors with x,y z coordinates) across the fish's body surface. The receptive field centers for each neuron within a column were mapped onto the body. All tuberous receptors within a neuron's receptive field boundary were assigned to that neuron, such that one receptor could belong to several neurons' receptive field centers. Using several neurons, we created a population response heatmap. Values from the neural response measures (e.g., firing rate, gain, vector strength) to the different spatial stimuli were appended to all receptors within the neurons' receptive field centers, and then averaged so that each receptor represented a single activation value for all its represented neurons. Unlike the discrimination analysis, for our heatmap analysis, we include

responses from both sides of the brain (i.e., left and right hemispheres). The purpose of the heatmaps is to provide a holistic representation of the population response, rather than to compare discrimination performance of stimuli.

Results

We investigated how a beat stimulus resulting from conspecific spatial interaction is encoded by ELL pyramidal cell populations. Importantly, the information content in a population of cells will depend on the number of units contained in the population, their sensitivity, and the amount of overlap (signal and noise correlations) in their responses. Previously published findings on *in*-vivo electrophysiological experiments have shown that there are differences in spatial coding accuracy across the ELL pyramidal cell populations (Milam and Marsat, 2023). To briefly summarize, it is known that deep-type pyramidal cells encode more accurately than superficial-type and intermediate-type pyramidal cells in spatial discrimination tasks. Furthermore, ON-type pyramidal cells outperform OFF-type, and pyramidal cells with larger receptive fields outperform those with smaller receptive fields. Here, we used an electric field model to simulate a sender fish at different locations around a focal fish (Ramachandra et al., 2023; we use sender' and 'focal' terminology, however both fish send and receive). A resulting electric image consisting of changes in beat contrast provided the input to the electroreceptor population model. The electroreceptor population provided a current input to the ELL pyramidal cells. To determine how the ELL network encodes spatial information from conspecific signals, we created model populations of leaky-integrate and fire model neurons were matched to empirical data on the response properties of the different ELL

pyramidal cells: ON and OFF; Superficial / Intermediate and Deep; and LS or CLS; resulting in a total of 12 LIF neuron subpopulations and a total of 4,620 neurons (Fig 1). The properties of each population were matched to the empirical average. Additionally, the various model parameters (threshold, noise, membrane time constant, etc.) were varied to replicate the range and distribution of properties observed *in-vivo* (Figure 2; Milam and Marsat, 2023; Bastian, 1986; Bastian et al., 2002; Bol et al., 2013; Krahe and Maler, 2014; Krahe et al., 2008; Maler, 2009a; Maler, 2009b). Pyramidal cells occupying the same column (150 columns for LS; 235 for CLS) received current inputs from electroreceptors within the associated receptive field center and surround (see Fig 3). Specific measures of the spiking response such as changes in firing rate, stimulus-response gain, and vector strength were quantified. The responses of several ELL pyramidal cells could then be pooled to create different population responses.

ELL pyramidal cell population modeling replicates encoding patterns for conspecific localization observed *in-vivo*

We first separated our full population of pyramidal cells into subpopulations based on the cells' response polarity (ON-type or OFF-type), position in the ELL layer (Superficial-type, intermediate-type, or deep-type), and location within a topographic map (LS or CLS). Using population heatmaps (see Methods), we assessed the subpopulations' responses to conspecific stimuli presented from different locations (Fig 4A). To compare differences between the subpopulations' responses we focused on stimulus-response gain as it quantifies information about response synchrony as well as amplitude. Overall, we found that for the model ON-type and deep-type ELL pyramidal cell subpopulations, stimulus-response gain varied as a function of

stimulus location. Furthermore, the contrasts of the heatmap pattern for these specific subpopulations were indicative of spatial dependency (Fig 4B). On the other hand, OFF-type, superficial-type, or intermediate-type pyramidal cells showed less of an indication of spatial dependency to conspecific stimuli in their heatmap population responses. Thus, a preliminary evaluation of gain responses to conspecific beat stimuli suggests differences at the population-level for encoding relevant spatial information.

ELL modeling validates known spatial coding differences observed in-vivo across pyramidal cell populations during a signal-source discrimination task

Knowing the spatial response pattern of heatmaps across different ELL subpopulations is particularly valuable for qualitative analysis, yet does not provide a quantitative measure for spatial coding. Therefore, we quantified the ability of ELL subpopulations to discriminate between conspecific stimuli presented from different locations, by comparing their responses using a weighted Euclidean decoder. Briefly, the analysis takes responses from several neurons in a subpopulation, runs a pairwise stimulus-discrimination task, and returns an accuracy estimate value to quantify successful discrimination (see Methods).

For our discrimination analysis, we used only the fish's left hemisphere of the brain to make a direct comparison to recordings in the ELL that are from just one side (Milam and Marsat, 2023). We first compared LS deep-type pyramidal cells to LS superficial-type pyramidal cells. We found that LS deep-type pyramidal cells displayed higher accuracy for signal-source discrimination. Whereas LS superficial-type pyramidal cells had lower discrimination accuracy (Fig 5A, 5B). We decided that because the deep-type cells were performing with higher

accuracy, we would ask whether there is any difference in discrimination accuracy between deep-type pyramidal cells with ON-type response polarity and those with OFF-type response polarity. Doing so, we found that deep-type pyramidal cells with ON polarity displayed higher accuracy than those with OFF polarity (Fig 5A, 5C). We then asked whether there were any differences in discrimination accuracy between topographic maps of the ELL. We compared deep-type pyramidal cells of the LS map with deep-type pyramidal cells of the CLS map. Deep-type LS cells achieved higher discrimination accuracy than deep-type CLS cells (Fig 5A, 5D). Overall, our modeling of full-scale ELL populations confirms patterns reported in experimental findings and supports that across subpopulations, accurate discrimination was feasible for all unique stimulus pairs that were simulated (7 locations, 3 azimuths, at a distance of 10cm away; see Methods). Thus, these findings show that there are differences between ELL pyramidal cell populations in their ability to accurately distinguish between conspecific beat stimuli across a multitude of spatial configurations.

Noise correlations are detrimental for localization accuracy

Noise correlations are inherent in the electrosensory system and most other sensory systems (Ecker et al., 2011; Ghim et al., 2008; Sompolinsky et al., 2001; Stein et al., 2005; Wiley, 2015). Each ELL pyramidal cell must integrate sensory information transmitted by several hundreds to thousands of electroreceptors located within the pyramidal cell's receptive field. Therefore, when comparing across several pyramidal cells, this shared input causes correlations in the transmitted signal as well as the background noise. Correlated noise can be beneficial in some situations, but is largely considered to be detrimental to information coding, particularly

at the population level when the noise cannot be averaged out (Bauermann and Lindner, 2019; Hunsberger et al., 2014; McDonnell and Ward, 2011; Nassar et al., 2021). To investigate the effect of noise correlations on stimulus encoding, we repeated the discrimination analysis using the same repetition to simulate recording from all cells at the same time. We found that noise correlations generally reduced the accuracy of discriminating between different stimulus pairs (Fig 6). This reduction in discrimination accuracy was consistent across various aspects of the neural response (i.e., mean firing rate, stimulus-response gain, vector strength). When noise correlations are present, we noticed a plateau in the accuracy as more neurons are added to the discrimination analysis, and that this trend was especially prevalent for populations in the CLS map (Fig 6C, 6D). For spatial coding, only a limited number of neurons overlap with each other, so the spatial information relies on averaging across a limited number of neurons. Interestingly, this means that correlated noise cannot be completely averaged out even when several neurons are considered. Overall, our analysis of noise correlations did not find any improvements in spatial coding of the unique pairwise stimulus combinations tested. Thus, noise correlations were detrimental to spatial discrimination accuracy of ELL pyramidal cell subpopulations.

Feedback and population response for conspecific localization

So far, we have shown that the electroreceptor population transmits the information necessary for permitting accurate spatial processing of conspecific beat stimuli by ELL pyramidal cell populations (see also Milam and Marsat, 2023). In addition to feedforward inputs, ELL pyramidal cells also receive feedback inputs that affect their spiking response. The indirect

feedback pathway, in particular, is driven by large receptive fields and we hypothesize that it influences the spatial representation across the population of cells (Berman and Maler, 1999; Maler, 2007). The impact of this feedback input on pyramidal cells response has been thoroughly characterized: it partially cancels the response to beats, be it on a cycle-per-cycle basis for low frequencies (Bol et al., 2013; Mejias et al., 2013). Responses to high frequencies are also affected, but not in a phase-specific manner (unpublished observations, Marsat). Despite this, it remains unclear how feedback affects spatial coding of conspecific signals at the population level.

We investigated the role of indirect feedback on spatial coding in subpopulations of ELL pyramidal cells. In our model of the ELL, only the superficial-type and intermediate-type pyramidal cells were supplemented with a feedback input, as the deep-type pyramidal cells serve as the source of the feedback (Berman and Maler, 1999; Clarke and Maler, 2017; Krahe and Maler, 2014; Maler, 2009a; Maler, 2009b; Milam et al., 2019). We determined its influence on spatial representation and accuracy of coding and compared them to model responses that did not include feedback. In adjusting our model to accommodate a feedback input, we had to alter the parameters slightly so that the response with feedback showed the characteristic suppression of low-frequency beats according to published data (Bol et al., 2011). The result of this adjustment was a decrease in coding accuracy even before the feedback is turned on (compare Figures 5B and 8C). Making the feedback active in this version of the model reduced the responses to the 5Hz beat (Fig 7). The quantitative coding analysis suggests that the feedback did not influence the accuracy of spatial coding. We suggest this might be due to the fact that the reduction in the response affects pyramidal cells uniformly for all locations. Our

analysis suggests that the spatial contrasts that support localization are not influenced by the feedback in this form. It is likely that feedback with additional non-linearities would affect spatial coding in a different manner. Further modelling efforts, paired with experimental data, will be required to assess more precisely how feedback affects spatial coding.

Discussion

In this study, we investigated how different neural populations in the ELL encode conspecific location. To do so, we implemented a large-scale modeling approach that: (1) characterizes the electrosensory signals generated during spatial interaction between two weakly electric fish; (2) quantifies the electroreceptor population response to changes in beat contrast; (3) computes the accuracy of spatial coding across ELL pyramidal cell populations using the output from the electroreceptor population as the input to the ELL model (see Fig 1 for more information). To accomplish this, we first generated a behavioral signal by using a previously published electric field model to simulate the electrosensory signals created during spatial interaction between two weakly electric fish. The combined signals created a series of beat contrasts that were fed into a population of electroreceptor model neurons (Ramachandra et al., 2023). Then, the output from the electroreceptor population was used as a current input to an ELL pyramidal cell population model. Our ELL model included several different types of pyramidal cell populations with heterogeneity, spatially mapped receptive field centers and surrounds, spike-frequency adaptation, noise correlations, and feedback cancellation (see Fig 2, Fig 3). We present for the first time in this system, a large-scale model of the ELL comprised of 4,620 heterogeneous pyramidal cells with a complex network dynamic that includes feedback.

The result is a full-scale model from signal to the output of the first sensory area. Lastly, we use a decoding algorithm to better understand the information contained in this population response. After simulating conspecific interaction in a variety of spatial arrangements, we analyzed the spike train output for changes in firing rate, stimulus-response gain, and vector strength. Using these measures, we pooled the responses of several neurons together to create a population response. This allowed us to compare the population responses between different stimulus locations, and to compute the populations' accuracy of encoding using a spike-distance metric (see Methods; Marsat et al., 2023).

Overall, our model confirms findings from electrophysiological data that pyramidal cells of the ELL are able to discriminate between beat signals that are emitted by a conspecific from different spatial locations. Specifically, we show that integration of feedforward electroreceptor inputs leads to accurate spatial coding. Our results support previous *in-vivo* findings that conspecific localization is possible for all subpopulations of pyramidal cells found in the ELL. In addition, our model replicated known performance differences across ELL subpopulations. We evaluated how accurate each subpopulation was by quantifying discrimination accuracy as a function of neural population size. The findings from our discrimination analysis support that pyramidal cells residing in the deep layer are more accurate discriminators of conspecific location, compared to pyramidal cells found in more superficial layers (see Fig 5). In addition, pyramidal cells with an ON-polarity preference were more accurate than those with OFF-polarity preference. Moreover, when separating pyramidal cells based on their topographic map position, we found that pyramidal cells of the LS map were more accurate than pyramidal cells in the CLS map (see Fig 6). Previous studies have shown that the LS map is more

specialized at coding for conspecific signals (e.g., chirps; Allen and Marsat, 2019; Krahe and Maler, 2014; Krahe et al., 2008; Marsat and Maler, 2010; Marsat and Maler, 2012; Marsat et al., 2012). Similarly, our data suggests that the LS map provides more accurate spatial coding of conspecific signals. Taken together, our model provides insights for what aspects contribute to spatial coding differences observed in ELL pyramidal cells. Future research using this model can explicitly test these aspects by varying the relevant parameters in a systematic way.

Our simplified model of an ELL population was calibrated using peak to trough firing rate across different beat contrasts, but not specifically to replicate changes in mean firing rate. We included an adaptation component, and while it was adjusted to provide reasonable changes to the pattern of the spiking response, the focus of the model was not to precisely match the rate of adaptation. This element could explain some of the discrepancies we observed in the model compared to responses observed *in-vivo* (Milam and Marsat, 2023). Certainly, further modeling and electrophysiological studies are needed to better understand the role ELL pyramidal cells for conspecific localization.

An especially interesting finding was that CLS deep-type pyramidal cells had lower spatial discrimination accuracy compared to LS deep-type pyramidal cells (see Fig 6). These differences between LS and CLS are particularly visible with noise correlations, and are likely the result of differences in averaging out noise based on variations in the size of the receptive field centers and surrounds for pyramidal cells in the LS and CLS maps. CLS pyramidal cells have smaller centers, with larger and stronger surrounds than LS pyramidal cells (Hofmann and Chacron, 2017; Maler, 2009a; Maler, 2009b; Shumway, 1989; Shumway et al., 1989), and our model is consistent with this pattern. In fact, the exact role of noise correlations is a topic of heavy

debate in the neuroscience research community. However, the overall consensus being that noise correlations are generally detrimental to information coding (Dayan and Abbott, 2001; Metzen and Chacron, 2021). This is met with several context-dependent exceptions that support the beneficial role of noise correlations (Bauermann and Lindner, 2019; Ecker et al., 2011; Hunsberger et al., 2014; McDonnell and Ward, 2011). In particular, one study demonstrated that higher noise correlations led to improvements in speed and robustness while learning a perceptual discrimination task (Nassar et al., 2021). Here, our results show that noise correlations are detrimental for encoding the spatial aspect of conspecific beat signals, specifically in a signal-source discrimination task. Across subpopulations in both the LS and CLS maps, a plateauing in the discrimination accuracy occurs even as more neurons are added to the discrimination analysis. This result indicates that correlations in the noise are lowering the amount of spatial information that is encoded by placing a limit on the population code. Each electroreceptor transmits a unique noise signature to several pyramidal cells in the population. However, due to the limited amount of receptive field overlap in the pyramidal cell population, noise correlations cannot be averaged out even when several neurons are considered. The situation we describe here differs from a temporal coding task, where discrimination curves will eventually reach perfect discrimination accuracy with enough neurons (albeit with a shallower slope). This is because even though some noise correlations exist, eventually with a sufficiently large population size, noise correlations can be averaged out. Here, however, they cannot be averaged out because only a limited number of neurons share a given “spatial information” (i.e., how the stimulus strength differs at a given location). Adding the spatial component provides a novel result for the role of noise correlations on neural coding and we did not find

any improvements in spatial coding accuracy of the unique pairwise stimulus combinations tested. Further studies are needed to investigate the effect of correlated noise on spatial coding during social interaction between multiple fish.

Field studies on interacting weakly electric fish have demonstrated that these fish are capable of detecting one another from over a meter away in difficult conditions (Henninger et al., 2018). Therefore, this challenging task requires the animal's nervous system to compute small differences in the low contrast beat signal. Pyramidal cells in the ELL must integrate responses from electroreceptors to the low contrast beats. This information must be transmitted downstream, from the ELL bottleneck to higher order brain areas, to guide social behaviors. To evaluate neural activity at the population level, we visualized the ELL population response to a conspecific beat stimulus by layering the receptive fields of each pyramidal cell along the fish's body. Our heatmap analysis qualitatively showed that there is a diffuse gradient with higher spatial contrast that corresponds to the stimulus location, indicative of a spatial dependency in the population response to a conspecific's location (see Fig 4). Our results indicate that the spatial contrast is higher in the ON-type pyramidal cell population than the OFF-type pyramidal cell population, though the topography of the gradient pattern is similar. One explanation for this finding might be attributed to the low-pass filtering that affects our model OFF-type pyramidal cells. The filtering will influence, to some extent, the spiking response and could alter the information used for discrimination. These findings suggest that ON-type cells might play a more direct role in neural coding of a conspecific's location. Furthermore, the heatmaps revealed that the deep-type pyramidal cell population responds to conspecific location similarly to the full electroreceptor population (Ramachandra et al., 2023).

An important distinction here is that the deep-type pyramidal cells do this while integrating the responses of up to several thousand electroreceptors per receptive field. Though the sensory image was weaker at the pyramidal cell level than at the electroreceptor level, the difference in integration might offer a higher resolution sensory image in downstream, higher order brain areas. This could allow for the sensitivity needed for localizing at further distances, where the higher image contrast indicates the direction of the conspecific's location in three-dimensional space. Importantly, this sensory problem is generalizable to other organisms that rely on various sensory modalities to navigate and interact within their environment. Further studies on distance coding and directional coding of conspecifics in three-dimensional space will be needed to support these hypotheses.

Lastly, we highlighted the possibility that in *A. leptorhynchus*, feedback pathways may influence the pyramidal cells' response properties to shape spatial coding. Visual inspection of the effect of feedback on the response of the pyramidal cells, as seen on the heatmaps, suggests that it reduces the response to the beat as expected. However, this reduction seems to be uniform for all the cells and consequently, feedback did not alter the accuracy of spatial coding (see Fig 8). Our simplified, negative-image feedback component contains a global receptive field and a static DC offset. It is possible that we have not included the key aspects of feedback that play a role in how it influences spatial coding of conspecific signals. Here, we cancelled the response in a uniform way using a negative-image feedback component that scales linearly with input strength. It is likely that the discrimination accuracy with and without feedback is similar because feedback is having the same effect on every cell, resulting in a uniform decrease in the population response, therefore the discrimination task is relatively

unchanged. However, one possibility for changing the feedback in a realistic way to elicit a stronger effect on spatial coding, could be to implement a non-linear intensity-response function for the feedback, particularly one that saturates at higher rates (e.g., an adaptation function). This would create less of an effect for the pyramidal cells that contribute more to the population coding (i.e., more pronounced changes in their spiking response). Certainly, more experiments and testing of population model interactions are necessary to determine the influence and mechanisms of how feedback shapes spatial coding. The way this spatial information is transformed and how it is used downstream may be an important mechanism for mediating accurate spatial processing of conspecifics.

References

Allen, K. M. and Marsat, G. (2018). Task-specific sensory coding strategies are matched to detection and discrimination performance. *J Exp Biol* **221**, jeb170563.

Allen, K. M. and Marsat, G. (2019). Neural Processing of Communication Signals: The Extent of Sender–Receiver Matching Varies across Species of Apteronotus. *eNeuro* **6**,.

Bastian, J. (1986). Gain control in the electrosensory system: a role for the descending projections to the electrosensory lateral line lobe. *Journal of Comparative Physiology A* **158**, 505–515.

Bastian, J., Chacron, M. J. and Maler, L. (2002). Receptive field organization determines pyramidal cell stimulus-encoding capability and spatial stimulus selectivity. *Journal of Neuroscience* **22**, 4577–4590.

Bauermann, J. and Lindner, B. (2019). Multiplicative noise is beneficial for the transmission of sensory signals in simple neuron models. *Biosystems* **178**, 25–31.

Benda, J., Longtin, A. and Maler, L. (2005). Spike-Frequency Adaptation Separates Transient Communication Signals from Background Oscillations. *Journal of Neuroscience* **25**, 2312–2321.

Berman, N. J. and Maler, L. (1998). Interaction of GABAB-mediated inhibition with voltage-gated currents of pyramidal cells: computational mechanism of a sensory searchlight. *J Neurophysiol* **80**, 3197–3213.

Berman, N. J. and Maler, L. (1999). Neural architecture of the electrosensory lateral line lobe: adaptations for coincidence detection, a sensory searchlight and frequency-dependent adaptive filtering. *Journal of Experimental Biology* **202**,.

Bialek, W. and Rieke, F. (1992). Reliability and information transmission in spiking neurons. *Trends Neurosci* **15**, 428–434.

Bodnar, D. A. and Bass, A. H. (1997). Temporal coding of concurrent acoustic signals in auditory midbrain. *Journal of Neuroscience* **17**, 7553–64.

Bol, K., Marsat, G., Mejias, J. F., Maler, L. and Longtin, A. (2013). Modeling cancelation of periodic inputs with burst-STDP and feedback. *Neural Networks* **47**, 120–133.

Borst, A. and Theunissen, F. E. (1999). Information theory and neural coding. *Nat Neurosci* **2**, 947–957.

Bratton, B. and Bastian, J. (1990). Descending control of electroreception: properties of nucleus-praeeminentialis neurons projecting directly to the electrosensory lateral line lobe. *Journal of Neuroscience* **10**, 1226–1240.

Bullock, T. H. (1969). Species differences in effect of electroreceptor input on electric organ pacemakers and other aspects of behavior in electric fish. *Brain Behav Evol* **2**, 85–118.

Carr, C. E., Maler, L., Heiligenberg, W. and Sas, E. (1981). Laminar organization of the afferent and efferent systems of the torus semicircularis of Gymnotiform fish: Morphological substrates for parallel processing in the electrosensory system. *Journal of Comparative Neurology* **203**, 649–670.

Carr, C. E., Maler, L. and Sas, E. (1982). Peripheral organization and central projections of the electrosensory nerves in gymnotiform fish. *Journal of Comparative Neurology* **211**, 139–153.

Chacron, M. J. and Bastian, J. (2008). Population coding by electrosensory neurons. *J Neurophysiol* **99**, 1825–1835.

Chacron, M. J., Maler, L. and Bastian, J. (2005a). Electroreceptor neuron dynamics shape information transmission. *Nat Neurosci* **8**, 673–678.

Chacron, M. J., Maler, L. and Bastian, J. (2005b). Feedback and feedforward control of frequency tuning to naturalistic stimuli. *Journal of Neuroscience* **25**, 5521–5532.

Clarke, S. E. and Maler, L. (2017). Feedback Synthesizes Neural Codes for Motion. *Current Biology*.

Clarke, S. E., Longtin, A. and Maler, L. (2014). A Neural Code for Looming and Receding Motion Is Distributed over a Population of Electrosensory ON and OFF Contrast Cells. *Journal of Neuroscience* **34**, 5583–5594.

Clarke, S. E., Longtin, A. and Maler, L. (2015). Contrast coding in the electrosensory system: parallels with visual computation. *Nat Rev Neurosci* **16**, 733–744.

Dayan, P. and Abbott, L. F. (2001). *Theoretical neuroscience: computational and mathematical modeling of neural systems*. Cambridge, MA: Academic Press.

Ecker, A. S., Berens, P., Tolias, A. S. and Bethge, M. (2011). The Effect of Noise Correlations in Populations of Diversely Tuned Neurons. *Journal of Neuroscience* **31**, 14272–14283.

Franke, F., Fiscella, M., Sevelev, M., Roska, B., Hierlemann, A. and Azeredo da Silveira, R. (2016). Structures of Neural Correlation and How They Favor Coding. *Neuron* **89**, 409–422.

Ghim, J.-W., Huh, N., Jung, M. W. and Oh, J.-H. (2008). Information transmission by stimulus-dependent modulation of noise correlation. *Neuroreport* **19**, 453–7.

Goldberg, J. M. and Brown, P. B. (1969). Response of binaural neurons of dog superior olivary complex to dichotic tonal stimuli: some physiological mechanisms of sound localization. *J Neurophysiol* **32**, 613–636.

Gussin, D., Benda, J. and Maler, L. (2007). Limits of Linear Rate Coding of Dynamic Stimuli by Electroreceptor Afferents. *J Neurophysiol* **97**, 2917–2929.

Henninger, J., Krahe, R., Kirschbaum, F., Grewe, J. and Benda, J. (2018). Statistics of natural communication signals observed in the wild identify important yet neglected stimulus regimes in weakly electric fish. *J Neurosci* 0350–18.

Hofmann, V. and Chacron, M. J. (2017). Differential receptive field organizations give rise to nearly identical neural correlations across three parallel sensory maps in weakly electric fish. *PLoS Comput Biol*.

Hofmann, V. and Chacron, M. J. (2018). Population Coding and Correlated Variability in Electrosensory Pathways. *Front Integr Neurosci* **12**, 56.

Hunsberger, E., Scott, M. and Eliasmith, C. (2014). The competing benefits of noise and heterogeneity in neural coding. *Neural Comput* **26**, 1600–1623.

Hupé, G. J. and Lewis, J. E. (2008). Electrocommunication signals in free swimming brown ghost knifefish, Apteronotus leptorhynchus. *J. Exp. Biol.* **211**, 1657–1667.

Ihlefeld, A., Alamatsaz, N. and Shapley, R. M. (2019). Population rate-coding predicts correctly that human sound localization depends on sound intensity. *Elife* **8**,.

Jung, S. N., Longtin, A. and Maler, L. (2016). Weak signal amplification and detection by higher-order sensory neurons. *J Neurophysiol* **115**, 2158–2175.

Krahe, R. and Maler, L. (2014). Neural maps in the electrosensory system of weakly electric fish. *Curr Opin Neurobiol* **24**, 13–21.

Krahe, R., Bastian, J. and Chacron, M. J. (2008). Temporal processing across multiple topographic maps in the electrosensory system. *J Neurophysiol* **100**, 852–67.

Lankarany, M., Al-Basha, D., Ratté, S. and Prescott, S. A. (2019). Differentially synchronized spiking enables multiplexed neural coding. *Proc Natl Acad Sci U S A* **116**, 10097–10102.

Lissmann, H. W. (1951). Continuous Electrical Signals from the Tail of a Fish, Gymnarchus niloticus Cuv. *Nature* **167**, 201–202.

Lissmann, H. W. (1958). On the Function and Evolution of Electric Organs in Fish. *Journal of Experimental Biology* **35**, 156-.

Litwin-Kumar, A., Chacron, M. J. and Doiron, B. (2012). The Spatial Structure of Stimuli Shapes the Timescale of Correlations in Population Spiking Activity. *PLoS Comput Biol* **8**, e1002667.

Maler, L. (2007). Neural strategies for optimal processing of sensory signals. In *Progress in Brain Research*, pp. 135–154.

Maler, L. (2009a). Receptive field organization across multiple electrosensory maps. II. Computational analysis of the effects of receptive field size on prey localization. *J Comp Neurol* **516**, 394–422.

Maler, L. (2009b). Receptive field organization across multiple electrosensory maps. I. Columnar organization and estimation of receptive field size. *Journal of Comparative Neurology* **516**, 376–393.

Maler, L. (2018). Current Biology. *Current Biology* **28**, R1328–R1330.

Maler, L., Sas, E., Johnston, S. and Ellis, W. (1991). An atlas of the brain of the electric fish Apteronotus leptorhynchus. *J Chem Neuroanat* **4**, 1–38.

Marsat, G. and Maler, L. (2010). Neural Heterogeneity and Efficient Population Codes for Communication Signals. *J Neurophysiol* **104**, 2543–2555.

Marsat, G. and Maler, L. (2012). Preparing for the unpredictable: adaptive feedback enhances the response to unexpected communication signals. *J Neurophysiol* **107**, 1241–1246.

Marsat, G. and Pollack, G. S. (2004). Differential temporal coding of rhythmically diverse acoustic signals by a single interneuron. *J Neurophysiol* **92**, 939–948.

Marsat, G., Longtin, A. and Maler, L. (2012). Cellular and circuit properties supporting different sensory coding strategies in electric fish and other systems. *Curr Opin Neurobiol* **22**, 686–692.

Marsat, G., Daly, K. C. and Drew, J. A. (2023). Characterizing neural coding performance for populations of sensory neurons: comparing a weighted spike distance metrics to other analytical methods. *bioRxiv* 778514.

McDonnell, M. D. and Ward, L. M. (2011). The benefits of noise in neural systems: bridging theory and experiment. *Nat Rev Neurosci* **12**, 415–425.

Mejias, J. F., Marsat, G., Bol, K., Maler, L. and Longtin, A. (2013). Learning Contrast-Invariant Cancellation of Redundant Signals in Neural Systems. *PLoS Comput Biol*.

Metzen, M. G. and Chacron, M. J. (2021). Population Coding of Natural Electrosensory Stimuli by Midbrain Neurons. *Journal of Neuroscience* **41**, 3822–3841.

Metzen, M. G., Huang, C. G. and Chacron, M. J. (2018). Descending pathways generate perception of and neural responses to weak sensory input. *PLoS Biol* **16**, e2005239.

Milam, O. E., Ramachandra, K. L. and Marsat, G. (2019). Behavioral and neural aspects of the spatial processing of conspecifics signals in the electrosensory system. *Behavioral Neuroscience* **133**, 282–296.

Nassar, M. R., Scott, D. and Bhandari, A. (2021). Noise Correlations for Faster and More Robust Learning. *Journal of Neuroscience* **41**, 6740–6752.

Pedraja, F., Perrone, R., Silva, A. and Budelli, R. (2016). Passive and active electroreception during agonistic encounters in the weakly electric fish Gymnotus omarorum. *Bioinspir Biomim* **11**, 065002.

Seriès, P., Latham, P. E. and Pouget, A. (2004). Tuning curve sharpening for orientation selectivity: coding efficiency and the impact of correlations. *Nat Neurosci* **7**, 1129–1135.

Shumway, C. A. (1989). Multiple electrosensory maps in the medulla of weakly electric gymnotiform fish. I. Physiological differences. *J Neurosci* **9**, 4388–99.

Shumway, C. A. and Maler, L. (1989). Gabaergic inhibition shapes temporal and spatial response properties of pyramidal cells in the electrosensory lateral line lobe of gymnotiform fish. *J Comp Physiol A* **164**, 391–407.

Shumway, C. A., Koch, C., Wessel, R. and Gabbiani, F. (1989). Multiple electrosensory maps in the medulla of weakly electric gymnotiform fish. II. Anatomical differences. *J Neurosci* **9**, 4400–15.

Simmonds, B. and Chacron, M. J. (2015). Activation of Parallel Fiber Feedback by Spatially Diffuse Stimuli Reduces Signal and Noise Correlations via Independent Mechanisms in a Cerebellum-Like Structure. *PLoS Comput Biol* **11**, e1004034.

Sompolinsky, H., Yoon, H., Kang, K. and Shamir, M. (2001). Population coding in neuronal systems with correlated noise. *Phys Rev E Stat Phys Plasmas Fluids Relat Interdiscip Topics* **64**, 11.

Stamper, S. A., Roth, E., Cowan, N. J. and Fortune, E. S. (2012a). Active sensing via movement shapes spatiotemporal patterns of sensory feedback. *Journal of Experimental Biology* **215**, 1567–1574.

Stamper, S. A., Madhav, M. S., Cowan, N. J. and Fortune, E. S. (2012b). Beyond the Jamming Avoidance Response: weakly electric fish respond to the envelope of social electrosensory signals. *Journal of Experimental Biology* **215**, 4196–4207.

Stamper, S. A., Fortune, E. S. and Chacron, M. J. (2013). Perception and coding of envelopes in weakly electric fishes. *Journal of Experimental Biology* **216**,.

Stein, R. B., Gossen, E. R. and Jones, K. E. (2005). Neuronal variability: noise or part of the signal? *Nat Rev Neurosci* **6**, 389–397.

Wiley, R. H. (2015). *Noise Matters: The evolution of communication*. Cambridge, MA: Harvard University Press.

Yu, N., Hupé, G., Garfinkle, C., Lewis, J. E., Longtin, A. and Fortune, E. (2012). Coding Conspecific Identity and Motion in the Electric Sense. *PLoS Comput Biol* **8**, e1002564.

Zhang, Z. D. and Chacron, M. J. (2016). Adaptation to second order stimulus features by electrosensory neurons causes ambiguity. *Sci Rep* **6**, 28716.

Figures and Legends

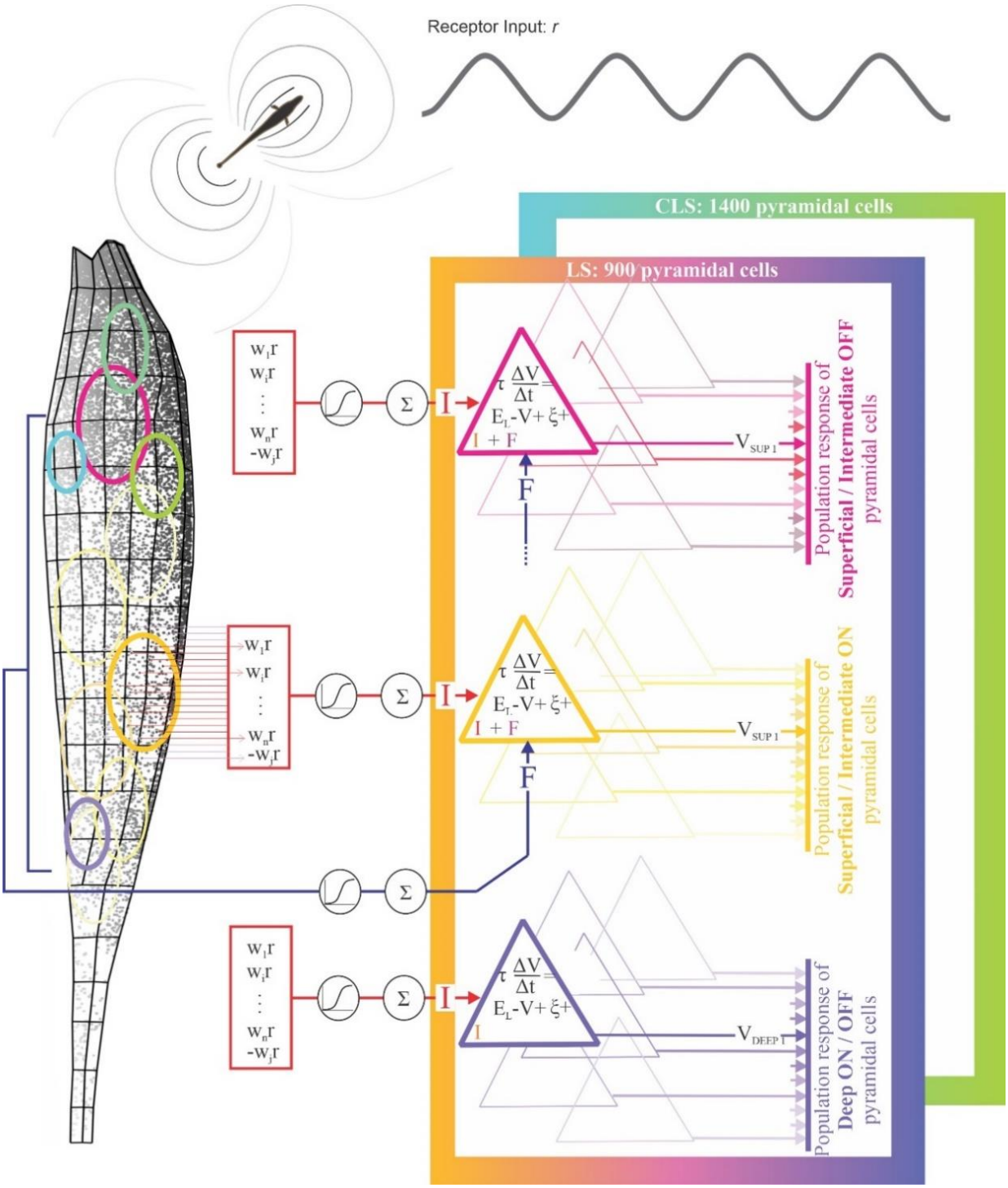

Figure 1. Schematic of the sensory transformation from electroreceptor input to neural representation by a heterogeneous model network in the ELL.

Schematic depicting how the model replicates the network elements present in the ELL, including population density, ON/OFF-type polarity preference, integration of electroreceptor input, *r*, for processing the spatial aspect of a conspecific stimulus, (top, gray), from overlapping receptive fields (left, colored circles on fish), and population specific feedback (*F*, purple) Pyramidal cells (center, multicolored triangles) in topographic maps of the ELL (right, colored boxes) have receptive fields mapping the electrosensory surface of the fish's body. Each leaky integrate-and-fire neuron (pyramidal cell of the ELL) will pool the stimulus-driven electroreceptor input and unique noise within the spatial extent of the pyramidal cell's receptive field. The parameters of each pyramidal cell will differ to precisely replicate the physiological responses of subpopulations of pyramidal cells as recorded from in-vivo extracellular electrophysiological recordings (*w* is the weight that will be determined based on the pattern of activation given by the electric field model, ξ is noise, τ is the time constant, *V* is voltage, E_L is the reversal-potential or "leak"). A spatially diffuse feedback component will only target the superficial and intermediate pyramidal cell types in both LS and CLS maps, and not the deep pyramidal cell types.

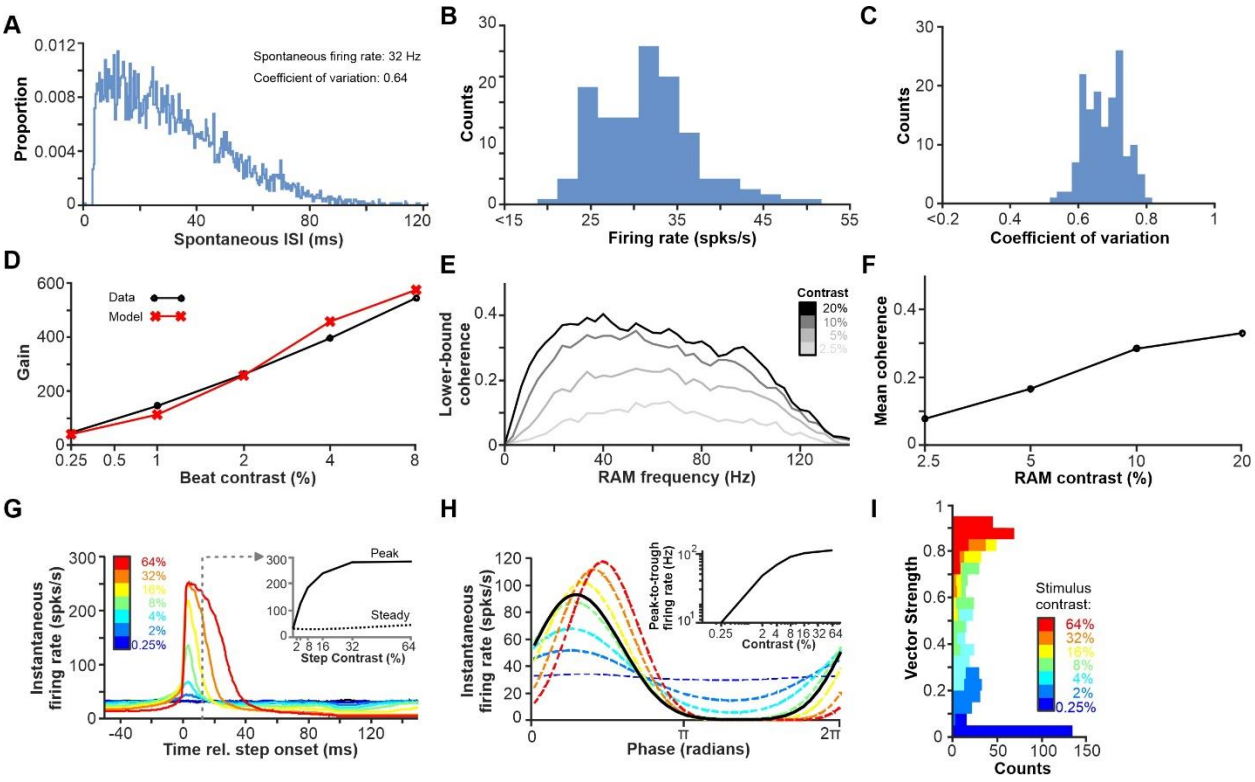

Figure 2. Model calibration for an example ELL subpopulation.

(A) Interspike interval histograms during spontaneous activity of the original seed for a deep pyramidal cell from the LS map with ON-type polarity. The mean firing rate and mean coefficient of variation are shown in the top right corner.

(B) Histogram of the mean firing rate during spontaneous activity for the full LS deep ON-type model pyramidal cell population (n=150).

(C) Histogram of the coefficient of variation during spontaneous activity for the full LS deep ON-type model pyramidal cell population (n=150).

(D) Comparisons of the stimulus-response gain from the experimentally documented average for LS deep ON-type pyramidal cells (Data, in black) to the original seed of an LS deep ON-type model pyramidal cell (Model, in red) using the output of the electroreceptor population to a 30 Hz SAM stimulus with different beat contrasts as the input.

(E) Lower-bound coherence of the original seed of an LS deep ON-type model pyramidal cell. The coherence is in response the output of the electroreceptor population to a RAM stimulus ranging from 0-100 Hz with different beat contrasts as the input.

(F) Mean lower-bound coherence of the original seed of an LS deep ON-type model pyramidal cell. The coherence is in response the output of the electroreceptor population to a RAM stimulus ranging at 30 Hz with different beat contrasts as the input. Coherence analyses are standard and described in previous publications (Allen and Marsat, 2019; Borst and Theunissen, 1999; Krahe et al., 2008). The lower-bound coherence represents the linear correlation between the stimulus and the response.

(G) Responses of the original seed of the LS deep ON-type model pyramidal cell to step increases in EOD intensity. The strength of the peak response, the steady-state response, and the adaptation time constant were approximately matched to experimental and published data (Milam and Marsat, 2023; Bastian, 1986; Bastian et al., 2002; Krahe et al., 2008; Maler, 2009a; Maler, 2009b). The dashed gray line indicates the starts of the window for averaging the steady-state response.

(H) Responses of the original seed of an LS deep ON-type model pyramidal cell to increasing beat contrast of a SAM stimulus at a 30 Hz beat frequency. The strength of the average peak-to-trough firing rate was fit to experimental and published data (Milam and Marsat, 2023).

(I) Histograms of the vector strength in response to a SAM stimulus with a 30 Hz beat frequency and different beat contrasts for the full LS deep ON-type pyramidal cell population (n=150).

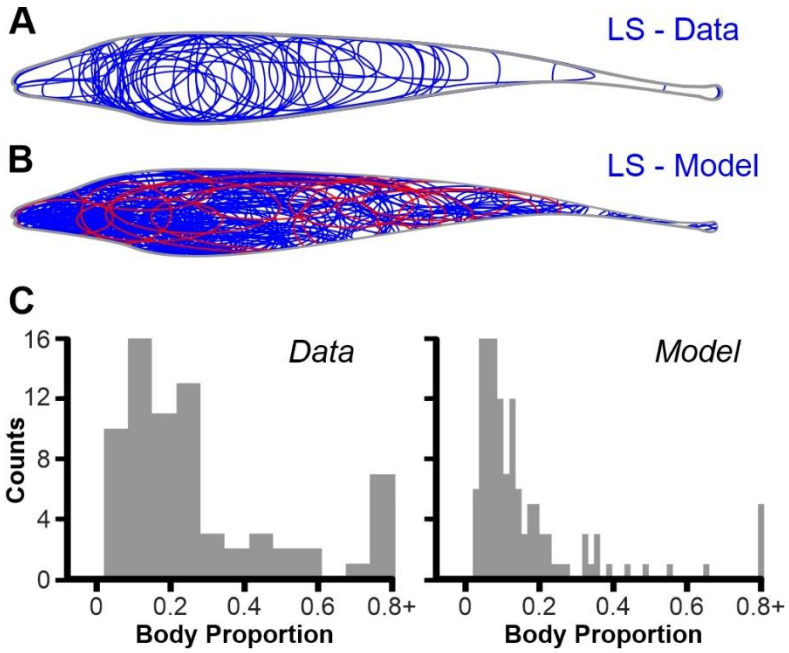

Figure 3. Spatial organization of pyramidal cell receptive fields. **(A)** Unfilled outlines of the perimeter of the receptive field centers for LS pyramidal cells recorded *in-vivo* using electrophysiology (n=55; Milam and Marsat, 2023). **(B)** Unfilled outlines of the perimeter of the receptive field centers for model LS pyramidal cells. There are 150 unique receptive field centers for the 150-column resolution of the model LS map. The LS map consists of 6 subtypes of pyramidal cells (ON and OFF; superficial, intermediate, and deep) using 150 receptive field centers resulting in (n=900) total LS model neurons. Note that both the data and model provide complete receptive field coverage of the body if receptive field outlines were illustrated as being filled in. For ease of visibility, a small subset (n=15) of receptive field outlines is shown in red.

(C) Histograms of receptive field center size represented as a proportion of the total body area of the 3D mesh model. We show the histograms as an approximate comparison of the distribution of receptive field center sizes between the data and the model. However, we note that these two are not fully comparable as the body proportion for the data are calculated as the length along the rostral to caudal axis of the fish, whereas the body proportion for the

model are calculated using the ratio of electroreceptors within a receptive field center to the total electroreceptor amount on the respective unilateral side of the body.

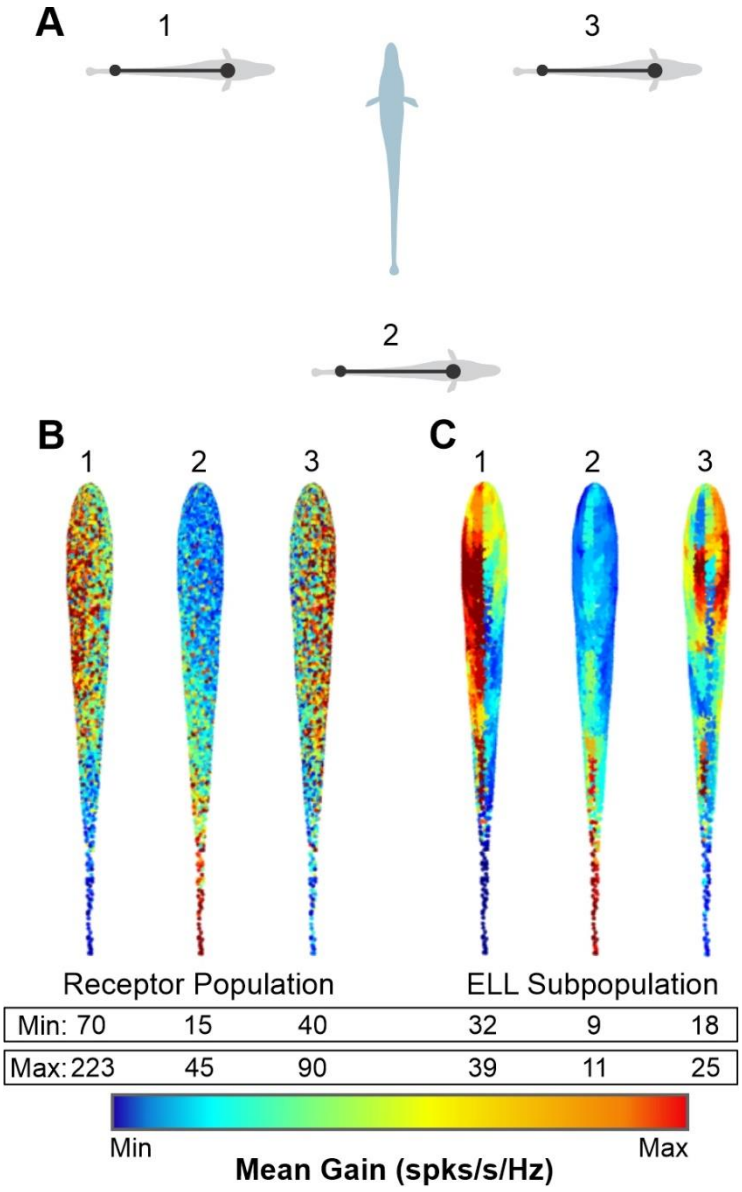

Figure 4. Responses to spatially realistic conspecific signals visualized as topographic heatmaps for the model electroreceptor population and model ELL subpopulation. The heatmaps allow a visualization of the population response to a conspecific stimulus played from various relative locations (from a distance of 10 cm away and oriented 90 degrees, shown in **A**). Each colored point on the heatmap represents a putative receptor on the skin of the fish (see Methods; and Ramachandra et al., 2023). A receptor can contribute to several neurons' receptive field and its color will reflect the average responses (e.g., gain) across these neurons. In the 6 heatmaps presented here, we see differences in the average gain across stimulus locations for **(B)** the electroreceptor population (n=8,195) and **(C)** the LS deep ON-type pyramidal cell population in the ELL (n=300 neurons with overlapping receptive fields integrating from 8,195 electroreceptors). The population responses show a spatial dependency, as the mean gain is higher on the side the body that corresponds to the source of the

conspecific stimulus. It is worth noting that we use individualized color scaling to highlight small differences in the patterns for a single location between populations, with a value range indicated by “Min” and “Max”. A normalized color scale to compare level differences between the stimulus locations could also be used, but occludes the spatial effect in the electric image so it is not shown here.

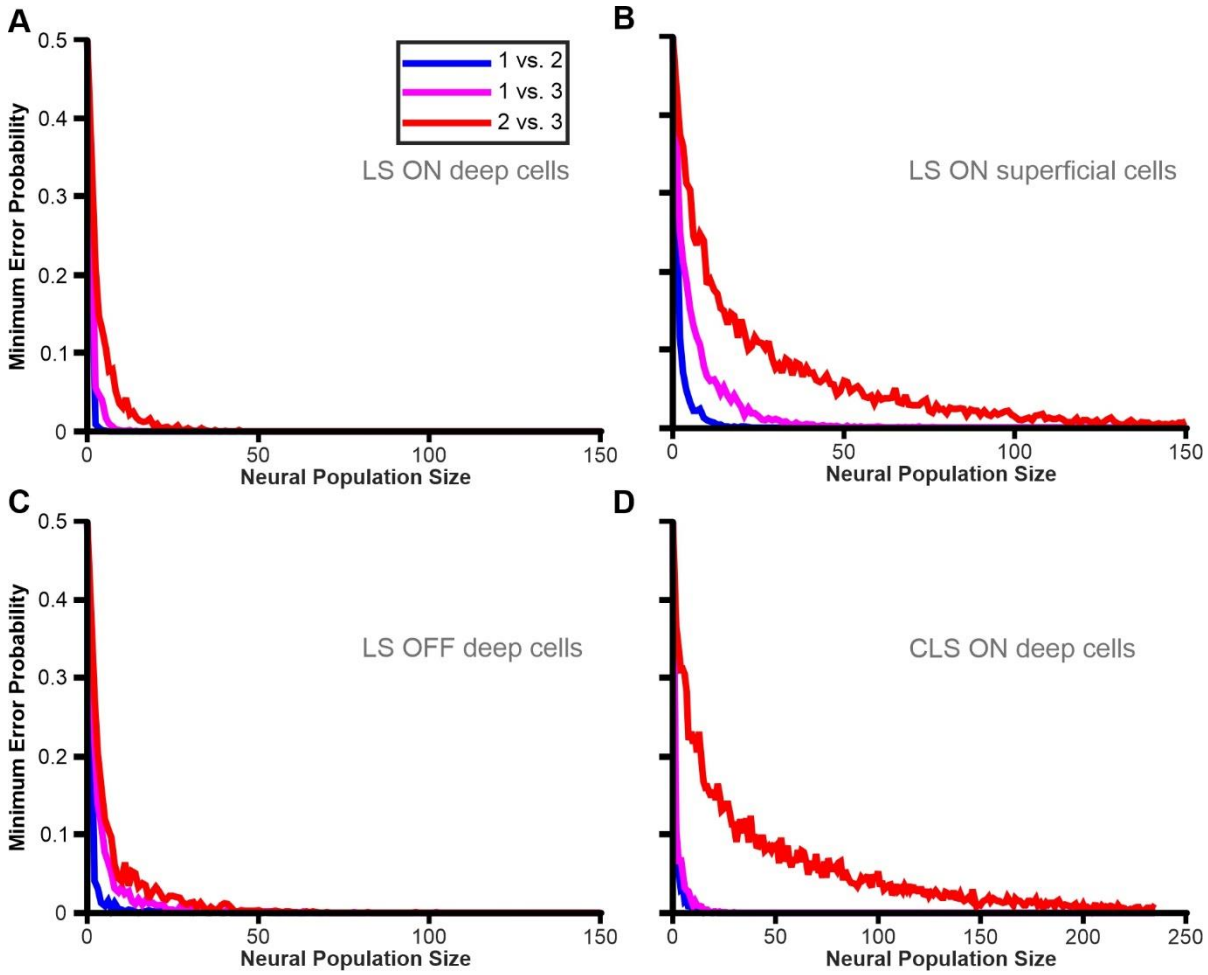

Figure 5. Deep pyramidal cells are highly accurate coders of conspecific location.

Pairwise stimulus discrimination using stimulus-response gain on full subpopulations of model pyramidal cells (n=150 for LS; n=235 for CLS). All unique paired combinations of conspecific 30 Hz beat stimuli are depicted by the top right inset of **(A)** and refer to the stimulus locations shown in Figure 4A. A discrimination accuracy level of 95% is obtained with fewer than 20 neurons for deep ON-type pyramidal cells in the LS map across all unique pairs of stimulus locations. **(B)** Superficial ON-type pyramidal cells reach a 95% accuracy level with less than 65 neurons across all unique pairs of stimulus locations. **(C)** A discrimination accuracy level of 95% is obtained with fewer than 25 neurons for deep OFF-type pyramidal cells in the LS map across

all unique pairs of stimulus locations. **(D)** A discrimination accuracy level of 95% is obtained with fewer than 100 neurons for deep OFF-type pyramidal cells in the CLS map, for certain stimulus pairs.

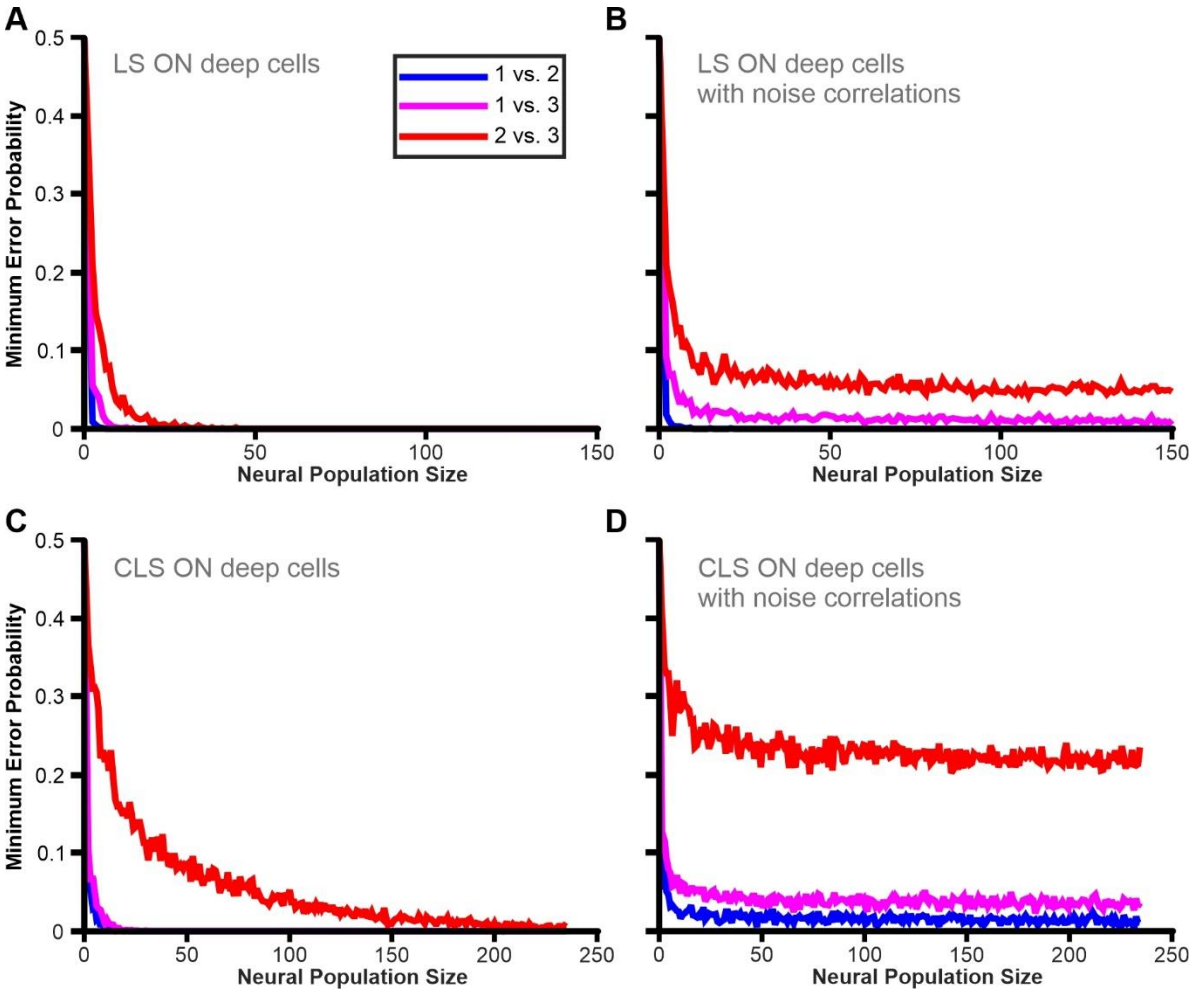

Figure 6. Noise correlations are detrimental to coding accuracy of conspecific location.

Pairwise stimulus discrimination using stimulus-response gain on full subpopulations of model pyramidal cells (n=150 for LS; n=235 for CLS). All unique paired combinations of conspecific 30 Hz beat stimuli are depicted by the top right inset of **(A)** and refer to the stimulus locations shown in Figure 4A. Without noise correlations, a discrimination accuracy level of 95% is obtained with fewer than 20 neurons for deep ON-type pyramidal cells in the LS map across all unique pairs of stimulus locations. **(B)** With noise correlations, deep ON-type pyramidal cells in the LS map achieve a discrimination accuracy of 95% for certain populations, but the accuracy is limited and remains mostly invariant to increasing population size. The population fails to

maintain a stable 95% accuracy level with 150 neurons for certain pairs of stimulus locations. **(C)** Without noise correlations, a discrimination accuracy level of 95% is obtained with fewer than 100 neurons for deep ON-type pyramidal cells in the CLS map, for certain stimulus pairs. **(D)** With noise correlations, deep ON-type pyramidal cells in the CLS map achieve a discrimination accuracy of 95% for certain populations, but the accuracy is limited and remains mostly invariant to increasing population size. The population fails to maintain a stable 95% accuracy level with 150 neurons for certain pairs of stimulus locations.

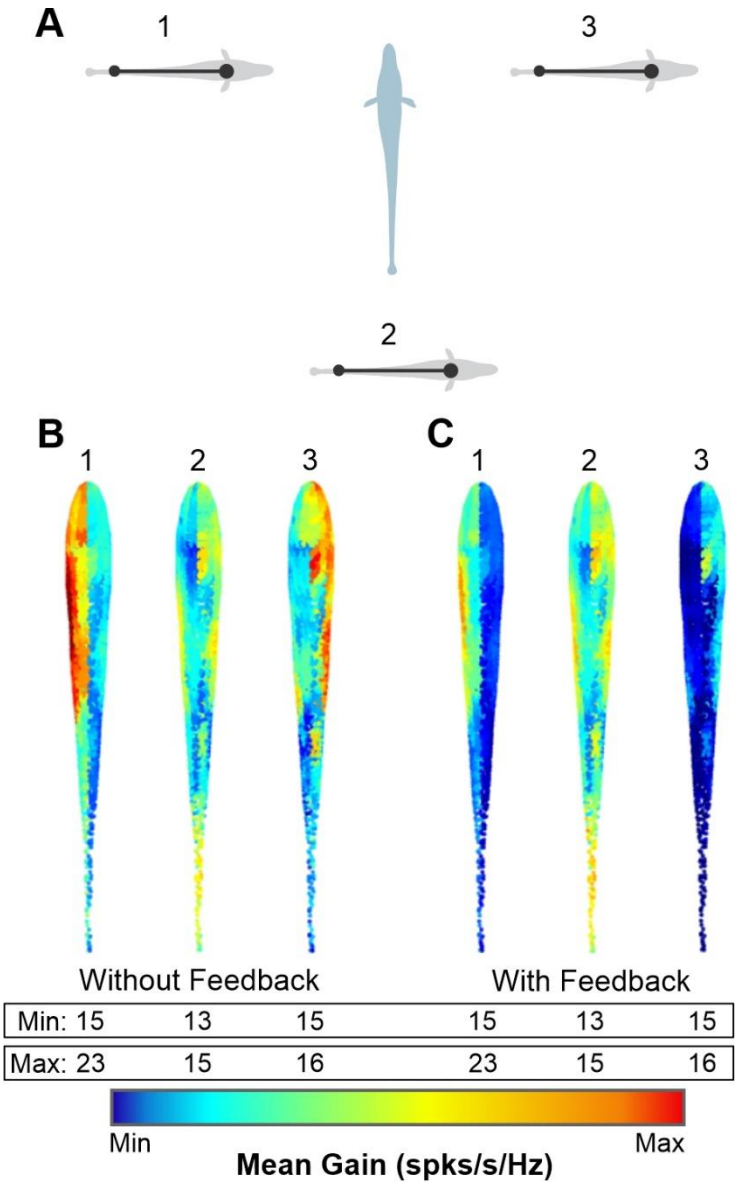

Figure 7. Responses to spatially realistic conspecific signals visualized as topographic heatmaps for an ELL subpopulation with and without uniform feedback.

(A) Illustration of a 5 Hz conspecific beat stimulus played from various relative locations (at a distance of 10 cm away and oriented 90 degrees). **(B)** Heatmaps of the mean gain across a population of superficial ON-type pyramidal cells of the LS (n=300) with feedback inputs **(C)** and without feedback inputs in response to different conspecific stimulus locations. Color scaling is indicated by the value range, “Min” and “Max”. Changes in the mean gain from the side of the body corresponding to the stimulus location compared to the other side are less pronounced in the population with feedback.

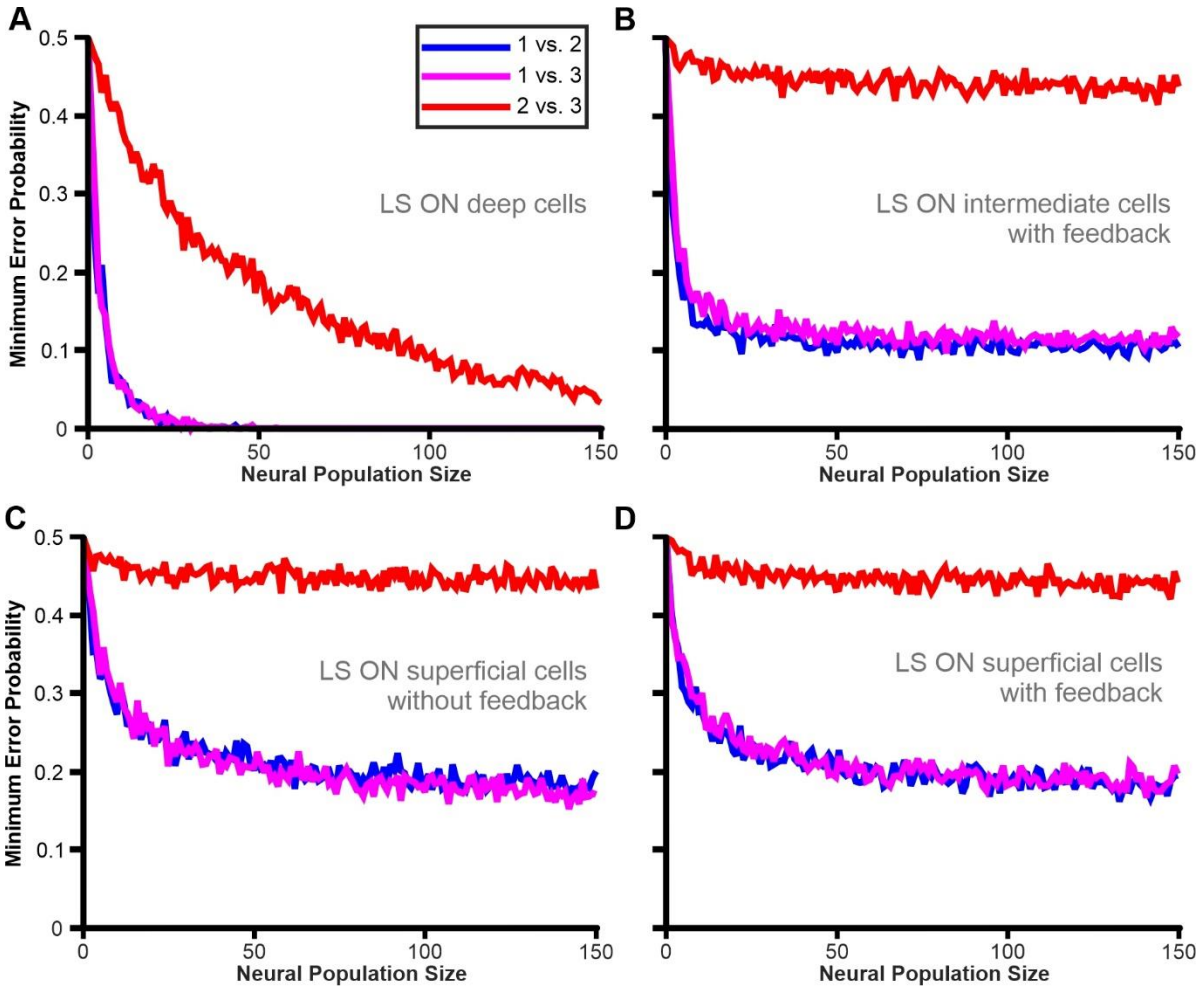

Figure 8. Feedback with uniform strength has minimal effects on coding accuracy of conspecific location.

Pairwise stimulus discrimination using stimulus-response gain on full subpopulations of model pyramidal cells (n=150 for LS). All unique paired combinations of conspecific 5 Hz beat stimuli are depicted by the top right inset of **(A)** and refer to the stimulus locations shown in Figure 4A and 7A. Deep pyramidal cells are the source of the feedback and achieve a discrimination accuracy level of 95% is obtained with fewer than 20 neurons for deep ON-type pyramidal cells in the LS map across all unique pairs of stimulus locations. **(B)** With noise correlations, deep ON-type pyramidal cells in the LS map achieve a discrimination accuracy of 95% for certain

populations, but the accuracy is limited and remains mostly invariant to increasing population size. The population fails to maintain a stable 95% accuracy level with 150 neurons for certain pairs of stimulus locations. **(C)** Without noise correlations, a discrimination accuracy level of 95% is obtained with fewer than 100 neurons for deep ON-type pyramidal cells in the CLS map, for certain stimulus pairs. **(D)** With noise correlations, deep ON-type pyramidal cells in the CLS map achieve a discrimination accuracy of 95% for certain populations, but the accuracy is limited and remains mostly invariant to increasing population size. The population fails to maintain a stable 95% accuracy level with 150 neurons for certain pairs of stimulus locations.

Chapter 5: Discussion

Summary of the Data

With this dissertation, I have evaluated how space is represented and transformed at different stages of electrosensory processing and demonstrated several important principles of neural coding and network properties that support population coding of conspecific signals. Specifically, I have shown how a signal's location modulates the activation pattern of the electroreceptor array (**Chapter 2**), and that this spatial information is encoded accurately by the heterogeneous population of pyramidal cells in the ELL (**Chapter 3**). I have provided evidence for the segregation of sensory information streams in the neural code, showing that neurons have specific functional roles based on their response properties, morphology, and connectivity in the network (**Chapter 3 and 4**). I have also examined aspects of the network dynamic that could influence spatial processing and thereby revealed core computational mechanisms operating in the early electrosensory circuit (**Chapter 4**).

The spatial aspect of conspecific signals is encoded by the electroreceptor sensorium

Chapter 2 of this dissertation demonstrates that in *A. leptorhynchus*, information about conspecific azimuth, position, and distance is carried within the beat and accurately captured by the electroreceptor array. The response of a single electroreceptor reliably encodes the strength of the beat at a single point on the skin, but does not convey substantial information about the location of the stimulus. However, by pooling several electroreceptors sensitive to different points along the body to create a population response, conspecific signals from different distances and locations can be discriminated accurately by the electroreceptor

population. I showed that spatial information from conspecific signals is encoded by differences in the peak-to-trough firing rate of the linear spiking response across several electroreceptors.

I quantified the spatial resolution ability of the electroreceptor population by testing the discrimination performance between different magnitudes of angular change. The electroreceptor populations tested can accurately discriminate small differences in angular resolution, and the accuracy performance is contingent on the number of beat cycles processed by the electroreceptor population. To investigate further the sensitivity of the electroreceptive periphery, I estimated the detectable range of conspecific signals and found that the full electroreceptor population could detect beat contrasts of less than a few percent at distances up to 75 cm away if integrating information over several EOD cycles. Furthermore, I show how the density distribution of electroreceptors enhances detection accuracy for signal sources around the fish, but contributes less towards accurately localizing conspecific signals. This is particularly true for the rostral end of the fish, which displays a much higher electroreceptor density, and is characteristic of an electrosensory fovea (Nelson and MacIver, 1999; Hofmann et al., 2017). I argue that the role of the electroreceptor distribution is multi-functional and dependent on the spatial structure of the sensory signal. For spatially diffuse signals, high receptor convergence contributes to increasing detection capacities, whereas for spatially delineated signals, receptor density can increase spatial resolution. These findings are in line with previously published behavioral observations of interacting fish from field and lab studies, and allude to the cues acquired by the peripheral nervous system to accomplish difficult conspecific localization tasks (Knudsen, 1975; Stamper et al., 2012; Henninger et al., 2018).

To gain a better insight into the mechanisms underlying the system's sensitivity for detecting and discriminating beat contrasts from conspecific signals, we must have a quantitative understanding of the transformation from the spatio-temporal structure of the signal at the electroreceptor level to its spatial representation in the ELL.

Population coding indicates that spatial information is segregated in the ELL

Neural coding of the temporal aspect of communication signals has been well documented in ELL pyramidal cells of *A. leptorhynchus* (Krahe et al., 2008; Marsat and Maler, 2010; Marsat and Maler, 2011; Marsat et al., 2012; Allen and Marsat; 2018). However, much less is known about how spatial information is processed by pyramidal cells of the ELL network. In this dissertation, I present foundational work that investigates extensively how the spatial aspect of conspecific beat signals are processed at the primary electrosensory level. I show that accomplishing a conspecific localization task relies on a heterogenous population of cells, and explain how the different elements of the population are leveraged to support accurate spatial coding.

In Chapter 3, I use a neurophysiological approach to investigate the accuracy of spatial coding for each pyramidal cell type of the ELL, by quantifying the localization performance based on the relevant information embedded in the beat stimulus. These data allow us to demonstrate that all ELL pyramidal cells are able to accurately discriminate signal location regardless of a change in azimuth. When evaluating the response of single neurons, I did not find a systematic pattern in the spiking response to different spatial stimuli. Indeed, the response of several neurons were largely heterogeneous, with some neurons displaying

distinct, spatially dependent responses, and other neurons where their responses were much noisier. Additionally, some neurons seemed to evoke more of a change in their firing rate response, whereas other neurons showed more of a shift in their response synchrony to different spatial stimuli. However, while this observation is unexpected from my initial predictions, I found that by pooling together a population of approximately 70 neurons, the population can achieve perfect accuracy when challenged with the location-based discrimination tasks that I tested in this study.

In Chapter 3, I assess the performance of the pyramidal cell subpopulations by estimating the spatial coding efficiency based on the discrimination accuracy rate for different azimuths and location of stimuli. The vector strength or synchronization coefficient was the most informative aspect of the neural response for localizing conspecific signals most efficiently. These results were significantly higher than the efficiency rates produced from measurements of firing rate and stimulus-response gain in most stimulus regimes.

Notably, I show that ON-type pyramidal cells perform better than OFF-type pyramidal cells of the ELL. The idea that ON-type cells are encoding a majority of the relevant spatial information could imply a supportive role for neighboring OFF-type cells in adjacent topographic columns. This disparity could act to increase contrast at small and large spatial scales, and has been alluded to in other recent studies (Clarke and Maler, 2017; Clarke et al., 2015; Haggard and Chacron, 2023).

Moreover, when exploring the dimensions of pyramidal cell receptive fields, I found that larger sized receptive fields outperformed smaller sized receptive fields. For conspecific stimuli that affect electroreceptors covering the entire body (i.e., a global stimulus), the high-

performing large receptive field neurons may have the advantage as they are able to integrate sensory information over a larger surface area containing more electroreceptors. Neurons with smaller receptive fields may be sufficient for this sensory task, but the results from the performance analysis provide clear support that larger receptive field neurons can accomplish this same task with significantly higher efficiency.

One of the most remarkable findings from the performance analysis is that the deep-type pyramidal cells are much more efficient than the superficial or intermediate-type pyramidal cells. Superficial-type neurons have been well-documented for excelling at temporal coding of communication signals (e.g., chirps). Here, I show for the first time that the deep-type pyramidal cells excel at spatial coding of conspecific signals. This is an especially important finding, given that deep-type pyramidal cells are the source of feedback to the superficial and intermediate-type pyramidal cells of the ELL, and receive no feedback themselves (Bratton and Bastian, 1990; Maler et al., 1991; Berman and Maler, 1999; see also Milam et al, 2019 for review). The differences in network connectivity combined with a clear distinction in spatial coding efficiency is indicative of a segregation of spatial information that begins at the ELL level.

In Chapter 4, I investigate population coding and the effects of correlated noise for spatially processing conspecific signals. Single unit recordings from pyramidal cell variants, while invaluable as a data source, are limited in sample size and offer a restricted scope for proposing candidate population codes. To circumvent this, I implement a large-scale modeling approach of all pyramidal cell types present in the lateral segment and centrolateral segment topographic maps of the ELL. The advantage to this modeling method is that it provides a way to expand on findings from *in-vivo* electrophysiological experiments at the full population scale. For certain

analyses, I combine the responses of the intermediate-type pyramidal cells with those of the superficial-type pyramidal cells, as their morphology, functional connectivity, and physiological responses overlap significantly. In support of my earlier findings from Chapter 3, ON-type pyramidal cells outperform OFF-type pyramidal cells, deep-type pyramidal cells are more efficient than those of the superficial or intermediate-type, and pyramidal cells with large receptive fields perform better than pyramidal cells with small receptive fields. Furthermore, the vector strength and stimulus-response gain provide significantly more information for accurately discriminating conspecific location than mean firing rate.

In Chapter 4, I quantify the effect of correlated noise that stems from the shared electroreceptor input that pyramidal cell populations receive due to their overlapping receptive field topography. In agreement with my hypothesis, I find that noise correlations are detrimental to the efficiency of the population, contributing to lower accuracy when resolving conspecific location. This is truly a remarkable insight from the model because it demonstrates that, in this specific network, noise correlations cannot be averaged out for spatial coding. For temporal coding, with a large enough number of neurons, noise correlations will eventually be averaged out. However, the mechanism is different for spatial coding because there is a limit to the amount of spatial information that can be shared between neurons within the population. I clearly demonstrate this principle as a stabilized plateauing in the discrimination accuracy even as neural population size increases. Despite the negative effects of noise correlations, discrimination of signal source location remains feasible (i.e., accuracy greater than chance level) even with a population of less than one hundred neurons. These findings suggest that by

pooling the information from all the different cell subtypes and topographic maps, less plateauing in the discrimination would occur as more cells with overlapping fields are included.

In Chapter 3, I employ a two-dimensional heatmap analysis to visualize qualitatively the response of specific pyramidal cell populations to different spatial stimuli. Though these tools are useful for visualizing the topographic responses to different conspecific locations, the heatmaps yield coverage that is incomplete and patchy resulting in a weak representation due to a restricted sample size. To circumvent limitations in sample size, I used computational modeling to expand my population to include several thousand neurons with complete receptive field coverage of the body. Surprisingly, this model that I presented in Chapter 4 was based on representative samples of neurons from electrophysiological experiments, and provides full coverage yet still shows a patchy heatmap (e.g., when compared to the electroreceptor heatmaps or to the EI). Therefore, this patchiness may not only be a consequence of low sample size, but might represent the reality of the variability of responses in this area. The response patterns produced by the heatmaps analysis revealed clear differences in population activity to stimuli presented ipsilaterally vs contralaterally. The response pattern differed most when comparing the vector strength of ON-type and OFF-type pyramidal cells, and also when comparing deep-type to superficial-type and intermediate-type pyramidal cells.

I show that producing heatmaps with increased population size and coverage result in a diffuse gradient with higher spatial contrast that corresponds to the stimulus location, indicative of a spatial dependency in the population response. The spatial contrast is higher in the ON-type pyramidal cell population than the OFF-type pyramidal cell population, though the

topography of the gradient pattern is similar. These results support the preliminary heatmaps findings made with responses from electrophysiological data, and suggest that ON-type cells are playing a more direct role in neural coding of a conspecific's location. Furthermore, the improved heatmaps reveal that the deep-type pyramidal cell population responds to conspecific location similarly to the full electroreceptor population. An important distinction here is that the deep-type pyramidal cells do this while integrating the response of up to several thousand electroreceptors per receptive field. In downstream brain areas, this could result in a higher resolution sensory image, where the higher image contrast indicates the direction of the conspecific's location in three-dimensional space.

The role of feedback in shaping spatial coding through a background suppression mechanism

Mechanisms of background suppression across modalities relies on spatially diffuse feedback to cancel noisy inputs and enhance contrast (Ölveczky et al., 2003; Baccus et al., 2008; Chen et al., 2005; Bratton and Bastian, 1990; Clarke and Maler, 2017). Similar elements are present in the electrosensory system, as the indirect feedback is driven by spatially diffuse inputs and can attenuate the response to conspecific signals (Milam et al., 2019; Bratton and Bastian, 1990; Berman and Maler, 1999; Clarke and Maler, 2017). The ELL receives indirect feedback inputs that influence the encoding of beats by canceling the response on a cycle-to-cycle basis (Bastian, 1986; Bol et al., 2011; Chacron et al., 2005). Superficial and intermediate-type pyramidal cells receive massive parallel fibers inputs onto their apical dendrites. Plasticity at these synapses adjusts the relative contribution of each fiber so that the overall input is in

antiphase to the feedforward input from the receptors, thus reducing the strength of the response in these cells (Bol et al., 2011; Harvey-Girard et al., 2010). For a pyramidal cell that is only weakly excited by the conspecific signal, because it is not ideally located relative to the conspecific location, the feedback might draw its inputs from a region that is maximally stimulated by the conspecific, and thus the beat would be effectively cancelled in these pyramidal cells. For cells strongly excited by the feedforward stimulation from the conspecific, the feedback might not completely cancel the beat response.

Chapter 4 of this dissertation explores the role of feedback pathways in influencing spatial coding in pyramidal cells. The effects of feedback on single neurons during parameter calibration to 5 Hz and 30 Hz beat stimuli, in addition to visual inspection of the population response from the heatmap analysis, suggest that it reduces the response to the beat as expected. However, this reduction appears to be affecting all cells uniformly and consequently, feedback did not alter spatial coding accuracy. Therefore, it is likely that I have not included the key aspects of feedback that influence spatial coding of conspecific signals. Specifically, the feedback component that I implemented cancelled the response in a uniform way using a negative-image that scales linearly with input strength. An alternative approach to incorporating feedback could be to include a non-linear intensity-response function, particularly one that saturates at higher rates (e.g., an adaptation function). This would create less of an effect for the pyramidal cells that contribute more to the population coding (i.e., more pronounced changes in their spiking response).

In the visual system, photoreceptors convey topographically organized visual input to retinal ganglion cells, whose activity is further influenced by amacrine cells to contribute to

mechanisms such as background-suppression (Ölveczky et al., 2003). However, for sound localization in the mammalian auditory system, the process operates differently and depends on a comparison of binaural inputs. Input from the ipsilateral side is sent to the lateral superior olive (LSO), while sensory input from the contralateral side is sent to the LSO by way of the medial nucleus of the trapezoid body. Direct excitatory inputs to the LSO and indirect inhibitory inputs illustrate an early mechanism of spatial processing in the auditory system (Carr and Konishi, 1990). Compared to the mechanisms operating in the visual and auditory systems, feedback in the electrosensory system contains the elements necessary to mediate localization and spatial processing of conspecifics.

As spatial information is transmitted from electroreceptors to the ELL, the suppression that originates from the high spatial contrast responses in deep-type pyramidal cell population, influences the responses of superficial-type and intermediate-type pyramidal cells through the feedback pathway. Here, the topography is conserved, and each deep-type pyramidal cell provides information to superficial-type and intermediate-type pyramidal cells in the same column of the topographic map. I posit that superficial-type and intermediate-type pyramidal cells play an important role for information transmission downstream, because the response with feedback appears suppressed relative to the response when feedback is absent. If spatial information from different pyramidal cell types or ELL layers are integrated in higher brain areas, then I argue that this suppression might be an important contributor for successfully localizing a conspecific signal from noisy background signals. Thus, supporting a topographically conserved, background suppression mechanism that helps to segregate spatial and temporal information to enable accurate spatial processing at the population level. Indeed, further

research on population model interactions will be needed to determine the role of feedback in shaping spatial coding.

Future Directions

Investigation of signal localization mechanisms in the vertical plane

I have shown in my work that there are several ways to encode spatial information, and that the method can differ depending on cell type and level of sensory processing (e.g., receptors, different maps of the ELL). From my physiological data, there is supporting evidence that some conspecific locations are more easily discriminable than others (e.g., lateral azimuth), and that certain pyramidal cell types outperform others in a localization task. Particularly, the ON-type, deep-type, and larger receptive field pyramidal cells achieve the highest efficiency, while other cell types provide significantly less spatial information. However, these findings resulted from experiments that presented conspecific stimuli along the horizontal plane of the fish's body. A more complete analysis of the spatial processing of conspecifics would require investigating localization along the vertical plane.

Using my current physiological data, I am limited to theorizing what specific aspects of the neural response and network dynamics might contribute most to spatial coding in the vertical plane. However, I would expect that responses at the electroreceptor level and deep-type pyramidal cell level would follow the same straightforward response pattern to conspecific stimuli presented from different locations along the vertical plane. The big difference being that the response pattern would be shifted more along the dorsal-ventral axis of the fish's body rather than the rostral-caudal axis. What is more variable might be the responses of the

superficial-type and intermediate-type pyramidal cells. These cells have much stronger receptive field surrounds, are more susceptible to feedback, and contain more dendritic sites for synaptic plasticity. This could mean that the responses of these cell types to conspecific stimuli presented along the vertical plane could be vastly different to those presented along the horizontal plane, as each of these mechanisms have complex, nonlinear effects on the neural response. In this scenario, one possibility is that the vector strength becomes a less informative measure of the neural response, and instead, cells must rely more heavily on changes in firing rate, stimulus-response gain, or another measure to accurately assess conspecific localization. Of course, this leaves much to the imagination, as a complete population code for localizing a conspecific in three-dimensional space may require a highly complex, and intricate balance of response synchrony and level differences across specific neuron subtypes.

Another insightful study to conduct with methods already accessible, would be to simply model the electric field interactions between two fish, while changing the vertical location and tilt of the fish, and keeping the horizontal location and azimuth unchanged. This would provide an electroreceptor population response and could enable a prediction of the deep-type pyramidal cell responses. This would certainly be a step in the right direction and similar to predictions based on the physiology data, I would expect that responses at the electroreceptor level and deep-type pyramidal cell level would follow the same straightforward response pattern to conspecific stimuli presented from different locations along the vertical plane (i.e., a population-wide spatial dependency). Thus, it is imperative to conduct follow-up modeling and electrophysiology studies to test whether the localization mechanism explained from Chapter 4

is a generalized, three-dimensional localization strategy and not restricted to localization only along the horizontal plane.

Spatial coding during motion

My work in this dissertation shows that the electroreceptor population and several subpopulations of pyramidal cell types in the ELL can accurately discriminate between conspecific stimuli presented from different locations. In the experiments conducted in Chapter 3, I deliver conspecific stimuli from different locations and azimuth from a stationary conspecific mimic. One behavioral component that remains unaddressed is the effect of motion on the spatial aspect of the signal and its influence on spatial processing. A stationary stimulus creates a beat (i.e., a first order stimulus) when the stimulus interacts with the electric field of the receiving fish. However, fish seldom remain completely stationary and even when they stay in the same location, they continually make small movements for active sampling. When a stimulus is moving, an envelope (i.e., a second order stimulus) is created between the stimulus and the electric field of the receiving fish. A beat arises in the presence of a conspecific and thus contains spatial information about the conspecific. Whereas envelopes arise during social contexts of more than two fish or when a conspecific is moving, thereby containing spatial information about motion (Metzen and Chacron, 2014; Stamper et al., 2013; Yu et al., 2012; Thomas et al., 2018).

Logically, a candidate future study would be to investigate neural coding of a moving conspecific stimulus. This study could quantify at several stages of analysis, how the strength of the envelope, the electroreceptor population, pyramidal cells of the ELL, and the influence of

feedback changes as one fish moves relative to another. An alternative study could investigate spatial processing in a freely swimming fish by using tethered or wireless recordings on pyramidal cells of the ELL. The freely swimming fish could be tasked with moving around a stationary conspecific stimulus, or by interacting with a moving conspecific stimulus with a programmed motion path. Certainly, further experiments on the spatiotemporal dynamics of beat and envelope coding are necessary to gain a more complete understanding of conspecific motion processing in the electrosensory system.

Spatial representation of conspecific signals in downstream topographic maps

In Chapter 3, I explore how the topographic representation of the ELL contributes to effectively encoding stimulus space, by mapping the receptive fields of pyramidal cells and quantifying their responses to a conspecific stimulus. I show that certain pyramidal cell populations, such as the deep-type pyramidal cells, display a straightforward pattern in their population response for encoding a spatial stimulus. Implementing a modeling approach, I show that the feedback acts to suppress the superficial and intermediate-type pyramidal cell populations' responses during spatial coding. However, the ELL is not the only area that contains topographic maps. In fact, electrosensory topographic maps are conserved downstream, in areas such as the midbrain torus semicircularis and the optic tectum (Carr et al., 1981, Carr et al., 1982, Maler et al., 1991). In the midbrain torus, there are several topographic maps that receive input from specific pyramidal cell types in the ELL. This begs the question, how is spatial information transformed from the ELL to the midbrain and optic tectum, and what are the functional consequences for localization? Furthermore, the midbrain

torus and optic tectum are areas that contain several connections for multisensory integration. This could mean that at these levels, information from several modalities (visual, mechanosensory, electrosensory, and sensorimotor) are contributing to successfully guide localization behavior. There are thus several open-ended questions that need to be researched further. What is the role of multiple topographic maps in the hindbrain, in the midbrain, and beyond? Are there certain aspects of the neural response that are more informative for a specific topographic representation? To what extent does feedback affect different topographic maps and what is the impact on behavior? Certainly, further studies will be required to elucidate mechanisms of spatial processing in higher brain regions that may serve as ultimate localization areas.

Conclusion

Detailing of how spatial information is processed requires analyzing the responses of the principal neurons in the primary sensory area as well as their network interactions (e.g., feedforward and feedback inputs). Such an analysis allows to clarify the role of the population and network dynamic in shaping spatial information and contributes to our general understanding of the mechanisms underlying spatial processing. This dissertation dissects how spatial information is represented in the electrosensory system, from the conspecific signal and its input onto receptors, to the primary electrosensory area (i.e., ELL). The significance of the contributions at each level of analysis is essential for uncovering how spatial information is coded in the early sensory system and how precise behavioral sensitivity is achieved. The research in this dissertation addresses this by: (1) characterizing the spatio-temporal structure

and the contrast of the conspecific signal as it reaches the receptors across the fish's body; (2) quantifying the coding of spatial information by heterogeneous pyramidal cells from empirical recordings in topographic maps of the ELL; and (3) upscaling to full populations through computational modeling to simulate the effects of feedback, receptive field interactions, and noise correlations on subpopulations of pyramidal cells in the ELL. Each finding in this dissertation provides unique insights into the functional role of the heterogeneous early electrosensory pathways for localizing conspecific signals. The results presented in this dissertation push sensory neuroscience research forward by laying the bases of a new area of focus using this model system, thereby allowing our understanding of spatial processing to benefit from a richer comparative perspective.

References

Allen, K. M., & Marsat, G. (2018). Task-specific sensory coding strategies are matched to detection and discrimination performance. *Journal of Experimental Biology*, *221*(6), jeb170563.

Bol, K., Marsat, G., Harvey-Girard, E., Longtin, A., & Maler, L. (2011). Frequency-Tuned Cerebellar Channels and Burst-Induced LTD Lead to the Cancellation of Redundant Sensory Inputs. *Journal of Neuroscience*, *31*(30), 11028–11038.

Baccus, S. A., Olveczky, B. P., Manu, M., & Meister, M. (2008). A retinal circuit that computes object motion. *The Journal of Neuroscience : The Official Journal of the Society for Neuroscience*, *28*(27), 6807–6817.

Bastian, J. (1986). Gain control in the electrosensory system mediated by descending inputs to the electrosensory lateral line lobe. *The Journal of Neuroscience*, *6*(2), 553–562.

Berman, N. J. and Maler, L. (1999). Neural architecture of the electrosensory lateral line lobe: adaptations for coincidence detection, a sensory searchlight and frequency-dependent adaptive filtering. *Journal of Experimental Biology* **202**.

Bratton, B. and Bastian, J. (1990). Descending control of electroreception: properties of nucleus-praeeminentialis neurons projecting directly to the electrosensory lateral line lobe. *Journal of Neuroscience* **10**, 1226–1240.

Carr, C., & Konishi, M. (1990). A circuit for detection of interaural time differences in the brain stem of the barn owl. *The Journal of Neuroscience*, *10*(10), 3227–3246.

Carr, C. E., Maler, L., & Sas, E. (1982). Peripheral organization and central projections of the electrosensory nerves in gymnotiform fish. *Journal of Comparative Neurology*, *211*(2),

139–153.

Carr, C. E., Maler, L., Heiligenberg, W., & Sas, E. (1981). Laminar organization of the afferent and efferent systems of the torus semicircularis of Gymnotiform fish: Morphological substrates for parallel processing in the electrosensory system. *Journal of Comparative Neurology*, *203*(4), 649–670.

Chacron, M. J., Maler, L., & Bastian, J. (2005). Feedback and feedforward control of frequency tuning to naturalistic stimuli. *Journal of Neuroscience*, *25*(23), 5521–5532.

Chen, L., House, J. L., Krahe, R., & Nelson, M. E. (2005). Modeling signal and background components of electrosensory scenes. *Journal of Comparative Physiology. A*, *191*(4), 331–345.

Clarke, S. E., Longtin, A. and Maler, L. (2015). Contrast coding in the electrosensory system: parallels with visual computation. *Nat Rev Neurosci* **16**, 733–744.

Clarke, S. E., & Maler, L. (2017). Feedback Synthesizes Neural Codes for Motion. *Current Biology*, *27*(9), 1356–1361.

Haggard, M., & Chacron, M. J. (2023). Coding of object location by heterogeneous neural populations with spatially dependent correlations in weakly electric fish. *PLOS Computational Biology, 19*(3), e1010938.

Harvey-Girard, E., Lewis, J., & Maler, L. (2010). Burst-induced anti-hebbian depression acts through short-term synaptic dynamics to cancel redundant sensory signals. *Journal of Neuroscience*, *30*(17), 6152–6169.

Henninger, J., Krahe, R., Kirschbaum, F., Grewe, J., & Benda, J. (2018). Statistics of natural communication signals observed in the wild identify important yet neglected stimulus regimes in weakly electric fish. *Journal of Neuroscience*, *38*(24), 5456-5465.

Hofmann, V., Sanguinetti-Scheck, J. I., Gómez-Sena, L., & Engelmann, J. (2017). Sensory Flow as a Basis for a Novel Distance Cue in Freely Behaving Electric Fish. *The Journal of Neuroscience*, *37*(2), 302–312.

Knudsen, E. I. (1975). Spatial aspects of the electric fields generated by weakly electric fish. *Journal of Comparative Physiology A*, *99*(2), 103–118.

Krahe, R., Bastian, J., & Chacron, M. J. (2008). Temporal processing across multiple topographic maps in the electrosensory system. *Journal of Neurophysiology*, *100*(2), 852–867.

Maler, L., Sas, E., Johnston, S. and Ellis, W. (1991). An atlas of the brain of the electric fish Apteronotus leptorhynchus. *J Chem Neuroanat* **4**, 1–38.

Marsat, G., & Maler, L. (2010). Neural heterogeneity and efficient population codes for communication signals. *Journal of neurophysiology*, *104*(5), 2543-2555.

Marsat, G., & Maler, L. (2011). Preparing for the unpredictable: adaptive feedback enhances the response to unexpected communication signals. *Journal of neurophysiology*, *107*(4), 1241-1246.

Marsat, G., Longtin, A., & Maler, L. (2012). Cellular and circuit properties supporting different sensory coding strategies in electric fish and other systems. *Current opinion in neurobiology*, *22*(4), 686-692.

Metzen, M. G., & Chacron, M. J. (2014). Weakly electric fish display behavioral responses to envelopes naturally occurring during movement: implications for neural processing. *J. Exp.*

Biol., *217*(Pt 8), 1381–1391.

Milam, O. E., Ramachandra, K. L., & Marsat, G. (2019). Behavioral and neural aspects of the spatial processing of conspecifics signals in the electrosensory system. *Behavioral neuroscience*, *133*(3), 282.

Nelson, M. E., & MacIver, M. A. (1999). Prey capture in the weakly electric fish Apteronotus albifrons: Sensory acquisition strategies and electrosensory consequences. *The Journal of Experimental Biology*, *202*(10), 1195–1203.

Ölveczky, B. P., Baccus, S. A., & Meister, M. (2003). Segregation of object and background motion in the retina. *Nature*, *423*(6938), 401–408.

Stamper, S. A., Madhav, M. S., Cowan, N. J., & Fortune, E. S. (2012). Beyond the Jamming Avoidance Response: weakly electric fish respond to the envelope of social electrosensory signals. *Journal of Experimental Biology*, *215*(23), 4196–4207.

Stamper, S. A., Fortune, E. S., & Chacron, M. J. (2013). Perception and coding of envelopes in weakly electric fishes. *Journal of Experimental Biology*, *216*(13).

Thomas, R. A., Metzen, M. G., & Chacron, M. J. (2018). Weakly electric fish distinguish between envelope stimuli arising from different behavioral contexts. *The Journal of Experimental Biology*, *221*(15), jeb178244.

Yu, N., Hupé, G., Garfinkle, C., Lewis, J. E., Longtin, A., & Fortune, E. (2012). Coding Conspecific Identity and Motion in the Electric Sense. *PLoS Computational Biology*, *8*(7), e1002564.